An Investigation into Regional Dependant Microglial Gene Expression and Function in the Control of Hippocampal Neural Stem and Progenitor Cell Regulation

A thesis submitted for the degree of Doctor of Philosophy

Emily Laura Adair

School of Medicine

Cardiff University

The Hodge Centre for Neuropsychiatric Immunology

Canolfan Hodge ar gyfer Imiwnoleg Niwroseiciatrig

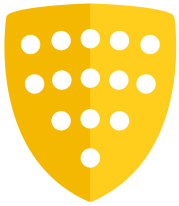

HODGE FOUNDATION

20th December 2022

Word count: 50,679

Abstract

Hippocampal neurogenesis is defined as the addition of new neurons to hippocampal circuitry and occurs continuously throughout adult life. What regulates this neurogenic phenomenon within the dentate gyrus (DG) of the hippocampus remains unclear. Previously, our group has suggested a role for microglia, showing the addition of hippocampal microglia to neural progenitor cells (NPC) has a positive neurogenic effect. Furthermore, recent studies have highlighted distinct regional transcriptional phenotypes of microglia, suggesting selective local functionality. I hypothesised that microglia possess differential neurogenic properties between distinct brain regions, which is underpinned by differential gene expression. Firstly, I investigated functional, regional-dependant, differential neurogenic properties of microglia in vitro via the addition of microglia or their conditioned media (CM) from separate brain regions, including the DG, rest of the hippocampus (RH) and cortex, to rat postnatal hippocampal NPC's cultures. This was assessed using immunocytochemistry and fluorescent microscopy, inspecting markers of the cell cycle, neuronal stem cells and immature neurons. Culture experiments revealed, the addition of microglia or their CM selectively increased NPC, but did not increase neuronal populations. This was consistent across all groups and as a result specialist phenotype of microglia are suspected to be lost during in vitro culture. Secondly, differential gene expression from acutely isolated microglia from mouse DG, RH and cortex was investigated using bulk RNA-sequencing. Significant differential gene expression was observed between microglia isolated from the DG and RH. Furthermore, GO enrichment analysis identified terms of interest including neurogenesis and neuron differentiation. In conclusion, DG microglia show significant differential gene expression compared to RH microglia which may contribute to a functional, regional specific, neurogenic microglial phenotype within the DG. Genes identified here may represent good biological targets to

undergo further investigation to prevent and/or slow down hippocampal neurogenesis dysregulation.

Acknowledgements

They say it takes a village to raise a child, I say, it takes a whole department to raise a PhD student. First and foremost, I would like to thank my supervisory team Professor William Gray and Professor Philip Taylor, without whom this work would not have taken place. Thank you for your invaluable guidance and support through some very challenging times and for never giving up on me, even when I wanted to give up on myself. Secondly, I would like to thank my generous PhD funders, the Hodge Foundation for supporting my work. To my PTY and final year supervisor Professor Vincenzo Crunneli and Professor Yves Barde, thank you for encouraging me and supporting me to pursue a career in academia. Thank you to my peers within the Gray lab and beyond who have supported me from day one of my PhD, including: Dr Malik Zaben, Dr Chloe Ormonde, Chen Liang, Dr Jo Brown, Dr Ying Zhu, Feras Sharouf and Leah Fallon. Thank you to Professor Anthony Isles, Professor Lawrence Wilkinson and Professor Nicholas bray for your guidance and support throughout the student progress monitoring process. An enormous thank you goes to Dr Neils Haan, Dr Mohammed Alsquati, Dr Nicholas Clifton, Dr Tom Chambers, Dr Laura Westacott, Dr Danni Casabeas, Mark Gurney, Elena Simmonanzi, and Jack Redaway for your practical help and guidance with my research. To the tireless work of the whole animal unit but particularly to Rhys Perry and Keely Samuel for always going above and beyond in supporting my research. To the admin, finance and lab support team, particularly Emma Dalton who always had the solution to every problem. I would like to particularly dedicate this body of work to Dr Jasmine Donaldson for your unwavering love, support and encouragement. This work would not have been written without you. Extra special thanks go to the friends that have supported me during this time with a special mention to Dr Aine Moylett, Sarah Quarmby, and the NMHRI lunch crew. To all the PhD students past and present who I have come to know throughout my time at Cardiff University, it has truly been a pleasure. Finally, to my parents James and Sheila, my brother Christopher and extended family, thank you for always believing in me and allowing me to make my own decisions, make my own mistakes and for always loving me.

List of abbreviations

ABX	Antibiotic-antimycotic
ANOVA	Analysis of variance
APC	Allophycocyanin
ATP	Adenosine triphosphate
Bdnf	Brain derived neurotrophic factor
BlbP	Brain lipid-binding protein
BrdU	Bromodeoxyuridine
BSA	Bovine serum albumin
C1q	Complement component 1q
C2	Curated gene set
C3	Compliment component 3
C5	Ontology gene set
Ccr2	Chemokine receptor 2
Cd11b	Cluster of differentiation 11b
Cd45	Cluster of differentiation 45
Cd68	Cluster of differentiation 68
cDNA	Complimentary DNA
CM	Conditioned media
CNS	Central nervous system
CO_2	Carbon dioxide
CRISPR	Clustered regularly interspaced short palindromic repeats
CR3	Complement receptor 3

Cre	Cre recombinase
Csf1r	Colony stimulating factor 1 receptor
Ct	Cycle threshold
Cux1	Cut like homeobox 1
CX	Cortex
Cx3cl	C-X3-C motif ligand 1
Cx3cr1	C-X3-C motif chemokine receptor 1
CyTOF	Cytometry by time of flight mass spectrometry
DAMPs	Damage associated molecular patterns
DAPI	4'6-diamidino-2-phenylindole
Dcx	Doublecortin
DEG	Differentially expressed gene
DG	Dentate gyrus
DIV	Days *in vitro*
DMEM	Dulbecco's modified eagle medium
DNA	Deoxyribonucleic acid
dPBS	Dulbecco's phosphate-buffered saline
Dsp	Desmoplakin
E	Embryonic day
EdU	5-ethyl-2-deoxyuridine
EDTA	Ethylenediaminetetraacetic acid
EGF	Epidermal growth factor
ES	Enrichment score
ESC	Embryonic stem cell

FACS	Fluorescence activated cell sorting
FBS	Fetal bovine serum
FDR	False discovery rate
FGF	Fibroblast growth factor
Fig	Figure
FIJI	FIJI is just imageJ
FIRE	Fms-intronic regulatory element
FSC	Forward side scatter
FITC	Fluorescein
FPKM	Fragments per kilobase of exon per million mapped reads
Gapdh	Glyceraldehyde-3-phosphate dehydrogenase
Gfap	Glial fibrillary acidic protein
(E)GFP	(enhanced) Green fluorescent protein
GO	Gene Ontology
GSEA	Gene set enrichment analaysis
H	Hallmark gene set
H_2O	Water
HBSS	Hank's balanced salt solution
HEK	Human embryonic kidney
hr	Hour
IB4	Isolectin GS-IB_4 conjugated to Alexa Fluor-488
Iba1	Ionised calcium binding adaptor molecule 1
ID	identification
IDT	Integrated DNA technologies

IGF1	Insulin-like growth factor 1
Il-(1α, 1β,4)	Interleukin- (1α, 1β,4)
iNOS	Inducible nitric oxide synthase
I.P.	Intra-peritonieal
iPSC	Induced pluripotent stem cell
KEGG	Kyoto Encyclopedia of genes and genomes
KO	Knock-out
LCM	Laser capture microdissection
Log	logarithim
LoxP	Locus of X over P1
LPS	Lipopolysaccharide
M1	Microglial phenotype 1: pro-inflammatory
M2	Microglial phenotype 2: Anti-inflammatory
MACS	Magnetic activated cell sorting
MAC-1-SAP	Saporin conjugated to CD11b monoclonal antibody
(h/c) MG	(hippocampal/cortical) Microglia
MGCM	Microglial conditioned medium
M-CSF	Macrophage colony stimulating factor
MGEnrichment	Microglia enrichment
Mhc	Major histocompatibility complex
Mrg1b	Meis-related gene 1b
mRNA	Messenger RNA
MSigDB	Molecular signatures database
NBA	Neurobasal A

NES	Normalised enrichment score
Neun	Neuronal nuclear protein
Nov	Nephroblastoma overexpressed gene
NPC	Neural progenitor cell
NSPC	Neural progenitor/stem cell
O_2	Oxygen
OCT	Optimal cutting temperature
P	Post-natal day
P2ry12	Purinergic receptor 2 , G-protein coupled 12
PC	Principal componant
PCA	Principal component analysis
PCR	Polymerase chain reaction
PBS	Phosphate buffered saline
PBS-T	Phosphate buffered saline + Triton-X 100
PE	Phycoerythrin
PFA	Paraformaldehyde
PI	Propidium Iodide
PLL	Poly-L-lysine
PMI	Post mortem interval
Ppp1r1a	Protein phosphatase 1 regulatory subunit 1A
Prox1	Prospero Homeobox 1
QC	Quality control check
Q-PCR	Quantitative polymerase chain reaction
RABID-seq	Rabies barcode interaction detection followed by sequencing

RH	Rest of the Hippocampus
RIN	RNA integrity number
rlog	Regularised log transformation
RNA	Ribonucleic acid
RNAseq	RNA sequencing
RT-PCR	Reverse transcription - polymerase chain reaction
SAP	Saporin
scRNA-seq	Single cell RNA sequencing
SEM	Standard error of the mean
SGZ/L	Sub granular zone/layer
smFISH	Single molecule RNA Fluorescence in situ hybridisation
SSC	Side scatter
Sox2	SRY (sex determining region Y)-box 2
SVZ	Sub ventricular zone
Tbr2	T-box brain protein 2
Tdo2	Tryptophan 2,3-dioxygenase
Tgf-β	Transforming growth factor beta
Tmem119	Transmembrane protein 119
TNF-α	Tumour necrosis factor alpha
Tuj1	Beta-Tubulin III antibody clone TUJ1
Vegf	Vascular endothelial growth factors
Vpac1	Vasoactive intestinal peptide receptor type 1
VST	Variance stabilising transformation
WH	Whole hippocampus

YFP	Yellow fluorescent protein
2D	2-dimensional
3D	3-dimensional
^{14}C	Carbon 14

Table of Contents

1.0 General Introduction

1.1.0 Hippocampal Neurogenesis

Hippocampal neurogenesis is the process whereby new functional granule neurons are born and integrated into existing neuronal circuitry within the dentate gyrus of the hippocampus from neural stem cells. This process is thought to be important for information processing critical for adaptive behaviour, including: learning and the formation of new memories, forgetting and emotionality (Kempermann et al. 2004b; Aimone et al. 2009; Akers et al. 2014; Kheirbek and Hen 2014; Anacker and Hen 2017). Hippocampal neurogenesis has been investigated since the 1960s from *in vitro* to *in vivo,* from rodents to humans and using a variety of techniques, including: histology, behavioural paradigms and electrophysiology (Altman and Das 1965; Eriksson et al. 1998; Anacker et al. 2018). Evidence from animal studies indicate that disruption to hippocampal neurogenesis is implicated in many neurological diseases and psychological disorders including Alzheimer's disease, depression and schizophrenia (Toda et al. 2019). This association is thought to underlie negative symptoms in these patient populations and may contribute to the progression of such diseases (Cho et al. 2015; Sheline et al. 1999). Hippocampal neurogenesis is defined as the generation and integration of new neurons within the hippocampus, specifically the birth of granule cells in the dentate gyrus. New born granule cells that manage to survive, migrate and integrate through to the granule cell layer (Cameron and Mckay 2001; Hayes and Nowakowski 2002; Kempermann et al. 2004a; Gonçalves et al. 2016; Pilz et al. 2018). Neurogenesis is a rare event in the brain and is thought to be limited to two structures: the hippocampus and the subventricular zone in mammals. A seminal paper by Eriksson (1998) utilised the thymidine analogue, bromodeoxyuridine (BrdU), in human post-mortem tissue to show hippocampal cells are

capable of self-renewal. Further studies have tried to quantify this event by retrospectively dating the birth of cells in the hippocampus based on relative levels of 14C in the genome of these cells compared with atmospheric levels. Using this method, it was estimated that adult humans, are capable of generating up to 700 new neurons each day in each hippocampus with only a small reduction in this renewing population with age (Spalding et al. 2013).

1.1.1 The anatomy and circuitry of the human Hippocampus

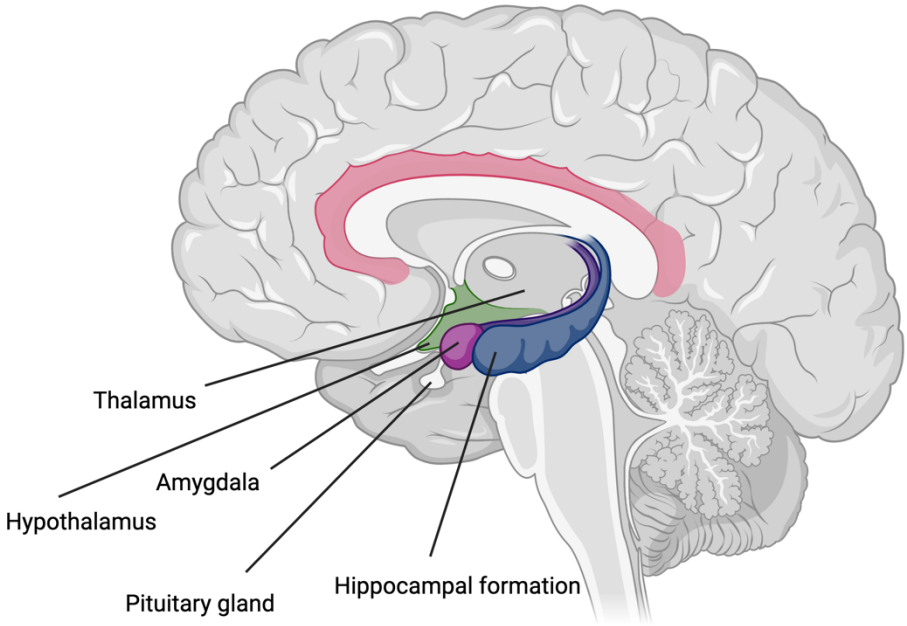

Figure 1.1 Sagittal view of the human brain identifying the hippocampal formation and structures that lie in close proximity including the amygdala, thalamus, hypothalamus and pituitary gland.

The hippocampi are a bilateral structure (**Fig.1.1**) that lies deep within the temporal lobes of the brain and which are highly conserved across mammals and birds (Insausti 1993; Atoji and Wild 2006; Manns and Eichenbaum 2006). Functional From animal and computational studies, we know that adult hippocampal neurogenesis is important for learning and the formation and integration of new memories as well as emotional processing (Bannerman et al. 2004; Chawla et al. 2005; Rolls and Kesner 2006; Leutgeb et al. 2007; Aimone et al. 2009). An inability to

regenerate hippocampal cells therefore is thought to underlie memory deficits associated with many neurological disorders (Shors et al. 2001; Zhao et al. 2008). The hippocampus consists of several distinct areas including the dentate gyrus, the hippocampus proper which is comprised of the cornu ammonis (CA)1, CA2, CA3 and CA4 (**Fig.1.2**) and finally the subiculum. These regions are connected in a serial path which begins with DG, followed by the CA3, CA1 and finally the subiculum. The dentate gyrus is further subdivided into three distinct layers: the sub granular zone (SGZ), the molecular cell layer and the granule cell layer. The SGZ is a highly vascularised region and the location where neural stem cells proliferate and differentiate into dentate granule cells (Palmer et al. 2000). The vascularised nature of the SGZ suggests that blood derived factors may play a role in the behaviour of neural stem cells in the DG. The hippocampi are situated in an ideal position in the brain to receive highly processed information including spatial and non-spatial information. They are well connected to neocortical structures via the entorhinal, perirhinal and parahippocampal cortical regions. While the hippocampus receives input from the entorhinal, perirhinal and parahippocampal cortices, the main source of sensory information to the hippocampus is received from layer II of the entorhinal cortex to the molecular layer of the DG, which is described as the perforant pathway. Projections from the DG in turn provide input to the CA3 region via mossy fiber projections of granule cells and the CA3 region provides the major input into the CA1 region through the Schaffer collateral pathway. Additionally, both the CA1 and subiculum receives direct projections from layer III of the entorhinal cortex. Most neurons in the CA1 are pyramidal cells which primarily project to the subiculum, however, projections are also known to extend to layer V of the entorhinal cortex. Finally, the subiculum sends projections to layers IV and V of the entorhinal cortex (Clark and Squirea 2013). Across the mammalian taxon, there exists neuroanatomical differences including size, connectivity and organisation of neocortical regions. However, across all mammals the distinctive structure of the DG and CA

regions can be identified in the hippocampus, with hippocampal connectivity remarkably well conserved (Manns and Eichenbaum 2006). Interestingly, structural asymmetry in hippocampi may have important functional consequences for example in spatial navigation (Jordan 2020a).

Despite the evolutionary conservation of hippocampal neurogenesis across species, some anatomical differences in the hippocampus have been observed. As mammals have evolved, the hippocampus appears to have been anatomically displaced and rotated, whereby in humans and non-human primates the hippocampus is located towards the base of the brain whereas in rodents the hippocampus is located much more dorsally (Kempermann 2012). There is also evidence that there is a larger degree of interhemispheric differences in human hippocampi compared to rodent hippocampi due to a reduction or weakened bilateral projections between hippocampal fields which is also reflected in the lateralisation of human hippocampal function (Jordan 2020b). One distinct difference between human and rodent hippocampal anatomy is the gross number of granule cells within the dentate gyrus. In rodents there are approximately 600,000 and 1 million granule cells whereas in humans, estimates vary between 9 and 18 million depending on the methods used (West and Gundersen 1990; Seress 2007).

1.1.2 Dynamics of Hippocampal Neurogenesis

The process of hippocampal neurogenesis can be divided into defined stages based on cell morphology and expression of key markers. Neural stem cells in the dentate gyrus are described in the literature as radial glial cells (RGLs) or type 1 cells. These cells are a quiescent population that reside in the SGZ of the dentate gyrus and are typically defined morphologically as having a triangular shaped cell soma and a prominent apical process

reaching up through the granule cell layer and branching out into the molecular cell layer (MCL) as seen in **Fig.1.2** (Kempermann et al. 2004a). Astrocytes which are also commonly found to express GFAP, can be distinguished from type 1 neural stem cells via the expression of S100β. (Savchenko et al. 2000). Type 1 cells can be identified by the expression of glial fibrillary acidic protein (Gfap) and Nestin, the transcription factor sox2 and vimentin (Kempermann et al. 2004a; Zhang and Jiao 2015). By their very definition, neural stem cells of the dentate gyrus should be capable of self-renewal and are multipotent (Bonaguidi et al. 2011). Chronic live imaging of hippocampal neurogenesis in adult mice has been used to asses RGLs self-renewal capacity. RGLs can be targeted by crossing tdTomato reporter mice with mice expressing a tamoxifen inducible Cre recombinase under the control of the Achete-scute homolog 1(*Ascl1*) promotor. Here injection of tamoxifen induces sparse labelling of RGLs which can be viewed via two-photon imaging. Using this technique one group observed the behaviour of individual RGLs for 2 months and the fate of their progeny was characterised through immunohistochemistry. Once RGLs entered the cell cycle, they were seen to generate a burst of neurogenic activity and commit to terminal neuronal differentiation rather than return to a quiescent state (Pilz et al. 2018). These contrasting reports may be reconciled by the existence of a heterogenous population of Type 1 neural stem cells which may explain differing rates of self-renewal as well as individual capacity to differentiate (Chaker et al. 2016). Therefore, it may be that *Ascl1* reporter mice do not capture the entire RGL cell population. Type 1 radial glial like cells generate intermediate transiently amplifying progenitor cells also known as type 2 cells which display a smaller more rounded morphology compared to type 1 neural stem cells and are highly proliferative. Type 2 progenitor cells can be further subdivided into two subtypes. Type 2a progenitors are characterised by the continued expression of Nestin and the down regulation of Gfap whereas Type 2b progenitor cells express Nestin and doublecortin (Dcx). Type 2b cells go on to give rise to neuroblasts also known as type 3 cells

which are positive for D and negative for Nestin expression. Neuroblasts will then further give rise to immature neurons identified by the expression of Dcx, Calretinin, Polysialated neuronal cell adhesion molecule (Psa-ncam), class beta III tubulin (Tuj1) and finally immature neurons develop into mature granule cells which express Neun and Calbindin (Kempermann et al. 2004a). Type 1 cells also facilitate the migration of newly born neurons by providing scaffolding within the dentate gyrus. Despite the high levels of energy expended in hippocampal neurogenesis, a relatively low level (40.4%) of new-born cells survive to mature and integrate into the functional neuronal circuitry, although this has been observed to vary along individual clonal lineages (Pilz et al. 2018). Two critical phases have been described: the first is an early phase which occurs in the first few days after cell birth and a second later phase which occurs one to three weeks after cell birth and is dependent on the cellular activity (Sierra et al. 2010). The factors that contribute to an individual newly born cells death remains elusive but may be due to multiple factors including: genetic alterations, aging factors, growth factor availability and levels of pro-inflammatory factors.

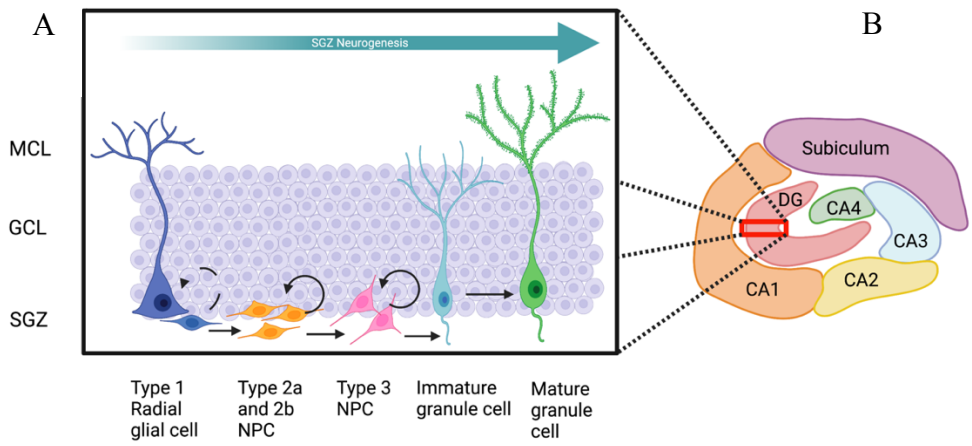

Figure 1.2 Hippocampal neurogenesis in the sub granular zone of the dentate gyrus. A diagram of an unravelled human hippocampus (B) with an enlarged sub section of the Dentate gyrus (A) including the molecular cell layer (MCL), granule cell layer (GCL) and sub granular zone (SGZ). A depiction of the proposed cellular continuum of hippocampal neurogenesis in the SGZ. Six stages have been proposed and can be identified by cell morphology and expression of neuronal stem cell and progenitor cell markers. The dentate gyrus is composed of three distinct layers: the molecular cell layer (MCL), granule cell layer (GCL) and sub granular zone (SQZ). Created with BioRender.com

1.1.3 Factors affecting hippocampal neurogenesis

Intrinsic factors that are known to regulate hippocampal neurogenesis include: morphogens, growth factors, cytokines, adhesion molecules, transcription factors, epigenetic modifiers, and neurotransmitters (Toda et al. 2019). These factors act to regulate hippocampal neurogenesis at different levels with some targeting Type 1 neural stem cells and others neuroblasts or immature neurons. For example, vasoactive endothelial growth factors (Vegf) an angiogenic growth factor has been shown to be secreted in large quantities by neural stem cells *in vitro* and *in vivo*. Secreted Vegf from neural stem cells appears to be important for maintaining population levels in the neurogenic niche as a loss of Vegf results in an impairment of stem cell maintenance (Kirby et al. 2015). In contrast brain derived neurotrophic factor (Bdnf) is a growth factor that has been described to possess differential effects on neurogenesis that is dependent on dosage in culture (Ahmed et al. 1995; Bartrup et al. 1997; Wei et al. 2015; Kowiański et al. 2018). Bdnf is seen to be capable of promoting differentiation as well as promoting neuronal maturation (Toda et al. 2019). Mice lacking the main receptor for Bdnf - Tyrosine kinase B, TrkB – in hippocampal neural progenitor cells show impaired proliferation and hippocampal neurogenesis (Li et al. 2008b). Additionally, when these mice voluntarily free run or are exposed to chronic administration of antidepressants – no change in hippocampal neurogenesis is observed. This indicates that Bdnf signalling via TrkB is an important factor in regulating hippocampal neurogenesis.

Extrinsic factors known to affect hippocampal neurogenesis include: exercise, environmental enrichment, diet, sleep, antidepressants and life events (Malberg et al. 2000; Mirescu et al.

2006; Fabel et al. 2009; Stangl and Thuret 2009). In experimental paradigms, rodents in standard laboratory settings are housed in relatively small cages with limited stimuli. Environmental enrichment is a practical approach of increasing cognitive stimulation in rodents that while increases animal welfare is also more representative of the human condition and therefore may improve the efficacy of rodent models used to investigate disease. Environmental enrichment can include cages with increased area, novel objects, nesting materials, tubes for hiding, a running wheel or changes to the number of individuals per cage. Environmental enrichment modules may by acute or long-term additions to the housing conditions depending on the set up. Rodents raised in environmental enrichment typically show increased hippocampal neurogenesis, increased cortical thickness and show enhanced performance in learning and memory tasks compared to rodents raised in standard laboratory housing (Fares et al. 2013). Similarly, exercise has been shown to increase hippocampal neurogenesis. This is typically referred to as voluntary wheel running in rodents and has been shown to selectively increase the proliferation of neural progenitors (van Praag et al. 1999; van Praag 2005). Interestingly, the role of an individual's diet is also becoming an increasingly Important factor in the regulation of hippocampal neurogenesis (Stangl and Thuret 2009). Some studies have suggested the ratios of omega-3: omega-6 fatty acids influence hippocampal neurogenesis, whereas others show that diets enriched in polyphenols and poly unsaturated fatty acids are pro neurogenic in the hippocampus (Beltz et al. 2007; Valente et al. 2009). While the factors that influence hippocampal neurogenesis is an ever-evolving field, it is clear that the regulation of hippocampal neurogenesis is a highly sensitive and complex. Therefore, further research is required to elucidate fully the mechanisms underlying the regulation of hippocampal neurogenesis.

1.1.4 Hippocampal Neurogenesis and brain health

Hippocampal neurogenesis is an energetically expensive process which is highly conserved across mammals. This would suggest that hippocampal neurogenesis serves an important function that is required throughout the lifespan of the organism that confers an evolutionary advantage. Several studies have shown that hippocampal neurogenesis in the healthy brain is required for many processes such as pattern separation, interference, forgetting, memory clearance, and cognitive flexibility. The overarching themes in these processes is the dealing with conflicting or overlapping information. Pattern separation, in the behavioural context, is the ability to distinguish between highly similar stimuli. In terms of electrophysiology, pattern separation, is the ability to minimise the overlap between neural activity that represents highly similar inputs (Madar et al. 2019). Computational models of pattern separation which have been validated in rodent electrophysiological recordings (Leutgeb et al. 2007; Madar et al. 2019). The overlap between two patterns of neural activity arriving from the cortex is thought to be reduced by sparse encoding in the granule cells of the DG which have strong projections to CA3 pyramidal cells. Knockdown of hippocampal neurogenesis in mice using temozolomide has added to the model of pattern separation by demonstrating a lack adult generated granule cells in dentate gyrus is associated with the inability of to a perform spatial memory task (Garthe et al. 2009). In addition, efforts to increase hippocampal neurogenesis show improvements in an animal's efficiency to delineate between overlapping contextual stimuli (Sahay et al. 2011). However, these results are not universally seen across all studies that have aimed to study the effect of varying rates of hippocampal neurogenesis upon pattern separation ability and this is thought to be due to experimental strategy (Toda et al. 2019). Hippocampal neurogenesis is also thought to play a role in memory clearance and forgetting. Mice which were first trained to perform hippocampus dependant memory tasks were later either kept

sedentary or were allowed to run on a wheel for six weeks. Mice that displayed increased levels of hippocampal neurogenesis, associated with wheel running, performed more poorly in in the hippocampus dependant memory tasks when tested again. Blocking the effect of wheel running on hippocampal neurogenesis prevented memory clearance (Akers et al. 2014). Cognitive flexibility is another process that hippocampal neurogenesis is implicated in. Cognitive flexibility, is the ability to use information from a previous experience and apply that knowledge in a new context. This has been demonstrated in mice that were trained to learn the location of a shock zone on a rotating platform. Mice whom underwent hippocampal ablation were able to learn that a shock was associated to a specific zone but were unable to apply this information when the shock zone was altered and therefore did not avoid the shock (Burghardt et al. 2012). The rate of hippocampal neurogenesis has been seen to be affected by multiple factors. These include environmental factors such as exercise and environmental enrichment as well as physiological factors or emotional state (Kempermann et al. 1997; van Praag et al. 1999; Malberg et al. 2000).

1.1.5 Hippocampal Neurogenesis and disease

Adult hippocampal neurogenesis is known to decline steadily with aging and is associated with cognitive decline and memory impairments. However, dysfunctional regulation of hippocampal neurogenesis is associated with many neurological and psychological disorders including: depression, schizophrenia, Alzheimer's disease (AD), Parkinson's disease, Huntington's disease and Epilepsy. There is good evidence in rodent and non-human primate studies that physical and psychological stresses can perturb adult hippocampal neurogenesis which suggests that similar processes could occur in humans (Gould et al. 1998; van Bokhoven

et al. 2011). There are various paradigms used to model the effects of stress in rodents which can be used in acute or chronic modalities. These include: social defeat, predator odour, physical restraint, electric shock and multiple mild stressors (Schoenfeld and Gould 2012). Depending on the specific paradigm used, stressors have been shown to decrease either rates of proliferation, rates of neuronal differentiation or rates of neuronal survival. Mice subjected to a chronic social defeat stress model display a reduced number of proliferating cells in the SGZ as labelled with BrdU, which recovers after 24hrs. Interestingly, four weeks after the chronic social defeat stress, mice that displayed social avoidance were seen to have increased hippocampal neurogenesis compared to mice that that did not show social avoidance (Lagace et al. 2010). This suggests that not only is hippocampal neurogenesis dysregulated by stress events but that in some individuals it is important in developing maladaptive response to stress. Stress induced dysregulation of hippocampal neurogenesis may further compound problems that have arisen due to pathological conditions.

Major depressive disorder (MDD) is classed as a mood disorder and has been linked to hippocampal neurogenesis primarily through experiments which have demonstrated that hippocampal neurogenesis is required for the beneficial effects of some antidepressants (Santarelli et al. 2003). While, the rate of hippocampal neurogenesis has been shown to increase through treatment with antidepressants, one group has demonstrated that hippocampal neurogenesis is required to reduce anxiety and depression related behaviour in mice subjected to a model of stress - chronic Corticosterone (CORT) (Malberg et al. 2000; Hill et al. 2015). A tamoxifen inducible transgenic mice line, where the pro-apoptotic gene *Bax* is deleted from neural stem cells and their progeny in the adult via Nestin-CreERT2 expression was used. In these transgenic mice there is an increase in hippocampal neurogenesis which was not associated with changes in baseline anxiety and depression related behaviours when tested with

the elevated plus maze and tail suspension test. Non-induced mice which were treated with CORT show a reduction in hippocampal neurogenesis as well as increase in anxiety and depressive live behaviour, as compared to vehicle treated mice. However, hippocampal neurogenesis and anxiety and depressive like behaviours appear to recover to vehicle treated levels in tamoxifen induced mice treated with CORT. As many studies like the one previously discussed are performed in rodents and non-human primates, it is important to consider what these results mean for human hippocampal neurogenesis. Similarities between rodent and human studies have been observed. For example, immunohistochemical assays have been performed on post mortem tissue to investigate the relationship between anti-depressant use in MDD patients and hippocampal neurogenesis. Anti-depressant use in MDD patients has been associated with hippocampal angiogenesis and progenitor cell proliferation compared to MDD patients who did not receive antidepressants (Boldrini et al. 2012). Further, evidence to support the importance of hippocampal neurogenesis comes from a meta-analysis of magnetic resonance imaging studies looking at hippocampal volume in MDD patients and controls. Here hippocampal volume has been demonstrated to be reduced in humans diagnosed with MDD compared to healthy controls (Campbell et al. 2004).

AD is the most common form of dementia which is characterised by accumulation of intracellular tau tangles and intercellular amyloid beta plaques. Clinical presentations of AD include functional memory impairment and cognitive decline. There is limited human data on the relationship between Alzheimer's and hippocampal neurogenesis due to the limited availability of human tissue and the ethical issues pertaining to human experimental practices. Therefore, the primary source of evidence comes from mouse models that have been engineered to overexpress genes linked to familial forms of AD such as mutant amyloid precursor protein (App) and presenilin (Psen). For example, a triple transgenic mouse model

of AD (3xTg-AD) carrying three mutations in β-amyloid precursor protein, presenilin-1 and tau genes has been used to demonstrate a reduction in hippocampal neurogenesis compared to control mice that begins at 9 months old and is completely abolished by 12 months of age (Rodríguez et al. 2008). However, there are conflicting reports on the effect of Alzheimer's disease on hippocampal neurogenesis with some groups observing decreases and others increases (Rodríguez et al. 2008; Yu et al. 2009; Wirths 2017). These differences are likely attributable to the different transgenic approaches as well as the stage of the disease that is assessed. Additionally, many of the transgenic mouse models that have been generated so far do not faithfully recapitulate AD pathology, for example the over expression paradigm can induce unwanted and unrelated phenotypes and this makes interpreting the results difficult. As the AD field has advanced, enhanced mouse models have emerged including mouse models that contain humanised mutations of the *App* gene which have partially resolved these problems (Sasaguri et al. 2017). AD pathology is known to begin in the entorhinal cortex and over time is seen to spread to the hippocampus and cortical regions. The hallmark pathology of AD is thought to result in synaptic and neuronal loss. As the entorhinal cortex is the primary source of input into the hippocampus, synaptic and neuronal loss in these regions may explain in part functional impairments in hippocampal neurogenesis. Similar to AD mouse studies, there is conflicting results with regards to the effect of AD on hippocampal neurogenesis (Jin et al. 2004; Boekhoorn et al. 2006; Li et al. 2008a; Crews et al. 2010). Again, these differences may be due to different stages of AD, APOE and TREM2 phenotypes as well as limitations of human post mortem immunohistochemistry.

A common symptom that is experienced in neurological and psychiatric disorders described above is cognitive impairment. Cognitive impairment in these patient populations is highly correlated with dysfunction in adult hippocampal neurogenesis and may underlie these

negative symptoms. There are currently no treatments that aim to restore cognitive impairment and memory loss or improve rates of hippocampal neurogenesis. A global understanding of the mechanism and regulators of hippocampal neurogenesis is still lacking. Therefore, investigations in to the mechanisms that regulate hippocampal neurogenesis is a good target for therapeutic action in these patient populations.

1.2.0 Microglia

1.2.1 Microglia in the context of the immune system

To understand the role of microglia in the brain it is important to have a clear understanding of the immune system as a whole. Humans and animals are in a constant state of threat from foreign bodies and pathogens that may be acquired by ingestion, inhalation, or direct contact. The first line of defence in immunological terms is a physical barrier between the inside of the body and the outside world. Our skin and the epithelial surfaces of our intestines, lungs and mouth can be considered our first line of defence, further aided by a mucosal layer which prevents adhesion of pathogens to the cell wall and can also provide a means of clearance by the beating of cell cilia. This barrier can fail, for example, when the skin becomes broken or where pathogens are able to invade the epithelial membranes. Crucially it is important that the immune system can delineate self from non-self. It is here that the innate and adaptive immune systems come into play to attempt to destroy the pathogen in a timely fashion without causing major harm to the host (Marshall et al. 2018).

Innate immunity is an evolutionarily older form of the immune system and as such its response is rapid and nonspecific. The innate immune system relies on conserved proteins and molecules that are commonly found on pathogens and not in the host. These conserved pathogenic features deliver a ‘go, no-go’ system that phagocytic cells are able to recognise and act upon. When a pathogen associated immune-stimulant is encountered such as cell surface molecules that are foreign to the host (e.g. Lipopolysaccharide on gram negative bacteria), two major responses are produced. Firstly, an inflammatory response and secondly a phagocytic response.

The innate immune system is a rapid responder and occurs rapidly regardless of whether the host has encountered this pathogen before or not. The components of the innate immune system include the complement system, pattern recognition receptors such as: toll like receptors and phagocytic cells. The complement system while playing a major role in innate immunity also mediates several biological processes including: host defence, synaptic pruning and modulation of metabolism. The complement system is comprised of approximately 20 interacting soluble proteins, some which act as pathogen recognition receptors which are largely synthesised by the liver. These proteins circulate in the blood and extracellular fluid and generally remain inactive until they are activated by an infection. There are three main activation pathways that have been identified by the complement system: classical, lectin and alternative. All three pathways converge to cleave C3 which is thought to be a pivotal component in this pathway. Ultimately the activation in these pathways result in an amplifying, proteolytic cascade that produces large and small by-products. The larger by-products adhere to pathogen cell walls and act as recognition sites for phagocytic cells. The smaller by-products act as signalling molecules to recruit phagocytes and lymphocytes to the site of pathogen invasion to engulf and destroy. By-products of the complement cascade are highly unstable and therefore inactivate quickly. This ensures that there is no long lasting and severe damage caused to the host even after the pathogen has been neutralised (Sarma and Ward 2011).

The adaptive immune system on the other hand, is a sophisticated and dynamic process that is highly specific to the pathogen it is responding to and as a result can provide long term protection. It can be said that the adaptive immune system imparts an immunological memory to the host and forms the basis for immunisation programs. An entity that is able to elicit an adaptive immune response is referred to as an antigen. The cells responsible for carrying out this process are lymphocytes of which there are two broad classes: B cells and T cells. When

activated B cells synthesise and secrete antibodies specific to a certain pathogen which is then circulated around the body through the blood and extracellular fluids. Binding of an antibody to its antigen inactivates the pathogen by preventing from binding with the receptors of host cells. T-cells on the other hand react directly to an antigen on the surface of a host's cell by killing it and or by recruiting macrophages to phagocytose the pathogen. In this way lymphocytes can recognise and distinguish between specific antigens on a pathogen which will elicits a highly specific immune response to target and destroy the invader. Immune cells need to communicate in order to induce an effective inflammatory response and they do this via signalling molecules known as cytokines. Cytokines comprise a large group of small proteins and glycoproteins that are largely synthesised and secreted by T-helper cells and macrophages. Whilst cytokines activate host cells in an antigen-non-specific way, they play a role in both the innate and adaptive immune responses as well as possessing non-immune functions in development (Flajnik and Kasahara 2009).

Historically, the brain was considered an immune privileged organ due to a limited immune response of tissue grafts in the brain compared to tissue grafts in the periphery which showed a much higher rate of rejection (James Murphy and Sturm 1923; Willis, A 1935; Medawar 1948). However, as the brain is a vital organ for normal bodily as well as cognitive functioning, one would expect a certain evolutionary advantage to some level of protection from dangerous molecules and pathogens. The CNS is of course protected by several layers of tissue including cerebrospinal fluid, the meninges and bone that surround the spinal cord and brain. However, the brain is principally protected from pathogens by the formation of the blood brain barrier. The blood brain barrier provides a strong wall of defence via tight junctions of capillary endothelial cells, the basal lamina and the end feet of astrocytes which prevent large and potentially dangerous entities from gaining entry to the brain. Circulating immune cells in the

blood as well as those that patrol and survey the meninges (macrophages) and brain (Microglia) provide an additional layer of protection (Muldoon et al. 2013).

1.2.2 Microglia origin and migration

Ramón Y Cajal, the founding father of neuroscience discovered the discrete units of the brain, terming these the first element (neurons), the second element (astrocytes) and the third element (Glia). However, advancements in methodological tools were needed to examine cellular structures at a higher level and to highlight previously unseen components of the brain parenchyma. Pío del Río Hortega was convinced that the so called 'third element' was not just a homogenous group of cells that orbited neurons. By modifying the metallic staining techniques used by Cajal to incorporate silver carbonate, Pío del Río Hortega was able to identify two distinct cell types based on cellular morphology: microglia and oligodendroglia and he also showed that these cells appeared to have differential distributions across grey and white matter (Pérez-Cerdá et al. 2015). Remarkably, at this time, Rio-Hortega was also able to attribute a functional relationship between microglial morphology and infection by observing that brain tissue from patients who died from meningitis displayed microglial cells with a rod-shaped morphology in the cerebral cortex in comparison to ramified microglia which was usually observed. These observations were later supported by experiments in rabbits where the investigator would 'produce a wound with bruising in the cerebral cortex'. In this way they way able to show by creating a necrotic focus in the tissue they were able to examine how microglial cells in close proximity to the focus responded in their morphology (del Río-Hortega Bereciartu 2020). Since these initial discoveries and observations of microglia in human and animal brain tissue, our knowledge of these cells has expanded exponentially. We now know that microglia are hugely important players in the central nervous system having major roles in maintaining brain homeostasis, immune protection, as well as roles in neuronal development and plasticity. Microglia are known as the innate macrophage cell of the brain, contributing approximately 10% of all cells in the CNS.

Formerly, it was widely believed that microglia, like oligodendrocytes and astrocytes, were of a neuroectodermal origin (Fujita and Kitamura 1975). This and several other theories regarding the origin of microglia arose over the years including the idea that microglia are derived from circulating blood monocytes originating from the bone marrow (Perry et al. 1985). Later, the field gained general consensus that microglia were likely of hematopoietic origin, with one hypothesis suggesting an intrinsic progenitor pool which was seeded in the brain and another predicting that progenitors were likely to be derived from the yolk sac (Alliot et al. 1991; Alliot et al. 1999). Several lineage tracing experiments since have definitively confirmed that microglia like tissue resident macrophages of the liver, epidermis and lung are derived from erythromyeloid progenitor cells in the yolk-sac (Ginhoux et al. 2010; Schulz et al. 2012; Kierdorf et al. 2013; Gomez Perdiguero et al. 2015; Hoeffel et al. 2015). To answer the question of whether microglia are derived from a circulating population of hematopoietic progenitors, Ginhoux *et al.* (2010) gave a sublethal dose of irradiation to *Cd45.2*$^{+}$ new born mice and repopulated these animals with hematopoietic progenitor cells from *Cd45.1*$^{+}$ mice. Crucially, they discovered that 95% of microglia in these mice were of host origin. In comparison over 30% of circulating leukocytes and tissue macrophages were of donor origin. This was then confirmed in parabiotic mice which share blood circulation to remove the need for radiation. These results indicate that postnatal microglia maintain populations independently of circulating hematopoietic progenitor cells or circulating monocytes and are most likely maintained by progenitors that are seeded in the brain before the formation of the blood brain barrier. In order to investigate microglial cell origin, *Cx3cr1*$^{GFP/+}$ mice were used as Cx3cr1 is known to be a marker for both early myeloid progenitor cells and microglia. They found that cells in the embryonic brain at day E9.5 showed positive expression of Cd45 a hematopoietic marker as well as mature microglial markers such as Cd11b, F4/80 and Cx3cr1 which was consistent with yolk-sac macrophages through development. Since these discoveries, others have gone on to further clarify the exact populations responsible for tissue resident macrophages. It is known that Csf1r-expressing cells give rise to tissue resident macrophage in mouse. Gomez *et al.* (2015) used

Csf1r^{icre} *Rosa26*^{YFP} and inducible *Csf1r*^{MeriCreMer} *Rosa26*^{YFP} mice in a time course analysis to identify the origin of microglial cells. Fate-mapping analysis showed erythromyeloid progenitor cells developing at embryonic day 8.5 and migrating towards the brain during the following days of embryonic development up until the formation of the blood brain barrier. Interestingly, this work has demonstrated that microglia originate from Tie2^{+} erythromyeloid progenitors and are distinct from haematopoietic stem cells (Gomez Perdiguero et al. 2015).

Once microglia have migrated to the CNS, there is a wave of microglial proliferation and levels are thought to peak during the early post-natal period, then decrease to a level that is maintained throughout adulthood (Nikodemova et al. 2015). During the first two postnatal weeks in mice, microglia have been shown to have a high mitotic activity, resulting in a surge of microglial number with microglia representing 1.7% of all CNS cells at P0 which jumps to 7.3% at P14 and plateaus at approximately 10-13% in adulthood (Alliot et al. 1999). Nikodemova et al. (2015) observed a 2.2-fold increase in the number of CD11b+ cells during the first two postnatal weeks which was followed by a sharp decrease in the third week. Furthermore, microglial cell numbers were seen to dramatically decrease by as much as 50% from their peak in the 2nd postnatal week. During development microglia resemble typical macrophages by taking on an ameboid morphology, with a large globular cell body and few short processes. Ameboid microglia are highly phagocytic, breaking down and removing cell debris that occurs from cell death in embryogenesis and late postnatal development, a state which is thought to be regulated through the expression of Runx1 (Zusso et al. 2012). Throughout this developmental period ameboid microglia have been shown to express cytokines associated with pro-inflammation including TNF-α, iNOS and arginase-I (Crain et al. 2013). With time, microglia gradually transition into a surveillant phenotype which is maintained into adulthood and characterised by a highly ramified morphology along with anti-inflammatory signalling molecules (Zusso et al. 2012; Crain et al. 2013).

1.2.3 Microglial turnover

Since the establishment of microglial origin within the yolk sac and their migration to the CNS, it was still unclear whether microglia populations were maintained. There were questions as to whether these populations were capable of self-renewal through resident proliferating cells, whether there was recruitment from the periphery (although this theory was becoming unclear from previous fate mapping experiments) or whether the cells that first migrated to the brain were maintained for life. Studies have shown that microglial cells are capable of re-populating the brain to near normal levels after transient but targeted depletions either by genetic or drug induced manipulations namely using Csf1r inhibitors which can lead to greater than 90% of depletion *in vitro* and *in vivo* across several weeks (Elmore et al. 2014; Bruttger et al. 2015; Coleman et al. 2020). Interestingly, microglial depletion has been shown to reduce inflammation and confer neuroprotective outcomes in some disease states (Rice et al. 2015; Li et al. 2017). To address the question of whether microglial populations are actively maintained by contributing circulating monocytes, Askew et al. (2017) compared the microglial density of *Ccr2*$^{-/-}$ and wild type mice. Monocytes in *Ccr2*$^{-/-}$ mice show poor withdrawal from the bone marrow and therefore in these mice if circulating monocytes contributed significantly to maintaining the microglial population, one would expect a reduction in the global microglial pool. However, when compared to wild type mice, *Ccr2*$^{-/-}$ mice showed comparable levels of microglia in both young and aged mice indicating that circulating monocytes are not important in maintaining this cell population. Although they could not rule out any contribution from patrolling monocytes. They then went on to assess proliferation rates of microglia in mouse and human brains using immunohistochemistry assessing BrdU and Iba1 co-staining. From their results they estimate that approximately 1.38% of the microglial population could be proliferating at any given time in mouse and that the entire population renews itself every 96

days for a potential 6 renewal cycles in a lifetime. The rate of microglial proliferation was also noted to be significantly higher within the dentate gyrus, which may reflect that microglia in this region reach their energetic capacity more quickly. In humans, microglia populations were seen to have a higher proportion (2%) of the population proliferating at any given time as well as an increase in the number of complete renewal cycles estimating in the hundreds. Another study published shortly after, agreed microglial population is maintained through a continuous turnover across the adult life but at a much slower rate than in mouse and also noted that some microglia were shown to last for more than two decades (Ré et al. 2017).

1.2.4 The many roles of microglia: development

Historically, the main role of microglia was thought to be similar to that of other tissue macrophages - surveying the local microenvironment for cellular debris and invading pathogens. However, a complex picture is now beginning to emerge regarding the functional role of these cells which can be divided into immune and non-immune function. As stated previously, microglial colonisation of the brain and subsequent proliferation coincides with the emergence of radial glial cells in embryogenesis and as such occupy the same developmental space as neural progenitors as early as embryonic day 11. Antony et al. (2011) investigated the role of microglia in embryonic cortical neurogenesis by generating neuronal precursor cultures from the cortex of E12-13 *Pu.1-/-* and *Pu.1+/+* mice. Cultures generated from *Pu.1-/-* mice lacked microglial cells and showed reduced precursor proliferation as well as reduced astrogenesis which could be reversed upon the reintroduction of microglia to the cultures. These results indicate that microglia are capable of regulating embryonic neuronal development at least in vitro and perturbations in microglia numbers at sensitive embryonic

timepoints could have detrimental effects on global neuronal populations. There are further reports that microglia act to regulate neuronal populations by indiscriminately phagocytosing neural progenitor cells within cortical proliferative zones in rats and macaques, thereby limiting the size of the progenitor pools. Tbr2+ and Pax6+ neuronal precursors were identified as populations that were targeted and phagocytosed by microglia in live organotypic slice cultures derived from embryonic cerebral cortex of rats and most interestingly, microglia were seen to phagocytose both live and apoptotic cells. In addition to this, deactivating or eliminating microglia in utero significantly increased the number of neuronal precursor cells (Cunningham et al. 2013). Genetic knock out of *Csf-1r* in mice are void of microglia and present with a reduced brain size and increased ventricular dimensions. In alignment from the previous study, they too report that *Csf -1r* mice lacking microglia show expanded pools of neural progenitor cells in the neocortex compared to wild type controls (Nandi et al. 2012). This suggests that microglia under normal conditions may act to prevent uncontrolled proliferation of neuronal progenitors in the embryonic and post-natal brain. In contrast, an astonishing study recently demonstrated that deletion of the *Csf1r* enhancer, *Fms*-intronic regulatory element (FIRE), in mice resulted in a near total depletion of microglia and other tissue macrophages but remained healthy in all other measured aspects and appeared neurological and developmentally normal (Rojo et al. 2019). Although further work remains to be seen on the effects of adult hippocampal neurogenesis, this study poses interesting questions for the requirement of microglia in brain health and development.

During postnatal development the brain undergoes a huge amount of sculpting and remodelling. In addition to the possibility of neuronal overpopulation through uncontrolled neurogenesis, there is also the issue of an overly connected neuronal circuit. It has been demonstrated that neurons make far more synaptic connections during the post-natal period

compared to that seen in adulthood for which in humans appears to peak at 1-2 years of age to approximately 50 percent more than the average number of connections in the adult (Huttenlocher. 1979). Microglia are thought to be active players in this reduction of synaptic connections across development by modifying or eliminating synapses through a process of synaptic pruning which is hypothesised to be driven through experience and therefore activity dependent (Sierra et al. 2010; Schafer et al. 2012a; Diaz-Aparicio et al. 2020). Time lapse imaging has shown microglia are highly dynamic cells in the healthy brain, capable of altering their morphology by protracting and extending their fine processes on the order of minutes they therefore appear to be highly suited to this role (Davalos et al. 2005; Nimmerjahn et al. 2005). Experience based synaptic alterations have been demonstrated in one-month old mice using quantitative electron microscopy and two-photon in vivo imaging, whereby the interaction between microglia and synaptic components was examined in the visual cortex (Tremblay et al. 2010). Of the examined microglia, most were found with processes in direct contact with a synaptic component. Furthermore, microglia were seen to change their morphology and activity during alterations in visual experience by housing mice in complete darkness for 6 days compared to controls. Even more interesting, mice deficient in key microglial signature genes – *Cx3cr1* or *P2ry12* - show dysregulation in synaptic development and weakened neuronal circuits (Paolicelli et al. 2011; Zhan et al. 2014; Sipe et al. 2016). To compliment this, mice which have undergone inducible microglial ablation via diphtheria toxin show a reduction in the percentage of neuronal spines that are eliminated or formed in the motor cortex compared to untreated mice (Parkhurst et al. 2013). Engulfment of synapses by microglia, at least in some cases, appears to rely on complement receptor 3 (CR3) expressed on the surface of microglia and its ligand C3 and C1q which are complement proteins which have been found to be enriched in synaptic structures and may therefore tag structures to be eliminated by microglia. Disruption of the CR3-C3 signalling pathway has also been shown to disrupt synaptic

remodelling (Stevens et al. 2007; Chu et al. 2010; Schafer et al. 2012b). More recent studies have begun to unravel the dynamic mechanisms through which these processes occur. Weinhard et al. (2018) suggests that unlike other macrophages that engulf debris and pathogens as a means to remove them, microglia instead 'nibble' at synaptic processes in a mechanism they define as "trogocytosis". Weinhard's team also present data that show microglia may induce spine head filopodia formation and translocation, which they propose could be a mechanism by which inefficient synapses are replaced.

Microglia also provide additional developmental roles such as, providing survival signals for newly born neurons, supporting oligodendrocyte progenitor development, normal mylinogenesis as well as aiding white matter tract formation (Ueno et al. 2013; Pont-Lezica et al. 2014; Hagemeyer et al. 2017). Layer V cortical neurons have been shown to require trophic support from microglia in order to survive. Experimental paradigms where microglia are depleted via the use of minocycline show an increased rate of neuronal apoptosis particularly in layer V sub-cerebral and callosal projection neurons. The molecule thought to be providing trophic support in this case was Insulin-like growth factor 1 (Igf1) (Ueno et al. 2013). Additionally, large numbers of activated microglia have been found in the sub ventricular zone of P1-P10 rats. Pharmacological suppression of these microglia via minocycline which acts to reduce the levels of proinflammatory cytokines significantly inhibited neurogenesis and oligogenesis in vivo in the SVZ and was corroborated with in vitro studies (Shigemoto-Mogami et al. 2014). Collectively, these studies further consolidate the importance of microglia in post-natal development by limiting cell numbers, sculpting neuronal circuits, providing trophic support as well as new roles which will undoubtedly unfold with time.

1.2.5 The many roles of microglia: Homeostasis

Microglia, once thought of as static bystanders in the adult brain are now known to be highly dynamic cells that survey the local milieu. From *in vivo* two-photon time lapse microscopy of transgenic mice expressing EGFP under the Cx3cr1 promotor, microglia could be observed through a thinned skull preparation. Remarkably, while the soma of most microglia was seen to remain in a fixed position, spontaneous thin process were observed extending and retracting in a cyclical fashion which enabled the scanning of the entire brain in a matter of a few hours (Nimmerjahn et al. 2005; Wake et al. 2009). This kind of microglial motility has been shown to be influenced by ATP gradients which are identified by P2y12 receptors (Davalos et al. 2005; Haynes et al. 2006). Naturally, as a product of such motility, microglia interact with all cell types within the brain.

Advances in genetic research tools have allowed transcriptional and chromatin profiles of microglia to be probed at new depths such as single cell sequencing and ATAC-seq. Microglia RNA expression has been shown to vary across developmental time points which may indicate highly adaptive changes in microglial function that are dependent on time and space (Doorn et al. 2015; Grabert et al. 2016; Matcovitch-Natan et al. 2016; Hammond et al. 2019; Kreisel et al. 2019; Sankowski et al. 2019). A study by Matcovitch-Natan (2016) described a dynamic alteration in microglial transcriptional phenotype, using Genome-wide chromatin expression profiling alongside single cell transcriptomics, they showed distinct microglial phenotypes that correlate with specific developmental time points defined as: yolk sac, early microglia, pre-adult and adult. They also show that the pattern of developmental gene expression in microglia is susceptible to perturbations when the system is challenged. For example, changes in gene

expression were observed following microbiome challenges and prenatal immune activation. To add to this body of work, (Grabert et al. 2016) have shown that not only do microglia display distinct developmental phenotypes but that they also show distinct spatial phenotypes with regards to transcriptional profiles. These new insights are leading us away from a dichotomous microglia phenotype (M1-pro-inflammatory/M2-anti-inflammatory) to a broad spectrum that is highly dependent on the local environment and its interactions (Ransohoff 2016).

1.2.6 The role of microglia in adult neurogenesis

As stated earlier, adult hippocampal neurogenesis is defined as the birth of new neurons within the dentate gyrus of the hippocampus. The phenomenon of adult neurogenesis is largely limited to discrete regions of the brain, namely the sub granular layer (SGL) of the dentate gyrus and the subventricular zone of rodents (Gage 2000). This sparks the question, why does adult neurogenesis occur in certain brain regions over others? Increasing evidence suggests that microglia are an essential component to this question. As with the many roles attributed to microglia during embryonic and post-natal neuronal development, so too are there many roles of microglia in adult hippocampal neurogenesis including removal of cells, regulation of proliferation and differentiation of neural progenitor cells as well as providing trophic support to newly born neurons. Sierra et al. (2010) demonstrated that newly born cells within the sub granular zone of mice undergo apoptosis within the first 4 days of their life during the transition from amplifying neural progenitor to neuroblast and that this process is preserved throughout adulthood. These apoptotic cells were shown to be phagocytosed by local ramified microglia indicating that these were unchallenged microglia. This was also confirmed by examining markers of activation Cd11b and Cd68 in SGZ microglia, both of which were shown to be

expressed at similar levels to non-phagocytic microglia in hippocampal CA2 regions and distinct from microglia in animals that had been challenged with LPS. Importantly, the mechanism of engulfment is performed in such a way as to not incur any damage to the surrounding tissue. It is thought that microglia undergoing phagocytoses do not release any damage associated molecular patterns (DAMPs) unlike in response to injury. In response to damaged cells microglia phagocytose cell debris through their soma, but in the neurogenic niche microglia phagocytose apoptotic new-born cells through a phagocytic pouch which is independent from the cell body which may indicate regional dependant functional roles. Additionally, the phagocytosis of newly born cells is indicated to be highly efficient with estimations suggesting that clearance time is 1.2-1.5hr per apoptotic cell which is similar to that observed in rat hippocampal slice cultures (Petersen and Dailey 2004).

Microglia may also contribute to adult Hippocampal neurogenesis by providing trophic support to neural progenitor and stem cells. Accumulating evidence suggests that microglia are capable of secreting various factors which can influence proliferation, differentiation and survival and even migration of neuronal cells. Cytokine action is regulated by two mechanisms, the first being the balance of pro and anti-inflammatory cytokines, the second being the presence of glucocorticoids and its downstream effectors. Glucocorticoids are released as consequence of activation of the hypothalamic-pituitary-adrenal axis. Therefore, to untangle the relationship between microglia and cytokine action, rodents undergo adrenalectomy. Upon adrenalectomy in male rats, there is a dramatic increase seen in the number of apoptotic cells in the dentate gyrus compared to sham. In parallel, there is also increased levels of neural progenitor proliferation, specifically type 2, and increased neuronal neurogenesis (Battista et al. 2006). In this model, microglia were seen to proliferate in adrenalectomized rats and the number of activated microglia was seen to be correlated with the increase in neurogenesis. Interestingly,

these microglia did not display a full macrophagic phenotype as denoted by a lack of ED1 (EDA)+ expression. When a cytokine panel was performed, there was significant upregulation of transforming growth factor-beta (Tgf-β) compared to other pro and anti-inflammatory cytokines indicating that Tgf-β secreted by microglia has a pro-neurogenic effect on neural progenitor cells in the dentate gyrus. The role of Tgf-β in neurogenesis was validated subsequently both *in vivo* and *in vitro*. In contrast to the pro-neurogenic effect of Tgf-β stimulation, one study has shown the surprising effect of selectively ablating the neurotrophic factor Bdnf from microglia. Upon genetic ablation of Bdnf, there was an increase in the production of new born neurons as shown by the significant increase in Tbr2 positive cells as well as double positive cells for Tbr2 and EDU stained cells in the SGZ compared to control animals (Harley et al. 2021).

Furthermore, several *in vitro* studies have also shown that microglia are capable of releasing soluble factors that are pro-neurogenic by using microglia conditioned media (Aarum et al. 2003; Morgan et al. 2004; Walton et al. 2006; Nunan et al. 2014). Including some evidence that microglia are capable of influencing the differentiation of precursor cells. Embryonic neural precursor cells were assessed for the number of neurons and astrocytes upon the addition of microglia conditioned media derived from: BV-2/N13 microglia lines, embryonic primary microglia and primary microglia treated with LPS. There was a significant increase in the number of neurons in precursors treated with conditioned media from BV-2/N13 microglia as well as primary microglia treated with LPS compared to control media. Additionally, there was no significant difference in the number of astrocytes compared to control media. However, astrocytes in treated cultures were seen to have longer processes and less compact than those that were in untreated cultures. Furthermore, only adult precursor cells treated with BV-2/N13

microglia conditioned media saw an increase in the number of neurons compared to control conditions (Aarum et al. 2003). The same group also provided some evidence that microglia are capable of influence the migration of neural precursor cells. Aarum et al. (2003) used modified Boyden chambers, where neuronal precursors were seeded and separated from microglia conditioned media via membrane which contains pores big enough for cells to pass through it. Conditioned media derived from embryonic primary microglia as well as LPS stimulated primary microglia conditioned media were both able to attract more precursor cells than control media. The biggest response in terms of migration however was in precursor cells treated with conditioned media from BV-2/N13 microglial cell lines which may reflect that the strength of the response depends on the phenotype of the microglia used.

Environmental enrichment has been shown to regulate adult hippocampal neurogenesis in rodents and microglia are thought to be responsible for this effect. There are many different approaches that have been used to provide environmental enrichment which are used in comparison to standard laboratory housing conditions. Environmental enrichment can include an increase in housing space by using larger cages and multi-level housing, an increase in social interactions by increasing the number of animals in a cage or by increasing the number of stimuli in the cage by providing toys, nesting material or novel foods. These environmental enrichments can be further combined to increase complexity or may be introduced to the animal for limited periods of time. Consequently, there has been a large amount of variability in experimental design between studies which makes comparisons difficult (Kempermann 2019). However, despite such variability there is largely consistent results demonstrating positive effects on hippocampal neurogenesis (Kempermann et al. 1997; Kempermann et al. 1998; van Praag et al. 1999; Ziv et al. 2006; Fabel et al. 2009; Fares et al. 2013). Rats housed in either standard conditions or 6 weeks of environmental enrichment, increased numbers of

BrdU/NeuN positive and BrdU/Iba1 positive cells were observed in the dentate gyrus of rats that had undergone enrichment compared to control (Ziv et al. 2006). This result indicates that the paralleled increase in microglia population to the neuronal population may be providing a supporting role. However, some studies suggest that there is an inverse correlation between the number of microglia and hippocampal neurogenesis in the context of environmental enrichment (Gebara et al. 2013). The contradiction in results between these two studies could be due the differences in BrdU injection schedules as in one study animals were injected over the course of a week and the other over the course of day. Other methods of enrichment such as exercise have also been shown to also improve adult hippocampal neurogenesis. One study has shown that this could be a mediated by microglia, by extracting microglia from mice that had undergone exercise (runner mice) and added these to cultures of neural precursor from sedentary mice (non-runner mice). In this paradigm they showed that the addition of microglia from runner mice to non-runner neural progenitor cells increased the percentage of neurospheres generated in culture. Additionally, when runner neural progenitor cells were cultured in the absence of their endogenous microglia, the increased percentage of neurospheres as compared to cultured non-runner neural progenitor cells was abolished, indicating that microglia played a pivotal role in the expansion of the neurospheres and were primed by the enrichment experience (Vukovic et al. 2012).

There is evidence to suggest that neurons and microglia engage in crosstalk via the chemokine Cx3cl and its receptor Cx3cr1. Cx3cr1 has been found to be mainly expressed by microglia and Cx3cl by neuronal populations indicating a unique dialogue between the two cell types (Harrison et al. 1998; Nishiyori et al. 1998; Tarozzo et al. 2003). Although, there have been conflicting studies which have shown that Cx3cr1 is also found in hippocampal neurons,

suggesting that Cx3c1 may have autocrine as well as paracrine activity (Meucci et al. 2000). Studies have since shown that Cx3cl is capable of supressing microglia activation.

Microglia depletion models have also provided interesting and sometimes contrasting insights into the possible roles of microglia in adult neurogenesis (Xavier et al. 2015; Reshef et al. 2017; Kreisel et al. 2019; Kyle et al. 2019; Willis et al. 2020). Rather than influencing the fate of neural progenitor offspring via differentiation, some studies have suggested that microglia play a greater role in supporting the survival and migration of immature neurons. In 12-week old mice containing an inducible human diphtheria toxin receptor allele, microglia were partially ablated via the injection of diphtheria toxin over 5 or 10 days. A significant reduction of Iba1 positive cells were observed in the dentate gyrus of mice injected with diphtheria compared to control animals which was accompanied by a reduction in the survival of neuroblasts in the granule cell layer (Kreisel et al. 2019). In addition, Willis (1935) showed that there was no significant difference in the percentage of immature neurons or intermediate neural progenitor cells in the dentate gyrus of mice that had received the Csf-1R inhibitor PLX5622 compared to sham mice that had received a control treatment. Some studies have investigated the loss of microglia in other neurogenic niches – the sub ventricular zone (SVZ). One study found whole brain microglia ablation using PLX5622, showed a significant reduction in proliferating neuroblasts in the SVZ at 7 days of PLX5622 treatment compared to control animals. However, this effect was lost at 14 days of PLX5622 treatment but showed a large degree of variability in the treatment group which may be improved by increasing the sample size. There were also no significant differences observed in the number of neural stem cells at day 7 or 14 of PLX5622 treatment as observed through the number of $Gfap^{+}Sox2^{+}$ cells (Kyle et al. 2019). Thus, indicating that in this paradigm, microglia were not needed for proliferation and differentiation of neural stem cells in the SVZ *in vivo*. However, a study using PLX5622 to

deplete microglia showed reduced spine density in adult born granule cells in the olfactory bulb of treated mice compared to controls indicating an important role for the maintenance of synapses on new-born neurons (Reshef et al. 2017). In another study whereby, microglia were ablated using a targeted injection of the saporin (SAP) toxin, which was conjugated to a monoclonal antibody Cd11b (Mac-1-SAP), into the SVZ. The partial ablation of microglia was seen to increase the general number of proliferating cells within the SVZ which were largely associated with pyknotic nuclei and concurrently disrupted neuroblast migration along the rostral migratory stream, indicating that microglia are important for neuroblast survival and migration in the SVZ (Xavier et al. 2015). Microglia depletion models are difficult to interpret as effects observed from depletion could be a response to a lack of microglial cells or a response to microglial cell death and therefore could be due to cytokines released from microglia reacting to the depletion method or by other surrounding glia and neurons in response to microglial cell death. Nonetheless, these reports add another layer of complexity to the relationship between microglia and hippocampal neurogenesis and highlight that it is not clear-cut area.

1.3 General Aims

The regulation of hippocampal neurogenesis as well as the effect of its dysregulation in patient populations is incomplete. This project aims to investigate functional and transcriptomic, regional dependant, differential neurogenic properties of microglia on hippocampal neural stem/ progenitor cells (NSPCs). I hypothesise that microglia show a regional dependant functional pro neurogenic property that is specific to the hippocampus and is underpinned by a pro neurogenic transcriptomic phenotype. This was assessed via a two-pronged approach.

firstly, by using a co-culture model to assess functional, regional dependant, neurogenic properties of microglia and secondly using bulk RNA-sequencing (seq) to investigate a regional dependant pro neurogenic microglia transcriptional phenotype.

- Aim 1: Phenotype and optimise NSPC cultures.
- Aim 2: Investigate regional dependant (hippocampal vs cortical) functional neurogenic properties of microglia using a co-culture paradigm whereby NSPC's were cultured with microglia or their conditioned media and assessed for changes in neuronal and neuronal stem/progenitor cell populations.
- Aim 3: Further investigate regional dependant (Dentate gyrus vs Rest of hippocampus vs whole hippocampus) functional neurogenic properties of microglia using a co-culture paradigm whereby NSPC's were cultured with microglia or their conditioned media and assessed for changes in neuronal and neuronal stem/progenitor cell populations.
- Aim 4: Optimise microglial isolation for bulk RNA-sequencing. Initially *Cx3cr1-GFP* mice were going to be utilised to for bulk-RNA sequencing analysis, but after further literature review wild type mice were chosen instead. Therefore, preparation of the bulk RNA-seq experiment was performed with *Cx3cr1-GFP* mice, however, the bulk RNA-seq was performed on wild type mice.
- Aim 5: Perform differential gene expression analysis between microglia that were acutely isolated from neurogenic (dentate gyrus) and non-neurogenic regions (rest of the hippocampus and cortex) which underwent bulk RNA-seq.

2.0 General Methods

2.1.0 Methods for cell culture

2.1.1 Animals

All experiments were performed using Postnatal day (P)7-10 Sprague-Dawley or Wistar rats (Charles River). Animals were housed in a 12hr light-dark cycle under controlled conditions (20-24^{o}C and relative humidity 55% ± 10%) and fed ad libitum. All animals were kept according to the Animal (Scientific Procedures) Act of 1986 and according to Cardiff University breeding procedures. Every effort was taken to minimise pain and suffering where possible.

2.1.2 Tissue collection

Animals were sacrificed one at a time via cervical dislocation and sprayed with ethanol (70%) before decapitation. All surgical equipment was sterilised with an autoclave to maintain sterility before use. Whole brains were extracted from the skull and hippocampi and/or sections of the cortex, were quickly dissected and placed into ice cold Gey's balanced salt solution (Sigma) supplemented with glucose (4.5mg/ml, Sigma). Tissue was then treated in parallel depending on brain region.

2.1.3 Generation of Neural Stem/Progenitor Cell (NSPC) Cultures

Typically, hippocampi from 7-12 pups were pooled tissue was sliced into 400µm thick sections using a McIlwain tissue chopper. An enzymatic solution was used to encourage cell dissociation. Slices were placed in a pre-warmed papain (22.0 U/mg, Sigma) solution (2mg/ml) for 30 mins at 37ºC containing Dulbecco's modified eagle medium (DMEM) supplemented with Glutamax (0.25mM), which was filtered (0.22µm syringe pore, Millex-GV, Millipore) before use. After a 30 min incubation with the papain solution, the mixture was transferred to a 15ml tube and centrifuged at 234 x g for 3 minutes to pellet the cells. The supernatant was removed and the pellet was resuspended initially in 1ml of Neurobasal A (NBA, Life technologies), 2% B27 supplement (Life Technologies), 0.25% Glutamax (Life technologies) and 1% antibiotic-antimycotic (ABX, Life technologies) and will hence be known as neuronal media. A single cell suspension was achieved via trituration approximately 15-20 times. The cell suspension was further diluted in another 5ml of neuronal media and passed through a 100µm cell strainer (VWR) to remove any remaining large clumps. Neural progenitor cells were enriched via a two-step OptiPrep™ (Sigma) gradient: 2ml of a 10% Optiprep™ solution was layered on top of 2ml of a 20% Optiprep™ solution. The cell suspension was then carefully layered on top and the gradient was centrifuged at 698 x g for 15 mins. The cell fraction situated at the interface of the 2 gradients was collected and resuspended in 2ml of neuronal media before centrifugation at 435 x g for 5 minutes to wash the Optiprep™ from the cells. The resulting pellet was then resuspended in 2ml of neuronal media and the cell density was estimated using trypan blue exclusion dye and a haemocytometer. Cells were plated at a density of 100,000 cells/ml. Depending on the experiment cells were seeded on poly-L-lysine (PLL)

pre-coated 24 well plates or pre-coated glass coverslips, 4 wells per condition, and cultured in a humidified incubator at 37°C, 5% CO_2 and 9% O_2. Hypoxic conditions were used to culture cells to mimic physiological conditions (Brewer and Cotman, 1989). Two hours post-plating, all media was replaced and experimental conditions added. Subsequently 2/3rd of culture media was replaced every 3 days.

2.1.4 Generation of pure microglial cultures from mixed glia

As with NSPC cultures, after a 30 min incubation of the dissected tissue with the enzymatic solution, the mixture was transferred to a 15ml tube and centrifuged at 234 x g for 3 minutes. The supernatant was removed and the pellet was resuspended in 1ml of Dulbecco Modified Eagle Medium (DMEM, Life technologies), 10% Fetal bovine serum (FBS, Life Technologies), 0.25% Glutamax (Life technologies) and 1% antibiotic-antimycotic (ABX, Life technologies) and will hence be known as glial media. A single cell suspension was achieved via trituration approximately 15- 20 times. The cell suspension was further diluted in another 5ml of glial media and passed through a 100µm cell strainer (VWR) to remove any remaining large clumps. Cells were then counted and plated at a density of $5x10^5$ cells/ml/well in glia medium. 2hrs post plating all media was changed to remove weakly attached cells and debris. Subsequently 2/3rd of media was changed at 3 days in vitro (3DIV). From 7-10 DIV, a confluent bilayer (Fig.2) has formed with astrocytes strongly attached to the bottom of the well and microglia sitting on top -weakly attached. Microglia were isolated by shaking culture plates at 1.61 x G for 20 minutes at 37°C whereby microglia become dislodged into the media. All media was immediately removed, pooled and centrifuged at 435 x g for 5 minutes. The cell pellet was then resuspended in glia media. Cells were counted and plated at the required density

in a 6 or 24 well plate. Two hours post-plating, media was switched to neuronal media and any experimental conditions were added.

2.1.5 Quantification of Cell death

Cell death was analysed using propidium iodide (PI) a well-known marker of cell death - in conjunction with 4'6-diamidino-2-phenylindole (DAPI), a nuclear stain. Propidium iodide is a highly polar molecule that can only enter dead or dying cells. It binds with nucleic acids and emits a signal at 490-590nm. DAPI is a non-polar molecule that binds to double stranded DNA and by doing so forms a stable fluorescent complex. As DAPI is not a polar molecule it is capable of entering both healthy and dying cells – particularly at high concentrations. Quantification of cell death can therefore be made by subtracting the number of PI positive cells from the total DAPI count. PI (5µg/ml) and DAPI(5µg/ml) were added to live cultures simultaneously for 40 mins at 37^{o}C prior to imaging. Fresh media was placed on cells to minimise autofluorescence and images were acquired quickly as both PI and DAPI are toxic to cells.

2.1.6 Live identification of isolated microglia in culture

Microglia were isolated as described 2.1.4. Cells were left to settle for 24hr before staining and imaging. Isolectin GS-IB$_4$ conjugated to Alexa fluor -488 (2.5µg/ml) was applied for 2 hours followed by DAPI (20µg/ml) for 40 mins prior to live imaging. Plates were washed once with dPBS and once with fresh media before imaging to remove background florescence and debris.

2.1.7 Generation of Microglia conditioned media

Microglia were isolated as described in 2.1.4. Culture media was switched to neuronal media two hours post-plating. Microglia were incubated in neuronal media for 24hrs before all media was removed, pooled, filtered (0.22µm syringe pore) and frozen at -80^{o}C until needed. Microglia conditioned media (MCM) was thawed on ice before use.

2.1.8 Immunocytochemistry

Cells were washed in phosphate buffered solution (PBS) to remove culture media and fixed in 4% paraformaldehyde (PFA) for 30 mins at 4^{o}C. Cells were then washed a further two times with PBS and either stored at 4^{o}C in PBS or used immediately for staining. Cells were blocked for non-specific binding in 0.01% PBS-T (Triton-x 100) with 5% donkey serum for 1 hour at room temperature followed by an incubation with primary antibodies overnight at 4^{o}C (**Table 1.**) diluted in 0.01% PBS-T and 5% donkey serum at 4^{o}C. Primary Antibodies were removed and cells were washed 3 times with PBS followed by a 2-hour incubation with secondary antibodies (**Table 1.**) at room temperature in the dark. Cells were washed 3 times with PBS followed by incubation with the nuclear marker DAPI (0.5µg/ml) for 6 mins diluted in PBS. Cells were then washed twice in double distilled H_2O and mounted on glass slides if plated on coverslips and imaged.

Antibody	Cat	Target	Dilution	Time course
Mouse anti-Nestin	MAB353	Type 1 and Type 2 NSPC	1 in 500	Overnight
Rat anti-GFAP	2.2B10	Astrocytes, Type 1 NSPC	1 in 1000	Overnight
Rabbit Anti-Beta III Tubulin (Tuj1)	Ab18207	Immature neurons	1 in 1000	Overnight
Rabbit Anti- Ki67	Ab15580	Cell cycle marker	1 in 500	Overnight
Click it Edu	C10340	S phase of cell cycle	10μM	24 hrs
Rabbit anti-Iba1	019-19741	General microglial marker	1 in 1000	Overnight
Rabbit Anti - Prox1	AB5475	DG specific neuronal population	1 in 5000	Overnight
Donkey Anti-Rabbit Alexa fluor® - 488	A-21206	Secondary Ab	1 in 500	2hrs
Donkey Anti-Mouse Alexa fluor® -555	A-31570	Secondary Ab	1 in 500	2hrs
Donkey– Anti Rat Alexa fluor® - 488	A-21208	Secondary Ab	1 in 500	2hrs
Donkey- Anti-Rabbit Alexa fluor®-647	A-31573	Secondary Ab	1 in 500	2hrs

Table 1. List of Antibodies used for immunofluorescence staining of primary monolayer cultures. Antibody (Ab).

2.1.9 Fluorescent cell imaging

Fluorescent images of live cells were taken on an inverted Leica microscope (Leica Microsystems UK Ltd., Milton Keynes, UK) attached to a temperature control unit and CO_2 regulator. Fluorescent images of fixed cells plated onto coverslips were imaged using an

upright Leica microscope (Leica Microsystems UK Ltd., Milton Keynes, UK). Six representative images at 20x were taken per well/coverslip in a clock like fashion with images taken at 12, 3, 6, and 9 with a further two images taken in the centre of the well/coverslip.

2.1.10 Data Analysis

Manual and automated cell counts of fluorescent images was were performed using FIJI (ImageJ) cell counter plugin. Average cell counts were taken from six representative images per well, 2 wells minimum, 5 wells maximum per condition. In all cases total cell counts were assessed from DAPI staining. T-test, One-way ANOVA and two-way ANOVA were performed using Prism Software (Graphpad, USA), appropriate post-hoc tests were used for further analyses.

2.2.0 Methods for microglial RNA-sequencing

2.2.1 Animals

Cx3cr1$^{+/+}$ and *Cx3cr1*$^{+/GFP}$ mice were kindly provided by Professor Philip Taylor, Cardiff University. *Cx3cr1*$^{+/+}$ and *Cx3cr1*$^{+/GFP}$ mice were bred and maintained under the project licence: P05D6A456. Mice were housed in sterile housing conditions (20-24˚C,45-65% humidity,12-hour dark/light cycle) and were fed *ad libitum*. Male C57B/L6J mice were supplied by Jackson laboratory (Maine, United States) and were housed in standard housing conditions (20-24˚C,45-65% humidity,12-hour dark/light cycle) and were fed *ad libitum*.

2.2.2 Tissue harvest

Mice were transported from the housing facility to the experimental facility 24 hours prior to isolation. One at a time, mice were euthanised via a lethal injection of dolethal (200mg/ml, I.P.) where both heartbeat and pedal reflexes were tested. Upon a loss of heartbeat and reflexes, the abdomen and chest were sterilised with 70 percent ethanol and an incision was made from the lower ribcage to the top of the thoracic cavity. The diaphragm was carefully opened and the ribs removed for clearer visualisation of the heart. The perfusion line containing sterile ice-cold PBS was inserted into the left ventricle and held in place via a suture clamp. An incision was then made in the right atrium to allow the release of pressure and the perfusion pump was turned on at the lowest setting. After a sufficient amount of time and where the fluid ran clear of blood, the pump was stopped and the brain was removed and placed into ice cold Gey's

solution (4mg/ml of glucose) and kept on ice. This was repeated until all mice were euthanised and brains extracted.

2.2.3 Immunohistochemistry

Mice were culled and perfused as described in 2.2.2 with 4% PFA and subsequently stored in 4% PFA for 24hrs. Specimens were then rinsed in PBS and submerged in a 30% sucrose solution (w/v) at 4°C until sunken. Brains were washed in PBS three times and then two coronal cuts were made, one at the level of the optic chiasm and the other half way through the cerebellum. The tissue was then snap frozen in OCT medium and stored at -80°C until needed. 40µm sections were generated using a cryostat (Leica) and placed into wells containing PBS and stored at 4°C. Sections were washed three times in PBS and blocked in 1% PBS-T + 10% donkey serum for 2 hrs at room temperature. Sections were incubated overnight with primary antibody (Iba1, Wako) in 1%PBS-T + 0.2% donkey serum at 4°C. Sections were washed again in PBS and incubated in secondary antibody (Donkey Anti-Rabbit Alexa Fluor® -647) for 2 hrs at room temperature. Finally, sections were washed in PBS and counter stained with DAPI (1 in 2000) and washed again before mounting. Sections were mounted onto a glass slide, coated in mowiol and covered with a glass cover slip. Sections were Imaged on a confocal microscope (Leica).

2.2.4 Brain Microdissection

Dissection instruments were sterilised prior to use using an autoclave or submersion in 70 percent ethanol for 24hrs. The dissection stage was left on ice prior to use in an effort to

maintain 4ºC temperature throughout processing. Dissection of the whole dentate gyrus (DG) and the rest of the hippocampus was performed following the protocol from (Hagihara *et al.*, 2009). Briefly, one brain at a time was transferred to a petri dish and was cut in the sagittal plane to divide the brain into two hemispheres using a single edged blade. Working under a dissection microscope and on one hemisphere at a time, the cerebellum was removed along with the hind and midbrain. The hemisphere was then placed medial side up and the diencephalon was carefully removed using fine forceps. This reveals the medial side of the hippocampus and the DG can be visualised. The whole DG was removed using a sharp 25-gage needle by inserting it between the boundaries of the DG and Ammon's horn and carefully sliding it along the boundaries to clear connective tissue and to separate it from the rest of the hippocampus. The whole DG was placed into a pre-weighed 1.5ml Eppendorf tube containing 1ml of Hank's balanced salt solution (HBSS) -/-. The rest of the hippocampus was then excised using a micro spatula and excess connective tissue was trimmed. The rest of the hippocampus was then placed in another pre-weighed Eppendorf containing 1ml HBSS -/-. In some experiments a section of the cortex was cut from each hemisphere and also collected and placed in a separate tube containing 1ml HBSS -/-. Samples were then placed back on ice while the next hemisphere was micro dissected. The processing of each brain was approximately 10-15 minutes and six animals were processed for microdissection at any one time. A wild type mouse was used as a unstained control at the same time and in this case the cerebellum was removed and the rest of the brain was placed in 1ml HBSS -/- until further processing.

2.2.5 RNA extraction and q-PCR

Brains were extracted and dissected as described in 2.2.2-3 from 3 mice and snap frozen on dry ice. QIAzol Cell lysis reagent (Qiagen, miRNeasy mini kit) was applied and the tissue was homogenised first by trituration with a p1000 pipette and subsequently with a needle and 1ml syringe. Cells were scraped from the bottom of the well using a pipette tip and subsequently passed through a 25-gauge needle to aid cell dissociation and membrane disruption. Purified RNA was extracted following the Qiagen miRNeasy on the column protocol for animal tissue. Purified RNA was eluted in 30µl of RNase free H_2O and frozen at -20^{o}C. The concentration of RNA was measured using Nanodrop spectrophotometer.

cDNA was generated using Quantitect reverse transcription kit (Qiagen) following the manufacturer's instructions including a step for the removal of genomic DNA. This kit allows the synthesise of first strand cDNA from RNA and eliminates genomic DNA contamination. cDNA quantity was assessed with Nanodrop. A master mix was prepared for each primer pair containing Quantitect syber green (Qiagen), forward primer, reverse primer and H_2O. High specificity and sensitivity in PCR are achieved by the use of the hot-start enzyme HotStarTaq DNA Polymerase together with a specialized PCR buffer. Samples were loaded into a 96 well in triplicate with a final reaction volume of 25µl and loaded onto a Step One™ real time PCR system (Applied Biosystems) with the following cycle parameters:

Step	Step length:	Temperature:	No of cycles
Activation step	15min	95 °C	X 40
Denaturation	15 sec	94 °C	
Annealing	30 sec	55 °C	
Extension	30 sec	72 °C	

Primer sequences were obtained from published literature and generated by Integrated DNA technologies (IDT) (Lein, Zhao and Gage, 2004; Parker *et al.*, 2006; Hagihara *et al.*, 2009; Zhang and Wang, 2011).

Primer	Sequence
Actin-β	F: AGTGTGACGTTGACATCCGTA, R: GCCAGAGCAGTAATCTCCTTCT
GAPDH	F: GTCGTGGATCTGACGTGCC, R: ATGCCTGCTTCACCACCTTC
TDO2	F: ATGAGTGGGTGCCCGTTTG, R: GGCTCTGTTTACACCAGTTTGAG
Desmoplakin	F: GCTGAAGAACACTCTAGCCC, R: ACTGCTGTTTCCTCTGAGACA
Ppp1r1a	F: ACGGAAGAAGATGACAAGGACC, R: TTGCCCTAGGTGATGTTCAACC
CNN3/Nov3	F: CCCAACAACCAGACTGGCATT, R: TACTGACAGTTCGGCTCAAAC
Mrg1b	F:CTGGCGAGATCACGATGACG, R: AAGCTACGCTGTTGTCTAACC

Table 2.List of primers used for qPCR

Melting curve analysis of the PCR products was performed to verify the specificity and identity of the PCR products. A threshold was set on the data at the exponential stage where the rate of amplification is at its greatest. The comparative Ct (ΔΔCt) was used to quantify relative gene

expression. The average of the two reference genes GAPDH and Actin-β was used to normalise the data.

2.2.6 Brain dissociation and myelin removal

Once all brains had been micro dissected, the samples were dissociated using the adult brain dissociation kit for mouse and rat (130-107-677, Miltenyi Biotec, Germany) following the protocol provided with a few minor alterations. Briefly, all enzymes were thawed on ice and all solutions were kept on ice throughout. Centrifuges were also set to 4°C. Once collected, samples were weighed and the approximate weight was calculated. For 6 animals, the average weight for DG was 45mg, the rest of hippocampus as 165mg, and whole brain was 500mg. The samples were transferred to C-tubes and the recommended amount of enzyme P (50µl), buffer Z (1900µl), buffer Y (20 µl) and enzyme A (10µl) was added. C-tubes were then placed on a GentleMACs Octodissociator (Miltenyi Biotec) with heated jackets and run on the program 37C_ABDK_01 for tissue > 100mg and program 37C_ABDK_02 for tissue 20-100mg for 30 mins. Upon completion of the GentleMACs program, tubes were then placed immediately back on ice. 1ml of HBSS +/+ was used to prewet a 70 µM cell strainer for each sample and the contents of each C-tube was passed through the cell strainer into a 50ml falcon tube. A further 9ml of HBSS +/+ was used to rinse each C-tube and this was also passed through the cell strainer. Single cell suspensions were centrifuged at 300 xg for 7 min. To remove debris and myelin, the supernatant was carefully aspirated and the pellet was resuspended with dPBS +/+ and transferred to a 15ml tube. Debris removal solution was added to each sample and mixed gently by inversion. Ice cold dPBS +/+ was then gently overlaid and samples were centrifuged for 10 min at 3000 xg (acceleration = 3 and brake =1) where upon three phases are formed.

The top two phases are discarded and the sample tube is then filled to the 15ml mark with dPBS +/+ and mixed gently by inversion. The samples were then centrifuged for 10 min at 100g. The supernatant was discarded completely as microglia are deposited in the pellet. In cases where brain perfusion was not performed, a red blood cell removal step was included. Briefly, cells were resuspended in a diluted (1:10) red blood cell removal solution for 10 min on ice. This was then stopped by washing the cells with 10mls dPBS +/+ containing 0.5% Bovine serum albumin (BSA).

2.2.7 Fluorescence activated cell sorting

Microglia were isolated using fluorescence activated cell sorting (FACS), whereby fluorescent antibodies or molecules are bound to a target cell of interest and then interrogated based on emitted wavelengths of light upon excitation. To prepare the samples for cell sorting, cells were washed with 10ml of 5mM EDTA buffer and centrifuged for 7 mins at 300 xg. Cells were then resuspended in 0.5% BSA dPBS -/- and counted using a Muse count and viability kit (MUSE cell analyser) or by trypan blue exclusion. Cells were stained on ice for 30 min with the pre-conjugated antibody P2ry12-PE (1in 200) in 0.5% BSA dPBS -/- and 5mM EDTA. Cells were then washed and resuspended in 200µl of 0.5% BSA dPBS and 5mM EDTA and passed through a cell strainer into FACS tubes ready for sorting and maintained on ice until required. DAPI (1µg/ml) was added to all relevant samples to identify dead cells. Cells were sorted into 200µl of 0.5% BSA dPBS -/- and 5mM EDTA in dPBS -/- using a BD FACSAria^{TM} and 100µm nozzle.

2.2.8 Gating Strategy

In order to accurately separate cell populations, gating parameters need to be set up and usually result in a negative population, single positive or double positive populations. Gates were established with an unstained control or wildtype control, single colour controls and a small fraction of the final sample to be assessed. Samples were first gated according to cell size using forward side scatter area (FSC-A) and side scatter area (SSC-A) and then for single cells using FSC-A and FSC- height (H). Live cells were identified using DAPI (1μg/ml). Fluorescence intensity for DAPI plotted against FSC-A was performed and live cells were identified by gating for DAPI negative cells. Of the live cells, only those that were only positive for GFP or double positive for GFP and P2Ry12 -PE were collected depending on the experiment. In experiments where only wild type animals were used, live cells for P2ry12-PE only were collected.

2.2.9 Post sort analysis

In order to perform offline analysis of the cell sorting procedure, gating parameters were recorded during each experiment for at least 10,000 events and analysed using FlowJo. In cases where more than 10,000 events were recorded I have used the 'DownSample' plugin to standardise the number of events being analysed. Events were gated and statistical parameters were obtained such as frequency of total, frequency of parent and mean counts.

2.2.10 Post FACS cell viability

The goal of this experiment was to extract a purified population of live microglia for RNA extraction and RNA sequencing. Therefore, the viability of the cells needed to be assessed post FACS as it is known that FACS is a highly stressful procedure on cells. LIVE/DEAD™ fixable far red stain (Invitrogen™) is an amine reactive dye which forms a covalent bond to intracellular and extracellular amines which is preserved after formaldehyde fixation, unlike other dead cell stains. The Far-red stain elicits a bright signal when excited with a red laser. Live and dead cells are discriminated by the intensity of the fluorescent staining. As dead cells possess a compromised membrane, the dye reacts with amines in the interior as well as the cell surface resulting in more intense signal compare to live cells. Post FACS, cells were incubated with a LIVE/DEAD™ fixable far red stain (Invitrogen™) according the manufacture's instruction and fixed with 4% PFA. The next day cells were washed and re-dissociated into a single cell suspension. 10,000 cells/sample were analysed using the BD Fortessa flow cytometer and data was further analysed using FlowJo.

2.2.11 RNA extraction for RNA sequencing

After cell sorting, cells were briefly spun down and washed in PBS. All surfaces and equipment were cleaned prior to extraction with 70% ethanol and RNase ZAP to reduce contamination from nucleases. Bulk RNA extraction was then performed on the column using the Nucleospin RNA XS kit according to the manufacturers protocol (Macherey-Nagel) and purified RNA was eluted in 10µl of RNase free water. Extracted RNA was stored at 4^{o}C for 24 hours and at -76^{o}C

for long term storage. The quantity of RNA extracted was assessed using the nanodrop and Qubit. RNA quality was assessed using a fragment bioanalyser and a high RNA sensitivity kit according to the manufacturers protocol. Samples that were used for RNA-sequencing were shipped on dry ice to Novogene (Oxford, UK) for quality checks. All RNA sequencing analysis was performed with 3 independent samples per region, where each sample was pooled from 6 mice.

2.2.12 RNA Library preparation and RNA sequencing

Novogene (Oxford, UK) performed RNA quality control (QC) on arrival with Nanodrop, Agilent 2100 and an agarose gel electrophoresis to assess RNA quantity as well as sample integrity and purity. As low yields of RNA were observed, RNA amplification was performed with SMARTer mRNA amplification kit (Clontech) and QC was performed again. Briefly, SMART-Seq™ v4 Ultra™ Low Input RNA Kit for Sequencing (Clontech) was used to generate cDNA. The first strand is synthesized (Total RNA is stored in RNase-free water to directly synthesize first strand), followed by the whole-length LD-PCR amplification. The amplified ds-cDNA (double-stranded DNA) is purified with AMPure XP beads and quantified with Qubit. The cDNA samples were sheared by the Covaris system, and then the sheared fragments were end-repaired, A-tailed, and ligated to sequencing adaptors. A size selection of about 200 bp is performed before the PCR enrichment. Library concentration was first quantified using a Qubit 2.0 fluorometer (Life Technologies), and then diluted to 2 ng/μl before checking insert size on an Agilent 2100 and quantifying to greater accuracy by quantitative PCR (Q-PCR) (library activity >2 nM). Libraries were pooled and loaded onto Illumina sequencers according to activity and expected data volume. Novogene performed paired end

(150bp reads) RNA sequencing on 9 samples with an approximate read depth of 30 million reads, on an illumina Novaseq.

Sequences of adaptor:

5' Adapter:

5'-
AATGATACGGCGACCACCGAGATCTACACTCTTTCCCTACACGACGCTCTTCCGA
TCT-3'

3' Adapter (The underlined 6bp bases is Index):

5'-
GATCGGAAGAGCACACGTCTGAACTCCAGTCACATCACGATCTCGTATGCCGTCT
TCTGCTTG-3'

SMART-Seq PCR primer:

5'-AAGCAGTGGTATCAACGCAGAGTAC-3'

2.2.13 Read mapping, transcript assembly and generation of feature counts

Fastq files were retrieved from Novogene. The mouse reference genome (GRCm39) was downloaded from ensemble database and indexed using STAR software (https://github.com/alexdobin/STAR). Prior to mapping, fastq files were trimmed using trimgalore software (https://github.com/FelixKrueger/TrimGalore) to remove residual illumina adapter sequences and trimmomatic software (http://www.usadellab.org/cms/?page=trimmomatic) to remove clonetech SMART CDS

primers which were over represented. Quality control (QC) checks were performed on raw and trimmed reads using fastqc software (https://www.bioinformatics.babraham.ac.uk/projects/fastqc/). Trimmed reads were mapped to the mouse reference genome using STAR which generated BAM files. The picard software (https://broadinstitute.github.io/picard/) was then used to mark and remove duplicate reads within each BAM file. A second QC was then performed using Bamtools (https://github.com/pezmaster31/bamtools/wiki) to see how effective the duplication removal has been. The featureCounts software (http://bioinf.wehi.edu.au/featureCounts/) was then used to generate raw read counts per gene.

2.2.14 Normalisation, visualisation and differential expression analysis

Normalisation, visualisation and differential expression were performed with the DESeq2 package (https://bioconductor.org/packages/release/bioc/html/DESeq2.html) which provides methods to test for differential expression using a negative binomial generalized linear models, the estimates of dispersion and logarithmic fold changes (Love, Huber and Anders, 2014). A count matrix of read counts was generated in R from the output of featureCounts. Genes with less than 1 count in all samples were filtered out prior to normalisation. Differential expression was performed on unnormalised counts and calculated with default parameters. For visualisation and clustering the count data was transformed using regularized log transformation (rlog, $\log2(qij)=\beta i0+\beta ij$). Results were visualised in R (version 1.4.1106, with packages: DESeq2, biomaRt, ggplot2, dplyr, corrplot, RcolorBrewer, ggbeeswarm, ashr, EnhancedVolcano, pheatmap, VennDiagram)

DESeqDataSET design Formula:

```
exptObject <- DESeqDataSetFromMatrix(
  countData = rawData_filt,
  colData = exptDesign,
  design = ~ condition
```

2.2.15 Gene Ontology term enrichment

In order to investigate which biological processes were enriched in the dataset. The Ensembl gene IDs for the top differentially expressed genes between pairwise comparisons where adjusted p-value < 0.01 were uploaded to the AmiGO 2 online tool (http://amigo.geneontology.org/amigo) term enrichment service, selecting biological process and Mus musculus. Fisher's exact test was performed with a false discovery rate of < 0.05.

2.2.16 Gene set enrichment analysis

Gene set enrichment analysis (GSEA) was performed inhouse by central biotechnology services (Mootha *et al.*, 2003; Subramanian *et al.*, 2005). Gene Set Enrichment Analysis (https://www.gsea-msigdb.org/gsea/index.jsp) was used to detect coordinated expression within samples of a predefined set of genes available from the Molecular Signatures Database (MSigDB, https://www.gsea-msigdb.org/gsea/msigdb/index.jsp) (Liberzon *et al.*, 2011). GSEA computes an enrichment score (ES) which reflects the degree to which a gene set is overrepresented at the top or bottom of the ranked list of the RNAseq data. The genes are ranked according to the difference in their expression between the experimental groups. These

are then ranked based on their adjusted p-values whereby only the significantly expressed genes are selected for the GSEA analysis. Here pairwise comparisons (DG v RH and DG v CX) were performed using differentially expressed genes with p-adjusted value less than or equal to 0.05. The ES score is determined by walking down the ranked gene list and increasing the running-sum statistic when a gene is encountered from the predefined gene set and decreasing the running-sum statistic when it is not encountered in the gene set. The gene sets database "MousePath_All_gmt-Format.gmt" was downloaded from http://ge-lab.org/gskb/ and the chip platform was set to "Mouse_ENSEMBL_Gene_ID_MSigDB.v7.0.chip". A total of 1000 permutations were performed for estimating the empirical p-values for the gene sets. The software was then used to calculate the enrichment scores with default parameters. The ES is the maximum deviation from zero which is encountered in the random walk which corresponds to weighted Kolmogorov–Smirnov-like statistic. As this was explorative analysis the differentially expressed gene sets were filtered with a false discovery rate (FDR) < 25%. MSigDB genesets: Hallmark, C2 – curated gene sets and C5 – ontology gene sets were used to investigated differences between DG and RH samples (Liberzon *et al.*, 2015).

2.2.17 Microglia enrichment analysis

Microglia enrichment (MGEnrichment) analysis is a web-based tool that was developed for non-programming wet lab scientists to easily and efficiently perform enrichment analysis (Jao and Ciernia, 2021). MGEnrichment is a simple enrichment tool which performs a one-tailed Fisher's exact test to compare overlap between the supplied list of DEG and the gene lists in the database where statistical significance is established relative to a background gene list and an FDR correction. Ensembl IDs of differentially expressed genes between DG and RH with a

P-value <0.01 and log fold change < -1 or >1 were loaded onto the platform with an FDR-value of 0.05. Gene list groups that were selected included: “microglia”, “microglia development”, “inflammation” and “neuropsychiatric & developmental disorders human brain”. The background query was set to “all mm10 Genes or hg38 Genes”. This data was not graphed.

3.0 A brief characterisation and optimisation of enriched Hippocampal neural progenitor cultures

3.1 Introduction

Hippocampal neurogenesis, is an attractive area of interest to the neuropsychiatric and neurodegenerative field. It represents a potential to harness the regenerative properties of neural progenitors to repair and replace damaged tissue in an effort to prevent and/or slow down disease progression where possible. However, hippocampal neurogenesis still eludes our full understanding in its regulatory mechanisms and in its contribution to many cognitive functions. In an attempt to bridge this gap, this body of work aims to examine the neurogenic potential of the immune cells of the brain - microglia – on stem cells within the hippocampal neurogenic niche and their interaction. In the first instance, this will be performed by generating hippocampal cultures that are enriched for neural progenitor/stem cells (NSPC) and co-culturing these with microglia or incubating them with microglial conditioned media (MGCM). This chapter aims to first briefly characterise and optimise the hippocampal NSPC cultures before exploring this relationship.

3.1.1 Rodent derived hippocampal neural stem/progenitor cell cultures

NSPC cultures have been generated from rodent brain tissue since the 1990s and have since been used for a variety of applications including developmental, pharmacological and electrophysiological studies. The discovery that NSPC's residing in the rodent brain could be differentiated and expanded in culture, provided significant support for continual generation of new neurons in the brain throughout life (Reynolds and Weiss 1992; Ray et al. 1993a; Palmer et al. 1995a). Early neurogenic studies using embryonic derived hippocampal neuronal monolayer cultures, showed these cultures were capable of proliferating and differentiating easily in high levels of basic fibroblast growth factor (bFGF) (Ray et al. 1993b). Embryonic hippocampal neurons responded to bFGF in a dose dependant manner, where low concentrations (1ng/ml) enhanced the survival of these cells and concentrations greater than or equal to 10ng/ml induced proliferation. In the absence of bFGF, cell survival was shown to decrease from day 4 in culture and by day 7, no cells remained. Immunostaining indicated that these hippocampal cultures lacked supporting cells such as astrocytes and oligodendrocytes and is suggestive that these cells are important to the survival of the neuronal cultures in the absence of bFGF. Unfortunately, the presence or absence of microglia was not reported in these cultures. There was no obvious attempt to remove debris resulting from the mechanical trituration which may have contributed to increased cell death, nor was there an effort to isolate specific cell populations in their cultures. As the use of bFGF and FGF-2 to promote cell survival and induce proliferation has been reported by other groups, the major success of (Ray et al. 1993b) was in maintaining primary hippocampal cells in culture long term that could be passaged, frozen, thawed and re-plated (Walickee et al. 1986; Walickei 1988; Palmer et al. 1995a; Brewer 1999; Babu et al. 2011). Other growth factors have been implicated in the survival and differentiation of embryonic hippocampal stem cells including epidermal growth

factor (EGF), brain derived neurotrophic factors (Bdnf), Neurotrophin-3 (Nt3) and glial derived neurotrophic factor (Gdnf) (Ahmed et al. 1995; Shetty and Turner 1998). Furthermore, studies which utilised postnatal derived NSPC cultures have identified additional pro-neurogenic factors such as Neuropeptide Y, Vasoactive intestinal poly-peptide and Il-4 (Howell et al. 2003; Namba et al. 2005; Zaben et al. 2009; Nunan et al. 2014).

Soon after the successful isolation and culture of embryonic NSPC's, cultures derived from adult hippocampal rodent tissue were also generated (Brewer 1997a; Palmer et al. 1997). (Brewer 1997a) used a four step Nycoprep density gradient to generate enriched neuronal cultures with reduced cellular debris that were capable of surviving for up to 3 weeks. Using this method, they were able to isolate approximately 900,000 viable neurons from the hippocampi of rats of any age. Furthermore, they showed that the application of FGF-2 enhanced the viability of cells by three-fold. In a later study, (Brewer 1999) demonstrated that the proliferative capacity of hippocampal neuronal cultures from both embryonic and adult rats in the absence of FGF-2 (5ng/ml) was almost non-existent. A potential reason for this could be the relatively low plating density used of 320 cells/mm^2 which resulted in a low live cell count. A low plating density is known to be associated with decreased cell viability, which is thought to be due to a lack of trophic support from surrounding neurons and glia particularly in serum free media (Banker 1980; Brewer et al. 1993).

The important question of whether different types of cells generated in culture arise from a multipotent progenitor or whether these are produced from separate individual cells already committed to a specific cell lineage was answered using used retroviral labelling (Palmer et al. 1997). Primary cultures were generated from the pooled hippocampal formation of 6 adult female Fischer 344 rats (160 -170g). Cells were grown to confluence and were passaged several

times using trypsin before experimental use. Importantly, the retroviruses used only labelled dividing cells and as the retroviral vectors insert themselves randomly in to the genome it was possible to identify the progeny of an infected cell through this unique identification. After selection and isolation of G418 resistant cells, they showed that when induced, cells from three major lineages (Oligodendrocytes, astrocytes and neurons) were represented in each clonal culture, suggesting that the cells within the culture originated from a single multipotent progenitor. To confirm their findings DNA was prepared from each clone before and after differentiation was induced and a southern blot was performed. The results confirmed that retroviral vectors are present before and after differentiation and that contaminated cultures could be identified by the visualisation of more than one band. It was also noted that cells plated at low density required the presence of 0.5% serum or 1ng/ml FGF-2 to maintain survival, whereas cells plated at high density survived in N2 media alone.

Monolayer cultures can be modified to a co-culture system in order to investigate cell to cell signalling *in vitro.* This can be achieved in a number of ways, for example, by directly co culturing two different cell types together providing direct cell to cell interaction via gap junctions. This is often used in neuronal cell lines where neurons are co-cultured with astrocytes to provide trophic support. Alternatively, paracrine signalling can be achieved by culturing different cell types together in the same defined medium separated by a thin membrane for example, using a trans well insert. (Ehret et al. 2015) used this co-culture system to investigate the influence of different cell types in parallel on hippocampal neural progenitors isolated from the dentate gyrus. All cell types used enhanced neural progenitor survival, however, endothelial cells were shown to stimulate proliferation of precursor cells and differentiation to a neuronal lineage. Although the primary cell cultures did not reach 100% purity, they demonstrate the highly adaptive nature of this approach. A co- culture system can

be manipulated to a high degree where elements can easily be added or removed based on experimental design unlike some 3D or *in vivo* approaches. An interesting addition to the co-culture paradigm is the use of scaffolds to recapitulate *in vivo* morphology. Scaffolds can be made from either natural or synthetic materials and provide cells support to functionally organise themselves and will perhaps aid issues surrounding cell morphology in traditional monolayer culture (Knight and Przyborski 2015). However, scaffolding within cultures can also cause technical issues depending on the downstream application. For example, depending on the material, transparency and scaffolding size, microscopy-based imaging can be difficult, whereas in other applications such as flow cytometry it may be hard to extract all cells as they would require dissociation from the scaffold itself (Antoni et al. 2015).

Alternatively, neurospheres and spheroids represent a scaffold free system whereby cells are dissociated into a single cell suspension and plated in a defined suspension media and through proliferation and differentiation, produce their own extracellular matrix components (Reynolds and Rietze 2005). Using low adherent substrates, cells are unable to attach to surfaces and as a they proliferate they form clusters. Neurospheres provide the complex 3D space and microenvironment that recapitulates an *in vivo- like* environment. However, due to the random nature of their formation, the ability to consistently reproduce uniformed spheres is a limitation of this methodology and spheroid size has been shown to affect cell differentiation in embryoid bodies (Messana et al. 2008). Another issue with long term culture of spheroids in culture is the formation of a necrotic core due to the limited diffusion of vital nutrients and waste products in and out of the aggregates (Edmondson et al. 2014). It is then not surprising that cellular location within a spheroid will affect the rate of proliferation and differentiation. An advancement in 3D culture systems has been the generation of organoids and specifically in relation to the field of neurogenesis – brain organoids. Organoids are self-assembled cell

aggregates resembling the development and cytoarchitecture of the embryonic brain, generated from pluripotent stem cells (Qian et al. 2019). Organoids can be produced through unguided differentiation which can result in heterogenous tissue that resemble more than one brain region or through guided differentiation via the application of various small molecules and factors. In this later approach organoids can be produced that resemble a defined brain region of interest. Typically, human embryonic or human induced pluripotent stem cells have been used to generate brain organoids which has been a great benefit to the field owing to a lack of human brain tissue available. Using self-organising human embryonic stem cells, functional hippocampal-like neurons have been generated in culture, an advance which will no doubt aid research into hippocampal related disorders (Sakaguchi et al. 2015). While the organoid model is great at integrating different cell types into a spontaneous 3D structure that is particularly suitable for developmental studies they, like Neurospheres, struggle to cope with the lack of nutrient diffusion into the centre of the organoid and are therefore limited to approximately 400μm in size.

A different approach used to recapitulate *in vivo* morphology and topology is the culture of organotypic hippocampal slices (Sadgrove et al. 2006). Here the hippocampus is cut in the coronal orientation to produce 400μm thick slices and cultured whole. In this way the cytoarchitecture of the hippocampus as well as the synaptic organisation is maintained (Opitz-Araya and Barria 2011). However, one of the major disadvantages of slice cultures are that cells lose their target innervation which is a primary cause of cell death (Humpel 2015). Interestingly, the granule cell layer in rat hippocampal organotypic slice cultures has been shown to undergo restructuring during two weeks in culture, with changes observed in cell density and area as well as showing that BrdU incorporation varies along the septotemporal

axis of the hippocampus (Sadgrove et al. 2006). This is thought to have major implications for studies assessing proliferation rates in these types of cultures. Another group has shown that there is marked reduction in neurogenesis in hippocampal slice cultures from mice after one week in culture thought to be a result of a marked increase in inflammation (Gerlach et al. 2016).

As I have described above, cell culture systems have been used to interrogate hippocampal neurogenesis and have evolved from the simple monolayer to complex 3D organoid systems. The neurogenic niche requires not only NSPC's but a supportive microenvironment which is likely to include supporting cells, cell-cell contact, extracellular matrix and supporting intrinsic and extrinsic factors. A hippocampal neurogenic model should then aim to fulfil these criteria. A neurogenic cell culture model not only allow us to investigate this rare phenomenon outside of a model organism but allows acute manipulations at the cellular and molecular level which would not otherwise be possible. This approach also provides the opportunity to disentangle this mechanism from multiple converging pathways. As a result of the limitations associated with human hippocampal cultures and the unparalleled efficiency of generating hippocampal cultures from rodent tissue, I decided to use postnatal hippocampal rat tissue to investigate the regional neurogenic effect of microglia on hippocampal NSPC's. Cultures generated from adult rodent brain tissue show poorer viability due to increased structural integrity and a decreased level of stem cells whereas embryonic tissue displays a less developed neuronal organisation and structure. Therefore, post-natal tissue finds itself in an intermediate state that will provide both increased viability and number of stem cells suitable for monolayer culture. Our group has had previous success in using this model to identify neurogenic properties of biological agents on the neurogenic niche including: neuropeptide Y, vasoactive intestinal polypeptide and the microglia Vpac1 receptor (Howell et al. 2003; Zaben et al. 2009; Nunan et al. 2014).

Using monolayer cultures will allow direct manipulation via the addition of microglia or microglia conditioned media (MGCM) and straightforward quantification and analysis using immunocytochemistry and microscopy to examine phenotypic changes in response to these conditions. I have chosen not to use exogenous growth factors such as FGF-2 or EGF in the culture media as this could conceal or alter the effects of the conditions that are used. Despite our group having previous success with post-natal NSPC monolayer culture, I am acutely aware of the reproducibility crisis that has been facing the research community in recent years, and therefore begin with characterising and optimising the hippocampal NSPC cultures that I have generated (Collins and Tabak 2014; Begley and Ioannidis 2015).

3.1.2 Aims

The general aim of this chapter was to characterise and optimise NSPC cultures for further experimental use.

- Aim 1: Briefly characterise the cell population of the hippocampal NSPC culture system used here derived from post-natal rat pups across five days *in vitro*.
- Aim 2: Optimise the hippocampal NSPC culture paradigm to increase levels of type 2 progenitor cells.

This chapter was used to validate the culture system and set a precedence so that potential regional neurogenic impacts of microglia from the hippocampus with other brain regions can be compared. Consistent with previous research in our lab, typical cell phenotypes expected of the neurogenic niche such as Type 1 (Nestin+Gfap+) and type 2 (Nestin+Gfap-) neural cells,

Beta III Tubulin (Tuj1) positive cells as well as a significant proportion of microglia were observed in these cultures.

3.2 Results

3.2.1 Characterising cell phenotypes in post-natal hippocampal NSPC cultures across five days *in vitro*

Hippocampal cultures were generated (General Methods 2.1.3) and at the relevant time point, immunocytochemistry was performed (General Methods 2.1.8) using antibodies against Gfap, Nestin, Tuj1 and the nuclear marker DAPI (**Fig.3.1**). Gfap and Nestin are both stem/progenitor cell markers and changes in the number and percentage of cells expressing these markers is a good indication of changes to the stem cell population. Tuj1 is a marker for immature neurons. A one-way ANOVA was performed and if significant a Tukey post hoc test was performed to compare the means between 1, 3 and 5 days in culture. The total number of cells per mm^2 was assessed using the DNA binding dye DAPI (**Fig.3.1 A, E, I**). There was a significant difference in DAPI counts ($F_{(2,39)} = 3.313$, $p = 0.0469$) between 1, 3 and 5 days in culture with post hoc tests demonstrating a significant decrease between 1 and 3DIV from 219 ± 30.85 cells/mm^2 to 138.8 ± 12.51 mm^2 respectively. This indicates that there was a drop off in cell survival in the initial days post plating. However, there was no significant difference between the number of DAPI counts between 1 and 5DIV, suggestive of a stable population.

There was a significant difference in the total number of Gfap (**Fig.3.1 B, J**) positive cells, representing radial glial cells, between 1, 3 and 5 days in culture ($F_{(2,39)}=5.859$, $p = 0.006$) with a significant increase between 1 and 5DIV from 27.30 ± 3.527 cells/mm^2 to 51.99 ± 6.481 cells/mm^2. The percentage of Gfap cells (**Fig.3.1 P)** was also significantly different across 5 days in culture ($F_{(2,39)} = 19.36$, $p < 0.0001$) with a significant increase from 1 and 3 DIV as well as 1 and 5 DIV with the latter increasing from 13.74 ± 1.198% to 28.77 ± 2.143%. The

total number of Nestin positive cells (**Fig.3.1 C, K),** representing radial glial and amplifying neural progenitors, was significantly different across 5 days in culture ($F_{2,39)}$ = 5.937, p = 0.0056) with a significant increase between 1 and 5 DIV from 21.6 ± 3.394 cells/mm^2 to 46.71 ± 6.585 cells/mm^2. The percentage of Nestin cells (**Fig.3.1 Q)** was also significantly different across 5 days in culture ($F_{(2,39)}$ = 19.19, p < 0.0001). Post hoc tests showed a significant increase in the percentage of Nestin cells between 1 and 3DIV as well as 1 and 5DIV with the latter increasing from 10.49 ± 1.132% to 25.13 ± 1.976%. There were no significant differences observed for Tuj1 positive cells (**Fig.3.1 D, L)** nor in its percentage (**Fig.3.1 R**) of total cells across 5 days in culture suggesting a steady state population. Interestingly, at 1DIV there is a significant number of Tuj1 positive cells suggesting that immature neurons are capable of surviving tissue dissociation. Overall, these results confirm that the cultures generated were supportive of Gfap, Nestin and Tuj1 positive cell types across 5 days in culture.

NSPC's in the neurogenic niche of the dentate gyrus can be segregated into subsets depending on where they are in their neuronal developmental stage. Type 1 cells are considered stem cells otherwise known as radial glial-like cells. These cells are known to express both Gfap and Nestin (Gfap+Nestin+) at the same time. Type 2 cells on the other hand are negative for Gfap but positive for Nestin (Nestin+Gfap-) and are highly proliferative (Kempermann et al. 2004a). There was a significant difference in the number of type 1 (Nesin+Gfap+) cells (**Fig.3.1 G, M**) per mm^2 across 5 days in culture ($F_{(2,39)}$ = 11.31, p = 0.0001). Post hoc tests showed a significant increase between 1 and 3DIV as well as 1 and 5DIV with the latter showing an increase from 12.18 ± 2.437 cells/mm^2 to 41.13 ± 5.503 cells/mm^2. The percentage of type 1 (Nestin+Gfap+) (**Fig.3.1 N)** with respect to DAPI was significantly different ($F_{(2,39)}$ = 30.44, p < 0.0001) across 5 days in culture, particularly between 1 and 3DIV and 1 and 5DIV (5.91 ± 0.8218% to 22.52

± 1.827%). There was also a significant difference in the percentage of type 1 (Nestin+Gfap+) cells with respect to the total number of Nestin cells ($F_{(2,39)} = 42.87$, $p < 0.0001$) (**Fig.3 .1O**) with increases between 1 and 3DIV as well as 1 and 5DIV (54.64 ± 3.723% to 89.36 ± 1.827%). This suggests that type 1 cells are proliferating across 5 days in culture.

For type 2 (Nestin+Gfap-) cells (**Fig.3.1 G, S**) there were also significant differences in cell numbers across 5 days in culture ($F_{(2,39)} = 4.149$, $p = 0.0232$) with a significant decrease between 1 and 3DIV from 9.427 ± 1.328 cells/mm^2 to 4.753 ± 0.9053 cells/mm^2. The percentage of type 2 (Nestin+Gfap-) with respect to the total number of cells (**Fig.3 T**) was significantly different ($F_{(2,39)} = 4.269$, $p = 0.0211$) with a significant decrease between 1 and 5DIV from 4.584 ± 0.5051% to 2.605 ± 0.4797%. There was also a significant difference in the percentage of Type 2 (Nestin+Gfap-) cells with respect to the total number of Nestin positive cells ($F_{(2,39)} = 42.87$, $p < 0.0001$) (**Fig.3.1 U**) with significant decreases between 1 and 3DIV as well as 1 and 5DIV (45.36 ± 3.723% to 10.64 ± 1.827). This suggests that there is a reduction in survival of type 2 cells across 5 days in culture. Overall, these results confirm that the hippocampal NSPC cultures contain both type 1 and type 2 neural stem cells. Type 1 cells were seen to steadily increase across 5 days whereas the number of type 2 cells decreased.

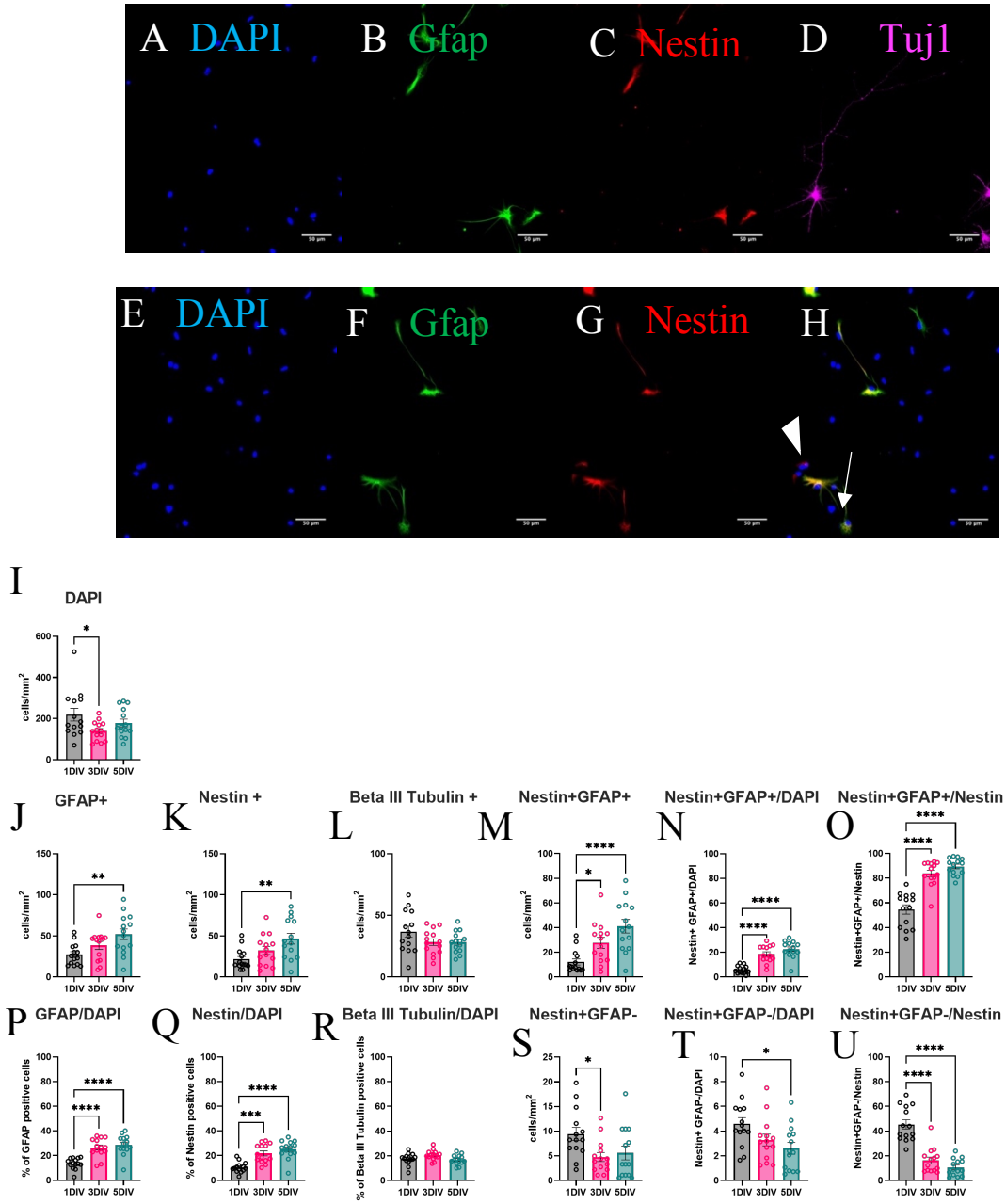

Figure 3.1 Gfap and Nestin positive cells increase, while Tuj1 positive cells remain stable across 5 days *in vitro* (DIV) in postnatal hippocampal NSPC cultures. Meanwhile, type 1 neural progenitor cells increase, while type 2 progenitors decrease across 5 days *in vitro* in postnatal hippocampal NSPC cultures.

An increase in Gfap positive cells is seen between 1 and 5DIV. Total cell count measured using DAPI per mm^2 (A, E, I), mean number of Gfap positive cells per mm^2 (B, J) and percentage of Gfap positive cells with respect to the total cell count (P). An increase in Nestin positive cells is seen between 1 and 5DIV. Mean number of Nestin positive cells per mm2 (C, K) and percentage of Nestin positive cells with respect to the total cell count (Q). Tuj1 population of cells remains stable between 1 and 5DIV. Mean number of Tuj1 positive cells per mm2 (D, L) and percentage of Tuj1 positive cells with respect to the total cell count (R). An increase in Type 1 (G, thick arrow) and a decrease in Type 2 (D, thin arrow) neural progenitor cells between is shown between 1 and 5DIV. Arrow head (G) shows Nestin-Gfap+ cell. Mean number of Nestin+Gfap+ cells per mm2 (M), percentage of Nestin+Gfap+ with respect to the total number of cells (N) and percentage of Nestin+Gfap+ positive cells with respect to the total Nestin count (O). Mean number of Nestin+Gfap- cells per mm2 (S), percentage of Nestin+Gfap- cells with respect to the total number of cells (T) and the percentage of Nestin+Gfap- with respect to the total number of nestin cells (U). N = 14 wells from 3 separate experiments. Data points represent mean ± SEM. One-way ANOVA with Tukey post hoc test. * = $p < 0.05$, ** = $p < 0.01$, *** = $p < 0.001$, **** = $p < 0.0001$.

3.2.2 Microglia represent twenty percent of cell content of postnatal hippocampal NSPC at day five in culture

Previous work in our lab has demonstrated that microglia may be washed off during fixing and washing, potentially due to the high motility that microglia possess (Nunan 2009). Therefore, in order to assess the microglial content of the hippocampal cultures, NSPCs were generated (General Methods 2.1.3). At 5DIV cells were stained with a pre-conjugated (IB4) antibody that is capable of staining microglia at all stages of cell activation. IB4 (2.5μg/ml) **(Fig.3.2 B, E)** and DAPI (5μg/ml) **(Fig.3.2 A, D)** were applied at 5DIV and two hours later were live imaged using an inverted fluorescent microscope (General Methods 2.1.6). At 5DIV 9.532 ± 0.87 IB4 positive cells per mm^2 were present in the hippocampal NSPC cultures **(Fig.3.2 E)**, representing 20.37 ± 2.892% of all cells in culture **(Fig.3.2 F)**.

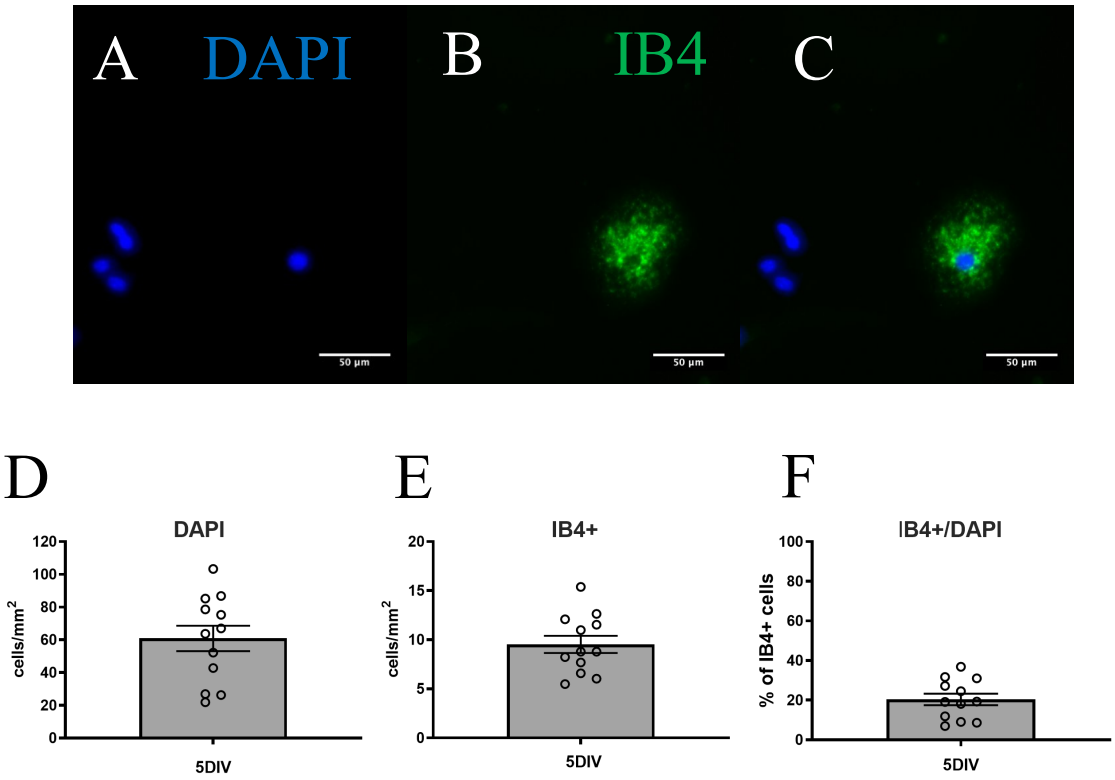

Figure 3.2 Microglia represent 20% of cells in hippocampal NSPC cultures at 5 days *in vitro*.

Hippocampal NSPC cultures were stained with IB4 and DAPI and live imaged using an inverted fluorescent microscope at 5DIV. Total cell count per mm^2 (A, D), total IB4 positive cell count (B, E) and percentage of IB4 with respect to DAPI (C, F) were calculated. N = 12 wells from 3 independent experiments. Data points represent mean ± SEM.

3.2.3 Cell viability of hippocampal NSPC increases over five days *in vitro*

To check the viability of the hippocampal NSPC cultures, parallel cultures were generated (General Methods 2.1.3) and grown for 1, 3 and 5 days in culture under standard conditions. At the appropriate time point cells were stained with DAPI and PI prior to live imaging (General Methods 2.1.5). One-way ANOVA showed that there was a significant difference between cultures in terms of total cell count **(Fig.3.3 A, E)** ($F_{(2,15)} = 33.75$, $p < 0.0001$), with Tukey's post hoc test showing a significant decrease between 1 (652.1 ± 24.82 cells/mm^2) and 3DIV (371.4 ± 35.3 cells/mm^2) and 1 and 5DIV (424.1 ± 10.85 cells/mm^2). This is consistent

with **Fig. 3** and suggests a drop off in cell survival from initial plating. A significant difference was seen in the number of PI positive cells across 5 days in culture ($F_{(2,15)} = 229.8$, $p < 0.0001$) with a significant decrease observed between 1 (397 ± 20.81 cells/mm^2) and 3DIV (73.31 ± 4.484 cells/mm^2) as well as 1 and 5DIV (55.32 ± 5.467 cells/mm^2), but not between 3 and 5DIV **(Fig.3.3 B, F)**. There was a significant difference in the percentage of PI positive cells across 5 days in culture ($F_{(2,15)} = 275.5$, $p < 0.0001$) with significant decrease shown between, 1 ($60.72 \pm 0.9645\%$) and 3DIV ($20.60 \pm 2.169\%$), 1 and 5DIV ($13.03 \pm 1.232\%$) as well as 3 and 5DIV **(Fig.3.3 G)**. These results show that the hippocampal cultures are supportive of the cell population, that cell death decreases over time, while the number of viable cells increases. The increase in viable cells across 5 days suggests that cells within the hippocampal NSPC cultures are proliferating.

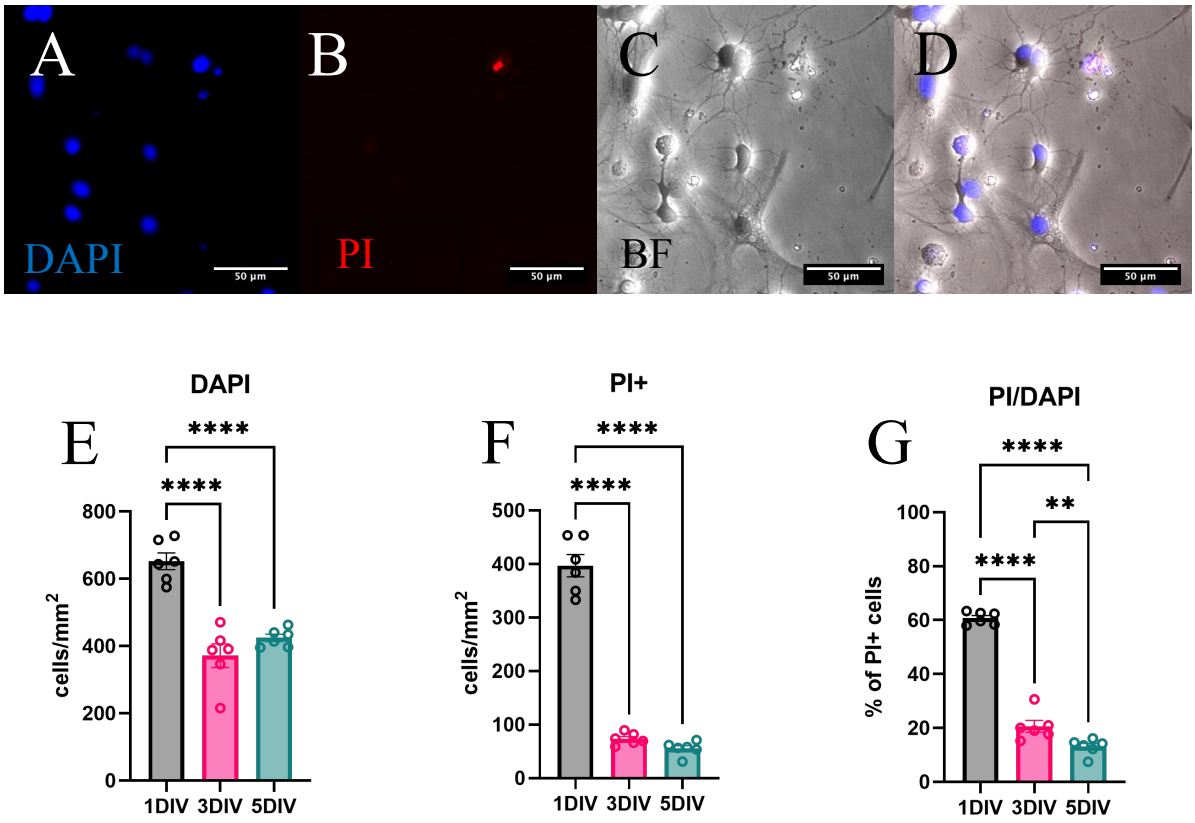

Figure 3.3The number of viable hippocampal NSPC's increases across five days *in vitro*.

Hippocampal cells were plated and grown as parallel cultures for 1, 3 and 5 days in culture. Live cells were stained with DAPI and PI two hours before live imaging. Representative images taken from 5DIV, C shows brightfield image. Total cell count (A, E) and total PI positive cells (B, F) were recorded. Percentage of cells that were PI positive (G). N = 6 wells from 1 experiment. Data points represent mean ± SEM. * = $p < 0.05$, ** = $p < 0.01$, *** = $p < 0.001$, **** = $p < 0.0001$.

3.2.4 Edu positive cells in postnatal hippocampal NSPC cultures show limited survival between 1 and 5 days *in vitro.*

To assess the survival of proliferating hippocampal NSPC's I used the s-phase marker EdU. EdU is a thymidine analogue which does not require harsh treatment of the cells to acid that is typical of the traditional BrdU treatment and therefore is much better at preserving cell integrity and morphology. Hippocampal cultures were generated (General Methods 2.1.3) grown in standard conditions for 1, 3 and 5 days in culture. EdU was applied 2 hours after plating and

washed out after 24 hours (General Methods 2.1.8). One-way ANOVA showed that there was a significant difference between the total number of cells between 1, 3 and 5 days in culture ($F_{2,22}$ =16.31, p <0.0001) **(Fig.3.4 A, D)**. Dunnett's post hoc test showed a significant decrease between 1 (175.5 ± 14.97 cells/mm^2) and 3DIV (122.4 ± 6.791 cells/mm^2) as well as 1 and 5DIV (106.6 ± 5.017 cells/mm^2) in line with previous results. There was a significant difference in the number of EdU positive cells between 1, 3 and 5 days in culture ($F_{2,22}$ = 7.249, p = 0.0038) with a significant decrease in the number of EdU positive cells between 1 (10.89 ± 0.9745 cells/mm^2) and 3 DIV (4.619 ± 0.9707 cells/mm^2) and 1 and 5DIV (6.489 ± 1.03 cells/mm^2) **(Fig.3.4 B, E)**. However, there was no significant difference ($F_{2,22}$ =2.996, p = 0.0707) in the percentage of EdU positive cells between 1 (6.271 ± 0.4779 %) and 3DIV (3.708 ± 0.7332 %) or 1 and 5DIV (6.074 ± 0.9296%) **(Fig.3.4 F)**. The results indicate that under the conditions applied here that there is limited survival of proliferating cells in these cultures.

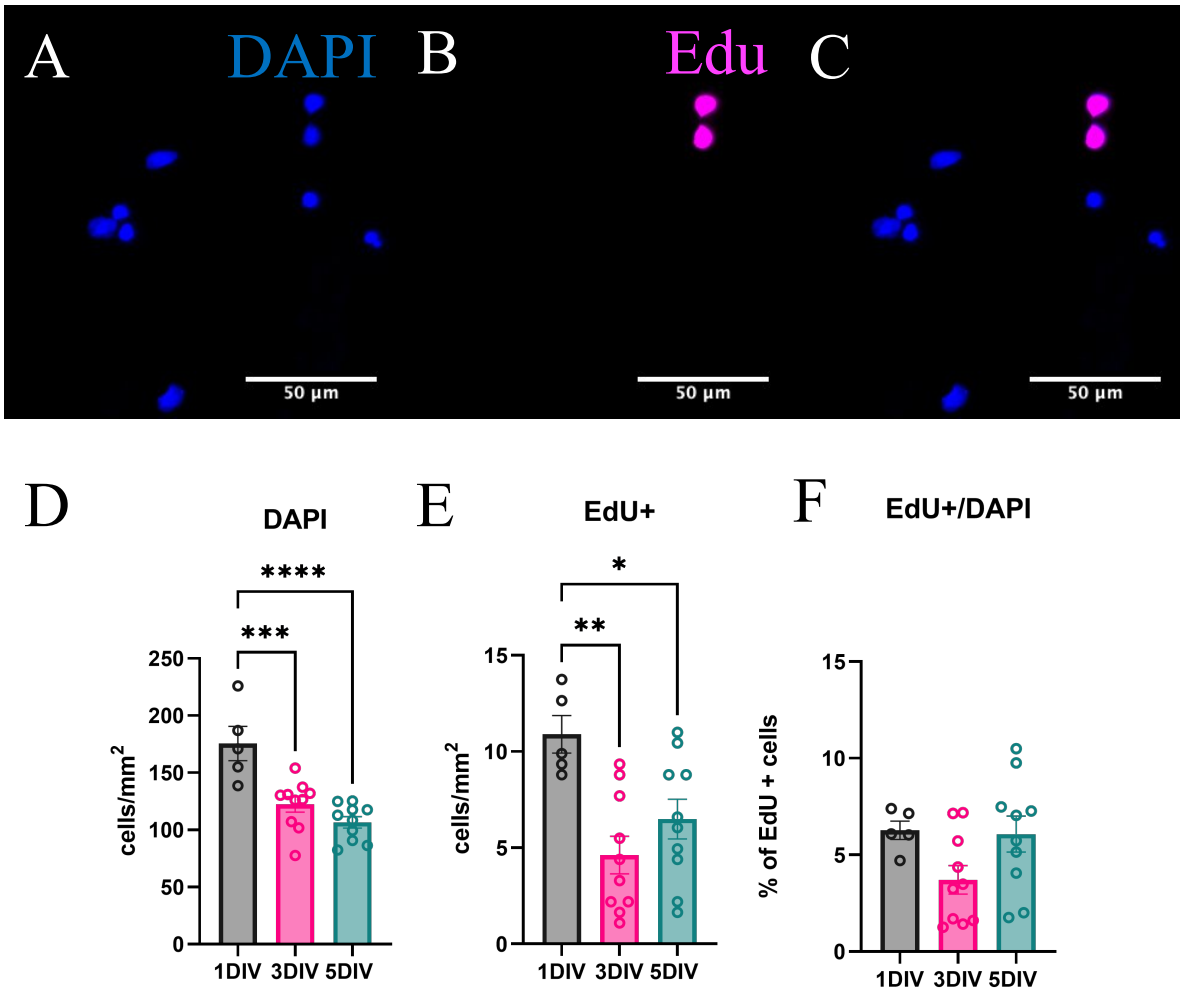

Figure 3.4 Postnatal hippocampal cells in s phase show limited survival between 1 and 5 days in vitro (DIV) when pulsed with EdU for 24hrs at 1 DIV.

Hippocampal cultures were treated with EdU for 24 hrs, 2 hrs after plating and then allowed to grow in standard conditions for 1, 3 and 5DIV. Cells were fixed and assessed for Edu incorporation, representative images from 1DIV. Total cell number (A, D), total EdU positive cells (B, E) and percentage of EdU (C, F) were recorded. N = 5 wells from 1 experiment for 1DIV. N = 10 wells from 2 independent experiments for 3 and 5DIV. Data points represent mean ± SEM. One-way ANOVA wit Dunnets post hoc test. * = $p < 0.05$, ** = $p < 0.01$, *** = $p < 0.001$, **** = $p < 0.0001$

3.2.5 Use of Muse cell counter provides higher estimates of Nestin and Gfap percentage in NSPC cultures

Live cell counting of cells in a suspension can be performed manually using trypan blue exclusion dye and a haemocytometer or it can be done with a commercially available

automated cell counter of which many exist. Both manual and automated cell counting are dependent on the sample used for analysis being representative of the total cell suspension. Manual cell counting is also susceptible to human error as it can be difficult to distinguish between live and dead cells by eye, therefore, in order to determine the accuracy of my cell counting of cells in suspension for plating I compared haemocytometer counts with those determined using the benchtop flow cytometer -Muse™ with the Muse™ count and viability kit. Cells were then plated for both conditions at two different densities: 100,000/ml and 200,000/ml according to haemocytometer and Muse™ total cell counts. NSPCs were generated (General Methods 2.1.3) and grown for 5DIV. Cells were fixed and stained for Gfap, Nestin, Tuj1 and with DAPI (General Methods 2.1.8). A statistically significant difference in average DAPI counts was observed for both plating density ($F_{(1,44)} = 27.24$, $p < 0.0001$) and method of cell counting ($F_{(1,44)} = 9.323$, $p = 0.0038$), though the interaction between these two factors was not significant ($F_{(1,44)} = 1.936$, $p = 0.1711$) **(Fig.3.5 A)**. A Bonferroni post hoc test comparing the means between the type of counter showed a significant difference between cells plated at 200,000 cells/ml for haemocytometer (142.433 ± 19.71 cells/mm^2) and Muse (236.93 ± 33.103 cells/mm^2), but not between cells plated at 100,000 cells/ml – although a similar trend can be seen.

Similar observations were made for average Gfap positive cells, average Nestin positive cells and Nestin+Gfap- cells. For average Gfap positive cells there was a significant difference for both plating density ($F_{(1,44)} = 25.29$, $p < 0.0001$) and type of counting method ($F_{(1,44)} = 9.975$, $p = 0.0029$) but the interaction between the two was not significant ($F_{(1,44)} = 1.137$, $p = 0.292$) **(Fig.3.5 B)**. Bonferroni post hoc tests comparing the mean between the types of counting method showed a significant difference between the haemocytometer (49.311 ± 8.502

cells/mm^2) and Muse (86.981 ± 13.941 cells/mm^2) at 200,000 cells/ml. Again, there was no significant difference observed for Gfap positive cells at 100,000 cells/ml between the two counting conditions (13.977 ± 2.602 cells/mm^2 to 32.629 ± 6.679 cells/mm^2). For average Nestin positive cells **(Fig.3.5 C)**, a significant difference was observed for both plating density ($F_{(1,44)}$ = 27.87, p < 0.0001) and counting method ($F_{(1,44)}$ = 9.634, p = 0.0033), with no significant difference for the interaction ($F_{(1,44)}$ = 1.234, p = 0.2726) between the two. Bonferroni Post hoc tests comparing the means between the counting methods identified a significant difference between the average number of Nestin positive cells plated at 200,000 cells/ml for haemocytometer (50.594 ± 8.148 cells/mm^2) and Muse (87.714 ± 14.231 cells/mm^2). For the average number of Nestin+Gfap- cells **(Fig.3.5 D)**, a significant difference was seen for both plating density ($F_{(1,44)}$ = 24.18, p < 0.0001) and method of cell counting ($F_{(1,44)}$ = 6.102, p = 0.0175) but no significant difference was observed for the interaction of these factors ($F_{(1,44)}$ = 0.678, p = 0.4147). Post hoc tests comparing the means between the counting methods showed a significant difference between the average number of Nestin+Gfap- positive cells plated at 200,000 cells/ml for haemocytometer (5.408 ± 0.869 cells/mm^2) and Muse (8.616 ± 1.664 cells/mm^2). No significant difference was observed at 100,000 cells/ml. For the average number of Tuj1 positive cells **(Fig.3.5 E)**, a significant difference was seen for both plating density ($F_{(1,44)}$ = 36.93, p <0.0001) and method of cell counting ($F_{(1,44)}$ = 6.894, p = 0.0118) but significant difference was observed for the interaction between the two factors ($F_{(1,44)}$ = 0.0084, p = 0.9274). Post hoc tests showed no significant differences between methods at either 100,000 cells/ml or 200,000 cells/ml. Unsurprisingly, a greater number of Tuj1 cells were found in cultures where cells were plated at 200,000 cell/ml.

Two-way ANOVA showed a significant difference for both the plating density ($F_{(1,44)} = 8.151$, $p = 0.0065$) and type of counter ($F_{(1,44)} = 8.087$, $p = 0.0067$) for the percentage of Gfap **(Fig.3.5 F)**, with no significant difference for interaction of these factors ($F_{(1,44)} = 2.514$, $p = 0.12$). Bonferroni post hoc tests were made between the counter types and showed a significant increase between haemocytometer (21.729 ± 3.045%) and Muse (32.555 ± 2.823%). Results also showed a significant difference in the percentage of Nestin cells for both the plating density ($F_{(1,44)} = 14.93$, $p = 0.0004$) and counter type ($F_{(1,44)} = 8.40$, $p = 0.0058$) **(Fig.3.5 G)**. The interaction of these two factor was also significant ($F_{(1,44)} = 5.361$, $p = 0.0253$). Bonferroni post hoc tests made between counter types showed a significant increase between haemocytometer (21.742 ± 2.681%) and Muse (32.559 ± 2.288%) at 100,000 cells/ml. Interestingly, this did not translate into a significant difference in plating density or method of counting for the percentage of type 2 neural progenitor cells or the percentage of Tuj1 cells between haemocytometer and Muse cultures **(Fig.3.5 H, I)**. The take home message is that using the Muse to count live cells for plating gave higher estimates of the percentage of Gfap and Nestin but had no effect on the percentage Nestin+Gfap- or Tuj1 positive cells.

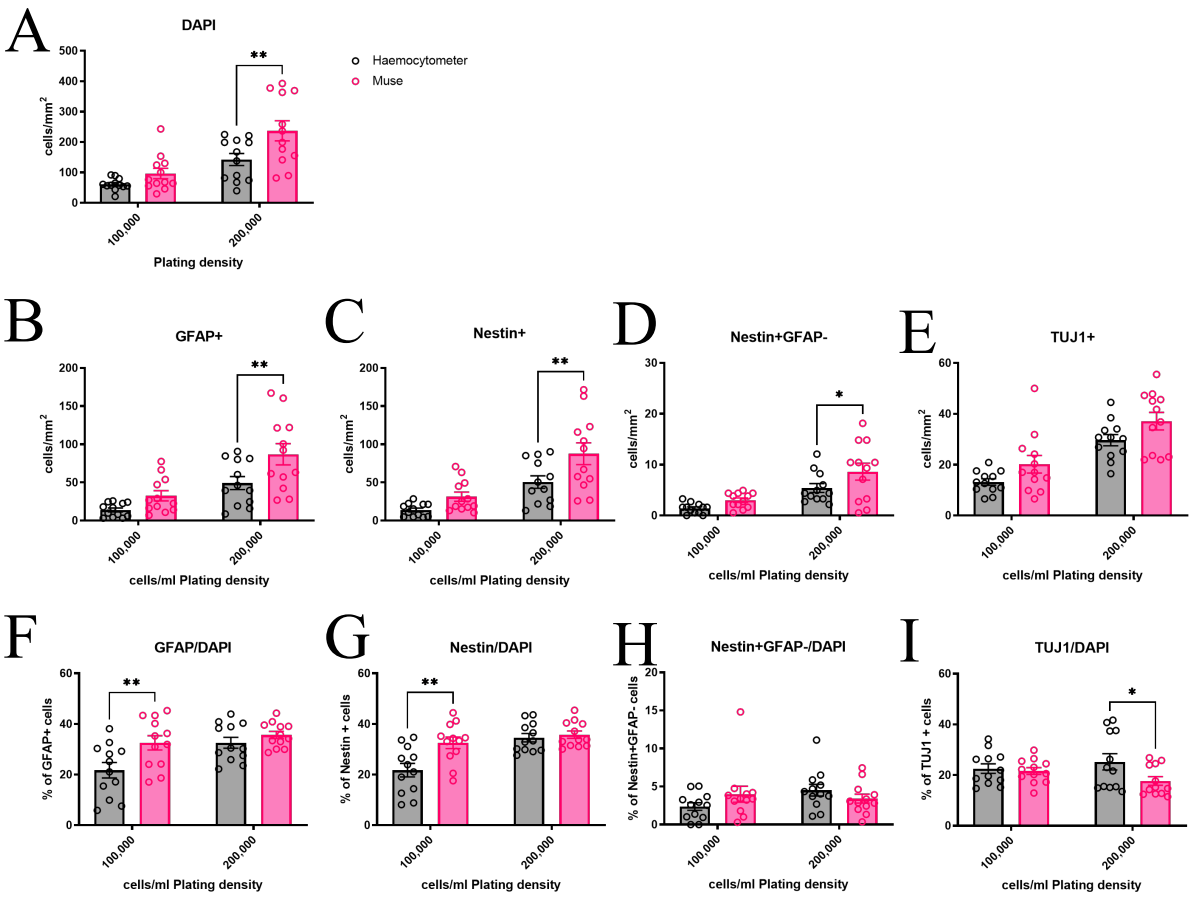

Figure 3.5 Significant differences observed between cell counting methods: Haemocytometer and Muse™.

Total number of cells (A), total number of Gfap positive cells (B), total number of Nestin positive cells (C), total number of Nestin+Gfap- cells (D) and total number of Tuj1 positive cells (E) were recorded. The percentage of Gfap positive cells (F), percentage of Nestin positive cells (G), percentage of Nestin+Gfap- cells (H) and the percentage of Tuj1 cells were calculated with respect to DAPI. N = 12 wells per condition from 3 separate experiments. Data points represent mean ± SEM. * = $p < 0.05$, ** = $p < 0.01$, *** = $p < 0.001$, **** = $p < 0.0001$.

3.2.6 Investigation of the OptiPrep™ gradient for isolating hippocampal NSPC

In order to investigate if there were stem cells remaining in the fractions of the OptiPrep™ gradient that were not usually used for plating, cells from the '2ml' fraction and the 'all' fraction (**Fig.3.6 A**) were plated. For previous hippocampal NSPC cultures, cells are usually taken and plated from the 2ml fraction. If stem cells remained in the other fractions then these could be captured by plating cells from the whole gradient. Cells from the '2ml' and 'all'

fraction of two different gradients were plated (General Methods 2.1.3) and at 5DIV cells were fixed in 4% PFA and stained for Gfap, Nestin, Tuj1 and DAPI (General Methods 2.1.8). No significant differences were observed between the two conditions for any of the parameters that were assessed as measured with an unpaired t-test. The mean total number of cells were 215.1 ± 16.47 cells/mm^2 and 198.3 ± 19.05 cells/mm^2 for '2ml' and 'all' fraction respectively **(Fig.3.6 B)**. The mean total number of Gfap positive cells were 60.81 ± 5.341 cells/mm^2 and 58.02 ± 6.451 cells/mm^2 with the percentage of Gfap 28.22 ± 1.154% and 29.09 ± 1.607% respectively **(Fig.3.6 C, G)**. The mean total number of Nestin positive cells were 65.12 ± 6.554 cells/mm^2 and 60.54 ± 7.881 cells/mm^2 with the percentage of Nestin 29.45 ± 1.496% and 29.88 ± 1.749% respectively **(Fig.3.6 D, H)**. The mean total number of Nestin+Gfap-positive cells was 9.340 ± 1.995 cells/mm^2 and 8.891 ± 2.085 cells/mm^2 with the percentage of Nestin+Gfap- 4.02 ± 0.888% and 4.224 ± 0.733% respectively **(Fig.3.6 E, I)**. The mean total number of Tuj1 positive cells was 31.71 ± 2.959 cells/mm^2 and 31.16 ± 2.41 cells/mm^2 with the percentage of Tuj1 15.19 ± 1.445% and 16.28 ± 0.9873% respectively **(Fig.3.6 F, J)**.

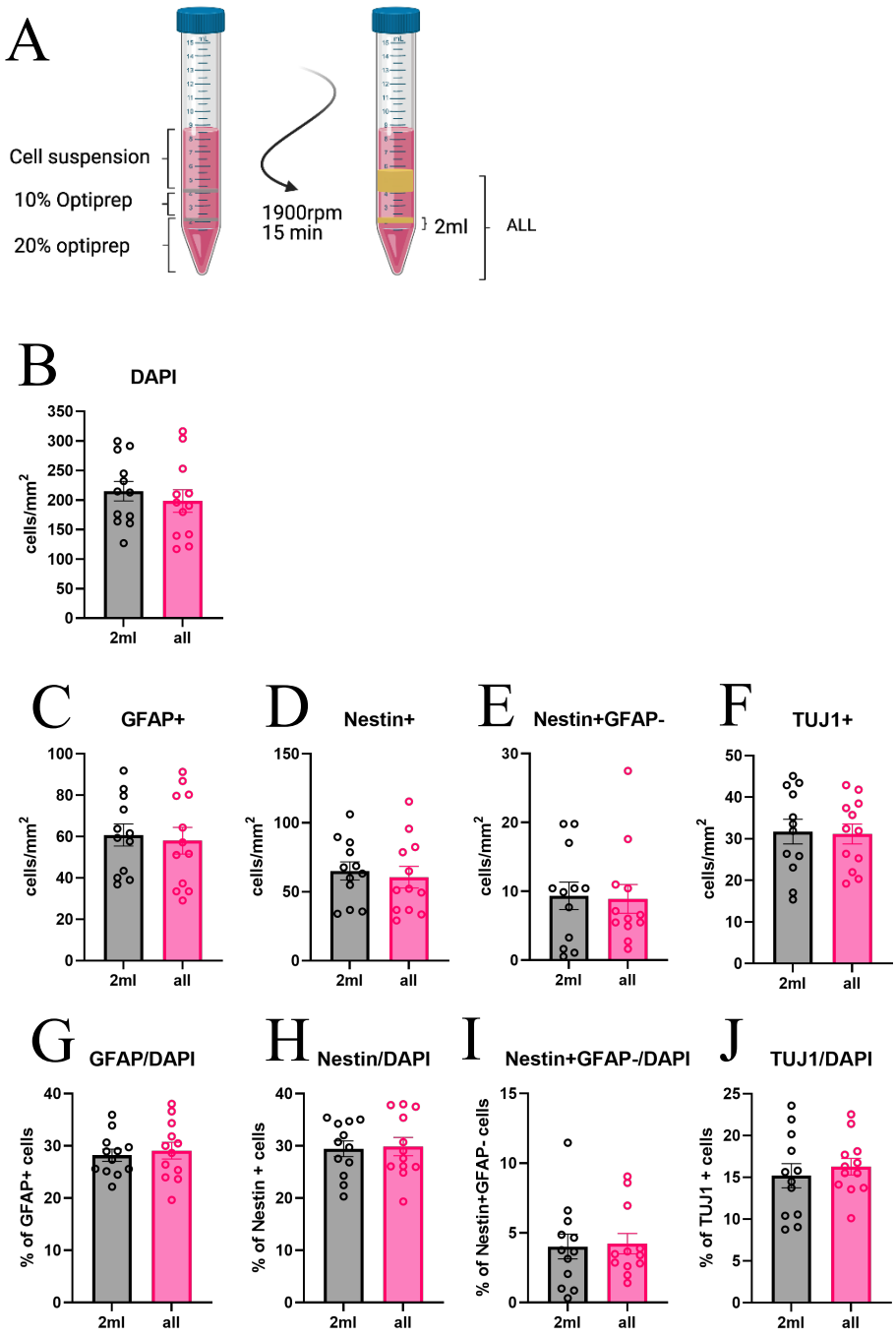

Figure 3.6 Interrogation of the OptiPrep™ gradient shows no difference in the phenotype of hippocampal NSPC cultures at 5DIV between cells taken at 2ml mark and cells taken from the 'all' fraction.

After the cell suspension was placed on top of the two-step OptiPrep™ gradient and centrifuged cells were taken either at the 2ml fraction or the 'all' fraction as shown in the schematic diagram (A) created with BioRender.com. Cells were plated and at 5DIV, fixed and stained. Total cell number (B), total number of Gfap (C), Nestin (D), Nestin+Gfap- (E), and Tuj1 (F) positive cells were recorded. Percentage of Gfap (G), Nestin (H), Nestin+Gfap- (I) and Tuj1 (J) with respect to DAPI were also calculated. N= 12 wells from 3 independent experiments. Data points represent mean ± SEM.

3.2.7 Further investigation of the Optiprep™ gradient for NSPC isolation

Fractions of the Optiprep™ gradient were further investigated by looking at the upper and lower phase of sedimented cells **(Fig.3.7 A)**. In parallel high (800 x G) versus a low (400 x G) centrifuge speed was also compared to see what effect this would have on the cell phenotypes of the hippocampal NSPC cultures. NSPC were generated (General Methods 2.1.3) and allowed to grow for 5DIV in standard culture media, then fixed in 4% PFA and stained for Gfap, Nestin, Tuj1 and counterstained with DAPI. A two-way ANOVA showed a significant difference in total DAPI count for the gradient fraction ($F_{(1,28)} = 4.4869$, $p = 0.0357$), however no significant differences were observed upon post hoc testing. There was no significant difference in centrifuge speed ($F_{(1,28)} = 0.1685$, $p = 0.6845$), nor was there a significant difference for the interaction between the two factors ($F_{(1,28)} = 0.1053$, $p = 0.7480$) **(Fig.3.7 B)**. For total Gfap counts there was no significant difference for the gradient fraction ($F_{(1,28)} = 0.1051$, $p = 0.7482$) or for the centrifuge speed ($F_{(1,28)} = 0.01153$, $p = 0.9153$) **(Fig.3.7 C)**. For the percentage of Gfap positive cells there was a significant difference in the gradient fraction ($F_{(1,28)} = 17.67$, $p = 0.0002$), where Tukey's multiple comparison showed a significant difference between upper (52.706 ± 4.659%) and lower (31.738 ± 3.233%) fractions centrifuged at 400 x G, between the upper fraction centrifuged at 400 x G and the lower fraction centrifuged at 800 x G (35.959 ± 4.117%) and between the upper fraction centrifuged at 800 x G (51.329 ± 5.06%) and the lower fraction centrifuged at 400 x G **(Fig.3.7 G)**. There was no significant difference in the percentage of Gfap for centrifuge speed and there was no significant difference in the interaction of the two factors. For the total of Nestin positive cells, there was no significant difference in gradient fraction ($F_{(1,28)} = 0.2021$, $p = 0.6565$), centrifuge speed ($F_{(1,28)} = 0.0086$, $p = 0.9265$) or in the interaction of these factors ($F_{(1,28)} = 0.0009$, $p =$

0.9755) **(Fig.3.7 D)**. For the percentage of Nestin positive cells, there was a significant difference in the gradient fraction ($F_{(1,28)}$ = 7.576, p = 0.0103) **(Fig.3.7 H)**. There was no significant difference in centrifuge speed and there was no significant difference for the interaction of these factors for the percentage of Nestin positive cells. There was no significant difference for Nestin+Gfap- cells in gradient fraction ($F_{(1,28)}$ = 1.136, p = 0.2956), centrifuge speed ($F_{(1,28)}$ = 0.2244, p = 0.6394) or in the interaction between the two ($F_{(1,28)}$ = 0.0035, p = 0.9532) **(Fig.3.7 E)**. There was also no significant difference for the percentage of Nestin+Gfap- cells for gradient fraction ($F_{(1,28)}$ = 1.976, p = 0.1708), centrifuge speed ($F_{(1,28)}$ = 0.2051, p = 0.6541) or the interaction between them ($F_{(1,28)}$ = 0.0782, p = 0.7818) **(Fig.3.7 I)**. For Tuj1 positive cells there was a significant difference for the gradient fraction ($F_{(1,28)}$ = 6.486, p = 0.0167), however, no significant differences were observed upon post hoc testing **(Fig.3.7 F)**. There was no significant difference in centrifuge speed or in the interaction between the two factors. Finally, for the percentage of Tuj1 cells, there was no significant difference in the gradient faction ($F_{(1,28)}$ = 0.01279, p = 0.9108), centrifuge speed ($F_{(1,28)}$ = 0.0138, p = 0.9073) or in the interaction between the two ($F_{(1,28)}$ = 0.4435, p = 0.5109) **(Fig.3.7 J)**.

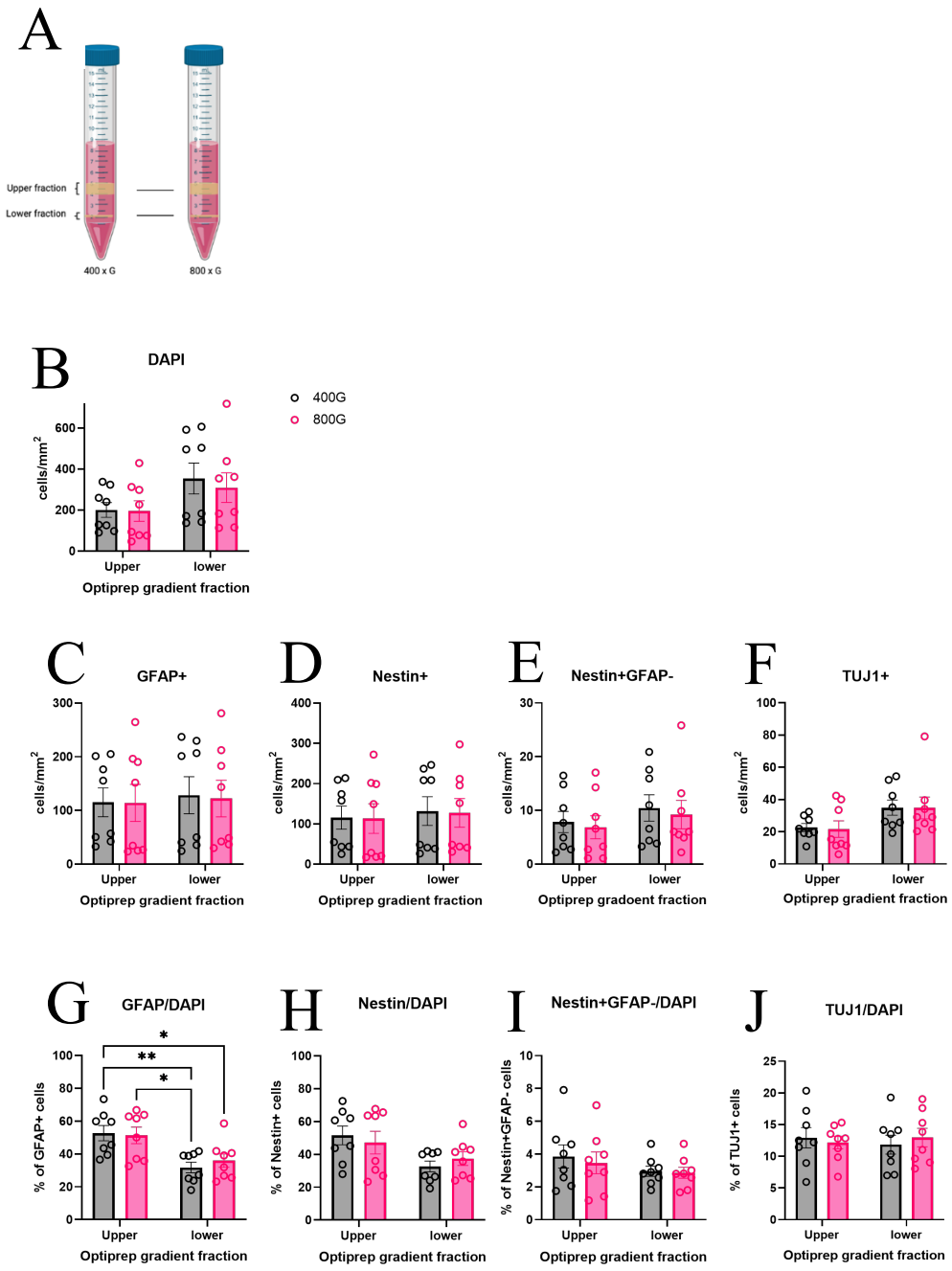

Figure 3.7 The upper fraction of the Optiprep™ gradient produces a significantly higher percentage of Gfap positive cells, however, no difference is seen regarding Tuj1 positive cells.

Hippocampal NSPC isolated from 2 different Optiprep gradients centrifuged at either 400 xG or 800 x G and from 2 different phases of the Optiprep gradient (A, Created with BioRender.com) were allowed to grow for 5DIV.Total number of cells (B), total number of Gfap positive cells (C), total number of Nestin positive cells (D), total number of Nestin+Gfap- cells (E) and total number of Tuj1 positive cells (F) were recorded. Percentage of Gfap (G), percentage of Nestin (H), percentage of Nestin+Gfap- (I) and percentage of Tuj1 (J) were calculated with respect total DAPI counts. N = 8 wells per condition from 2 separate experiments. Data points represent mean ± SEM. * = $p < 0.05$, ** = $p < 0.01$.

3.2.8 OptiPrep™ vs Percol as a separation medium to enrich NSPCs in a cell suspension

In order to assess the ability of an OptiPrep™ gradient to generate an enriched NSPC population from a heterogenous cell suspension and debris, cell cultures generated (General Methods 2.1.3) from a two-step OptiPrep™ gradient were compared with cell cultures generated with a Percol gradient. After 5DIV cells were fixed in 4% PFA and stained with antibodies for Gfap, Nestin, Tuj1 and with DAPI to assess the total number of cells in culture (General Methods 2.1.8). There was a significant difference in the total number of cells as assessed by DAPI (Unpaired t-test, $t_{(22)} = 2.712$, $p = 0.0127$) with 184.3 ± 29.92 cells/mm^2 and 90.78 ± 17.12 cells/mm^2 for cultures generated with OptiPrep™ and Percol respectively **(Fig.3.8 A)**. Significant differences were also observed in the total number of cells positive for Gfap (Unpaired t-test, $t_{(22)} = 2.511$, $p = 0.0199$) from 60.81 ± 11.76 cells/mm^2 to 26.86 ± 6.674 cells/mm^2 **(Fig.3.8 B)**, as well as Nestin (Unpaired t-test, $t_{(22)} = 2.821$, $p = 0.01$) from 64.02 ± 11.1 cells/mm^2 to 28 ± 6.309 cells/mm^2 **(Fig.3.8 C)**, Nestin+Gfap- (Unpaired t-test, $t_{(22)} = 3.127$, $p = 0.0049$) from 7.607 ± 1.031 cells/mm^2 to 3.758 ± 0.6730 cells/mm^2 **(Fig.3.8 D)** and Tuj1 (Unpaired t-test, $t_{(22)} = 2.195$, $p = 0.039$) from 28.83 ± 6.077 cells/mm^2 to 13.52 ± 3.422 cells/mm^2 **(Fig.3.8 E)**. However, there were no significant differences between the two culture conditions in terms of the percentage of each cell type **(Fig.3.8 F, G, H, I)**.

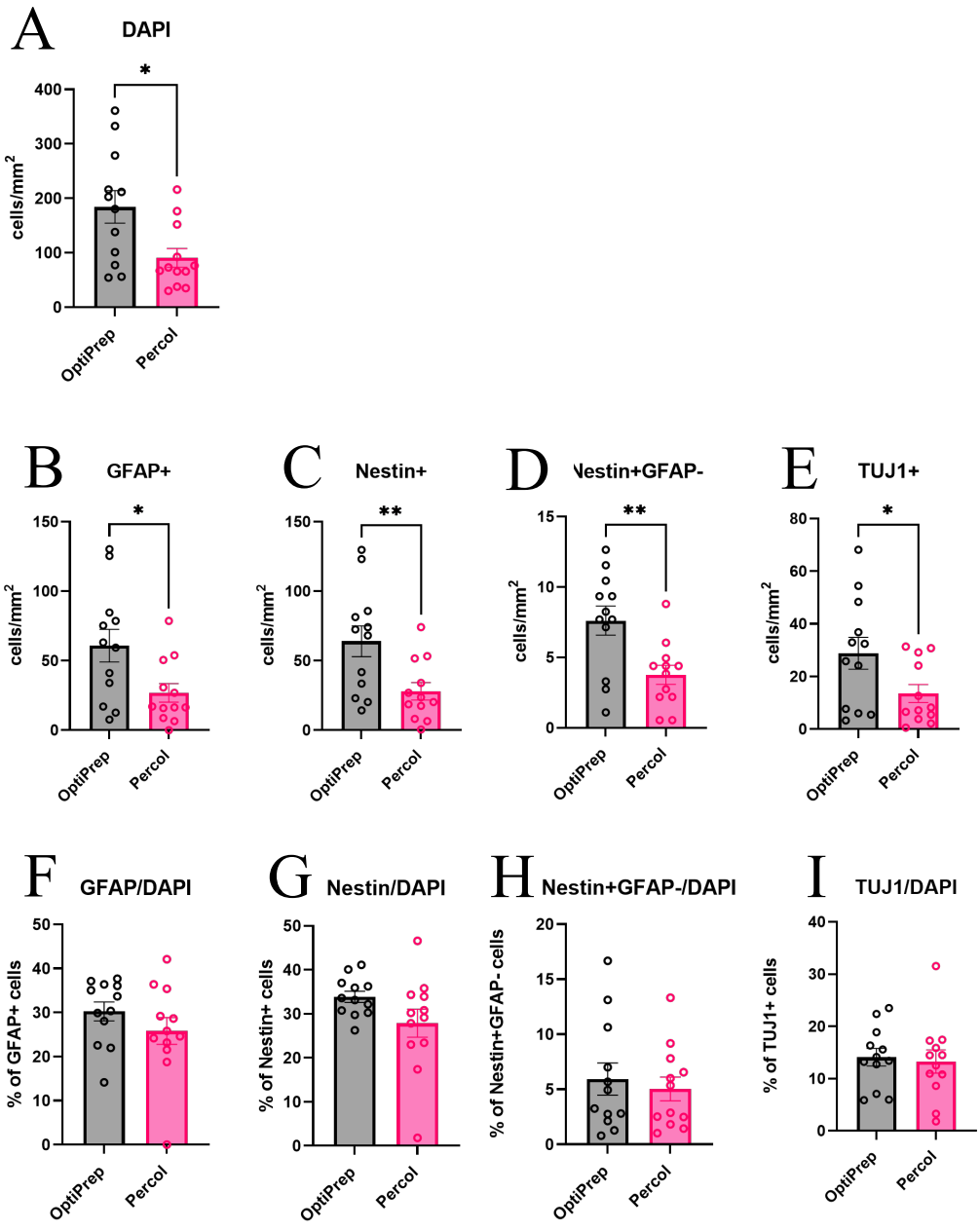

Figure 3.8 No difference is seen from using Percol over OptiPrep™ to isolate hippocampal NSPC's for culture experiments.

Hippocampal cell suspensions were split evenly between a Percol and OptiPrep™ gradient, plated and allowed to expand for 5DIV at which point cells were fixed and stained for Gfap, Nestin, Tuj1 and with DAPI. Total number of cells (A), total number of Gfap positive cells (B), total number of Nestin positive cells (C), total number of Nestin+Gfap- cells (D) and total number of Tuj1 cells (E) were counted. The percentage of Gfap (F), Percentage of Nestin (G), percentage of Nestin+Gfap- (H) and percentage of Tuj1 cells (I) with respect to DAPI was calculated. (N= 12 wells from 3 independent experiments. Data points represent mean ± SEM * = $p < 0.05$, ** = $p < 0.01$, *** = $p < 0.001$, **** = $p < 0.0001$.

3.3.0 Discussion

The aim of this chapter was to briefly characterise hippocampal NSPC cultures across 5 days in culture that were derived from postnatal day (P) 7-10 Sprague-Dawley rat pups in preparation for further experimental manipulation. The overarching aim is to use these hippocampal cultures to investigate a potential regional-specific neurogenic effect of microglia on neural stem cells. Therefore, a phenotypic base line of these cells needed to be established. Firstly, I have demonstrated that the cultures generated were stable across 5 days in culture and were capable of expanding NSPC cell populations as shown through expression of NSPC markers Nestin and Gfap with a smaller but stable neuronal cell population as observed through Tuj1 positive cells. I also showed that these cultures contained a substantial population of microglia. Secondly, the viability of hippocampal NSPC's improved considerably across 5 days in culture with greater than 80% of cells PI negative by day five. The fact that the number of viable cells across 5 days in culture increases, indicates that there are proliferating cells within this culture system, however, this would need to be confirmed with markers for proliferation. Thirdly, the number and percentage of type 1 neuronal progenitors increased across 5 days, while the number and percentage of type two neural progenitor cells was seen to decrease across this time point. Fourthly, attempts to optimise the NSPC cultures to increase levels of type 2 cells showed limited efficacy. This characterisation demonstrates this is a useful model to explore the effects of microglia on type 1 and type 2 NSPC populations.

Hippocampal neurogenesis is a process made possible by the existence of a pool of neural stem and progenitor cells within the neurogenic niche of the dentate gyrus. To model this *in vitro*, hippocampi from 8-16 Sprague-Dawley rat pups were enzymatically and mechanically

dissociated and enriched for neural progenitor cells using a two-step density gradient. This protocol was established by (Brewer 1997a) and adapted (Howell et al. 2003; Zaben et al. 2009; Nunan et al. 2014) to incorporate Optiprep™ a non- toxic solution comprised of iodixanol in water. Cells were plated on poly-L-lysine coated 24 well plates and maintained in culture for up to five days in culture using media devoid of serum and growth factors. In a mixed neuronal cell population derived from the neurogenic niche, one would expect representation of the main cell types including: neurons, progenitor cells and glial cells. In order to characterise these cultures, I examined the expression of typical markers associated with each of the main cell types found within the neurogenic niche which include Gfap for astrocytes and type 1 progenitor cells, Nestin for type 1 and type 2 progenitor cells, Tuj1 for immature neurons and IB4 for microglia in line with earlier studies (Howell et al. 2003; Zaben et al. 2009; Nunan et al. 2014). Previous work from our group demonstrated that at 5DIV the percentage of Nestin positive cells in hippocampal cultures under control conditions was 37.3% (± 3.4 SEM), Tuj1 positive cells 25.1% (± 2.4 SEM) and Gfap positive cells 28.4% (± 3.8 SEM) (Howell et al. 2003). Using the same methodology, at 5DIV my hippocampal cultures contained 25.13% (± 1.976 SEM) of Nestin positive cells, 16.74% (± 1.061 SEM) of Tuj1 positive cells and 28.7% (± 2.143 SEM) of Gfap positive cells (**Fig.1**). Although the levels of Gfap appear to be similar across studies, there is roughly a ten percent difference in the levels of both Nestin and Tuj1 positive cells. This might have been explained by the difference in sample size (n) used to assess the cultures. For Gfap the number of wells examined in both studies was 14, but for Nestin and Tuj1, Howell et al. (2003) used a much larger n number of 22 and 29 respectively. From a larger sample size, I would expect a smaller standard error of the mean, however this is not the case between these two experiments. In addition, Zaben *et al.* (2009) in one experiment showed that in control conditions the proportion of Gfap and Tuj1 cells was close

to 40% which may indicate inherent user to user variability present in producing these cultures despite using the same methodology. Inherent strain differences in neural progenitor populations between the two different strains of rat used could also explain these results. Here I used Sprague-Dawley rat pups whereas the studies above utilised Wistar rats. In accordance with this work, the number of Tuj1 positive cells in Howell *et al.* (2003) do not appear to significantly change across 5 DIV.

Type 1 progenitor cells also known as radial glial-like like cells are seen to be the putative progenitor cell of the sub granular zone. In histological mouse sections they have distinct morphology including a triangular shaped cell body with a distinct apical process reaching out and branching into the molecular cell layer (Kempermann et al. 2004a). To identify progenitor cells, I have examined Gfap and Nestin co-expression. Both Gfap and Nestin are types of intermediate filament protein and are traditional markers used to identify type 1 progenitor cells. These cells are thought to represent two thirds of the Nestin positive population *in vivo.* Type 1 cells can be quiescent or proliferative and are capable of dividing symmetrically or asymmetrically (Doetsch et al. 1999; Seri et al. 2001; Kriegstein and Götz 2003; Garcia et al. 2004; Kempermann et al. 2004a). Type 1 cells were seen to increase across 5 days in culture and contributed to 22.52% of total cells by day 5 (**Fig.2**). Interestingly, these cells comprised 89% of all Nestin positive cells by day 5 in culture. It is thought that type 1 cells are slowly dividing cells and account for only 5% of cell divisions in Nestin expressing cells, facilitated by asymmetrical cell division *in vivo*. Type 1 cells give rise to type 2 cells which show Nestin but not Gfap expression and are thought to be highly proliferative. Type 2 progenitor cells decreased across 5 days in culture from 4.6% at 1DIV to 2.6% at day 5DIV. Nunan (2009 – thesis) reported a Nestin+Gfap- population of 9.1% at 5DIV, whilst Zaben et al. (2009) showed a proportion greater than 1.5 with respect to the total cell population in one experiment under

control conditions. In perfect conditions I would expect type 1 progenitors to follow the neuronal lineage by first down regulating expression of Gfap and later upregulating doublecortin expression. As the cells differentiate into a post mitotic state doublecortin is down regulated and markers for immature and mature granule neurons can be visualised including NeuN, calretinin, calbindin, Tuj1 and Prox1 (Kempermann et al. 2004a). This differentiation pathway is by no means guaranteed as these cells are highly sensitive to changes in the microenvironment. There are therefore, many reasons that could underlie the differences observed between the studies mentioned above, including: a reduced mitotic activity of type 2 progenitors, a reduced capacity of type 1 progenitors to differentiate or there could be a drop off in survival of type 2 progenitors across time. In terms of microglia, (Nunan et al. 2014) reported that they comprised 11.38% of their hippocampal cultures as measured with IB4 staining at 5DIV, whereas I have reported almost double that with 20.37% of microglia (**Fig.3**). An increased population of endogenous microglia in these cultures' is could also be affecting the behaviour of the progenitor pool. Again, these disparities could be due to a strain differences in neurogenesis which has been demonstrated in the literature (Epp et al. 2011).

As well as showing that the hippocampal cultures contained the main cell types across 5 days in culture, I also showed that the cultures were highly viable (**Fig. 4**). After 5 days in culture over 80% of cells were shown to be PI negative. This in accordance with previous work in our lab which has shown a viability of 85% at 5DIV (Nunan 2009). In addition to this, there was an increase in the number of PI negative cells from 1DIV to 5DIV, indicating that there is cell proliferation within this culture paradigm. A traditional method used to assess proliferation and survival of cells whether that be *in vivo* or *in vitro* is to pulse cells with the thymidine analogue, 5-bromo-2-deoxyuridine (BrdU) which incorporates itself into the DNA of cells undergoing 'S' phase of the cell cycle. However, recently 5-ethynyl-2′-deoxyuridine (EdU) has been

favoured as its detection does not require harsh treatments of Hydrochloric acid like BrdU which can be damaging to sub nuclear structures. Instead of antibody binding, EdU uses a 'Click-it' technology which is seen to be more efficient and representative due to the strong linear relationship between EdU incorporation and detection (Salic and Mitchison 2008). To look at the survival of proliferating cells a pulse of EdU was applied to hippocampal cultures 2 hours after plating for 24hrs (**Fig.5**). After which the EdU was washed out. Parallel cultures were grown for 1, 3 and 5 days in culture and once processed showed that there was limited survival of proliferating cells. The long exposure time could have induced cell toxicity. A study using mouse embryonic stem cells treated with EdU for 30-minute pulse saw a marked reduction in the relative number of cells compared to BrdU and untreated controls after washout and a 48hr incubation with fresh media. A much longer pulse of 15hrs was also assessed, and this was seen to induce cell death zero hours post labelling. Cells treated with EdU for 30 minutes were also seen to have high rates of DNA damage compared to BrdU treatment or untreated controls (Kohlmeier et al. 2013). In hindsight, for my hippocampal cultures a much shorter pulse time frame should have been used and EdU toxicity could have been examined.

Several attempts were made to interrogate and optimise the culture methods used to generate the hippocampal cultures presented here. I examined plating density, fractions of the Optiprep™ gradient, speed of centrifugation, alternative density gradient mediums, rat strain and cell culture media. The principal method used for calculating cell plating density was trypan blue exclusion using a haemocytometer. A viable cell count is important particularly for cell culture as the aim is for viable cells to proliferate and differentiate in culture which has been shown to be highly dependent on cell density where paracrine signalling of growth factors from supporting cells and neurons is needed. It has been suggested that cells plated at less than

10^4 cells/cm^2 die within days (Kaneko and Sankai 2014). Trypan blue exclusion performed with a haemocytometer is a traditional method of cell counting whereby a sample of cells is taken from a single cell suspension and trypan blue is applied. Once mixed the sample is applied across a haemocytometer and the number of live cells is determined using a light microscope, with the convention that bright cells that have not taken up the dye are alive and those that have are dead due to a compromised cell membrane. While it is fairly inexpensive method of determining cell viability, it is dependent on the experience of the user being able to accurately discriminate between live and dead or dying cells. Although manual cell counting has been shown to produce similar results to automated techniques there is always going to be an element of human error (Cadena-Herrera et al. 2015). I compared manual cell counting using trypan blue exclusion with an automated method- the Muse – a bench-top flow cytometer in conjunction with a live/dead labelling kit. At the same time, I compared plating density of 100,000 cells/ml with 200,000 cells/ml. Cells plated using Muse cells counts produced a greater number of total cells at both plating densities but was only significantly different from the manual count when plated at 200,000 cells/ml. A similar pattern was seen for both Nestin and Gfap counts. For cells plated at 100,000 cells/ml with Muse counts, the percentage of Nestin and Gfap approximately equalled those plated at 200,000 cells/ml in both conditions. There was no positive impact on type 2 progenitor cells or Tuj1 positive cells from plating density or the counting method used. From this experiment I established that cells counted using the Muse and plated at 100,000 cells/ml were most optimal.

Next, I proceeded to interrogate the Optiprep™ gradient which was used to enrich for neural progenitor cells and reduce cellular debris. Enriched cells used for plating were usually taken from the interface of the two Optiprep™ fractions. However, I was concerned that I could be

missing some important cells that were left within the gradient. I compared plated cells taken from the phase at the interface of one column with cells plated from a second column where the whole gradient was taken. On the premise that if there were a missing population of cells in the gradient then it would be present when cultured. Upon analysis, there were no significant differences between cells plated from the Optiprep™ interface and cells plated from the whole gradient after 5 DIV under standard conditions. This was further investigated in a second set of experiments whereby the speed of which the centrifuge was spun to pellet the cells within the Optiprep gradient was examined alongside the two phases of cells that are visible upon centrifugation. After centrifugation of the Optiprep™ gradient, two cell bands become apparent. One at the interface of the two Optiprep™ fractions termed the lower fraction and another band which sits on top of the 10 % Optiprep™ fraction termed the upper fraction which should largely be composed of cellular debris. Centrifuge speeds were chosen from previous studies in our lab and the original paper on which the method was adapted from (Brewer 1997b; Howell et al. 2003). There were no significant differences observed between the two centrifuge speeds which were compared. The lower fraction of the Optiprep™ gradient showed a trend for a greater number of total cells compared to the upper fraction although there was a large amount of variance. The only parameter which was significantly different between the upper and lower fraction was the percentage of Gfap was increased in the upper fraction. Again, no gains were made in Nestin+Gfap- or Tuj1 positive cell populations.

Then, I investigated whether a different density gradient would have any impact on the number of type 2 progenitor cells in culture at 5DIV. The use of a density gradient to isolate distinct cell populations relies on cell types within a heterogenous population to sediment at a separate isopycnic point. This is where the density of the cells and the density of the media are equal. I

compared plated cells at 5DIV from 2 density gradients, one made with Optiprep™ using our standard isolation protocol and the other using a Percoll density gradient using the protocol from (Walker and Kempermann 2014). Like Optiprep, Percoll is a commercially available medium. Percoll consists of colloidal silica particles coated with polyvinylpyrrolidone which has a low osmolarity and low viscosity. Many groups have used Percoll density gradients to isolate neural progenitors from primary tissue with successful results (Ramírez-Rodríguez et al. 2009; Babu et al. 2011; Walker and Kempermann 2014). Cells plated from the Optiprep™ density gradient out performed those generated from the Percoll density gradient for total cell count, Gfap count, Nestin count, Nestin+Gfap- count and Tuj1 count. Despite this, there were no significant difference in the percentages of these cell populations between the cells plated from the two types of gradients used. These results indicated that both media were satisfactory for enriching and generating neural progenitor cultures, however in this case Optiprep™ performed marginally better. While density gradients are an inexpensive method of cell separation and enrichment, they can display low specificity, low purity and low throughput. Some studies have taken enrichment protocols a step further using fluorescence activated cell sorting (FACS) and magnetic activated cell sorting (MAC) to isolate and enrich neuronal progenitors for cell culture. (Bowles et al. 2019) used MAC to enrich for neural progenitor cells from iPSC derived cells using Cd271- and Cd133+ selection markers. MAC isolation was seen to improve neural progenitor homogeneity and reduce contaminating cell types such as glia. While this may be beneficial for generating homogenous iPSC lines it is a relatively expensive method and I was not concerned with homogeneity in the cultures presented here.

Some groups advocate the use of growth factors such as Epidermal growth factor (EGF) and Fibroblast growth factor (FGF-2) to promote survival and expansion of NSPC's *in vitro*

(Pollard and Conti 2007). FGF-2 has also been used to induce proliferation of quiescent neural progenitors from non-neurogenic brain regions including, the septum and striatum of adult rats (Palmer et al. 1995b). I have chosen not to use growth factors in these cultures as hippocampal neurogenesis is an inherently complex process for which the use of exogenous growth factors has the potential to conceal effects of the conditions applied. This is supported by the demonstration that hippocampal NSPC's are capable of secreting large quantities of endogenous vascular endothelial growth factor (Vegf) *in vivo* and *in vitro* (Kirby et al. 2015). Endogenous Vegf secretion may promote the expansion of NSPC's via EGF receptor signalling and may also promote the expansion of microglia (Kreisel et al. 2019; Liu et al. 2019). In addition, during the generation of these hippocampal cultures serum free media has been used. Serum is a component of some cell culture media that provides vital metabolites and growth factors. However, serum also contains blood borne factors that microglia in the healthy CNS would not normally come into contact with, which has the potential to activate them (Bohlen et al. 2017).

3.3.1 Limitations

A critical limitation of the monolayer model is the lack of recapitulating the morphological structure and typical behaviour that is found within the brain. For example, it has been noted that 2D culture of fibroblasts and osteogenic cells leads to altered morphology including cell flattening and changes to internal cytoskeletal architecture (Knight and Przyborski 2015). Alterations in cell shape can be driven by environmental factors such as temperature, plasma osmolarity and surface interaction. As a consequence, the shape of the nucleus can also be affected and this has been shown to be associated with changes in gene expression via

chromatin remodelling (Bidwell et al. 1993). However, where 2D culture systems lack in recapitulating *in vivo* morphology they make up for by allowing for a highly controlled model system that provides a platform for standardised assays, for example: cells in a monolayer system receive uniform exposure to experimental conditions that is not necessarily true of 3D models. The more complex a system the less control you have over it, therefore, by utilising the monolayer system, the microenvironment can be tightly controlled, regulated and manipulated, providing reproducible results. Individual cells can be monitored and investigated with regards to motility, morphology and other phenotypic parameters in a way which is not feasible in 3D models. Monolayers are an artificial and reductionist model but they provide the opportunity to disentangle mechanism from multiple converging pathways. As with all *in vitro* models: they show what cells are capable of doing, but not necessarily what they actually do *in vivo*.

3.4 Conclusion

In conclusion, I have established that the hippocampal NSPC cultures generated from p7-10 rat pups are stable and viable across 5 days in culture in growth factor and serum free conditions. The cultures show characteristic cell types including Nestin, Gfap, Tuj1 and IB4 positive cells which are indicative of astrocytes, stem cells, immature neurons and microglia. I have also demonstrated that there are both type 1 and type 2 neural progenitor cells present in these cultures, denoted by the presence of Gfap+Nestin+ and Nestin+Gfap- cells respectively. These cultures were seen to have a low surviving rate of proliferating cells that were pulsed on day 0 for 24hrs, however, as a long exposure to EdU can be toxic to cells this should be further investigated with a shorter pulse of EdU. Further investigations would endeavour to assess the phenotype of these cultures to a higher depth by utilising a greater range of markers for stem

cells (Sox2, Blbp), mature astrocytes (S100b) and neuronal populations (Dcx, NeuN). The presence of oligodendrocytes and other cell types could also be looked at as well as further investigating the source of the proliferating population with both EdU and ki-67. Additional investigations aimed to increase the abundance of type 2 neural progenitors showed limited differences to control conditions. Further investigations could look at the adherent substrate as well as media components. Previous groups in our lab have also used different strains of rat, so this could also be another investigative factor. I decided to move forward with this model and apply experimental parameters in the next chapter.

4.0 Investigating the neurogenic role of microglia in hippocampal neural stem/ progenitor cells in culture

4.1.0 Introduction

A common denominator among many neurological and psychiatric disorders is cognitive impairment, a condition that can include: learning and memory impairments, difficulties in concentrating and problems with making decisions that affect an individual's everyday life. These include neurodegenerative and mood disorders such as Alzheimer's disease and depression. Age related disorders particularly are on the rise globally with the world health organisation predicting the proportion of the world's population over sixty years old will double to approximately two billion people. This will result in many more people with neurodegenerative disorders and will be a major contributor to disease burden worldwide with huge socioeconomic consequences. (Aimone et al. 2009; Anacker and Hen 2017; Toda et al. 2019). Therefore, the neurogenic niche of the hippocampus may represent a good target to develop preventative, curative and replacement therapeutics. Despite its importance, adult hippocampal neurogenesis is a poorly understood biological process. What controls and regulates this phenomenon in neurogenic niches as well as drivers of its perturbation remain uncertain. One approach to investigating these questions is to look directly at how its dysregulation is caused and contributes to neurological dysfunction. Alternatively, investigating the regulation of hippocampal neurogenesis under 'normal' conditions may

provide a means of 'turning up the volume' in a targeted way on this process. A logical place to begin investigating is the local microenvironment of the neurogenic niche. There are many components that could be explored but here I have chosen to focus on microglia the resident macrophage of the brain. They are highly dynamic cells that have various roles in the brain including surveillance, homeostasis, synaptic pruning, phagocytosis, cell signalling and clearance of waste without initiating an inflammatory response. Previous work in our lab has demonstrated the addition of microglia or microglia conditioned media to hippocampal NSPC increased cell survival as well as proliferation of Nestin positive cells (Nunan et al. 2014). This as well as other reports in the literature make microglia an attractive player to investigate further in terms of their neurogenic potential.

4.1.1 Evidence for pro-neurogenic effect of microglia in embryonic neurogenesis

Embryonic neurogenesis begins in the early days of embryogenesis, peaking at embryonic day 17 in mice and gestation week 25 in humans, where upon the phenomenon is largely relegated henceforth to the neurogenic niches of the SVZ and SGZ (Malik et al. 2013). This lends to the idea that microglia in the SGZ of the adult dentate gyrus and other neurogenic niches retain an embryonic-like phenotype. Evidence suggests that during embryonic neurogenesis, microglia play an important role in regulating the size of the progenitor pool (Tong and Vidyadaran 2016). Not inconsequentially, microglia are known to infiltrate the brain at the same time as the emergence of radial glial cells during mid-gestation and cluster in regions such as the ventricular and sub ventricular zones and thus places them at key neurogenic zones (Ginhoux et al. 2010a; Arnò et al. 2014). Furthermore, *Csf-1r* and *Pu.1* knockout (KO) models have provided insights into the possible roles of microglia during embryo-neurogenesis (Ginhoux et

al. 2010b; Nandi et al. 2012; Kierdorf et al. 2013) *Csf-1r* KO mice, whilst lacking microglia, show expanded populations of Nestin positive neural progenitor cells in the neocortex compared to wild types. This uncontrolled proliferation of neural stem cell populations in *Csf-1r* KO mice may indicate that microglia, under normal conditions in embryos, play a role in neurogenesis by acting to promote neural precursor cells to exit their proliferative state. E15.5 and P20 mice lacking Csf-1r also display reductions of mature excitatory neuronal subtypes demonstrated by reduced numbers of Ctip2+ and Cux1+ cells compared to wildtypes, suggesting microglia play a further role in neuronal differentiation (Nandi et al. 2012). These studies position microglia as an important player in embryonic neurogenesis by influencing the behaviour, differentiation or survival of neural progenitor pools and their progeny. This pro-neurogenic phenotype of microglia observed across the brain in embryonic neurogenesis may be maintained postnatally and into adulthood, in regions where neurogenesis is preserved such as the SGZ and SVZ.

4.1.2 Evidence for pro-neurogenic effect of microglia in postnatal neurogenesis

Increasing evidence demonstrates that unchallenged microglia play important roles in the neurogenic zones by clearing apoptotic cells (Sierra et al. 2010; Diaz-Aparicio et al. 2020). (Sierra et al. 2010) showed that in mice there is a large proportion of apoptotic cells within the sub granular layer of the dentate gyrus compared to other hippocampal regions and that these cells die within the first four days of their creation during the transition from amplifying neural progenitor to neuroblast. Microglia that phagocytosed apoptotic cells in the SGZ displayed a ramified morphology indicating an unchallenged state which was further corroborated by a negative expression of Cd68, a marker known to be expressed in activated microglia. This

important phagocytic action of unchallenged microglia prevents the toxic contents of cells spilling out causing a detrimental inflammatory response to the surrounding neuronal tissue (Nagata et al. 2010). Furthermore, by chronically impairing phagocytosis pathways using *P2ry12* KO and *MerTK/Axl* KO mouse models, (Diaz-Aparicio et al. 2020) showed that adult hippocampal neurogenesis was impaired compared to wildtype controls demonstrated by a reduction in doublecortin positive cells. Microglia can also contribute to the neurogenic environment by releasing proliferative agents such as Tgf-β and Bdnf (Battista et al. 2006; Parkhurst et al. 2013). Microglia co-culture studies where microglia have been pre-treated with pro or anti neurogenic agents before culture with neuronal progenitor cells show that microglial phenotype can have a direct consequence on the proliferation and differentiation of progenitor cells within their local microenvironment (Butovsky et al. 2006). Previous work in our own lab, has demonstrated that the addition of untreated hippocampal microglia or their conditioned media to hippocampal NSPC cultures display a pro-neurogenic effect at 5DIV (Nunan et al. 2014). However, to my knowledge it has not been shown functionally whether microglia from different brain regions have a differential effect on the proliferation and differentiation of hippocampal neural progenitor cells. I would expect microglia from the hippocampus to have a greater proliferative effect on neural progenitor cells compared to microglia from other brain regions owing to the fact that the hippocampus contains a proliferative region known as the dentate gyrus and therefore microglia from this region may have a phenotype suited to this role.

4.1.3 Transcriptomic data supports regional dependant differential microglial gene expression

Advancements of genetic tools in recent years have produced results supporting the idea that microglia possess distinct time and regional dependant phenotypes. These advances have allowed phenotypic profiles of microglia to be probed at new depths specifically with advances in single cell sequencing and multi-omic technologies. Studies have now shown that microglia RNA expression varies across developmental time points as well as brain location, which may reflect adaptive changes in microglial function that are dependent on local microenvironment (Doorn et al. 2015; Grabert et al. 2016; Matcovitch-Natan et al. 2016; Hammond et al. 2019). One study using genome-wide chromatin expression profiling alongside single cell transcriptomics has demonstrated dynamic alterations in microglial transcriptional phenotype. Microglial phenotypes were seen to correlate with specific developmental time points defined as: yolk sac, early microglia, pre-adult and adult. The pattern of developmental gene expression in microglia was also shown to be susceptible to perturbations when the system is challenged (Matcovitch-Natan et al. 2016). For example, changes in gene expression were observed following microbiome challenges and prenatal immune activation. To add to this, microglia have been shown to possess distinct region-specific phenotypes with regards to their transcriptional profiles throughout the adult lifespan (Grabert et al. 2016). By isolating microglia from the cortex, cerebellum, hippocampus and striatum through density gradients and immuno-magnetic separation, principal component analysis showed that microglia RNA clustered away from each other in a regional dependant manner. These new insights are leading the field away from a dichotomous view of microglia phenotype (M1-pro-inflammatory/M2-

anti-inflammatory) to a broad spectrum that is highly dependent on the local environment and its interactions (Ransohoff 2016). Furthermore, microglia in the dentate gyrus show a differential gene expression to microglia in the CA1 of the hippocampus (Kreisel et al. 2019). Altogether, by showing that the microglial transcriptome varies along the spatiotemporal axis, these studies support the hypothesis that microglia in neurogenic zones could have a unique transcriptional phenotype which is reflective of the function in their local microenvironment. This has not been functionally demonstrated so far in the literature and here I aim to do so.

4.1.4 Isolation of primary microglia

Microglia, the innate immune cells of the central nervous system have proven a fascinating cell population to investigate in recent years, as demonstrated by the vast expansion of work in this area. Microglia research has branched out from solely looking at their role in immune function to investigating potential non-immune functions such as synaptic pruning (Weinhard *et al.* 2018). Microglia possess a reactive immune function which is vital for an organism's protection from pathogens. As microglia are known to be highly sensitive to their microenvironment any isolation protocol is likely to alter its basal phenotypic state, thus adding a layer of complexity in their isolation and study (Ju et al. 2015; Lin et al. 2017; He et al. 2018). For this reason, is it important to select an isolation method not only appropriate to the experimental design but also in which minimises endogenous changes in microglia phenotype. Isolation procedures of microglia from primary tissue are generally split into two main threads: direct isolation either by Cd11b+ magnetic beads and FACs, or downstream isolation from mixed glia cultures (Bohlen et al. 2019).

Culture of microglia has historically been the most widely used paradigm to investigate their phenotypic and functional properties due to its simplicity and relative in-expense (Chamak and Mallat 1991; Appel ' et al. 1995; Tanaka et al. 1998; Kitamura et al. 2000; Duke et al. 2004; Tamashiro et al. 2012; Ju et al. 2015; Lam et al. 2017; Lin et al. 2017). To generate microglia from mixed glia cultures, primary tissue is dissociated into a single cell suspension via mechanical and or enzymatic digestion and re-plated in the presence of serum -which promotes the expansion of glia cells. Mixed glia are then grown *in vitro* for 7-10 days depending on plating densities and the presence or absence of growth factors such as M-csf. When cell culture vessels are coated with an adherent substrate such as poly-L-lysine astrocytes strongly attach to the bottom of plastic ware with microglia weakly attached on top of the astrocytes. Microglia can then be isolated to a high degree of purity either by physical shaking of the culture plates or by using trypsin to enzymatically detach microglia. In both cases microglia become detached and float in the culture media which can subsequently be collected re-suspended and used in experimental paradigms. However, recent evidence suggests that the gene expression of microglia is altered by the culturing process (He *et al.* 2018). As a result, direct isolation procedures of microglia from tissue have arisen and allow for highly sensitive gene sequencing assays to be performed. One method utilises Cd11b, a common cell surface maker for monocytes, macrophages and microglia. The protocol exploits magnetic beads which have been bound to a Cd11b antibody (Marek et al. 2008). Cd11b bound magnetic beads are incubated with a mixed population of cells in suspension, which is then applied to a magnetic column, whereby cells expressing Cd11b will bind with the beads and are attracted to the magnetic column. In this way microglia can be removed from a mixed cell suspension and moved to a separate solution by removal of the magnetic field. The second method for direct isolation utilises flow cytometry technology to sort microglia that are fluorescently labelled. This can be achieved either by incubation with a microglial specific fluorescently labelled

antibody or through the use of transgenic animals whereby microglia are fluorescently labelled for example, with GFP under a microglial specific promotor such as *Cx3cr1*. Both of these direct methods as well as general handling of cells have the potential to alter intrinsic microglia gene expression, however, this is thought to be minimal (Box et al. 2020). One way to reduce these effects further has been to implement a cold isolation procedure where cells are kept at 4^{o}C throughout such as that used by Hammond *et al.* (2019). Here, microglia were generated from mixed glial cultures and further extracted via shaking so that the population can be expanded for experimental use and so that the replication of previous work can be achieved.

4.1.5 Aims

This general aim of this chapter was to investigate whether there are functional, differential regional neurogenic effects of microglia on hippocampal NSPCs. This question was investigated *in vitro* using microglia - hippocampal NSPC co-culture paradigm where cells were derived from postnatal Sprague-Daley rat pups unless stated otherwise. This was evaluated using immunocytochemistry and immunofluorescence microscopy by examining markers associated with neuronal progenitor populations and immature neurones.

- Aim 1: Assess the purity and viability of microglia obtained from mixed glial cultures post isolation.
- Aim 2: Investigate the neurogenic potential of microglia on hippocampal NSPC cultures in a microglial regional dependant manner.

There were no significant differences observed between hippocampal NSPC cultures treated with hippocampal and cortical microglia or their respective conditioned media. However, hippocampal NSPC cultures were shown to have increased rates of Nestin progenitor cells when treated with hippocampal microglia at high concentrations compared to control conditions suggesting a trophic action.

4.2.0 Results

4.2.1 Microglia isolation from mixed glial cultures by shaking at 1.61 x g

In order to assess the purity of microglial isolated from mixed glial cultures hippocampal and cortical mixed glial cells generated (General Methods 2.1.4) and grown in parallel for 7DIV or until confluent. Plates were then shaken at 1.61 x g for 10 or 20 mins at 37°C. All media was collected and pooled, and cells were re-plated at 100,000cells/ml. 24hrs after plating, cells were stained with IB4 and DAPI for 2 hours prior to live imaging (General Methods 2.1.6). An unpaired t-test showed no significant difference for total cell counts of hippocampal derived cells ($t_{(14)} = 1.617$, $p = 0.1282$) between 10 (193.8 ± 26.89 cells/mm^2) and 20 (333.6 ± 82.16 cells/mm^2) mins, although a trend can be seen (**Fig.12 A**). There was also no significant difference in the total number of IB4 positive cells ($t_{(14)} = 1.599$, $p = 0.1322$) or in the percentage of IB4 positive cells ($t_{(14)} = 0.2594$, $p = 0.7991$) between hippocampal derived cells at 10 or 20 minutes (**Fig.12 B, C**). Importantly, the percentage of IB4 positive cells for both 10 ($92.92 \pm 0.7035\%$) and 20 ($92.69 \pm 0.5688\%$) minutes exceeded 90%.

For cortical derived cells, a significant difference can be seen in total cell counts between 10 (158.1 ± 22.28 cells/mm^2) and 20 (329.2 ± 30.05 cells/mm^2) minutes of shaking ($t_{(14)} = 4.575$, $p = 0.0004$) (**Fig.12 D**). A significant difference in the total number of IB4 positive cells was also seen between 10 (142.1 ± 25.24 cells/mm^2) and 20 (311.3 ± 31.64 cells/mm^2) minutes of shaking ($t_{(14)} = 4.179$, $p = 0.0013$) (**Fig.12E**). No significant difference in the percentage of IB4 positive cells ($t_{(14)} = 0.9383$, $p = 0.3556$) was seen in cortical derived cells but again both cells obtained at 10 ($92.04 \pm 0.9501\%$) and 20 ($93.01 \pm 0.3975\%$) mins of shaking reached a purity

above 90% (**Fig.12 F**). From this data, I decided to obtain microglia from this point onwards using a speed of 1200 rpm for 20 mins as the greatest number and greatest purity could be obtained.

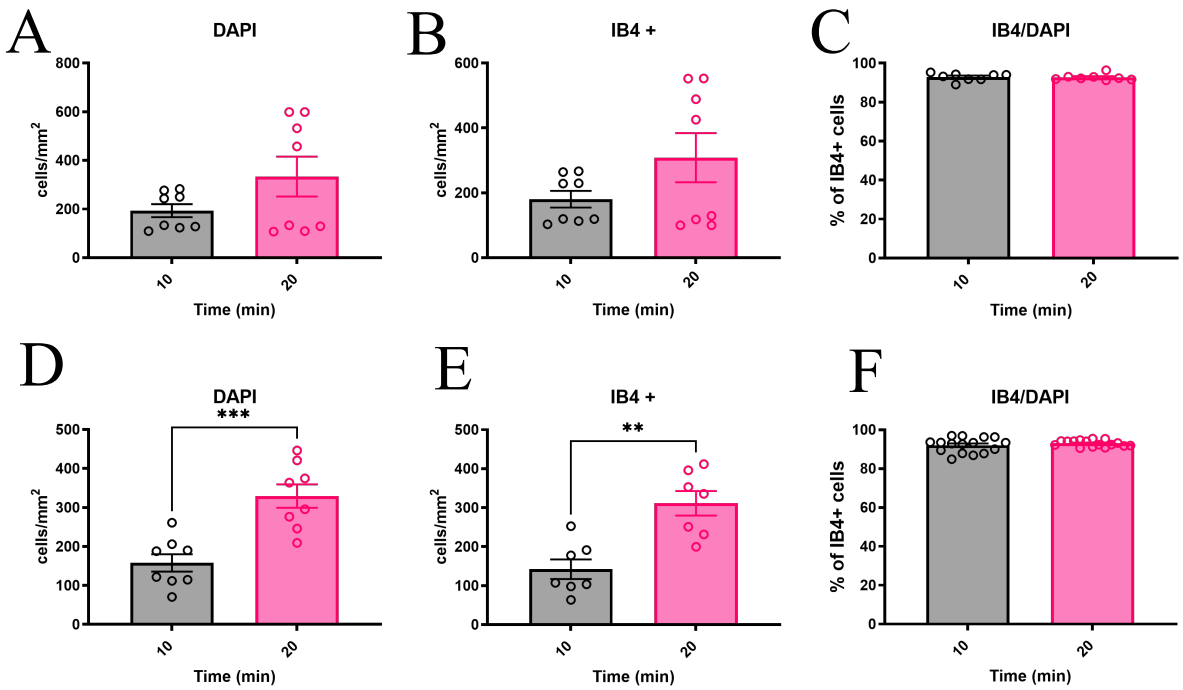

Figure 12. Microglia isolated from mixe glia display over 90% purity.

Mixed glial cultures were shaken at 1.61 x g for 10 or 20 minutes, the media was collected, and the resulting cells were replated. Hippocampal microglia (A-C) were live imaged 24hrs later, total cell count (A), total IB4 positive cell count (B) and percentage of IB4 positve cells (C) were recorded. Cortical microglia (D-F) were assessed in the same way, for total cell count (D), total IB4 positive cell count (E), and percentage of IB4 positive cells (F). N = 8 wells from 2 separate experiments. Data points represent mean ± SEM. * = $p < 0.05$, ** = $p < 0.01$, *** = $p < 0.001$, **** = $p < 0.0001$

4.2.2 Microglia are viable 24hrs post isolation

To determine microglial viability post isolation from mixed glial cultures, hippocampal microglia were isolated as previously stated (General Methods 2.1.4). Cells were then live imaged 24hrs post plating. 2hrs prior to imaging cells IB4, PI (a marker for dead cells) and DAPI were applied and subsequently washed off (General Methods 2.1.6). Total number of

DAPI positive cells (**Fig.13 A**) (334.2 ± 39 cells/mm^2), total number of IB4 positive cells (232.1 ± 40.55 cells/mm^2) and total number of PI positive cells (1.237 ± 0.346 cells/mm^2) were recorded. Percentage of IB4 positive cells (**Fig.13 B**) (93.65 ± 1.536 %), percentage of PI positive cells (**Fig.13 C**) (0.4108 ± 0.087 %) as well as the percentage of live microglia (**Fig.13 D**) (99.59 ± 0.106 %, IB4+PI-/DAPI) were calculated (Fig.3). This indicates that the majority of microglia survive isolation by shaking for at least 24hrs.

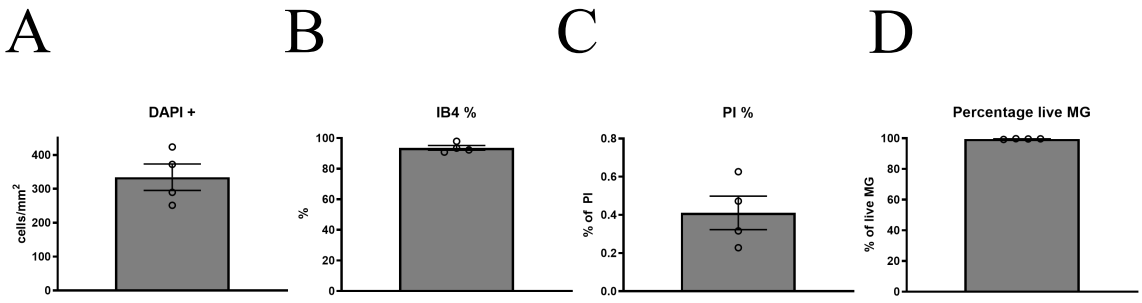

Figure 13. Microglia are viable 24hrs post isolation.

Mixed glial cultures were shaken at 1200 rpm for 20 minutes, cells in suspension were collected, counted and replated. Cells were live imaged 24hrs later, total cell count (A), percentage of IB4 positve cells (B), percentage of PI positive cells and the percentage of live cells (C) were calculated. N = 4 wells from 1 experiment. Data points represent mean ± SEM.

4.2.3 NSPC treated with cortical or hippocampal microglia

In order to investigate the effect of adding microglia directly to hippocampal NSPCs. Microglia were isolated from the hippocampus and neocortex and expanded in parallel in mixed glial cultures and then further isolated (General Methods 2.1.4). Microglia were directly applied to hippocampal NSPCs at 100,000 cells/ml, 500µl/well, 2hrs post plating. A one-way ANOVA was performed which showed a significant difference in the total number of cells ($F_{2,9}$=7.257, p = 0.0133) with post hoc tests demonstrating a significantly greater total number of cells in hMG (192.1 ± 26.25 cells/mm^2) and cMG (215.8 ± 35.85 cells/mm^2) treated cultures compared

to control (85.24 ± 5.129 cells/mm^2) treated cells (**Fig.14 A**). This is an expected result as a significant amount of microglia were added directly to the NSPC cultures. There was no significant difference in the total number of Gfap, Nestin or Tuj1 positive cells between groups (**Fig.14 B, C, D**). There was however, a significant difference in the percentage of GFAP positive cells ($F_{2,9}$= 7.075, p = 0.0142) (**Fig.14 E**). Post hoc testing showed a significant decrease from control (34.74 ± 5.052%) to cMG (18.38 ± 0.4191%) conditions but no difference was observed between hMG and cMG conditions. Similarly, there was a significant difference in the percentage of TUJ1 cells ($F_{2,9}$= 15.75, p = 0.0011), with post hoc tests showing a significant reduction from control (15.27 ± 1.436%) to hMG (7.011 ± 1.697%) and control to cMG (4.256 ± 1.147%) (**Fig.14 G**). There was no significant difference between hMG and cMG. The reduction in GFAP and TUJ1 percentage is most likely attributed to the increase in total cell number caused by the addition of microglia.

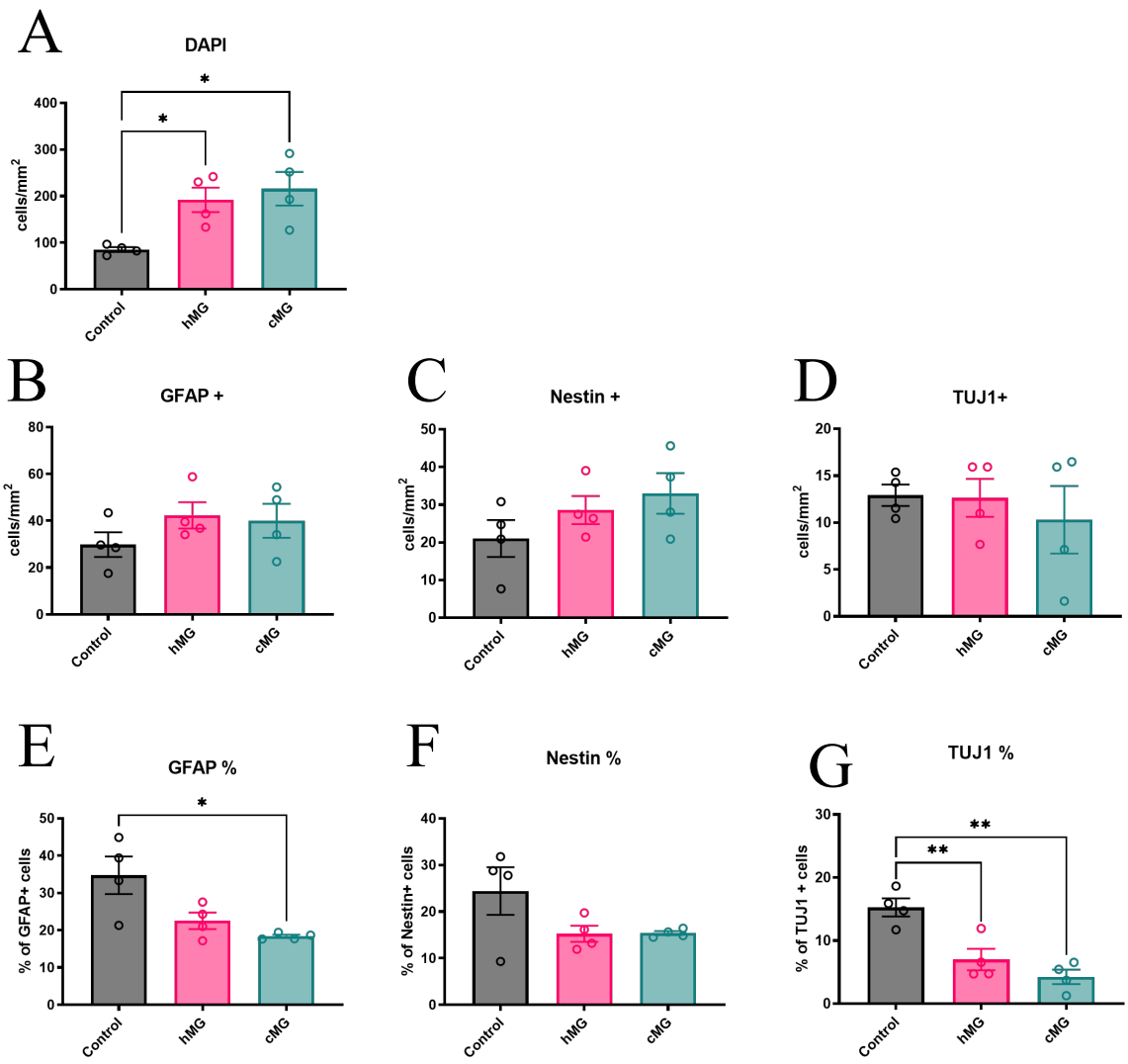

Figure 14. Addition of microglia at 100,000 cells/ml has no effect on phenotype of NSPC.

Total number of cells (A), total number of GFAP positive cells (B), total number of Nestin positive cells (C) and total number of TUJ1 cells (D) were recorded. Percentage of GFAP (E), percentage of Nestin (F) and percentage of TUJ1 cells (G) were calculated. N = 4 per condition from 1 experiment. One-way ANOVA with Tukey post hoc tests. Data points represent mean ± SEM. * = $p < 0.05$, ** = $p < 0.01$.

4.2.4 NSPC treated with cortical or hippocampal microglial conditioned media

Previously our group has demonstrated that the addition of hippocampal microglia or its conditioned media to hippocampal NSPC cultures produced a significant pro-neurogenic effect (Nunan et al. 2014). This was shown to induce an increase in the total number of Nestin and

TUJ1 positive cells as well as increasing the proportion of Nestin positive cells compared to control conditions. This led to the hypothesis that microglia in the hippocampus display distinctive pro-neurogenic properties compared to microglia in non-neurogenic regions. In order to test this hypothesis, microglia were isolated from the hippocampus and cortical regions and expanded in parallel in mixed glial cultures and then further isolated (General Methods 2.1.4). The microglial conditioned media was generated (General Methods 2.1.7) and upon collection, filtered and snap frozen if necessary. Conditioned media generated from cortical and hippocampal microglia were applied to separate wells of hippocampal NSPC's 2 hours after plating as well as control group which received conventional media. At 3DIV cultures 2/3rds of the microglia conditioned media or control media was changed. At 5DIV cells were washed, fixed and later stained for Gfap, Nestin, Tuj1 and counter stained for DAPI. After imaging and counting a one-way ANOVA was performed between control, hMGCM and cMGCM treated cells. There were no significant differences between groups in the total number of cells, total number of Gfap, Nestin or Tuj1 positive cells or in their respective percentages (**Fig.15**).

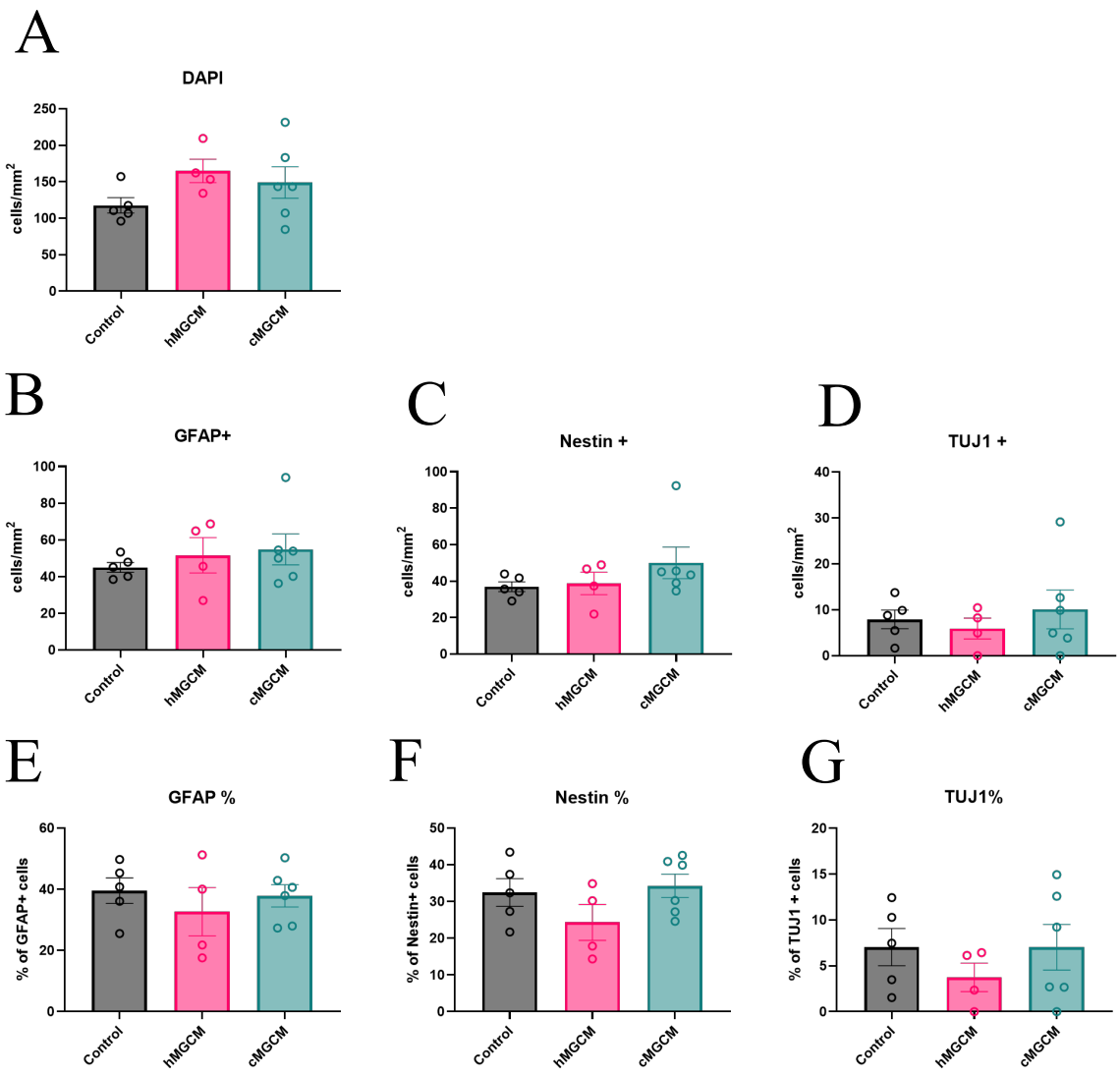

Figure 15. No significant differences observed between hippocampal microglia conditioned media (hMGCM), cortical microglial conditioned media (cMGCM) on the phenotype of hippocampal NSPC's at 5DIV.

Total number of cells (A), total number of GFAP positive cells (B), total number of Nestin positive cells (C) and total number of TUJ1 cells (D) were recorded. Percentage of GFAP (E), percentage of Nestin (F) and percentage of TUJ1 cells (G) were calculated. N = 5 wells for control, 4 wells for hMGCM, 6 wells = cMGCM from 1 experiment.

4.2.5 Dose response of hippocampal microglia on hippocampal NSPC

To determine the effect of different microglia concentrations directly applied to hippocampal NSPC cultures (General Methods 2.1.3), microglia were harvested from mixed glial cultures, washed, counted and added to the hippocampal cultures at the concentration specified (General

Methods 2.1.4). Cultures were grown for 5DIV with a 2/3rd media change at day 3. At 5DIV cells were fixed and stained for Nestin, Gfap, Tuj1 and counterstained for DAPI (General Methods 2.1.8). A one-way ANOVA showed a statistically significant difference for the total number of cells ($F_{2,9}$= 10.98, p =0.0038), with Tukey's multiple correction showing a significant increase between control (85.24 ± 5.129 cells/mm^2) vs 100,000 MG/ml (192.1 ± 26.25 cells/mm^2) and control vs 400,000 MG/ml (240.2 ± 31.67 cells/mm^2) but not between 100,000 MG/ml vs 400,000 MG/ml (**Fig.16 A**). There was a significant difference in the total number of Nestin positive cells between groups ($F_{2,9}$=5.452, p = 0.0281) with post hoc tests showing a significant increase from control (21.03 ± 4.8 cells/mm^2) to 400,000 MG/ml (56.51 ± 12.42 only cells/mm^2) only (**Fig.16 B**). Similarly, for the total number of Gfap positive cells there was a significant difference between groups ($F_{2,9}$= 6.843, p =0.0156) with post hoc tests showing a significant increase from control (29.83 ± 5.296 cells/mm^2) to 400,000 MG/ml (68.33 ± 10.46 cells/mm^2) only (**Fig.16 C**). There were no significant differences observed between groups for both Nestin and Gfap percentages (**Fig.16 E, F**). There were no significant differences observed between groups when looking at the total number of Tuj1 positive cells (**Fig.16 D**), however the percentage of Tuj1 cells was significantly different ($F_{2,9}$= 12.33, p = 0.0026). Post hoc tests revealed a significant decrease in control (15.27 ± 1.436%) vs 100,000 MG/ml (7.011 ± 1.697%) and control vs 400,000 MG/ml (5.778 ± 1.240%) but not 100,000MG/ml vs 400,000 MG/ml (**Fig.16 G**). These results are difficult to interpret as the addition of microglia directly to the cultures significantly alters the total number of cells, however, the addition of microglia at both conditions had no significant effect on the number of Tuj1 positive cells.

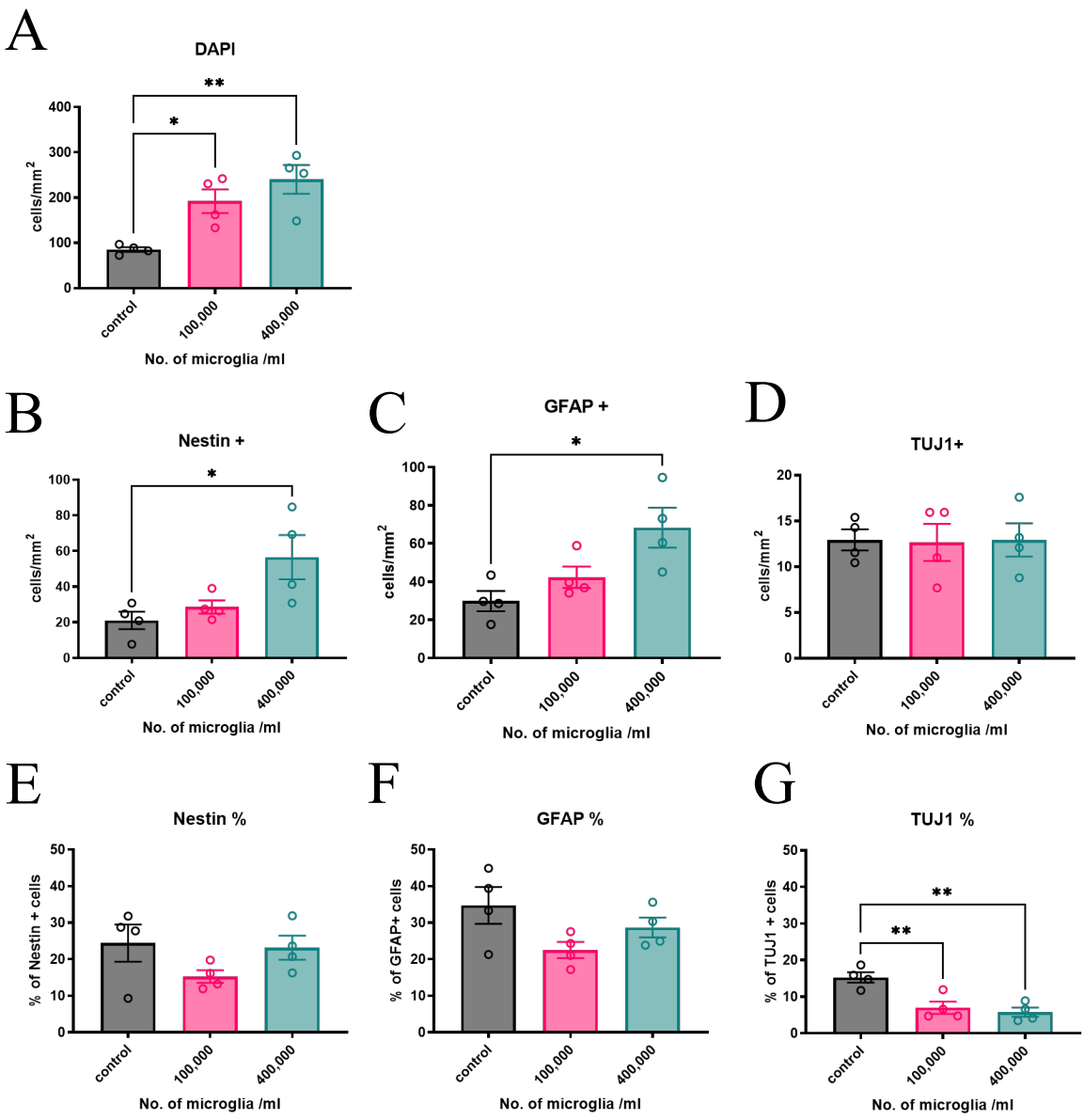

Figure 16. Addition of 400,000 hippocampal microglia/ml showed a significant increase in the total number of Nestin and Gfap positive cells compared to control conditions. The addition of microglia at 100,000 cells/ml and 400.00cels/ml decreased the percentage of TuJ1 positive cells with respect to control conditions.

Microglia (100,000 cells/ml, 400,000 cells/ml) or control media were directly applied to hippocampal NSPCs 2 hours post plating at grown for 5DIV. Total number of cells (A), total number of Nestin positive cells (B), total number of GFAP positive cells (C), and total number of TUJ1 positive cells (D) were recorded. The percentage of Nestin positive cells (E), percentage of GFAP positive cells (F), and the percentage of TUJ1 (G) cells were calculated with respect to DAPI. N = 4 wells per condition from 1 independent experiment. Data points represent mean ± SEM. One-way ANOVA with Tukey post hoc tests. * = $p < 0.05$, ** = $p < 0.01$.

4.2.6 Dose response of hippocampal microglia conditioned media

In order to assess how the percentage of microglia conditioned media would affect hippocampal NSPC cultures, parallel cultures were generated (General Methods 2.1.3) and 2 hours post plating the corresponding microglial condition media was applied (General Methods 2.1.7). Cells were treated with 0% (standard NSPC media), 25%, 50% 75% or 100% microglial conditioned media. Cells were allowed to grow for 5DIV at which point they were fixed in 4% PFA and stained for Nestin, Tuj1 and counterstained with DAPI (General Methods 2.1.8). One-way ANOVA showed a significant difference in total DAPI counts between conditions (**Fig.17 A**). ($F_{4,35} = 7.793$, $p = 0.0001$). Dunnett's post hoc tests were all conditions were compared to the control (0%) showed a significant difference between 0 (77.4 ± 6.5 cells/mm^2) and 50% (152.5 ± 16.77 cells/mm^2), 0 and 75% (172.3 ± 23.48 cells/mm^2) and 0 and 100% (227.1 ± 29.21 cells/mm^2). There was a significant difference in the total number of Nestin positive cells between conditions (**Fig.17 B**) ($F_{4,35} = 6.825$, $p = 0.0004$). Dunnett's post hoc tests showed a significant difference between 0 (28.39 ± 3.47 cells/mm^{2}5) and 50% (67.71 ± 7.025 cells/mm^2), 0 and 75% (81.87 ± 13 cells/mm^2) and 0and 100% (104.4 ± 16.56 cells/mm^2). There was also a significant difference in the percentage of Nestin positive cells (**Fig.17 D**) ($F_{4,35} = 2.677$, $p = 0.0477$). Post hoc tests showed a significant difference between 0 (36.31 ± 2.681%) and 75% (46.70 ± 2.36%) and 0 and 100% (45.71 ± 2.69%) of conditioned media. There was no significant difference between conditions in the total number of Tuj1 positive cells as assessed by one-way ANOVA ($F_{4,35} = 0.7218$, $p = 0.5829$) (**Fig.17 C**). However, there was a significant difference in the percentage of Tuj1 cells between conditions ($F_{4,35} = 33.2$, $p < 0.0001$) (**Fig.17 E**). Dunnett's post hoc test showed a significant difference between 0% and all other levels, 0 (28.17 ± 1.916%) and 25% (18.55 ± 1.241%), 0 and 50% (13.77 ± 1.01%), 0 and 75% (12.38

± 0.6738%) and 0 and 100% (10.95 ± 0.8128%). Surprisingly, the addition of MGCM at all levels appeared to produce a marked decrease in the percentage of Tuj1 cells and interestingly the highest levels of MGCM display an increased percentage of Nestin positive cells.

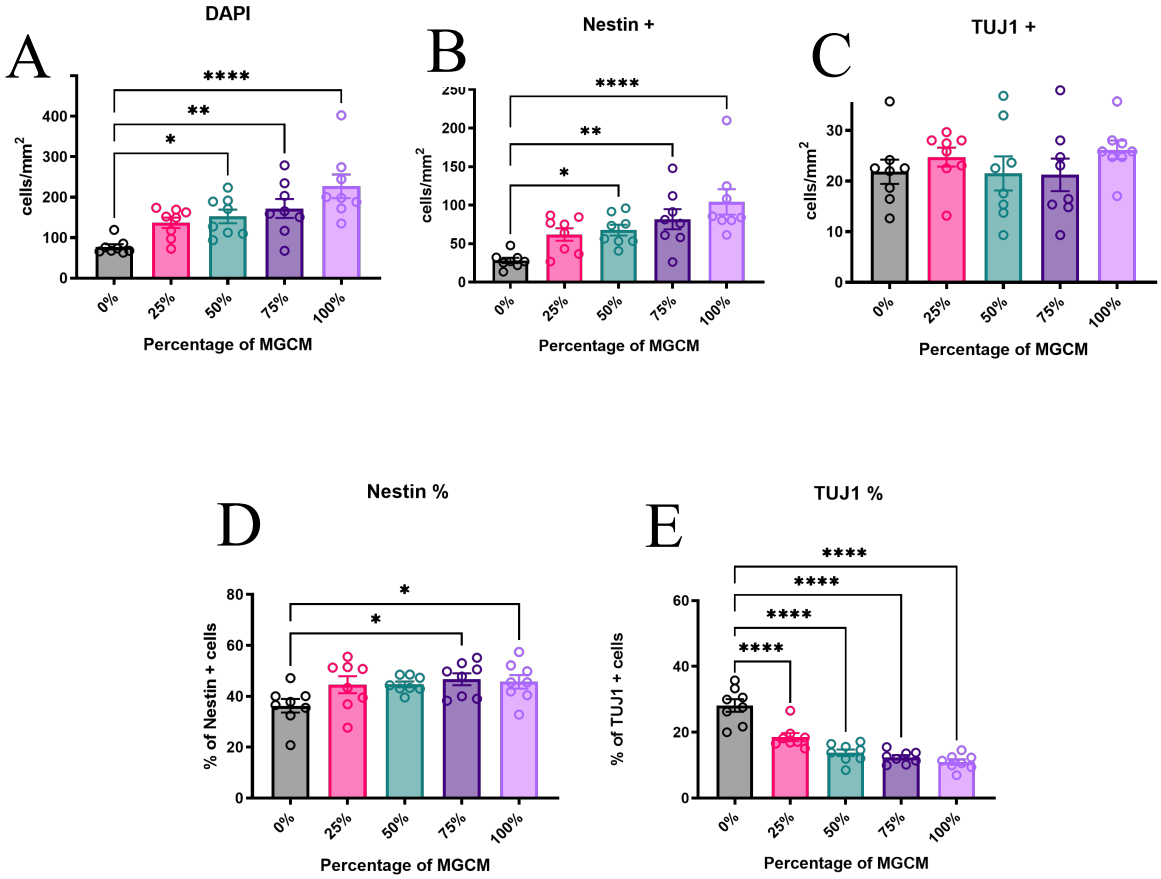

Figure 17. The addition of hippocampal microglia conditioned media to hippocampal NSPC's decreases the percentage of Tuj1 positive cells at all levels.

Hippocampal NSPC cultures were generated and two hours later microglial conditioned media (MGCM) was added to parallel cultures at 0, 25, 50, 75 and 100%. Cells were allowed to expand for 5DIV with a 2/3rd media change at 3DIV. Cells were were fixed and stained. Total number of cells (A), total number of Nestin positive cells (B) and total number of Tuj1 cells (C) were recorded. Percentage of Nestin cells (D) and percentage of Tuj1 positive cells (E) were calculated from the total number of cells. N = 8 wells from 2 separate experiments. Data points represent mean ± SEM. One-way ANOVA with Tukey post hoc tests. * = $p < 0.05$, ** = $p < 0.01$, *** = $p < 0.001$, **** = $p < 0.0001$.

4.2.7 NSPC treated with a high concentration of cortical or hippocampal microglia

Hippocampal NSPC cultures showed significant differences in total numbers of Gfap and Nestin positive cells where hippocampal microglia were added at a concentration of 400,000 cells/ml. Therefore, to determine if these effects where specific to microglia derived from the hippocampus, microglia were isolated and expanded from hippocampi and cortex p7-10 rat pups *in vitro*. Once microglia had expanded sufficiently they were isolated (General Methods 2.1.4) and then directly applied at 400,000 microglia/ml to hippocampal NSPC cultures (General Methods 2.1.3) 2hrs after plating. At 5DIV cultures were washed, fixed and stained for Nestin, Gfap, Tuj1 and counterstained for DAPI (General Methods 2.1.8). A One-way ANOVA was performed which showed significant differences in the total number of cells ($F_{2,9}$= 21.38, p = 00004), with post hoc tests showing a significantly greater number in cultures where hMG (240.2 ± 31.67 cells/mm^2) and cMG (285.4 ± 22.74 cells/mm^2) had been added compared to control (85.24 ± 5.129 cells/mm^2) (**Fig.18 A**). There was no significant difference between hMG and cMG treated wells for total number of cells. As in **4.2.5** the difference in total cell number is likely due to the addition of a significant number of cells. There was a significant difference between groups observed in the total number of Gfap positive cells ($F_{2,9}$= 5.128, p = 0.0326), with post hoc testing showing a greater number of Gfap positive cells in cultures where hMG (688.33 ± 10.46 cells/mm^2) were added compared to control (48.12 ± 8.909 cells/mm^2) but no difference was observed between cultures treated with hMG an cMG (**Fig.18 B**). There was no significant difference observed between groups for total number of Nestin positive cells (**Fig.18 C**). There was no significant difference observed between groups for total number of Tuj1 positive cells (**Fig.18 D**). In terms of percentages, there was a significant difference in Gfap ($F_{2,9}$= 7.133, p = 0.0139) with post hoc tests showing a significant

decrease from control (34.74 ± 5.052%) to cMG (16.44 ± 1.921%) treated cultures only (**Fig.18 E**). There was also a significant difference across groups for the percentage of Tuj1 ($F_{2,9}$= 26.98, p = 0.0002) in cultures that were treated with hMG (5.778 ± 1.240%) or cMG (4.173 ± 0.6330%) compared to control (15.27 ± 1.436%) but not between hMG and cMG which is likely a reflection of the significant increase in total cell number due to the direct addition of MG (**Fig.18 G**). There were no significant differences in the percentage of Nestin positive cells across groups (**Fig.18 F**). These results suggest that there were no observed differential effects of microglia derived from the two different brain regions at high concentrations on the number of immature neurons generated or number of stem cells in culture.

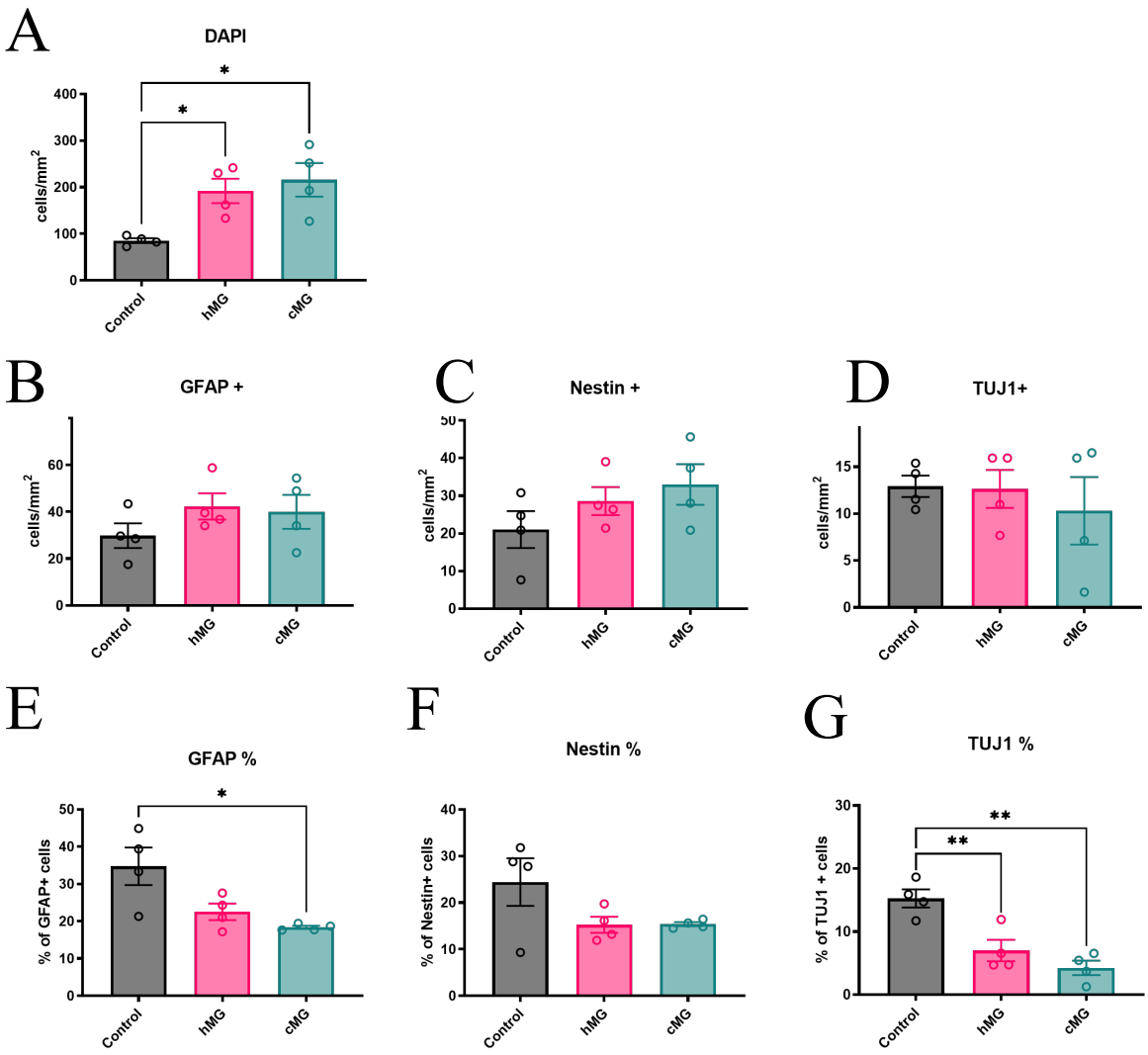

Figure 18. The addition of 400,000 Hippocampal derived microglia show an increased percentage of Gfap positive cells.

Microglia were isolated from either the hippocampus or the cortex and expanded in mixed glial cultures. Once isolated microglia were applied to hippocampal NSPC cultures 2hrs post plated. AT 5DIV cells were fixed and stained. Total cell number (A), total number of GFAP positive cells (B), total number of Nestin positive cells (C), and total number of TUJ1 positive cells (D) were recorded. The percentage of GFAP positive cells (E), percentage of Nestin positive cells (F) and percentage of TUJ1 positive cells (G) were then calculated. N = 4 wells per condition from 1 independent experiment. Data points represent mean ± SEM. One-way ANOVA with Tukey post hoc tests. * = $p < 0.05$, ** = $p < 0.01$, *** = $p < 0.001$.

4.2.8 No observed difference between Sprague-Dawley or Wistar derived microglial conditioned media on hippocampal NSPCs

Using Wistar $P_{7\text{-}10}$ rat pups, (Nunan et al. 2014), demonstrated that the addition of microglial conditioned media to hippocampal NSPC cultures increased cell survival and NSPC

proliferation as compared to control conditions. Whilst attempting to replicate these results, as described above, both microglia (General Methods 2.1.4) and hippocampal NSPC cultures were generated (General Methods 2.1.3) using Sprague-Dawley rat pups. There is some evidence that strain differences in neurogenic responses exist in rodents (Epp et al. 2011). To determine whether there are strain differences in the neurogenic potential of microglia, microglia conditioned media was generated from both Wistar and Sprague-Dawley $p_{7\text{-}10}$ pups as previously described for microglial densities of 50,000cells/ml, 100,000 cells/ml and 200,000cells/ml. Hippocampal NSPC cultures were generated from Sprague-Dawley pups as described previously and the microglia conditioned media was applied 2hrs post plating with two thirds of the media changed at 3DIV. At 5DIV cells were washed and fixed in PFA and later stained for Gfap, Nestin, Tuj1 and counterstained with DAPI (General Methods 2.1.8). Cells were then imaged using a fluorescent microscope. A two-way ANOVA showed no significant differences observed in the total number of cells, total number of Gfap positive cells, total number of Nestin positive cells, total number of Tuj1 positive cells and in the percentage of TUJ1 positive cells between cells treated with Wistar and Sprague-Dawley derived microglial conditioned media (**Fig.19 A, B, C, D**). For the percentage of Gfap positive cells (**Fig.19 E**) there was a significant difference between microglial density ($F_{2,34}$=6.809, p =0.0033), however, there was no significant differences for rat strain or for the interaction between them. Similarly, for the percentage of Nestin positive cells (**Fig.19 F)** there was a significant difference in microglial density ($F_{2,34}$= 6.146, p = 0.0053), however, there were no significant differences for rat strain or for the interaction between them. This set of results indicates that under these specific parameters there are no discernible differences between the effects of Sprague-Dawley and Wistar derived microglia conditioned media on Sprague-Dawley derived hippocampal NSPCs.

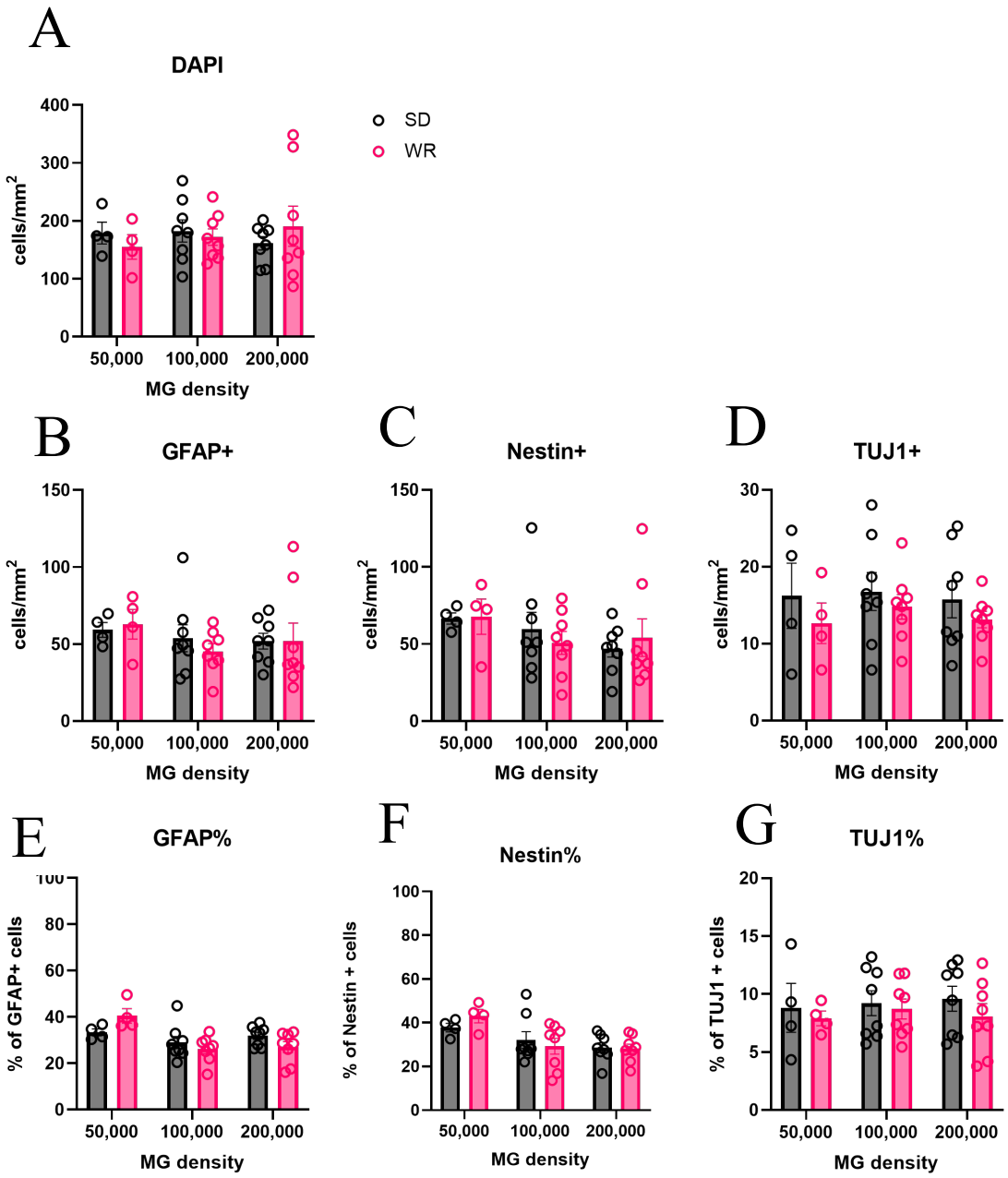

Figure 1. No significant difference in phenotypes was observed between hippocampal NSPC treated with Sprague-Dawley or Wistar derived microglia conditioned media.

Hippocampal NSPC cultures generated from Sprague-Dawley P7-10 rat pups were treated with microglial conditioned media which was generated either from Sprague-Dawley or Wistar rat pups at varying microglial densities. After 5DIV cells were fixed stained and imaged. Total number of cells (A), total number of GFAP positive cells (B), total number of Nestin positive cells (C) and total number of TUJ1 cells (D) were recorded. Percentage of GFAP positive cells (E), percentage of Nestin (F) and percentage of TUJ1 positive cells (G) were then calculated. (N= 8 wells from 2 independent experiments. Data points represent mean ± SEM * = $p < 0.05$, ** = $p < 0.01$.)

4.2.9 No effect of media type used to generate microglial conditioned media on hippocampal NSPCs at 5DIV

To generate microglia for direct application or to produce microglial conditioned media, mixed glial cultures were first made. Microglia were then subsequently isolated by a method of shaking (General Methods 2.1.4). Mixed glial cultures were produced by dissociating neuronal tissues and plating resulting cells in a serum containing medium. The main component of this media is DMEM. Once microglia are isolated and allowed to settle for two hours, the media is switched to a serum free media of which the main component was neurobasal A (NBA) and B27. To determine if the switching of the main component of the media used to generate microglia for microglia conditioned media affected the phenotype of hippocampal NSPCs treated with microglial conditioned media, parallel hippocampal NSPC cultures were generated (General Methods 2.1.3) and treated with microglia conditioned media generated as previously described or from media that was generated from mixed glial cultures that were grown exclusively in NBA containing media. Cells were fixed at 3 and 5DIV and stained and imaged (General Methods 2.1.8). A two-way ANOVA was performed where no statistical differences were observed for the total number of cells (**Fig.20 A)**, the number and percentage of Gfap positive cells (**Fig.20 B, E)** and the number and percentage of Tuj1 cells (**Fig.20 D, G)** for media type or DIV. There was no significant difference for the total number of Nestin positive cells (**Fig.20 C)**, however, for the percentage of Nestin positive cells (**Fig.20 F)** there was a significant difference for media type ($F_{1,24}$ =4.122, p = 0.0484) which was confirmed by post hoc testing to show a greater percentage of Nestin positive cells for NBA (29.135 ± 2.777%) than DMEM (22.827 ± 1.03%) at 3DIV but not at 5DIV. These results suggest that the media the microglia were first plated and expanded in (mixed glial cultures) generally had no significant effect on hippocampal NSPC phenotype at 5DIV in these set of experiments.

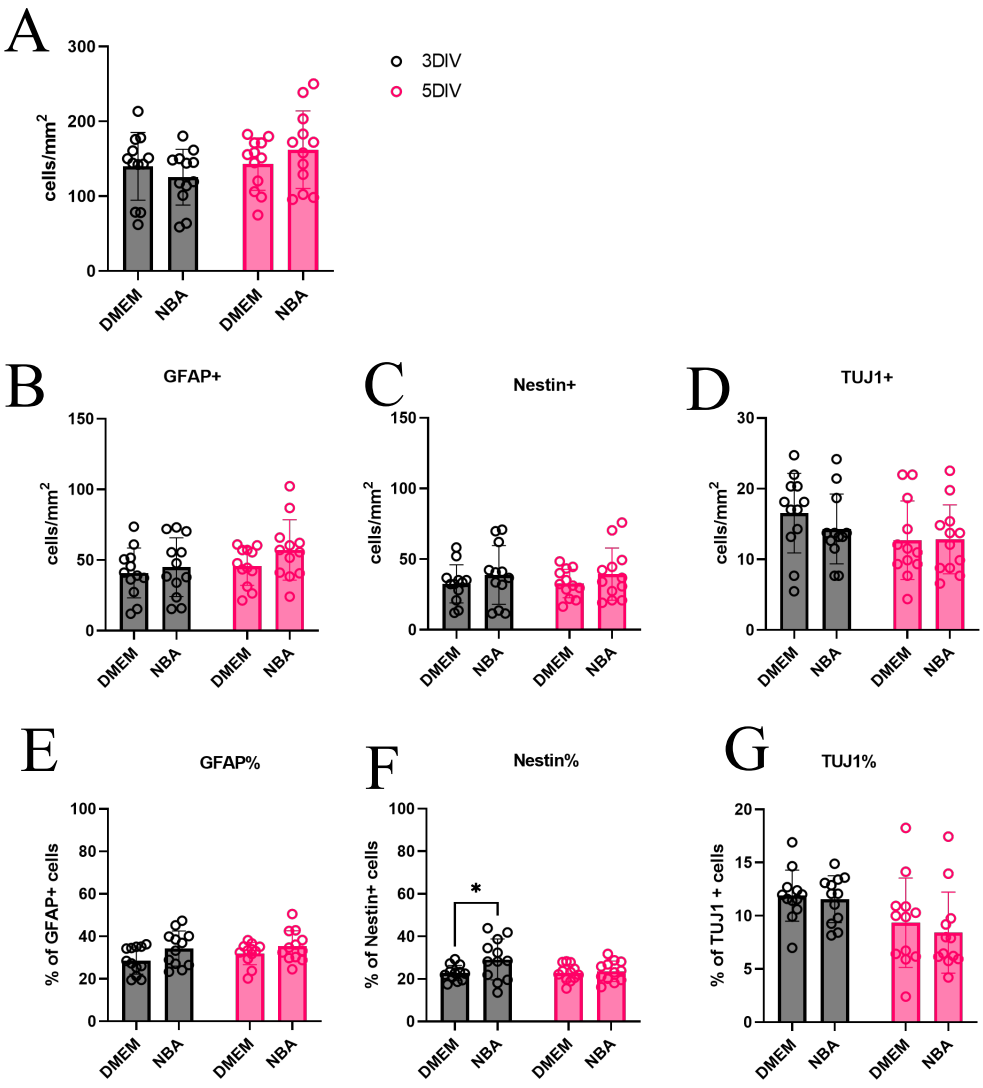

Figure 2. No effect of media type used to generate microglial conditioned media on hippocampal NSPC's at 5DIV.

Hippocampal NSPC cultures were treated with microglial conditioned media which was generated from microglia which were generated in medium containing DMEM or Neurobasal A (NBA). After 3 or 5DIV cells were fixed stained and imaged. Total number of cells (A), total number of GFAP positive cells (B), total number of Nestin positive cells (C) and total number of TUJ1 cells (D) were recorded. Percentage of GFAP positive cells (E), percentage of Nestin (F) and percentage of TUJ1 positive cells (G) were then calculated. (N= 12 wells from 2 independent experiments. Data points represent mean ± SEM * = $p < 0.05$)

4.3.0 Discussion

The aim of this chapter was to examine potential functional, regional differences in the neurogenic effect of microglia upon hippocampal NSPC cultures derived from postnatal day (P) 7-10 rat pups and examine potential variables that could contribute to discrepancies seen in this and previously published data. Firstly, I have demonstrated that microglia isolated from mixed glial cultures via shaking were isolated to a high degree of purity and were viable 24hrs after isolation. Secondly, I compared the addition of hippocampal microglia (or their conditioned media) to hippocampal NSPC's to the addition of cortical microglial to hippocampal NSPCs. Here, no significant differences were observed between the addition of hippocampal and cortical microglia at previously reported concentrations on the populations of neural progenitors or neuronal populations. Thirdly, hippocampal microglia or their conditioned media added to hippocampal NSPC cultures at high concentrations (400,000 MG/ml or 75% and 100%) produced an increase in Nestin positive populations compared to control conditions, suggesting a trophic effect. When microglia from the cortex and hippocampus were then compared at high density or high concentration in conditioned media, there were no significant effects on hippocampal NSPCs between the two conditions. However, microglia isolated from both the cortex and hippocampus showed a reduced population of immature neurons compared to control conditions. as the proportion of Tuj1 positive cells remained consistent throughout investigations.

It is important to be able to distinguish microglia from other myeloid cells when purifying them from other cell types. However, to date there are limited markers that display definitive expression across all microglial states and that are effective across different methodologies. A

common method used to delineate between microglia and other myeloid cell contaminants is fluorescence activated cell sorting (FACS) using an immune panel of antibodies that is expressed in both microglia and other myeloid populations with differential bimodal expression patterns. Typically, Cd11b and Cd45 are the markers of choice which are both cell surface markers expressed in these populations. In microglia the expected pattern of expression is Cd11b+/Cd45low and in other myeloid cells such as monocytes it is Cd11b+/Cd45high (Sedgwick et al. 2006). These markers are highly effective for use in FACS where gating parameters allow a high degree of specificity, however these show limited efficacy in immunocytochemistry assays when using multiple markers. The marker, Iba1 is a pan microglial marker that's is used widely in both rodents and human studies (Ito et al. 1998). However, Iba1 has also reportedly been shown to be upregulated in microglia of tissue that has undergone damage and therefore may be an indication of an activated microglial state (Ito et al. 2001). More recently, Tmem119, a transmembrane protein highly expressed on the cell surface of microglia has been described as a highly specific microglia marker (Bennett et al. 2016; Satoh et al. 2016). However, since publication, Tmem119 has been shown to be highly expressed in mouse and human cells but not in rat. Here, microglia were isolated from mixed glial cultures from both the hippocampus and cortex (not shown) to a high degree of purity by detaching microglia via shaking. This was visualised and assessed with a pre-conjugated Isolectin B4 (IB4) antibody, a classical microglial marker shown to be expressed at all stages of microglial activation (Lünemann et al. 2006). In their native environment, microglia are known to be highly ramified, however, under stress conditions this phenotype is lost and they take on an ameboid like morphology (Ziebell et al. 2015). As a consequence, it is difficult to recapitulate the ramified morphology of microglia in culture and therefore it is possible that I will be observing the effects of stressed microglia in culture to some degree. Whether regional differences remain in this stressed state is to be investigated.

Previously in our group, it was shown that the addition of hippocampal microglia (100,000 cells/ml) to hippocampal NSPC cultures produced a significant pro-neurogenic effect (Nunan et al. 2014). The addition of microglia as well as its conditioned media was shown to induce an increase in the total number of Nestin and Tuj1 positive cells as well as increasing the proportion of Nestin positive cells compared to control conditions. This led us to hypothesise that microglia in the hippocampus displayed distinctive pro-neurogenic properties compared to microglia in non-neurogenic regions. In order to test this hypothesis, microglia were isolated from the hippocampus and cortical regions and expanded in parallel in mixed glial cultures and then further isolated. Upon purification, microglia were either directly applied to hippocampal NSPC cultures or were used to generate microglia conditioned media. The use of microglial conditioned media allows microglial derived signals to be applied to NSPC without reciprocal action of microglia then responding to that effect, e.g. microglia may start to perform excessive pruning or apoptosis in response to proliferative effect. The addition of hippocampal and cortical microglia or their conditioned media to hippocampal NSPC's were then compared between each other and with control media. There were no significant differences observed between hippocampal and cortical microglia on hippocampal NSPC populations under these conditions. As a consequence of these results, the microglial cell density and concentration that were applied to the hippocampal NSPC cultures were investigated. In hindsight, pre-labelling of microglia with a pre-conjugated antibody such as IB4 before adding to the NSPC cultures would have been beneficial in teasing out the effects on cell type specific proportions and provided a more accurate representation of Nestin/Gfap and Tuj1 populations. When using a high density or high concentration of microglial conditioned media I was able to show an increase in the number of Nestin positive cells in alignment with previous work, however, this was accompanied with a decrease in the proportion of Tuj1 positive cells. Microglia from

hippocampal and cortical regions were then compared at high density and concentration but again there were no significant differences observed between their effects oh hippocampal NSPCs. This coupled with the decrease in the proportion of Tuj1 cells observed upon the addition of microglia conditioned media led me to interrogate my basal hippocampal NSPC cultures further.

As stated earlier, prior work in our lab has demonstrated a pro-neurogenic effect on hippocampal NSPCs via the addition of hippocampal microglia using primary cells derived from Wistar rats (Nunan et al. 2014). During this study I have extracted microglia and generated hippocampal NSPC's from Sprague-Dawley rat tissue. It is known that there can be strain specific differences in rodents in terms of behaviour, physiology and sensitivity to stimuli (Epp et al. 2011; Cacao et al. 2018). For example, strain differences between Sprague-Dawley and Long Evans rats have been examined using the, hippocampus dependant, Morris water task followed by a comparison of neurogenesis (Epp et al. 2011). They showed that spatial learning increased cell survival and the number of immature neurons in Sprague-Dawley rats compared to Long-Evans rats. This may provide some explanation with regards to opposing results where studies have used a similar paradigm. Therefore, I sought to examine whether there were neurogenic strain differences in microglia between Sprague-Dawley and Wistar rats. I compared the effect of hippocampal microglial conditioned media generated from Sprague-Dawley and Wistar rats on Sprague-Dawley hippocampal NSPC's at varying microglial concentrations. Microglia conditioned media was preferred over the addition of microglia directly to the cultures as this would lead to results that were more easily interpretable, but there is always a question of whether it is direct signal or contact from the microglia themselves which is needed. No significant differences were observed between NSPC cultures treated with Sprague-Dawley and Wistar hippocampal microglia conditioned media at any density of

microglia density. To fully examine this question, it would have been beneficial to also examine the conditioned media upon hippocampal NSPC cultures generated from Wistar rats, however, due to poor rat breeding there was not enough animals to provide sufficient tissue. In addition to investigating differences in rat strain, the type of media used to generate mixed glial cultures were also investigated to see if this had a significant impact on the effect of the isolated microglia. Previous studies have isolated pure microglial from mixed glial cultures using media containing Neurobasal A or DMEM (Moussaud and Draheim 2010; Tamashiro et al. 2012; Nunan et al. 2014; Ju et al. 2015; Lin et al. 2017). No significant differences were observed at 5DIV between cultures that were treated with microglia generated from mixed glia cultures whose media was based in DMEM or Neurobasal A. As there was no observable difference between NSPC treated with microglia isolated in different types of media, this may demonstrate the strong effect of serum on microglia phenotype and function (Bohlen et al. 2017).

4.3.1 Limitations

Due to unforeseen events, some of the experiments here have not been repeated or have reduced numbers of wells used. This was due to a lack of tissue availability resulting from inconsistent rat breeding. An additional problem when trying to examine the effect of microglial concentration on NSPC is generating enough microglia to accommodate all conditions which also made replicating experiments challenging. Furthermore, in this chapter, microglia that were isolated to generate microglia conditioned media or for direct application to NSPC were derived from the hippocampus and the neocortex of post-natal rats. A pro neurogenic microglia phenotype may be specific to the dentate gyrus of the hippocampus and therefore this effect

may be masked by microglia from the rest of the hippocampal regions. Moreover, experimental paradigms were evaluated over 5DIV and it could be that microglial effects on hippocampal NSPC appear over a longer time course. I try to further explore the latter two of these issues in the next chapter.

4.4 Conclusion

In conclusion, I have shown that the addition of hippocampal derived microglia at high density or concentration is capable of increasing the Nestin positive cell population in culture. However, there were no observable differences between adding hippocampal or cortical microglia to hippocampal NSPC under these conditions. Despite attempts to investigate methodological there were no significant changes in cell phenotypes. As a result, in the next chapter I examine the effects of microglia on NSPC that are derived specifically from the neurogenic niche -the dentate gyrus. Future work should characterise the phenotype of the isolated microglia used to a deeper extent and investigate the generation of microglia under serum free conditions. The media of the hippocampal NSPC treated with microglia could be assessed to look for levels of cytokines or trophic factors in response to this stimulus to give an indication as to what the state of these cultures are. The use of an alternative co-culture cell model could also be investigated, for example, one that uses a trans well membrane so that there was less stress acted upon the microglia. The work performed here also hints that microglia heterogeneity may be tissue dependant and that future work should also include *in situ* approaches such as spatial transcriptomics.

5. Examining the neurogenic effect of microglia derived from the Dentate Gyrus on hippocampal NSPC cultures

5.1.0 Introduction

In the previous chapter, it was hypothesised that there is a functional, regional dependant, neurogenic property of microglia located within the neurogenic niche. This was investigated in a co-culture model whereby hippocampal NSPC monolayer cultures were treated with either microglia or microglia conditioned media from the hippocampus and cortex. A functional neurogenic effect of microglia that was regionally dependant was not demonstrated which could be due to the fact that it is microglia specifically within the dentate gyrus (DG) that display a pro-neurogenic effect. Therefore, as microglia were harvested experimentally from the whole hippocampus, pro-neurogenic signalling could have been diluted from microglia derived from beyond the boundaries of the DG. To further investigate this hypothesis, co-cultures of hippocampal NSPC cells with DG microglia or their conditioned media were examined. This was compared to microglia derived from the rest of the hippocampus and/or microglia derived from the whole hippocampus.

5.1.1 Evidence for a unique neurogenic phenotype of microglia within the dentate gyrus

There are divergent thoughts in the field as to whether true subpopulations of microglia exist or whether microglia are a homogenous population with differences in phenotype arising due to differences in local microenvironments and which is supported by the results of the previous chapter. It has already been demonstrated that there is large variation in the distribution and morphology of microglia throughout the CNS with particularly dense populations found in the hippocampus and olfactory telencephalon (Lawson et al., 1990). Evidence in favour of microglia subpopulations suggest that microglia do not all react to stimuli in the same way (Pannell et al., 2014). In one study, both freshly isolated and cultured microglia have been isolated and exposed to different neurotransmitters and neurohormones. In all cases examined, only a small percentage of microglia responded to each stimulant at any one time as measured through calcium imaging. Even when pre -treated with LPS, Interferon -γ or Il-4 to model pro and anti-inflammatory phenotypes there was no stimulus that elicited a response from all microglia. Co-culture experiments have examined the neurogenic properties of microglia from the neurogenic region -sub ependymal zone and the cortex, where microglia derived from the sub ependymal zone were shown to possess intrinsic characteristics that were independent of the *in vitro* environment (Marshall et al., 2014). Similar observations have also been made of microglia found in the sub ventricular and rostral migratory zone (Xavier et al., 2015). The DG is the neurogenic niche found within the hippocampus and it consists largely of three main layers: the granule cell layer, the molecular cell layer and the sub granular zone. Neural progenitor cells reside largely in the sub granular zone and emerging evidence suggests that microglia within the dentate gyrus display a pro-neurogenic effect (Kreisel et al., 2019). In favour of this hypothesis a diphtheria microglia depletion model, has shown that a reduction

of microglia within the DG reduced the survival of newly born neuroblasts. Additionally, DG microglia were shown to have an increased response to hippocampal Vegf overexpression in a tetracycline regulated *Vegf164* model, compared to CA1 microglia, whereby microglia density as well as cell soma were increased indicative an activated morphology. Vegf overexpression was shown to induce hippocampal neurogenesis, however, when microglia were ablated this effect was abolished indicating that DG microglia are integral to Vegf induced hippocampal neurogenesis. Interestingly microglial activation was seen to occur prior to angiogenesis and neurogenic responses (Kreisel et al., 2019).

5.1.2 Aims

The general aim of this chapter was to assess whether there are functional, differential regional neurogenic effects of microglia specifically isolated from distinct regions of the hippocampus on hippocampal neural progenitor/stem cells (NSPC).

- Aim 1: Investigate a functional regional dependant (Dentate gyrus, rest of the hippocampus, whole hippocampus) neurogenic effect on hippocampal NSPC using a co-culture paradigm or by using microglia conditioned media where cells were derived from postnatal day 7-10 Sprague-Dawley rat pups.

I evaluated this question using immunocytochemistry and immunofluorescence microscopy by examining markers associated with neuronal progenitor populations and immature neurons across 5DIV.

5.2.0 Results

5.2.1 Microglia plating density had no significant effect on Hippocampal NSPC treated with dentate gyrus derived microglia conditioned media 5DIV

As there were no significant differences observed in neural progenitor or neuronal populations between hippocampal NSPC cultures treated with microglia conditioned media from the DG, RH and WH, I wanted to examine the effect of microglial density used to generate the DG, RH and WH microglia conditioned media. To do this, microglia conditioned media derived from the DG, RH and WH were generated (General Methods 2.1.7), as stated previously, from microglia plated at 3 different densities: 50,000 cells/ml, 100,000 cells/ml and 400,000 cells/ml. Once generated the conditioned media was applied to hippocampal NSPC microchamber cultures 2 hours after plating (General Methods 2.1.3). Parallel cultures were grown for 5DIV and were then washed in PBS, fixed and stained for Nestin, Prox1 and counterstained with DAPI (General Methods 2.1.8). Cells were imaged with a fluorescent microscope and analysed via imageJ and a two-way ANOVA was performed. There was no significant difference in the total number of cells (**Fig.21 A**) as determined by total DAPI count for microglial plating density or factor interaction, however there was a significant result observed for microglia source (Two-way ANOVA, $F_{(2,21)} = 4.260$, $p = 0.028$). For the total number of Prox1 positive cells, there was no significant result observed for microglia density nor in the factor interaction. There was a significant result for the microglial source for total number of Prox1 positive cells (Two-way ANOVA, $F_{(2,21)}=10.06$, $p =0.0009$) (**Fig.21 C**). Upon testing for multiple comparisons there were a significant difference between RH-50,000 cells/ml (23.2 ± 8.3%) and WH-50,000 cells/ml (12.4 ± 7.4%) as well as RH-400,000 cells/ml

(27.1 ± 6.2%) and WH-400,000 cells/ml (14.3 ± 0%). There were no significant results observed for the percentage of Prox1 positive cells between experimental groups (**Fig. 21.E**). For the total number of Nestin positive cells there was no significant result observed microglial density or factor interaction (**Fig. 21 B**). However there was a significant result for source of microglia (Two-way ANOVA, $F_{(2,21)}$ =4.5, p=0.0236). Upon multiple comparison post hoc testing, no significant pairwise comparison was maintained. For the percentage of Nestin positive cells, there was a significant result for both microglia density (Two-way ANOVA, $F_{(2,21)}$ = 4.56, p = 0.0227) and for microglial source (Two-way ANOVA, $F_{(2,21)}$ = 10.74, p = 0.0006) but not for the interaction between them (**Fig.21 D**). Tukey's post hoc test showed a significant difference between DG – 100,000 cells/ml (24.4 ± 3.9%) vs WH– 100,000 cells/ml (44.927 ± 1.696%) and RH-100,000 cells/ml (31.5 ± 4.3%) vs WH- 100,000 cells/ml. These results suggest that the plating density of microglia used to generate microglia conditioned media had no significant effect on the neural progenitor or neuronal population regardless of the microglial source. Furthermore, a large amount of variation was observed between repeated experiments which may be resolved with a greater n number.

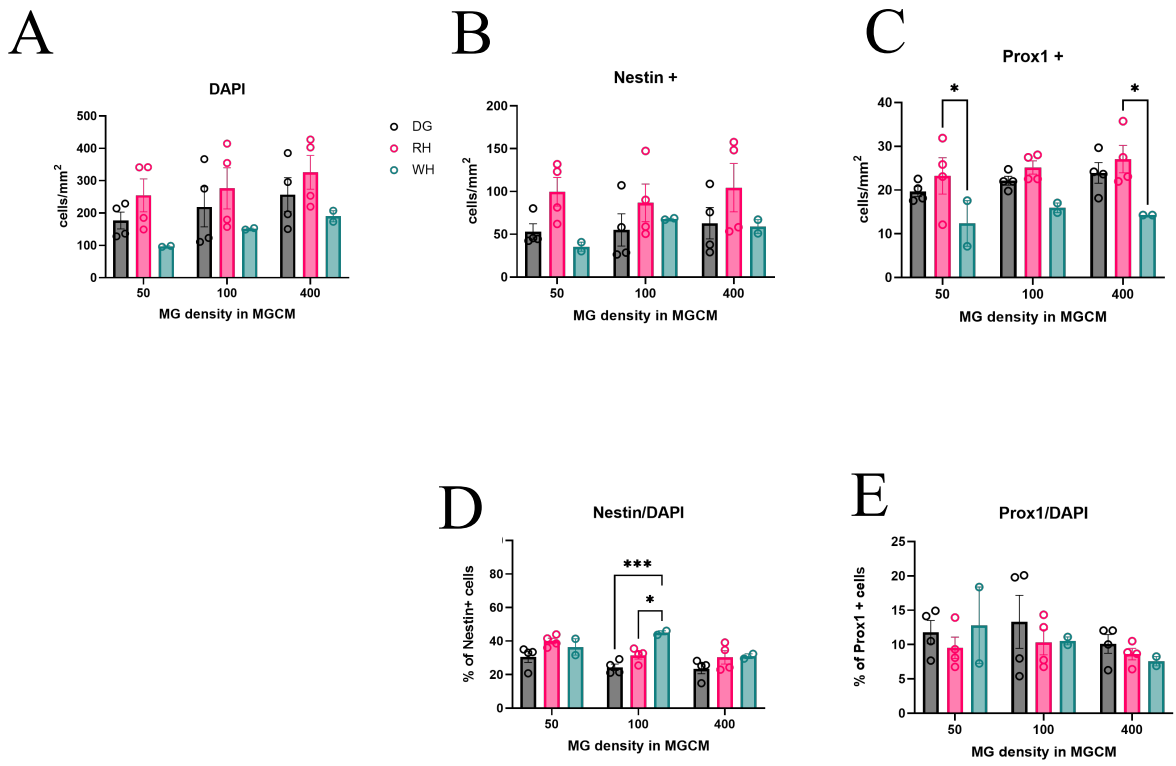

Figure 21. Hippocampal NSPC's treated with DG, RH and WH microglial conditioned media grown for 5DIV show no significant difference in Nestin or prox1 population at 50,000, 100,000 or 400,000 MG. N = 4 wells from 2 separate experiments for all except WH where N= 2 wells from 1 experiment. Total number of cells (A), total number of Nestin positive cells (B), and total number of Prox1 positive cells (C) were counted. The percentage of Nestin positive cells (D) and the percentage of Prox1 positive cells (E) were calculated. Data points represent mean ± SEM. * = $p < 0.05$, *** = $p < 0.001$.

5.2.2 No differential neurogenic effect of dentate gyrus derived microglial conditioned media on Hippocampal NSPC at 5DIV

In previous culture experiments in which microglia from the hippocampus and cortex were isolated and applied directly or used to generate microglia conditioned media, I was unable to show a regionally distinct neurogenic effect on hippocampal NSPC across 5 days *in vitro*. I had hypothesised that microglia from the hippocampus would have a regionally distinct pro-neurogenic effect when applied to hippocampal NSPC in culture based on previous work in our lab (Nunan et al., 2014). As this effect was not observed, I considered that microglia

specifically found within the DG may provide pro-neurogenic properties compared to microglia found within the greater hippocampal area. With this reasoning, it could be that pro-neurogenic signalling from DG microglia was diluted by signalling from non-DG microglia. Therefore, in order to investigate whether microglia derived from the DG possessed a unique functional neurogenic property that was regional distinct, mixed glia cultures were generated from the dentate gyrus (DG), rest of the hippocampus (RH) or whole hippocampus (WH) of P7-10 rat pups as shown in **Fig.22 A**. Microglia conditioned media was generated (General Methods 2.1.7) and applied to hippocampal NSPC's 2 hours after plating (General Methods 2.1.3). Microglia used to generate microglial conditioned media were plated at 100,000 cells/ml for all conditions. Parallel cultures were allowed to grow for 5DIV and were then washed in PBS, fixed and stained for Nestin, prox1 and counterstained with DAPI (General Methods 2.1.8). Nestin is a filament protein and a marker for neural progenitor cells whereas Prox1 is a transcription factor found within the granule cell lineage and therefore is useful as a DG specific neuronal marker (Iwano et al., 2012). There was no significant difference in the total number of cells as determined by total DAPI count (One-way ANOVA, $F_{(3,40)} = 2.158$, $p = 0.108$, **Fig.22 B**), nor in the total number of Nestin cells (One-way ANOVA, $F_{(3,40)} = 0.4303$, $p = 0.7324$, **Fig.22 C**) or in the total number of Prox1 cells (One-way ANOVA, $F_{(3,40)} = 0.5071$, $p = 0.6796$, **Fig.22 D**). There was also no significant difference in the percentage of Nestin positive cells as assessed by one-way ANOVA ($F_{(3,40)} = 1.553$, $p = 0.2157$, **Fig.22 E**) or in the percentage of Prox1 positive cells ($F_{(3,40)} = 0.08128$, $p = 0.9698$, **Fig.22 F**). These results suggest that in this instance there were no observable differences in the effect of microglia conditioned media derived from the DG, RH and WH when applied to hippocampal NSPC's for 5DIV.

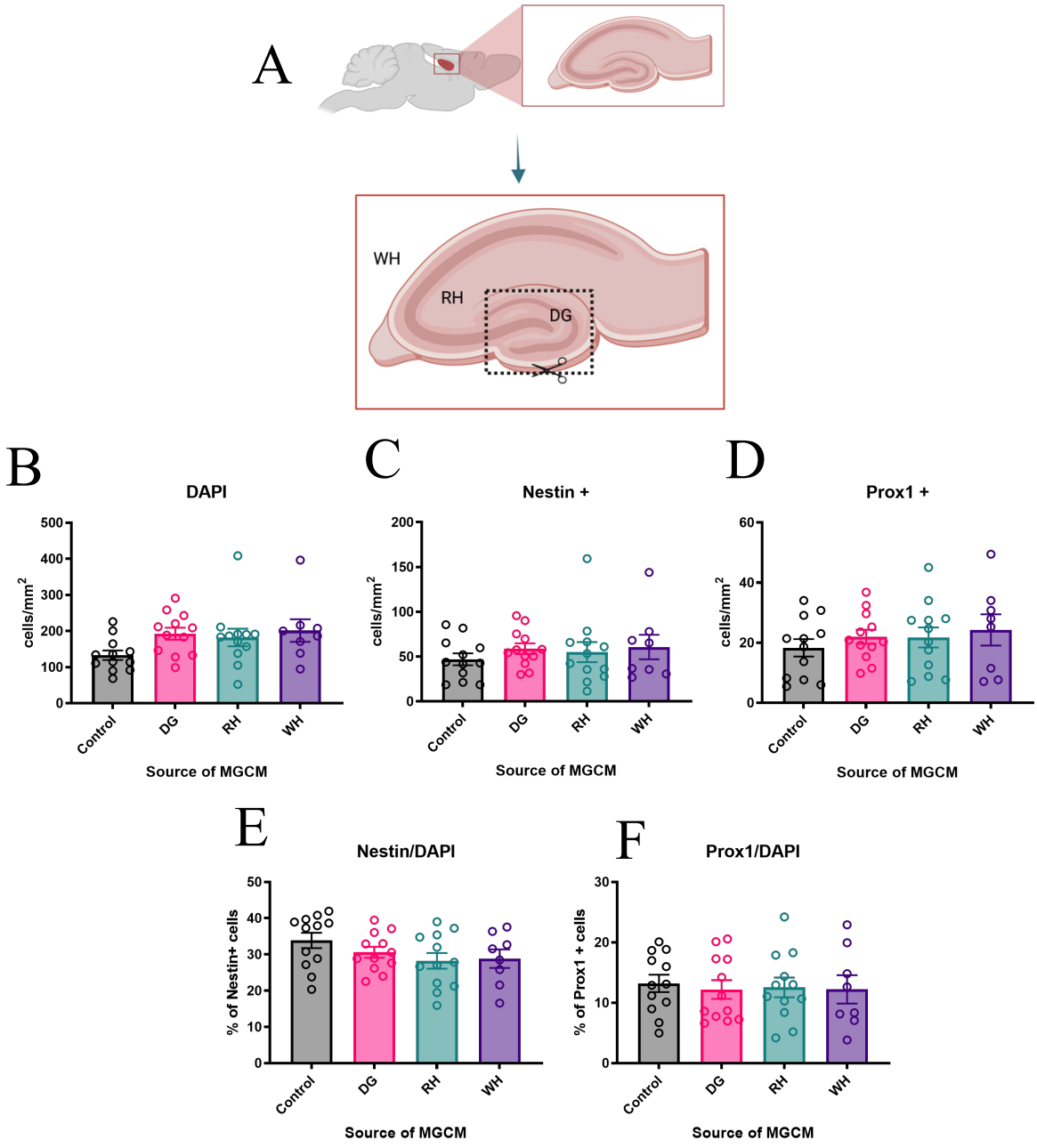

Figure 22. No significant difference was observed between hippocampal NSPC cultures treated with microglial conditioned media derived from the dentate gyrus (DG), rest of the hippocampus (RH) or whole hippocampus (WH) for 5DIV.

(A) Schematic diagram of microglial source from rodent brain. A coronal section of the rodent hippocampi is enlarged depicting whole hippocampus (WH), dentate gyrus (DG) and rest of the hippocampus (RN). Total cell number (B), total number of Nestin positive cells (C), total number or prox1 positive cells (D) were recorded. Percentage of Nestin (E) and percentage of prox1 were calculated (F). N = 12 wells from 3 separate experiments for control, DG and RH. N = 8 wells from 2 separate experiments for WH. Data points represent mean ± SEM. (A) Created with BioRender.com.

5.2.3 No differential neurogenic effect of dentate gyrus microglia conditioned media on hippocampal NSPC's at an extended 7DIV

In the experiments conducted thus far, I have only observed phenotypic changes in the make-up of hippocampal NSPC cultures up to 5DIV. At this timepoint I have, in some experiments, seen an increase in the percentage of Nestin positive cells upon the addition of microglia conditioned media or microglia added directly to cultures but there have not been any significant differences in neuronal populations. Therefore, I wanted to investigate whether an extended culture end point would change these observations. To do this, parallel hippocampal NSPC's were generated (General Methods 2.1.3) in microchamber cultures and 2 hours post plating MGCM (General Methods 2.1.7) from the DG, RH and WH were applied and allowed to grow for 7DIV. At the same time, I also examined the plating density of microglia used to generate MGCM. Microglia used to generate MGCM were plated at 50,000, 100,000 or 400,000 cells/ml. At 7DIV, cultures were washed in PBS, fixed and stained for Nestin, EdU, Prox1 and counterstained for DAPI (General Methods 2.1.8). EdU is a thymidine analogue which is incorporated into the DNA of cells undergoing the 'S' phase of the cell cycle and therefore can be used as an indicator of cell proliferation. A two-way ANOVA showed no significant differences in total DAPI counts between conditions for microglial density ($F_{(2,61)}$ = 1.648, p = 0.2008), source of microglia ($F_{(2,61)}$ = 0.07399, p = 0.9288) or for the interaction between the two factors ($F_{(4,61)}$ = 1.475, p = 0.2210) (**Fig.23 A**). There was no significant difference in the number of Nestin positive cells for microglial density ($F_{(2,61)}$ = 1.202, p = 0.3077), source of microglia ($F_{(2,61)}$ = 1.303, p = 0.2792) or for the interaction between the two ($F_{(4,61)}$ =1.374, p = 0.2536) (**Fig.23 B**). There was no significant difference in the percentage of Nestin positive cells for microglial density ($F_{(2,61)}$ = 0.1547, p = 0.857), source of microglia

($F_{(2,61)}$ = 2.424, p = 0.0971) or the interaction between the two factors ($F_{(4,61)}$ = 0.8160, p = 0.5199) (**Fig.23 F**). There was no significant difference in the number of EdU positive cells for microglial density ($F_{(2,61)}$ = 0.0144, p = 0.9857), source of microglia ($F_{(2,61)}$ = 0.1080, p = 0.8978), or for the interaction between these two factors ($F_{(4,61)}$ =1.249, p = 0.3001) (**Fig.23 C**). There was no significant difference in the percentage of EdU positive cells for microglial density ($F_{(2,61)}$ =2.212, p = 0.1182), the source of microglia ($F_{(2,61)}$ =0.5881, p = 0.5585) or for the interaction between the two factors ($F_{(4,61)}$ = 1.403, p = 0.2436) (**Fig.23 U**). There was no significant difference in the number of cells that were positive for both Nestin and EdU for microglial density ($F_{(2,61)}$ = 0.9376, p = 0.3971), source of microglia ($F_{(2,61)}$ = 1.006, p = 0.3716) or for the interaction between the two factors ($F_{(4,61)}$ = 2.069, p = 0.0959). There was a significant difference in the percentage of cells that were positive for both Nestin and EdU for microglial density ($F_{(2,61)}$ = 3.845, p = 0.0268) but this did not withstand post hoc testing. There was no significant difference for the source of microglia ($F_{(2,61)}$ = 0.09215, p = 0.9121) nor for the interaction between the two factors ($F_{(4,61)}$ = 0.2955, p = 0.8798). There was no significant difference in the number of prox1 positive cells for microglial density ($F_{(2,61)}$ =1.078, p = 0.3467), source of microglia ($F_{(2,61)}$ = 0.8752, p = 0.4219) or for the interaction between the two factors ($F_{(4,61)}$ = 1.217, p = 0.3128) (**Fig.23 E**). Finally, there was no significant difference in the percentage of prox1 positive cells for microglial density ($F_{(2,61)}$ = 0.9569, p = 0.3898), source of microglia ($F_{(2,61)}$ = 0.4748, p = 0.6243) or in the interaction between the two factors ($F_{(4,61)}$ = 8144, p = 0.5209) (**Fig.23 I**). These results indicate that an extended culture timepoint of 7DIV did not result in any changes in the neuronal populations of hippocampal NSPC's treated with microglia conditioned media from the DG, RH or WH.

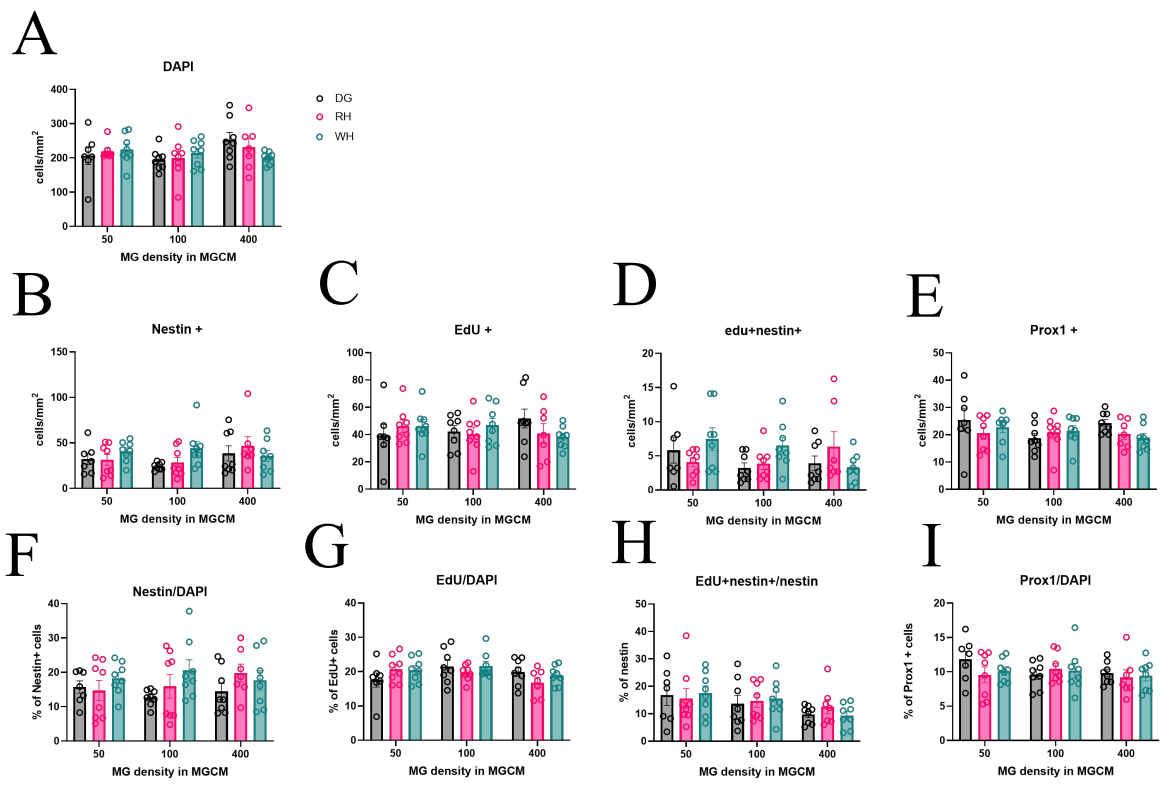

Figure 3. Hippocampal NSPC's treated with DG, RH and WH microglial conditioned media and grown for 7DIV show no significant difference in Nestin, EdU or prox1.

Total number of cells as measured by DAPI (A), total number of Nestin positive cells (B), total number of Edu positive cells (C), total of double Edu and Nestin positive cells (D) and total number of prox1 positive cells were calculated (E). Total percentage of Nestin positive cells (F), percentage of Edu (G), percentage of double EdU and nestin positive cells of the total nestin population (H) and total percentage of prox1 posiitve cells (I) were calculated. N = 8 wells from 2 separate experiments for all conditions except DG -50,000 and RH- 400,000 where N=7 wells. Data points represent mean ± SEM.

5.3.0 Discussion

The aim of this chapter was to investigate potential functional, regional dependant, neurogenic effects of microglia from the DG on hippocampal NSPC cultures derived from P7-10 rat pups. Conversely, this may also help to understand if unique regional dependant microglia characteristics are lost once microglia are removed from their native micro environment. Firstly, I examined the addition of microglia conditioned media from the DG, RH and WH on hippocampal NSPC at 5DIV. In this instance microglia conditioned media was generated from microglia seeded at 100,000 cells/ml for each condition and upon addition no significant differences were observed between regionally derived microglia conditioned media treatments. Secondly, I investigated the effect of microglial seeding density on microglia conditioned media from the DG, RH and WH. Microglia were plated at 50,000 cells/ml, 100,000cells/ml and 400,000 cells/ml for generation of microglia conditioned media. Within each regional source of microglia, there was no significant effect from microglial seeding density. Finally, I examined the effect of extending the culture end point to 7DIV on hippocampal NSPC treated with microglia conditioned media from the DG, RH, and WH at the plating densities mentioned above. Again, there were no significant differences observed on the population of neural progenitor or neuronal populations that could be explained by microglia seeding density or microglial regional source. These results appear to be consistent with previous experiments from the last chapter where there has been no significant change in neuronal populations upon the addition of microglia or their conditioned media.

In this chapter I have investigated potential neurogenic properties of DG derived microglia using microglia conditioned media. It is worth acknowledging that in using microglia

conditioned media instead of adding microglia directly to the hippocampal cultures themselves, neurogenic signalling that may require direct cell to cell contact or prolonged exposure to microglia themselves will have been missed, however time restrictions left me unable to further explore these factors. There is also the possibility that, through freezing, some factors within the microglia conditioned media may have been compromised and therefore it would be useful to compare freshly generated microglia conditioned media with that of its frozen counterpart for completeness. It is worth noting that frozen microglia conditioned media did not appear to have a detrimental effect on the hippocampal NSPC even when compared to control media. However, there is some transcriptomic evidence which suggests microglia once removed from their local microenvironment revert to a macrophage-like phenotype and could potentially lose any specialisation that they may have had (He et al., 2018). Owing to the fact that the results seen here are consistent with results from the previous chapter where upon in some instances microglia were directly added to the cultures, these results could be explained by the idea that the microglia isolated from distinct brain regions have lost their phenotypic specialization whilst expanded in culture. It could therefore be interesting to compare the effect of adding microglia expanded in culture to hippocampal NSPC cultures with the addition of other macrophages. There are also additional factors that could have influenced these results as mentioned in the previous chapters. The lack of neurotrophic factors used in the cultures that I have generated may have reflected some of the results observed. Some groups advocate the use of neurotrophic factors, such as EGF and FGF, in NSPC cultures (Marshall et al., 2014). Likewise, in microglial cultures some groups have used macrophage colony stimulating factor one (mCSF-1) in their culture medium to provide trophic support. I have not used such factors in my cultures as previous results in our group demonstrated that these were not essential and may also provide a simpler paradigm to untangle (Nunan et al., 2014).

There are conflicting reports in the literature as to the pro-neurogenic phenotype of microglia. Some studies indicate that activated microglia are capable of eliciting neurogenic properties such as those induced by LPS (Nikolakopoulou et al., n.d.). Here, microglia derived from rats treated with LPS where shown to produce greater numbers of neurons in culture compared to controls. Other groups claim that anti-inflammatory microglial phenotype drive pro neurogenic properties. For example, in an adrenalectomy model, it was found that increased proliferation of type 2 neural progenitor cells (Nestin+Gfap-) in the DG correlated with stage 2 and stage 3 of activated microglia as defined by altered morphology. Upon cytokine analysis via real time RT-PCR of the DG of adrenalectomized rats, modest increments were observed in proinflammatory cytokines such as Il-1α and Il-1β. Interestingly, there was a 10-fold increase in the levels of Tgf- β in the DG of adrenalectomized rats compared to control animals (Battista et al., 2006). Single cell RNA sequencing of the dentate gyrus has demonstrated that microglia appear homogenous but largely express markers such as Ccl2, Gas6, and Tgfbi which have been associated with an M2 or anti-inflammatory phenotype (Artegiani et al., 2017). In this study they speculate that microglia in the DG display a neuro protective phenotype. These studies present a greater question of whether microglia culture models or activated microglia models reflect in vivo neurogenic mechanisms.

5.3.1 Limitations

A major limitation of this work was using micro-dissected regions of the hippocampus to generate mixed glia cultures for microglial isolation. Due to the small nature of the tissue limited amounts of mixed glial cultures could be generated. In addition, as microdissection of the dentate gyrus involved a protocol that is significantly longer than dissection of the whole

hippocampus a decrease in cell viability cannot be ruled out. However, when comparing DG, RH and whole hippocampal, cells used to generate these microglia were all treated in the same way so that any negative effects of the procedure on cell viability is spread equally across groups.

5.4 Conclusion

In conclusion, I found no distinct regional dependant neurogenic effect of microglia conditioned media derived from DG microglia. This indicates that microglia isolated from the dentate gyrus do not show a functional neurogenic phenotype in these cultures. Future work would endeavour to replicate these experiments with microglia from the DG and RH directly applied directly to hippocampal NSPC cultures to check whether their physical presence or cell to cell contact is important for a pro neurogenic effect on hippocampal NSPC. Furthermore, it would also be interesting to look at the effects of differentially activated microglia on neural progenitor and neuronal populations for example with Tnf-α and see if results are consistent with published work. Likewise, comparing DG microglia with microglia found in other neurogenic niches such as the subventricular zone would also be of interest.

6. Acute microglial isolation from mouse brain in preparation for RNA - sequencing

6.1.0 Introduction

Microglia are highly dynamic and sensitive cells that have been shown to alter their activity, morphology, and transcriptional output rapidly and dramatically depending on their environment (Matcovitch-Natan et al. 2016; Hanamsagar and Bilbo 2017; Lam et al. 2017). I hypothesised that microglia found within the dentate gyrus (DG) possess distinct neurogenic properties that are not seen elsewhere in the brain. However, as discussed in the previous chapter, thus far, I have been unable to demonstrate a regional dependant functional neurogenic property of microglia isolated from mixed glial cultures via the traditional culture and shake off method. Despite this outcome I still favour this hypothesis, as the fact that microglia are so highly susceptible to their environment implies that there could be functional variation between microglia found in different brain regions with regards to neurogenesis (Nimmerjahn et al. 2005; Lund et al. 2006; Grabert et al. 2016; Matcovitch-Natan et al. 2016). I aim to perform RNA-sequencing (seq) of mouse microglia derived from the dentate gyrus (DG), the rest of the hippocampus (RH) and cortex to identify differentially expressed genes that may relate to the neurogenic function of microglia. In order to generate purified samples of microglia for RNA-seq it is important to limit interference with their normal state as much as possible by choosing a suitable isolation methodology. Research in the field has struggled to recapitulate endogenous phenotypes and transcriptional profiles of microglia from traditional culture methods when

compared to *in vivo* or freshly isolated microglia (He et al. 2018). For this reason, alternative, physical separation methods of isolating microglia have been utilised including: magnetic activated cell sorting (MACS) and fluorescence activated cell sorting (FACS). Both of these methodologies rely on identifying target cells from a heterogenous population by labelling either the target or the unwanted cells and filtering accordingly. The limiting factors are then, what are the best markers at identifying your target population and which is the best way to label them. This chapter aims to answer some of these questions.

6.1.1 Cell separation techniques for primary tissue

There are several methods of separating out cell populations from dissociated primary tissues, the oldest of which rely on either adherence or cell density. Cell separation based on adherence is possibly the simplest and cheapest of all the methods. It relies on the target population having preferential adherence properties to precoated glass or plasticware and or involves promoting the expansion of the target population to outcompete unwanted cells. The latter, utilises the differential density of different cell types relative to a graduated separation medium under centrifugation and is a method that is highly valuable in clinical settings. However, both of these methods suffer from low purity and cannot distinguish between subpopulations of cells within a cell type (Tomlinson et al. 2013). Newer methods such as FACS and MACS have become major players in cell separation, both of which allow distinct populations of cells to be isolated from a heterogenous population. They both rely on antibody binding to cell identifying surface antigens (in the case of live separations) to perform cell separation. For FACS, antibodies are raised to target antigens which are conjugated to fluorescent labels such as fluorescein (FITC), allophycocyanin (APC) and Phycoerythrin (PE). A heterogenous cell

population is incubated with specific fluorescently labelled antibodies and run on a FACS machine in which the cells are separated based on the emitted signals from laser excitation of the bound fluorophore as well as cell size and granularity. The advantage of FACS is that it produces highly purified populations due to the fact that it can discriminate individual cells based on multiple fluorescently bound antibodies simultaneously. In this way FACS is regarded as a single cell technology. The cost for this specificity however is time. For MACS, antibodies for specific antigens are bound to magnetic microbeads which can be bought commercially. Once the population of cells has been incubated with the antibody bound beads, a magnetic field is applied to the cell suspension across a column and the unwanted cells are washed away (positive separation). Once the magnetic field is removed the target population can be collected. In this fashion only one antibody can be used at a time but the result is a quick and efficient method of isolating bulk populations of cells at once. MACS is considered to be considerably more cost and time effective than FACS and can be setup so that multiple separations are set up in parallel, vastly increasing the yield (Sutermaster and Darling 2019). Both MACS and FACS are powerful tools in biological research across many fields including immunology, cancer and regenerative medicines.

6.1.2 Isolation of microglia using antibody-based cell sorting

Microglia activation is a key physiological process that aims to protect the brain parenchyma from potential threat (Chen and Trapp 2016). Generally, microglia become activated via the stimulation of a number of immune related receptors (e.g. toll like receptors) which result in morphological and biochemical changes including the production of inflammatory cytokines. As microglia are highly sensitive cells, it is important to consider sample preparation methods

that have minimal effects on microglial activation. Interestingly, a study looking at the transcriptomic effect of cell dissociation and FACS on mouse muscle stem cells noted that some cell populations were strongly affected by the cell dissociation of their tissue. One subpopulation of muscle stem cell was seen to express high levels of *Socs3*, heat shock proteins and immediate early genes such as *Fos,* in single cell RNA-seq (scRNA-seq) experiments. These highly expressed genes could not be detected later in muscle cryo-sections when single molecule RNA fluorescence *in situ* hybridization (smFISH) against these genes was performed, suggesting that expression of these genes may be affected by the tissue processing and handling prior to sequencing (van den Brink et al. 2017). The authors suggest that this could also apply to other tissue types as dissociation protocols are highly similar across fields and interpretation of transcriptomic data should be evaluated with caution.

To further emphasise the importance of tissue preparation conditions, it is known that cell viability will begin to drop upon isolation from the lack of vital nutrients and enzymatic action and therefore the speed of tissue processing is vital. One way to negate these effects is to perform cell isolation procedures at consistently cold temperatures (4°C) where possible to slow down cell metabolism and delay degradation which occurs at ambient temperatures (Tomlinson et al. 2013). Unlike primary culture protocols used to generate microglia which can get away with ambient temperatures, the general consensus around fresh preparations for transcriptomic studies are that they should be performed under consistently cold conditions where possible and to minimise the use of serum (Nikodemova and Watters 2012; Bohlen et al. 2017; Hammond et al. 2019a). Cell viability can also be further improved using oxygenation and appropriate transport media such as those that mimic interstitial fluids or in the case for microglia -cerebrospinal fluid.

For microglial RNA-seq studies, generally two approaches are favoured for cell isolation: FACS or MACS. These both rely on microglial specific antibodies to isolate cells from a heterogenous population. There are many different markers used to differentiate microglia from other cell types each with different expression profiles and binding affinities such as Cd11b, Cx3cr1, P2ry12 and Tmem119. Despite this, for MACS preparations of microglia the Cd11b micro bead is the predominant antibody that is in use (Gonzalez-Pena et al. 2016; Grabert et al. 2016; He et al. 2018; McCarthy et al. 2018). In simple experimental set ups where there are major differences in the expression of cell identifying genes such as in mixed glial cultures, MACS has been used to separate cells easily into separate fractions of microglia and astrocytes using Cd11b micro beads, where the microglia remain bound to the column and the astrocytes are flushed through (He et al. 2018). Furthermore, from whole brain cell suspensions $Cd11b^{+}$ cells can also be easily extracted to high degree of purity (97%) without neuronal or astrocytic (<1%) contamination whilst retaining their *in vivo* phenotype (Nikodemova and Watters 2012). It has also been shown that microglia isolated via MACS show a greatly reduced activation profile compared to those isolated by shake off methods (Ju et al. 2015). Whilst these are promising results, MACS preparations only allow for the identification of a single cell type via the binding of one antibody at a time. The disadvantage of using Cd11b as a microglial marker is that its expression is not restricted to microglia but is also expressed by infiltrating monocytes and macrophages. Microglia can be differentiated from infiltrating monocytes with the use of Cd45 antibody. It is largely considered that $Cd11b^{+}/Cd45^{high}$ expression level are indicative of infiltrating monocytes (E. Hirbec et al. 2017). In (Nikodemova and Watters 2012) MACS separations, $Cd11b^{+}$ cells were further analysed using flow cytometry and stained with antibodies against Cd45, two populations become apparent: $Cd45^{high}$ and $Cd45^{low}$. They found that 88-96% of cells were $Cd11b^{+}/ Cd45^{low}$. Matters can be complicated further as there is some evidence that under pathological conditions microglia may

show increased expression levels of Cd45 (Noristani et al. 2017). If infiltrating monocytes are not a concern or if you can remove this contamination post analysis for example in scRNA-seq analysis this maybe an attractive option.

Alternatively, FACS provides the user with the ability to use multiple biological targets providing the corresponding conjugated antibody has been manufactured and that there are enough lasers present within the FACS machine to accommodate multiple fluorophores. It is also capable of examining multiple biological parameters at the same time such as cell size, granularity and viability which may improve efficiency of isolation. The most widely used markers to identify microglia using FACS are $Cd11b^{+}/Cd45^{low}$ (Matcovitch-Natan et al. 2016; Noristani et al. 2017; Hammond et al. 2019a; Delbridge et al. 2020). (Hammond et al. 2019a) FACS sorted microglia from whole brains for scRNA-seq using $Cd11b^{+}/Cd45^{low}$ followed by $Cd11b^{high}/Cx3cr1^{high}$ expression profiles. They profiled mice spanning embryonic day 14.5 – post natal day 540 and noted that there was an increase in the number of $Cd45^{high}$ populations in younger mice. This was thought to be from circulating blood monocytes where embryos could not be perfused. $Cd11b^{+}/Cd45^{low}$ FACS expression profiles of microglia have been further corroborated with the use of antibodies against the transmembrane protein Tmem119, which is thought to be a microglia specific marker in both mouse and human (Bennett et al. 2016; Martin et al. 2017). Another advantage of FACS is that antibodies against unwanted cell types can also be used simultaneously to further aid specificity. For example, Ccr2 can be used to differentiate infiltrating macrophages from resident or activated microglia (Mizutani et al. 2012; Martin et al. 2017). Due to advances in reporter mice, FACS can also be performed without the use of antibodies where cells have had a fluorescent protein such as green fluorescent protein (GFP) inserted into a target gene and expression is restricted to a specific cell type. For all the advantages of FACS there are limitations. Cells undergoing sorting

experience extreme conditions including high pressure, high decompression, the application of an electric charge and high shear forces which may contribute to low viability yields compared to MACS which is a gravity driven process (Sutermaster and Darling 2019).

6.1.3 Isolation of microglia using reporter mice

The *Cx3cr1*^{GFP} reporter mouse is a widely used line to isolate microglia in which GFP is expressed under the *Cx3cr1* promoter. Cx3cr1 is a seven transmembrane G-protein coupled receptor which has a high affinity for the chemokine Cx3cl1. Cx3cl1 and Cx3cr1 are thought to be widely found across tissues but remain expressed in specific cell types. In the central nervous system (CNS) Cx3cl1 is reported to be confined to neurons whereas *Cx3cr1* expression is restricted to microglia (Nishiyori et al. 1998). As homeostatic microglia express high levels of Cx3cr1, reporter mice will exhibit microglia that will strongly express GFP. The *Cx3cr1*^{GFP} reporter mouse was first generated by (Jung et al. 2000) to investigate the interactions and physiological properties of the Cx3c chemokine fractalkine (FKN also known as Cx3cl1) and its receptor. To create the *Cx3cr1*^{GFP} mouse line a vector consisting of a 1.2kb fragment immediately upstream of the *Cx3cr1* start codon, 8kb fragment spanning the *Cx3cr1* coding exon and the 3' flanking DNA was constructed. A GFP-neomycin cassette replaced the first 390bp of the Cx3cr1 gene with loxP sites flanking the Neogene. Embryonic stem cells (ES) were transfected with the vector and colonies displaying double resistance to G418-gancyclovir were selected for further analysis. ES cells displaying the correct targeted homologous recombination were further transfected with a vector expressing Cre recombinase to perform loxP excision of the Neogene. ES therefore, that were not resistant to G418 were isolated and injected into mice blastocysts to generate chimeric mice. Mice that harboured the transgene in

the germline were then backcrossed on a BALB/c background. *Cx3cr1*$^{+/GFP}$ possess only one functional allele of the *Cx3cr1* gene, whereas *Cx3cr1*$^{GFP/GFP}$ are functionally Cx3cr1 knockout (KO) mice. In generating this line, the *Cx3cr1* gene was replaced with an enhanced green fluorescent protein (EGFP) reporter gene. This allowed not only an investigation into the functional properties of this gene in monocytes, NK cells, dendritic cells and microglia but also resulted in the tagging of these cells with a visual marker via the expression of GFP which could be further exploited. Importantly, the loss of Cx3cr1 at that time did not appear to show an overt phenotype in the mice nor did it have a detrimental impact on microglial injury response in peripheral nerve injury (Jung et al. 2000).

Cx3cr1$^{+/GFP}$ mice have been used to investigate transcriptional differences between brainstem microglia isolated by FACS and laser capture microdissection (LCM) (Solga et al. 2015). Downstream analysis demonstrated that there were large numbers of common RNA sequences from microglia derived from the two isolation procedures, but that each method also displayed unique signatures. 519 transcripts were differentially expressed between FACS and LCM isolated microglia. Analysis of the transcripts strongly expressed from FACS isolated microglia showed genes involved in transcriptional control, lymphocyte activation and inflammatory processes. Conversely microglia isolated by LCM showed highly expressed genes associated with neurons and oligodendrocyte function. These results were confirmed by mRNA fluorescence in situ hybridization (FISH), however, immunohistochemistry did not show evidence of protein translation of neuron and oligodendrocyte transcripts suggesting that these transcripts could be left over from microglial phagocytosis. The fact that 94% of transcripts were identified in both methods suggests that both FACS and LCM are suitable isolation tools in studies looking at global transcript expression. Interestingly, the studied also

compared the transcriptomes of microglia from *Cx3cr1*$^{+/GFP}$ mice with wild types. Of the detected differentially expressed genes only 0.5% differed.

Beyond characterising the transcriptional effects of different isolation procedures, *Cx3cr1*^{GFP} mice are being used in transcriptomic studies to examine the gene expression profile of microglia across time, space and in disease. (Matcovitch-Natan et al. 2016) has used *Cx3cr1*$^{+/GFP}$ mice to investigate chromatin and gene expression profiles of microglia across development. By performing RNA-seq, they demonstrated microglia undergo three distinct temporal changes in parallel with brain development defined as: early, pre and adult microglia. A large number of genes were found to be differentially expressed across nine timepoints from yolk sac to adulthood. Early microglia were associated with genes involved in cell cycle and differentiation whereas typical microglial associated genes were expressed only in adulthood. Interestingly, adult microglia from the cortex, hippocampus and spinal cord displayed only a small amount (76 genes) of differential gene expression across regions, which is surprising given the differing functional roles that microglia are thought to play in these regions. Genes highly represented in the pre-microglia stage were related to neural migration, neurogenesis and cytokine secretion. Some groups suspect that this pre-microglial phenotype is maintained in the hippocampus where similar to the developing brain, new neurons are generated in the DG. The fact that each developmental stage of microglia was associated with a different pattern of gene expression and that those genes were aligned with different functions represents a sign that perturbation of these transitions could have developmental consequences for the brain.

(Matcovitch-Natan et al. 2016) also utilised the *Cx3cr1*$^{+/GFP}$ mouse for single cell transcriptomics. As previously mentioned, this group looked at the developmental changes in transcription of microglia and here they used ScRNA- seq to assess the heterogeneity of

microglial at each transitional phase. The study showed that by and large, microglia perform co-ordinated shifts in transcriptional phenotype across pseudo time at the single cell level. However, when the ScRNA-seq data was compared to bulk RNA-seq time points, several yolk-sac populations aligned closer to early microglia expression – demonstrating some heterogeneity in the yolk-sac microglia population.

A different study used *Cx3cr1*$^{+/GFP}$ mice to perform bulk RNA sequencing of microglia isolated from the DG and CA1 regions. DG and CA1 regions were micro dissected and GFP positive cells were cell sorted from dissociated cell samples (Kreisel et al. 2019). Here, 41 genes were found to be differentially expressed between DG and CA1 microglia, among those included genes linked with fatty acid metabolism as well as genes associated with both M1 and M2 microglial phenotypes. An additional group of experimental mice were exposed to vascular endothelial growth factor (Vegf) for 1 week and RNA-seq of microglia from the DG and CA1 of these mice was performed. In this way they investigated the regional transcriptional differences between the DG and CA1 as well as the differential transcriptional effect of Vegf on both of these regions. Stimulation with Vegf saw a further 349 genes differentially expressed between the two regions, including those associated with cell proliferation and M1 phenotype which were upregulated in DG microglia. Three of the genes that were highly expressed in DG microglia were further validated by qPCR: *Clec7a, Spp1 and Axl.* From these results, it hints that microglia residing in the DG represent a unique subset of microglia with a unique responsiveness to Vegf which may indicate a specialised role in hippocampal neurogenesis

Overall, the *Cx3cr1*^{GFP} mouse line has proved to be highly useful not just in studies involving microglia isolation but also to investigate the microglial- neuron relationship under

physiological and pathological conditions (Davalos et al. 2005; Nimmerjahn et al. 2005). However, like many other markers used to identify microglia, *Cx3cr1* expression is not solely restricted to microglia and is also observed in border associated macrophages, peripheral monocytes, dendritic cells and NK cells. There have been large efforts to identify markers that are more specific to microglia from bulk and single cell RNA-seq studies. Several candidates have been put forward including, Tmem119, P2ry12, Sall1, Siglech, Fcrls among others. As a result of these efforts several other microglial reporter mouse lines have become available including $Tmem119e^{GFP}$, $Tmem119^{TdTomatoe}$, $Sall1^{GFP}$ and $Hexb^{TdTomato}$ (Takasato et al. 2004; Kaiser and Feng 2019; Masuda et al. 2020; Ruan et al. 2020). These are great advances in the field but even these have limitations as many of these signatures microglial genes including *Tmem119* and *Sall1* are seen to be downregulated under pathological conditions (Vankriekelsvenne et al. 2022).

6.1.4 Aims

The general aim of this chapter was to prepare for RNA sequencing of acutely isolated microglia. $Cx3cr1^{+/GFP}$ mice were used to test and optimise microglial isolation using FACS and P2ry12-PE antibody staining, however, in the next chapter wild type mice were used for bulk RNA-seq as there is evidence to suggest that $Cx3cr1^{+/GFP}$ and $Cx3cr1^{GFP/GFP}$ mice show deficits in hippocampal dependant learning and synaptic plasticity.

- Aim 1: Validate the $Cx3cr1^{+/GFP}$ mouse model through immunohistochemistry using Iba1.
- Aim 2: Validate micro-dissection of the whole DG from the rest of the hippocampus.

- Aim 3: Evaluate and Isolate microglia from dentate gyrus, rest of hippocampus and neocortex into a purified population and show that these cells are viable post isolation.

6.2.0 Results

6.2.1 Iba1 antibody co-localises with GFP expression in *Cx3cr1*$^{+/GFP}$ mice

In order to confirm that *Cx3cr1*$^{+/GFP}$ mice expressed GFP in microglial cells, mice were culled (General Methods 2.2.2), brains were swiftly removed, fixed and frozen in OCT embedding medium. 40µm thick sections were generated and stained for the microglial marker Iba1(0.5µg/ml) and DAPI (0.5µg/ml) (General Methods 2.2.3). Representative confocal images demonstrate GFP expressing cells are widely distributed across the dentate gyrus. Iba1 staining was shown to visually co-localise with GFP expression (**Fig. 24**.).

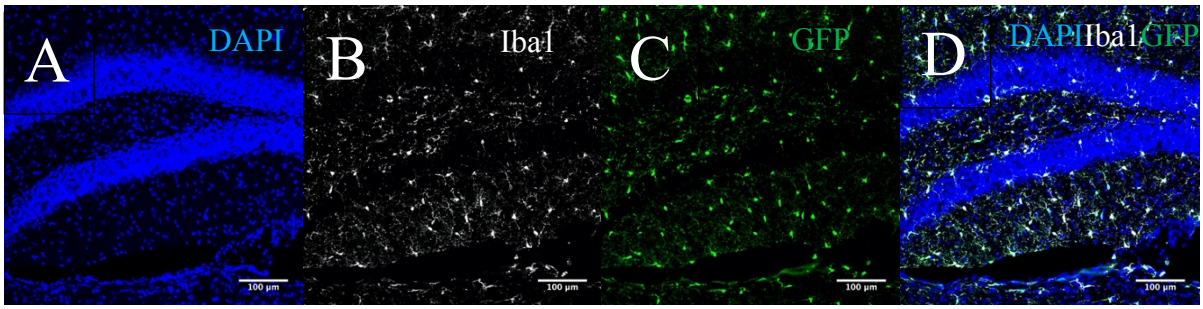

Figure 4. A representative image of GFP expression and Iba1 antibody staining in a brain section of the dentate gyrus from Cx3cr1$^{+/GFP}$ mouse. Brain sections were stained with DAPI (A) and Iba1 (B). GFP (C) expressing cells were distributed across brain sections and align with Iba1 antibody staining.

6.2.2 GFP positive cells are successfully isolated from the hippocampus and cortex and confirmed with Iba1 antibody.

In order to quickly assess whether GFP positive cells could be isolated from the cortex and hippocampus of *Cx3cr1*$^{+/GFP}$ mice, tissues were dissociated using the adult brain dissociation kit (Miltenyi Biotec) (General Methods 2.2.6). 50µl of the cell suspension acquired was placed on a glass slide with a coverslip and immediately viewed using an upright fluorescent microscope (Leica). The acquisition of GFP positive cells was visually confirmed (**Fig. 25A**). Remaining hippocampal and cortical cells in suspension were plated at 100,000 cells/ml for 2 hours at 37^{o}C before fixation with 4% PFA. The resulting samples were permeabilised, stained with DAPI (0.5µg/ml) and Iba1 (0.5µg/ml) antibody and imaged using a fluorescent upright microscope (Leica) (**Fig. 25B**). GFP and Iba1 co-staining was assessed between hippocampal and cortical samples using an unpaired t-test. Total number of cells as measured with DAPI were significantly different between hippocampal and cortical cells (**Fig.25C**), 291.5 ± 4.9 and 213.6 ± 6.3 cells/mm^2 respectively ($t_{(4)}$ = 9.735, p = 0.0006). There was no significant difference between the raw number of GFP cells between the two samples (**Fig.25D**) or for the raw number of Iba1 cells (**Fig.25E**), however, cells derived from the cortex displayed a significantly higher proportion of GFP positive cells (**Fig.25G**), 56.50 ± 1.6% and 70.37 ± 1.5% ($t_{(4)}$ = 6.236, p = 0.0034). This was also true for the proportion of Iba1 positive cells (**Fig.25H**), 56.94 ± 1.9% and 70.54 ± 1.5% ($t_{(4)}$ =5.719, P = 0.0046). Importantly, the percentage of cells that expressed GFP and Iba1 staining as a proportion of GFP were greater than 99% for both hippocampal and cortical samples.

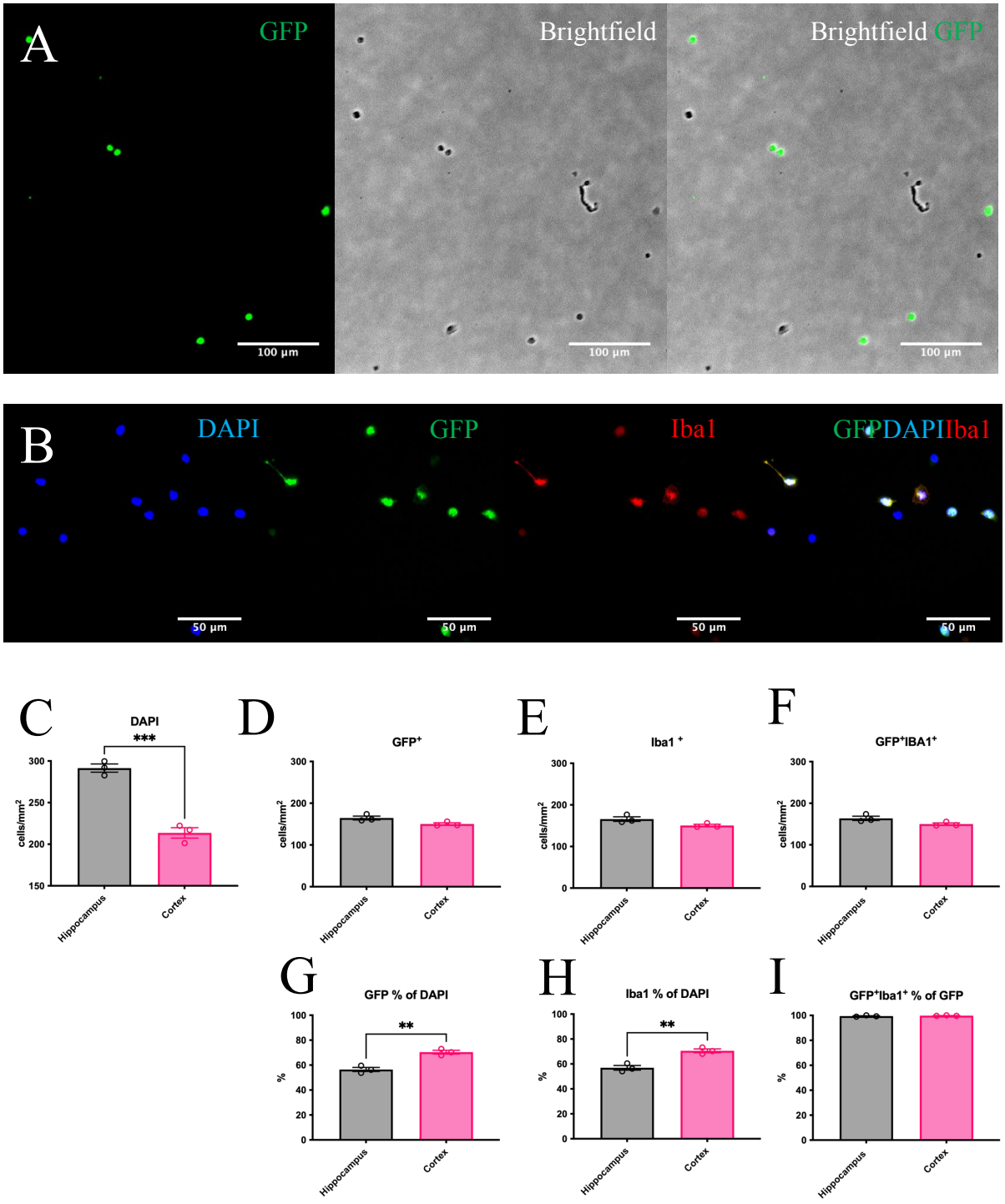

Figure 5. Unsorted GFP positive cells are successfully isolated from *Cx3cr1*$^{+/GFP}$ mouse and are positive for Iba1 antibody staining.

A drop of cell suspension was placed on a glass slide and the isolation of GFP positive cells was assessed visually (A). The unsorted cell suspension was plated 2 hours before fixation then stained for Iba1 and DAPI (B). Total cell number (C), number of GFP positive cells (D), number of Iba1 positive cells (E), number of cells that were positive for both GFP and Iba1 (F), percentage of GFP positive cells (G), percentage of Iba1 positive cells (H) and the number of cells that were positive for GFP and Iba1 as a percentage of GFP cells (I). Data represents mean ± SEM from a sample of 3 wells/condition (N=1). Unpaired t-test (** = p ≤0.01, *** = p≤0.001).

6.2.3 Over 45% of total events are viable during cell sorting.

To investigate what proportion and number of viable microglia could be obtained from the whole hippocampus and cortex, six *Cx3cr1*$^{+/GFP}$ mice were culled. The brains were swiftly removed and the hippocampi and cortex were dissected out and dissociated (General Methods 2.2.6). Cortical (**Fig. 26 A-D**) and hippocampal **(Fig. 26 E-H)** cells were then washed, stained with DAPI (1μg/ml) and FAC sorted (**Fig.26**) (General Methods 2.2.7). A whole wild type mouse brain served as an unstained control sample (**Fig. 26 I-L**). Ten thousand events of the total sample were recorded for post sorting analysis. In a population of cells, viability can be discerned whilst performing FACS by staining with DAPI (1μg/ml). As DAPI is predominately an impermeant dye to live cells it can be used to stain a dead population were the cell membrane has become compromised. In one experiment 29.2 and 26% of total events were DAPI negative and GFP positive for cortex and hippocampus respectively (**Fig.26 M**). In a second experiment 47.4 and 45.9% of cells were DAPI negative and GFP positive for cortex and hippocampus respectively (**Fig. 26 M**). Sorted cells were used to test RNA extraction.

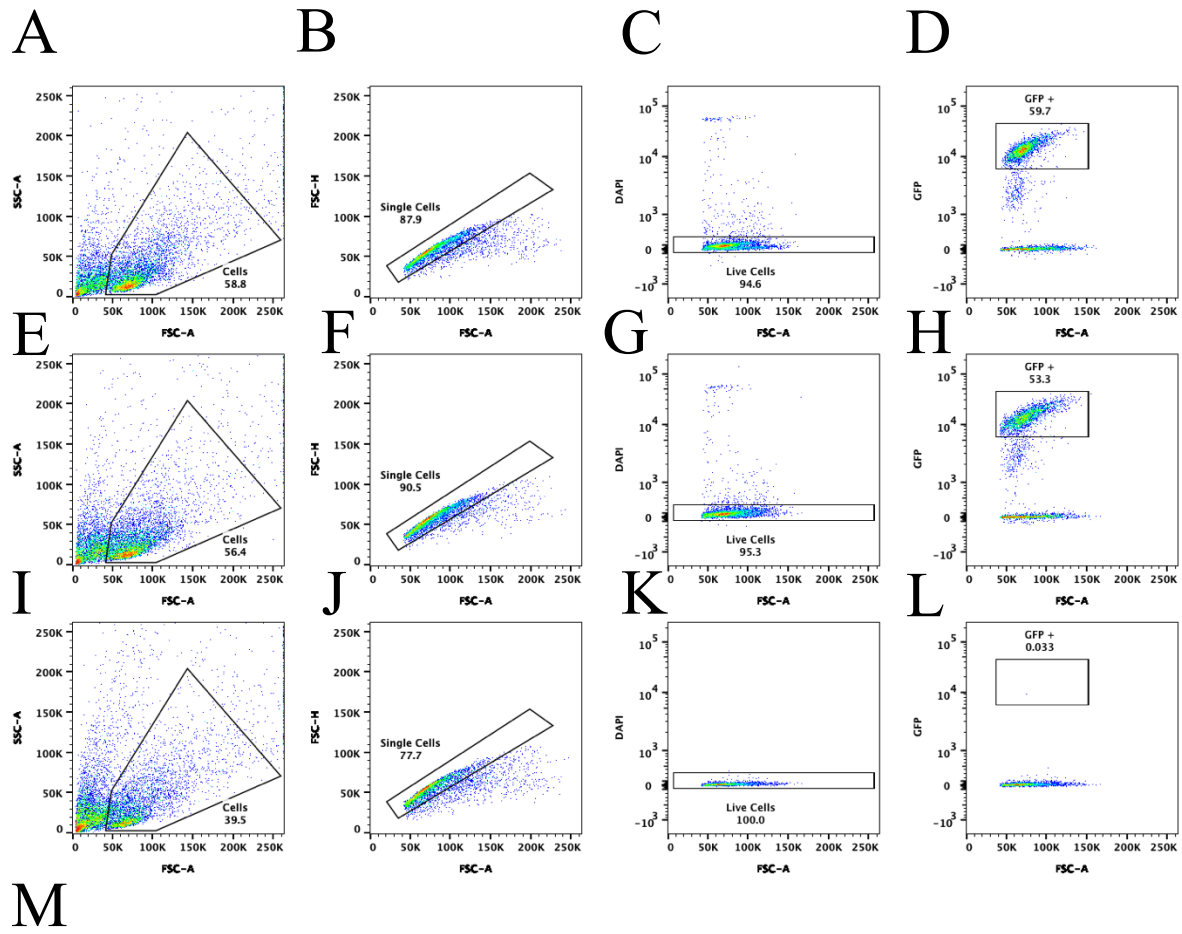

Sample	Ungated count	Freq of total: Cells	Freq of total: Single Cells	Freq of total: Live cells	Freq of total: GFP +	GFP+ count
1 - Cortex	10000	58.8	51.7	48.9	29.2	2921
1 - Whole Hippocampus	10000	56.4	51.1	48.7	26	2598
2 – Cortex	10000	56.6	50	47.4	47.4	2928
2 – Whole hippocampus	10000	53	48.1	45.9	45.9	2587

Figure 26. An example of cell sorting strategy for extracting viable GFP positive cells from the cortex (A-D) and whole hippocampus (E-H) from 10,000 recorded events.

An example of post sorting analysis of mouse Cx3cr1$^{+/GFP}$ microglia using the BD FACSAria^{TM} Fusion cell sorter. Pooled cortex (A) and hippocampus (B) cell suspensions from six mice stained with DAPI to differentiate live and dead cells. Cells were then sorted based on the gating strategy: Cells (A, E, I), single cells (B, F, J), live cells (C, G, K) and GFP positive cells (D, H, L). A whole wild type mouse was used as a negative control (I-L). Table shows the summary statistics of 2 experiments where 10,000 events have been recorded per sample (M). Side scatter -area (SSC-A), forward side scatter-area (FSC-A), Green fluorescent protein (GFP).

6.2.5 Whole dentate gyrus dissections confirmed with qPCR.

To validate micro dissection the whole dentate gyrus (DG) from the hippocampus of mice using a stereomicroscope (General Methods 2.2.4), RNA expression of genes associated within the DG, CA1 and CA3 were examined in my micro dissected tissue. I looked at the expression of three genes associated with the dentate gyrus (*Tdo2*: Tryptophan 2,3- dioxygenase, Dsp: *Desmoplakin*, *Ppp1r1a*: Protein phosphatase 1 regulatory subunit 1A) and two genes associated with the CA1 and or CA3 regions (*Mrg1b*: Meis-related gene 1b, *Nov*: Nephroblastoma overexpressed gene) that have been previously published (Lein et al. 2004; Hagihara et al. 2009). Following the dissection protocol from (Hagihara et al. 2009), DG and rest of the hippocampus (RH) were generated and qPCR was performed (General Methods 2.2.5). Results following a one-way ANOVA demonstrated that there were significant differences in levels of *Tdo2* (**Fig. 27A**) expression between brain regions ($F_{(2,6)}$=1619, P<0.0001), Dunnett's post hoc tests showed a marked increase in relative expression levels in the dentate gyrus compared to the RH with a mean relative expression of 8.787 ± 0.206 (P<0.0001). Whereas, the DG associated genes Dsp (**Fig.27B**) and Ppp1r1a (**Fig.27C**) did not show a statistically significant difference in relative gene expression between brain regions (P= 0.0734, P =0.0720). One way ANOVA results show that there is a significant difference in relative gene expression between brain regions for both NOV ($F_{(2,6)}$ = 83.19, P <0.0001) (**Fig.27D**) and Mrg1b ($F_{(2,6)}$ = 44.56, P = 0.0003)(**Fig.27E**). A marked decrease in relative gene expression in the DG with a mean relative gene expression of 0.02 ± 0.01 (P<0.0001) for *Nov* and 0.062 ± 0.043 for *Mrg1b* (P=0.0201) as compared to the rest of the hippocampus. Data represents $2^{(-\Delta\Delta CT)}$ values where DG and CTX have been normalised to RH.

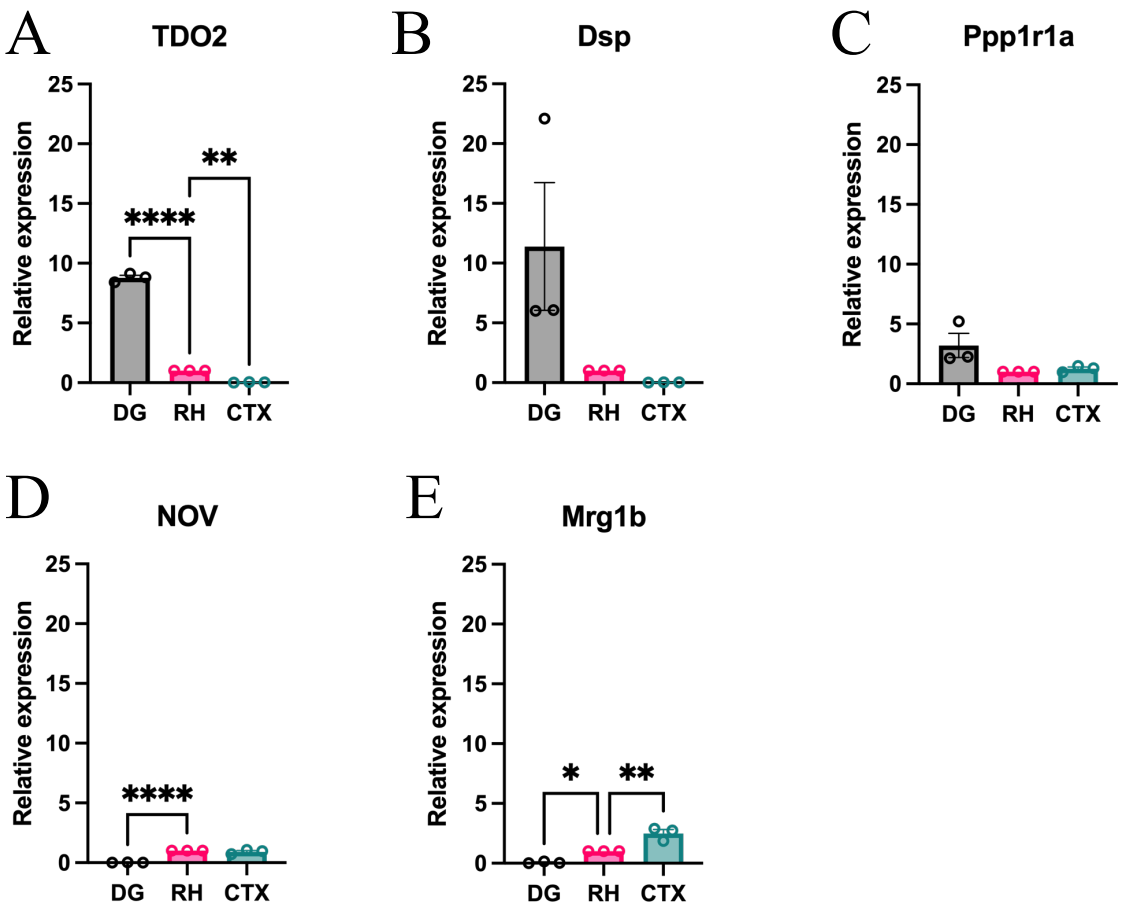

Figure 27. Validation of whole dentate gyrus micro dissection from mouse brain by qPCR.

RNA from dentate gyri (DG), hippocampus-DG (RH) and cortical (CTX) samples was converted into cDNA for qPCR. Primers for Tryptophan 2,3- dioxygenase (TDO2), Desmoplakin (Dsp), Protein phosphatase 1 regulatory subunit 1A (Ppp1r1a), Meis-related gene 1b (Mrg1b) and Nephroblastoma (NOV) were used as discriminatory gene expression markers for DG and CA1/CA3 enriched regions. Where TDO2 (A), Dsp (B) and Ppp1r1a (C) expression have been associated with the DG, whereas, NOV (D) and Mrg1b (E) are associated with CA1/CA3 regions. Data represents $2^{(-\Delta\Delta CT)}$ values from mean ct values where DG and CTX have been normalised to RH (n=3 independent experiments, *= P<0.05, ** = P< 0.01, **** = P<0.0001).

6.2.6 Microglia are successfully extracted from the Dentate gyrus

To assess the proportion and number of cells that could be isolated from the DG (**Fig. 28 A**) and RH (**Fig.28 B**), whole DG and RH were micro-dissected from six *Cx3cr1*$^{+/GFP}$ mice one brain at a time (General Methods 2.2.4). Single cell suspensions were generated (General Methods 2.2.6) and stained with DAPI (1µg/ml) and P2ry12-PE (1 in 200). Cells were FAC sorted (General Methods 2.2.7). A whole wild type mouse brain served as a control sample

(**Fig. 28 C**). Ten thousand events per sample were recorded for post sorting analysis. 3.9% ± 1.24 and 21.38% ± 2.77 of total events were sorted for DG and RH samples respectively (**Fig. 28 D**). The mean total number of events sorted for DG was 15653.33 ± 22077 and for RH 54323.33 ± 8641. This provides an estimate of the number of cells that will be recovered for RNA extraction. The marked difference in total events sorted between DG and RH is likely due to differences in total volume of starting tissue for each sample and potentially a greater number of cells are damaged from initial dissection in DG samples.

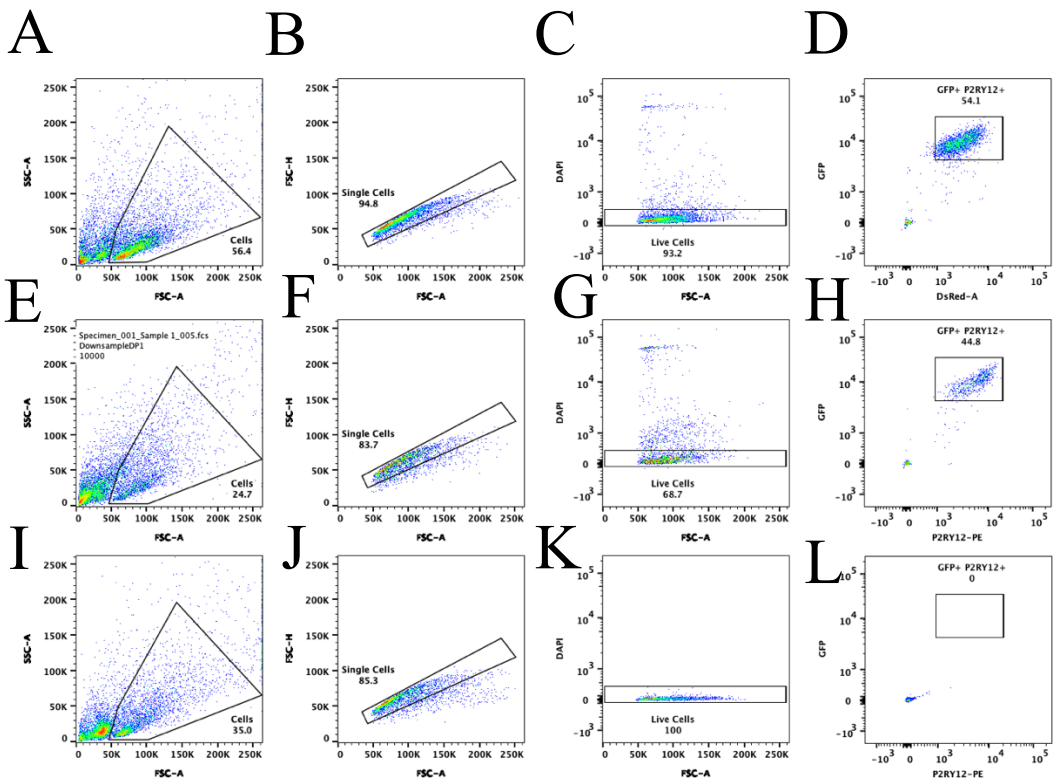

M

Sample	Mean ungated count	Mean Freq of total: cells	Mean Freq of total: single cells	Mean Freq of total: Live cells	Mean Freq of total: GFP+ P2ry12+	Total sorted mean GFP+ p2RY12+ count
Hippocampus -DG (RH)	10000	46.26	43.40	39.59	21.38	54323.33
DG	10000	18.25	14.04	8.93	3.9	15653.33

Figure 28. Example cell sorting of mouse *Cx3cr1*$^{+/GFP}$ microglia using the BD FACS Aria.

Rest of the hippocampus (RH, A-D) and dentate gyrus (DG, E-H) from six mice were pooled. Cell suspensions were stained with P2ry12-PE and DAPI to differentiated from monocytes and dead cells respectively. Cells were then sorted based on the gating strategy: Cells (A, E, I), single cells (B, F, J), live cells (C, G, K) and GFP and P2ry12-PE double positive cells (D, H, L). 3.9% and 21.38% of total events were recorded as microglia for DG and hippocampus- DG respectively (D). A whole wild type mouse was used as a negative control (I-L). Table (M) shows the summary statistics of 2 experiments where 10,000 events have been recorded per sample (M). Side scatter -area (SSC-A), forward side scatter-area (FSC-A), Green fluorescent protein (GFP). N =3 independent experiments.

6.2.7 The estimated number of events sorted by the FACSAria™ Fusion is decreased after purity check

In order to assess the accuracy of the readout of sorted cells (General Methods 2.2.7) from the hippocampus-DG (RH) and DG samples, 5µl of the sorted cell suspension from each sample was added to a small amount of FACS buffer and passed through the sorter again using the same gating strategy as was initially applied (**Fig. 29 A-H**). Across 3 experiments a range of purity was observed in these samples from 31.4% to 78.6% resulting in big differences in some samples between estimated numbers of cells sorted and corrected no of cells sorted, which is summarised in **Fig.29 I**. In the worst example where the purity was deemed to be 31.4% there is a difference of more than 20,000 cells in estimation. Sample 2-DG was not assessed for purity as the cell number was already considered to be low and was needed for further downstream analysis.

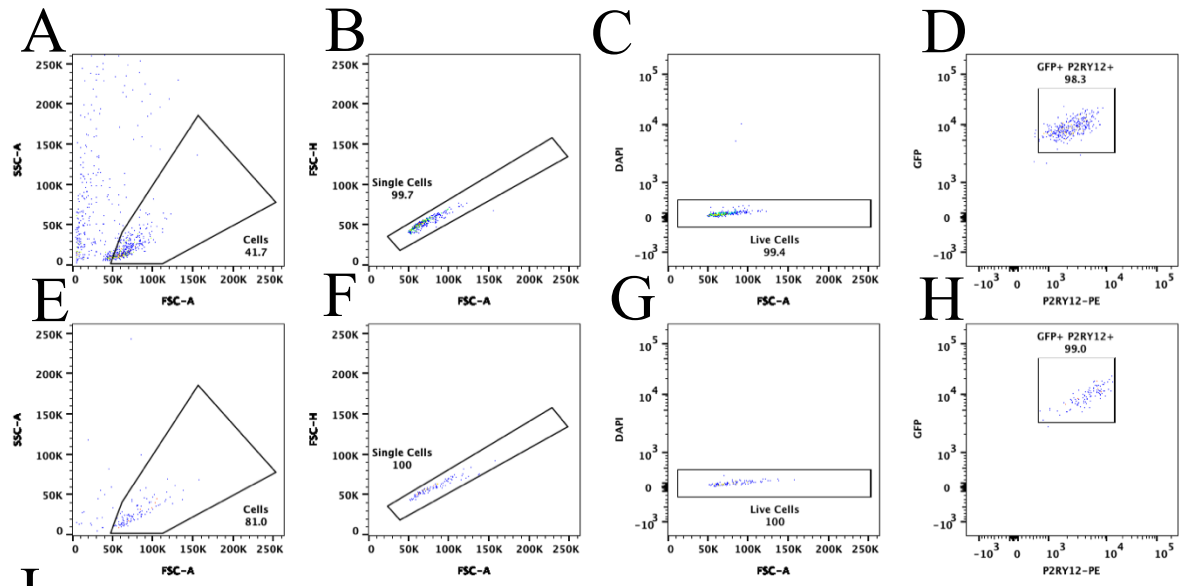

I

Sample	No. of Events sorted	Purity Check %	Adjusted no. of events sorted
1 – DG	14300	78.6	11239.8
1 – RH	62210	40.8	25381.68
2 – DG	1409	-	-
2 – RH	12757	37.7	4809.389
3 – DG	31251	31.4	9812.814
3 – RH	88003	72.2	63538.166

Figure 29. Number of events sorted is not a reliable estimate.

5µl of a sorted cell suspension was added to a small amount of buffer and passed through the sorter again. Dot plots represent an example from one experiment from the hippocampus-DG (A-D) and DG (E-H) with the gating strategy applied: Cells (A, E), single cells (B, F), live cells (C, G) and GFP and P2ry12-PE double positive cells (D, H). Table (I) shows a summary of the estimated number of sorted events acquired before and after the purity check had been performed from 3 separate experiments. Adjusted no pf events sorted = (No. of events sorted/100)*purity check.

6.2.8 A purified population of microglia are viable after cell sorting

DNA binding dyes such as DAPI and Propidium iodide are fluorochromes that can be used to assess cell viability. They identify dead cells in a population as they can only enter a cell if the membrane has been perturbed either due to cell death or from permeabilization. Therefore, they are not good candidates to identify cell viability after cell fixation as cell membranes are permeabilised by the fixation process. Addition of these DNA binding dyes would incorporate into all cells and give the misleading result that all cells are dead as they would not enter live

cells under normal conditions at low concentration. To assess the proportion of cells that are viable post cell sorting, DG (**Fig.30 A**) and RH (**Fig. 30 B**) cell sorted microglia populations were washed and stained with the fixable live/dead aqua-647 stain (Thermo Fisher) according to the manufacture's protocol (General Methods 2.2.10). A positive control was generated by heating a sample of sorted unstained cells to 60^{o}C for 5 mins prior to staining (**Fig 30 D**). Cells were analysed the following day using the BD Fortessa flow cytometer. Previous unstained and single stain control samples were carried over (**Fig. 30 C**). In the first attempt at this experiment 9.2% and 1.48% of total events were considered to be viable post sorting for RH and DG respectively. 7.8% and 0.94% of total events were GFP+ P2ry12+ for RH and DG. This poor outcome may reflect a very low total cell count in each of the samples. In a second attempt, where cell counts were much higher, 85.1% and 71.7% of total events were considered to be viable post sorting for RH and DG respectively. While 83.2% and 70% of total events were analysed as GFP+P2ry12+ for RH and DG samples respectively (**Fig. 30 D**). The data represents two experiments. Due to Covid-19 restrictions I was unable to replicate these findings further.

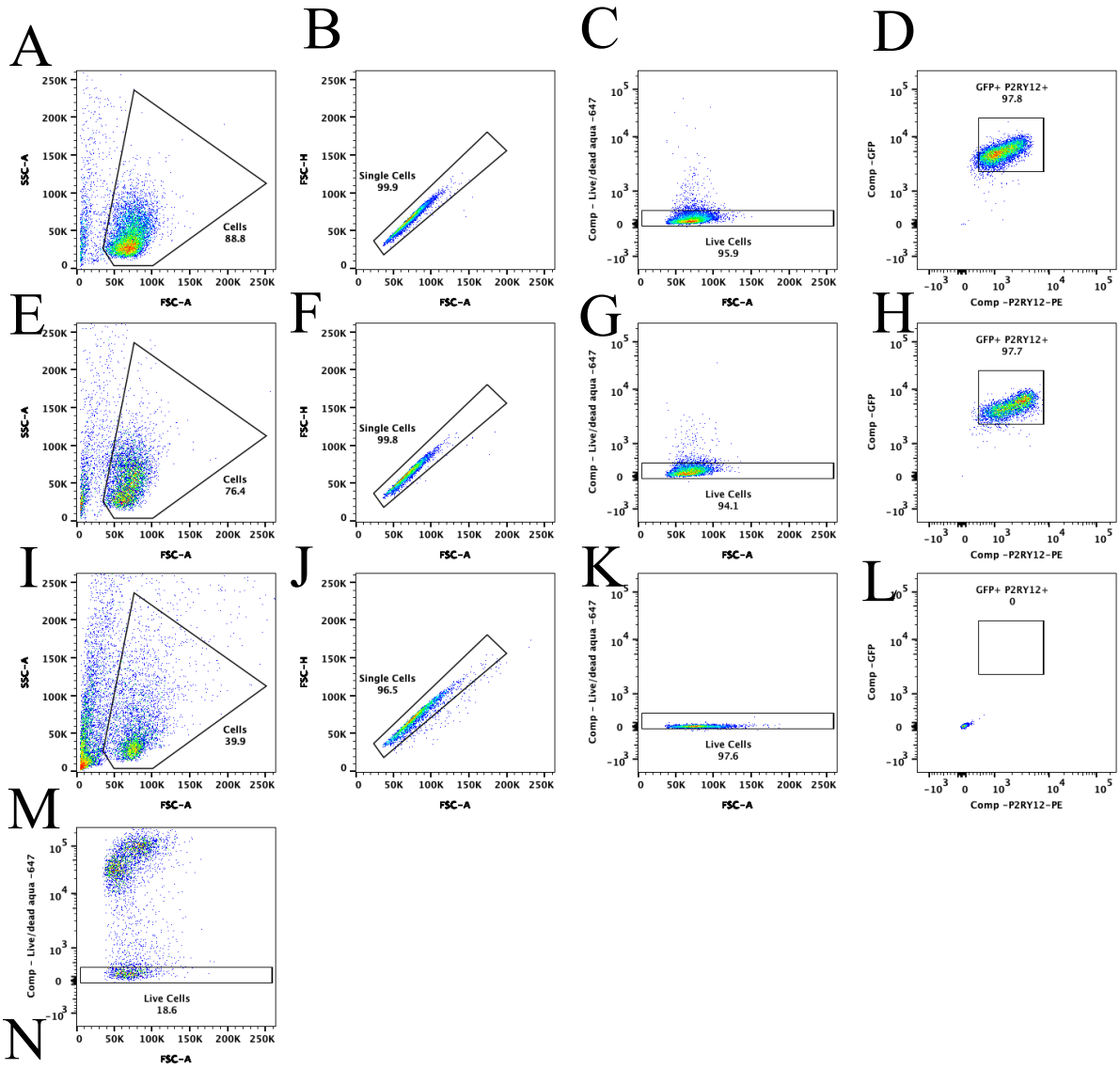

Sample	Total count	Freq of total: Cells	Freq of total: Single cells	Freq of total: Live cells	Freq of total: GFP+ P2ry12 +
1 - Hippocampus-DG (RH)	1141	9.38	9.38	9.20	7.8
1 - DG	742	1.62	1.48	1.48	0.94
2 - Hippocampus-DG (RH)	10,000	88.8	88.8	85.1	83.2
2 -DG	6274	76.4	76.2	71.7	70.0

Figure 30. Example analysis of mouse *Cx3cr1*$^{+/GFP}$ microglia after sorting looking at cell purity and viability.

Sorted cells from the hippocampus-DG (A) and DG (B) and were stained with a fixable live/dead stain -647 for 30 mins, washed and fixed in 4% PFA. Fixed cells were left overnight at 4ºC before analysis. A positive control (M) was generated by heating a sample of cells to 60ºC for 5 min prior to staining. Gating strategy applied: Cells (A, E, I), single cells (B, F, J), live cells (C, G, K) and GFP and P2ry12-PE double positive cells (D, H, L). These results represent recorded events for all samples post sorting.). Table (N) shows the summary statistics of 2 independent experiments. Side scatter -area (SSC-A), forward side scatter-area (FSC-A), Green fluorescent protein (GFP).

6.2.9 RNA is successfully isolated from FACS sorted MG cells.

In order to evaluate the feasibility of performing bulk RNA-sequencing I wanted to assess both the quantity and quality of RNA that could be extracted from FACS sorted microglia. Samples for the DG and RH were generated (General Methods 2.2.6), RNA was extracted using the manufacturers protocol (Macherey-Nagel, Nucleospin RNA XS micro kit) (General Methods 2.2.11). RNA was eluted in 10µl of RNA free H_2O and the quantity of extracted RNA was first measured using a Nanodrop 2000 spectrophotometer (Thermo Fisher) and 1µl of sample. DG was recorded as containing 5.2 ng/µl of RNA and RH 4 ng/µl. Samples were left at 4^{o}C overnight and then measured using Qubit^{TM} fluorometer (Thermo Fisher) and Qubit^{TM} RNA HS Assay kit as this instrument is thought to be more sensitive and 1µl of sample. DG sample was recorded as too low to detect and the RH as 3.33 ng/µl. To assess the quality of the RNA, 1µl of each sample was run on the BioAgilent fragment analyser. DG **(Fig. 31 A)** was recorded as having an RNA integrity number (RIN) score of 8 and RH **(Fig.31 B)** of 9.1. It is widely thought that a RIN score > 7 is preferable for downstream applications (Imbeaud et al. 2005). The genomic contamination seen suggest further treatment with DNase should be performed. Subsequent RNA samples used for bulk RNA-seq were sent to Novogene (Cambridge, UK) for quality control (QC), library prep and sequencing.

A

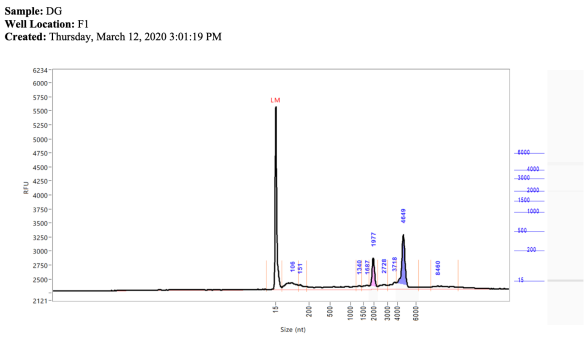

B

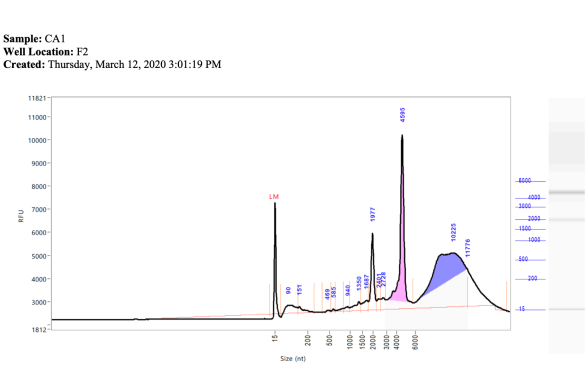

Figure 31. RNA extraction from FACS sorted GFP and P2ry12 double positive cells.

Microglia from Cx3cr1$^{+/GFP}$ mice were isolated from the DG and RH and FACs sorted. Positive events were sorted and RNA was extracted following the manufacturers protocol (Macherey -Nagel, Nucleospin RNA XS micro kit). Fragment analyser analysis of RNA extracted from the DG (A) and RH (B). RH RNA shows some genomic contamination on the far-right hand side. The lower marker (LM) is used to align the sample with ladder. Pink peak (18S ribosomal band), Purple peak (28S ribosomal band).

6.2.10 Microglia stained with P2ry12-PE captures Cx3cr1-GFP positive population

Disturbances in measures of hippocampal neurogenesis as well as hippocampal associated cognitive deficits have been observed under a *Cx3cr1* haploinsufficiency as well as a *Cx3cr1* KO in mice (Rogers et al. 2011). After evaluating the literature, it was decided that it would be preferable to use wild type over *Cx3cr1-GFP* mice and instead use P2ry12-PE antibody staining solely to selectively isolate microglia using fluorescence activated cell sorting (FACS). As all my attempts to selectively isolate microglia from mouse brain thus far were conducted using GFP expression in *Cx3cr1-GFP* mice I needed to check that P2ry12-PE staining alone would isolate the same population of cells. In order to validate the use of P2ry12-PE antibody to selectively isolate microglia from wild type mice, I analysed previously acquired FACS data where both GFP expression and P2ry12-PE antibody staining on *Cx3cr1*$^{-/GFP}$ mice were used to sort microglia (General Methods 2.2.9). The P2ry12-PE positive population was back gated onto the GFP positive population in a recorded sample of 10,000 events per experiment. Gating strategy: Cells>single cells>DAPI -ve cells >P2ry12-PE +ve population >GFP +ve population. 2225.67 ± 264.74 and 400 ±125.4 events were recorded as P2ry12-PE positive for Hippocampus-DG and DG samples respectively. 98.8% ± 0.2 and 96.8% ± 0.31 of P2ry12-PE events back gated to GFP for hippocampus-DG and DG respectively (**Fig.32 A**, N=3). We were confident therefore, that using P2ry12-PE antibody to isolate microglia would isolate the representative population from our samples in wild type mice.

A

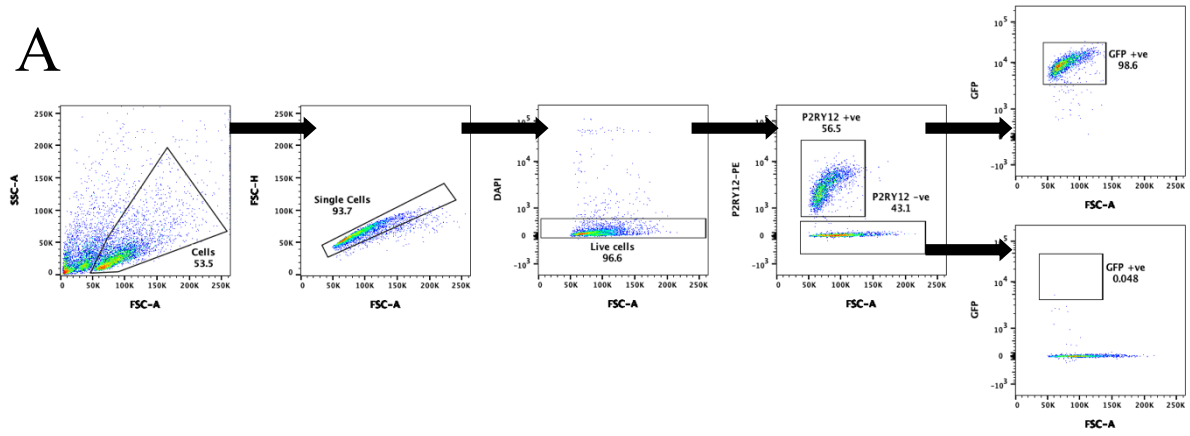

B

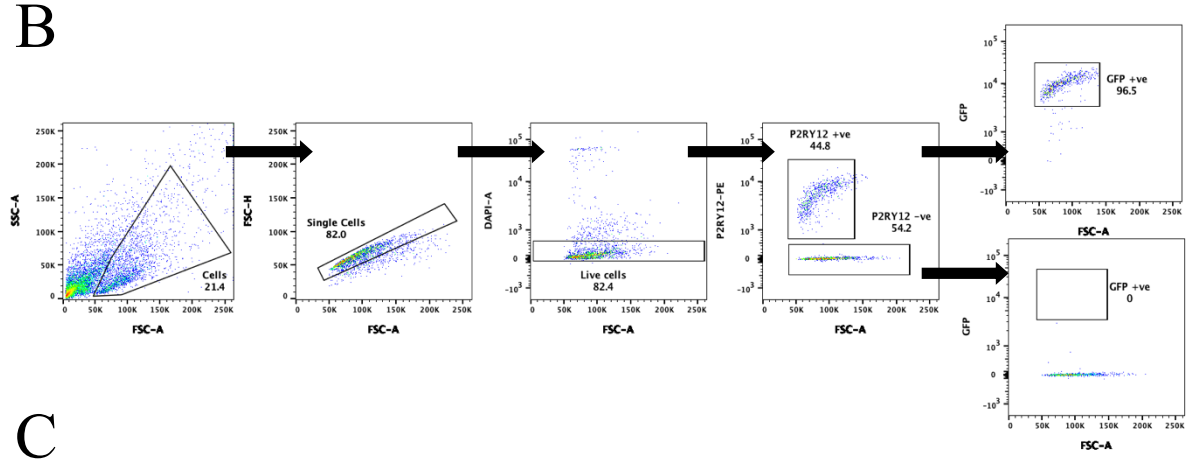

C

Sample	Ungated count	P2ry12-PE + counts	P2ry12-PE - counts	% GFP + of P2ry12-PE +	% GFP + of P2ry12-PE -
Hippocampus-DG (RH)	10000	2225.67	1231.75	98.82	0.01
DG	10000	400	506	96.83	0

Figure 32. P2ry12-PE antibody staining captures more than 96% of GFP expressing microglia.

Example of fluorescence-activated cell sorting and gating strategy (A, B) from a sample of 10,000 events. Offline analysis was used to back-gate GFP expression on to P2ry12-PE antibody staining from samples containing microglia derived from the hippocampus -DG (A) and DG (B). Summary table (C) shows that > 96% of P2ry12-PE stained cells show GFP expression in hippocampal-DG and DG samples (N=3 independent experiments, 6 mice per experiment).

6.3.0 Discussion

This chapter served to investigate the feasibility of performing bulk RNA sequencing of microglia from the DG and other discrete brain regions using the *Cx3cr1*$^{+/GFP}$ transgenic mouse. The overarching aim is to perform bulk RNA sequencing of microglia isolated from the DG, RH and cortex as I hypothesise that there are differential functional neurogenic properties of microglia from these regions. I have shown that GFP expression in the *Cx3cr1*$^{+/GFP}$ mouse brain sections aligned with Iba1 antibody staining as assessed by visual confirmation, indicating that expression of GFP in the brain was restricted to microglia. Furthermore, microglia were successfully sorted based on GFP fluorescence from the DG, RH and cortex and were found to be sufficiently purified and viable post sorting. I also established that RNA extraction could be performed from small populations of FACS sorted cells. There is literature to suggest that there are deficits in hippocampal related memory tasks as well as in metrics of hippocampal neurogenesis in *Cx3cr1*$^{+/GFP}$ and *Cx3cr1*$^{GFP/GFP}$ mice (Rogers et al. 2011). Therefore, after careful consideration, I made the decision to use wild type instead of *Cx3cr1* $^{GFP/+}$ mice for RNA sequencing. I will use P2ry12-PE antibody staining to selectively isolate microglia and I have shown through back gating that P2ry12-PE antibody staining captures more than 96% of the GFP population.

The *Cx3cr1*^{GFP} transgenic mouse line has been widely used in microglial research since its generation by (Jung et al. 2000). Here I have confirmed that GFP expression aligns with the macrophage/microglial marker Iba1 through antibody staining in our cohort of *Cx3cr1*$^{+/GFP}$ mice (**Fig 1, 2**). There is evidence that Iba1 is expressed by other myeloid cells including meningeal, perivascular, and choroid plexus macrophages as well as infiltrating monocytes but

only after they have invaded the brain parenchyma and matured (Ajami et al. 2011; Prinz and Priller 2014). While this is not ideal, it is thought that all microglia express Iba1 and that non-parenchymal macrophages and infiltrating monocytes represent a small population of our sample. One might have expected a higher number of GFP^+ cells to be present in hippocampal cell suspensions compared to the cortex as studies looking at distributions of microglia across the brain have demonstrated high density of microglia within the hippocampus (Lawson et al. 1990). This experiment was only performed once as it served to further confirm that Iba1 and GFP colocalised so it is difficult to draw any broader conclusions. However, it could be speculated that non-microglial cells from the hippocampus had a greater viability post isolation and therefore microglia yield was diluted by this population upon seeding.

During cell sorting, there appears to be a main population of cells that highly express GFP and a smaller less discrete proportion of cells that display a low/intermediate expression of GFP (**Fig 3, 4**). I initially suspected that this population could represent classical circulating monocytes particularly in early experiments where mouse brains were not perfused with PBS (Geissmann et al. 2003). Therefore, in subsequent experiments I perfused brains with ice cold PBS and stained cell suspensions with P2ry12 antibody in an effort to differentiate microglia from any remaining monocytes left over (Butovsky et al. 2014). Unfortunately, blocking steps were omitted before FACS so the data shown will display some non-specific antibody binding and therefore it is difficult to speculate what these populations represent from the current data set. The low/intermediate GFP expressing population could also be interpreted as a population of infiltrating macrophages, as they have been reported to display low Cx3cr1 mRNA expression compared to tissue specific macrophages (Jung et al. 2000; Si et al. 2010). Further antibody testing would be required to establish if these are microglia that express low levels of Cx3cr1-GFP or if they belong to a different cell type. Future microglial FACS experiments

should include sufficient blocking steps that include Fc receptor blocking. Fc receptors are expressed by leukocytes including monocytes, macrophages, B cells and dendritic cells. Of these cell types macrophages and monocytes have the highest expression rates of these receptors. Fc receptors can bind antibodies to their Fc domain non-specifically which can lead to false positives (Andersen et al. 2016). Of interest, one group has demonstrated that blood derived myeloid cells in mouse were minimally affected by Fc blocking and this is thought to be because Fc receptors were saturated with blood plasma immunoglobulins (Kuonen et al. 2010).

As the DG is a relatively small region to dissect out of the mouse brain and is particularly difficult to distinguish in a perfused brain, I wanted to validate my microdissection by RTqPCR. I chose five genes from the literature to examine the accuracy of my dissections, three that have previously been shown to display restricted or enriched gene expression in the DG (*Tdo2, Dsp* and *Ppp1r1a*) and two genes associated with the CA1 and or CA3 regions (*Mrg1b* and *Nov*) (Lein et al. 2004; Hagihara et al. 2009). Using the Allen brain atlas (Yamasaki et al. 2008) identified *Tdo2* and *Dsp* as genes which showed selective expression in the dentate gyrus of wild type mice, they went on to show that expression of these two genes were downregulated in a mouse model for psychiatric disorders (*alpha-CaMKII*$^{+/-}$*)* which was confirmed by micro array. Tdo is an enzyme encoded by the gene *Tdo2* which catalyses the oxidation of L-tryptophan in the kynurenine pathway. Here, T*do2* was significantly upregulated in terms of RNA expression which aligns with previously reported data from (Hagihara et al. 2009). Other groups have demonstrated *Tdo2* expression in the whole hippocampus, but have failed to further investigate whether this was global *Tdo2* expression or region specific. *Tdo2* is also known to be expressed in the cerebellum owing to its granule cell population (Ohira et al. 2010; Wu et al. 2013). *Desmoplakin* forms part of desmosomal

tight junctions and has also been reported to be exclusively restricted to granule cells in the dentate gyrus by in situ hybridisation (Lein et al. 2004; Lein et al. 2007). I did not report a significant difference in *Dsp* expression between DG and RH samples, however a large trend to significance can be observed. I repeated the RTqPCR for the *Dsp* data point which looked like it could be an outlier but the results were maintained suggesting that either the other two data points are compromised or that there was some variability of the dissection between animals. Ppp1r1a is a potent protein phosphatase 1 inhibitor involved in many physiological events including protein synthesis and cell division and is reported by (Lein et al. 2004) to also show restricted expression in the DG (Luo et al. 2018). Again, my RNA expression data for *Ppp1r1a* was not significantly different between DG and RH samples although, as with Dsp there is a trend to significance. *Nov* is a gene that encodes a growth factor and its expression has been reported to be limited to the CA1 region within the hippocampus (Liu et al. 1999; Zhao et al. 2001; Lein et al. 2004). My RTqPCR results align well with these reports as Nov was significantly down regulated in DG compared to RH. Finally, expression of the transcription factor *Mrg1b* is thought to be restricted to pyramidal cells of the CA1-CA3 regions of the hippocampus and importantly the portion of the CA3 most proximal to the DG has not been shown to demonstrate labelling (Lein et al. 2004). My results for Mrg1b RNA expression are concordant with previous results showing down regulation in the DG relative to RH and upregulation in the cortex. Through RTqPCR validation, I am confident I have micro dissected the DG from the RH accurately.

The protocol I use for generating microglia for RNA- sequencing is lengthy (9hrs +) and it was important to assess cell viability before and after FACS sorting. Cell viability during cell sorting varied between samples, with cell viability greater than 45% as a percentage of all events captured for both cortical and whole hippocampal samples. This was markedly reduced

in DG and RH samples with 8.92% and 39.48% respectively. This is likely due to a reduced volume of starting tissue and the fact that DG and RH samples spent a greater amount of time on ice due to the additional process of microdissection. This could possibly be remedied by having multiple people process the tissue simultaneously. Importantly, a large proportion of the purified cell samples were found to be alive when I examined cell viability post cell sorting with 85.1% for RH and 71.7% for DG, again of the total events. (Nikodemova and Watters 2012) utilise a similar isolation protocol and report cell viability of Cd11b+ isolated cells using trypan blue exclusion as 93%. Here they compared the cell viability of isolated microglia after 3 methods for the removal of myelin as myelin is known to interfere with downstream analysis. They compared the viability of microglia after Percol, anti-myelin beads or sucrose prior to flow cytometry and found that Percol demonstrated the highest percentage of cell viability. They also replicated this using a fixable live/dead stain and flow cytometry analysis and found 97% viability using Percol. The elevated cell viability seen using the fixable live/dead stain is likely due to the human error rate that is seen in trypan blue exclusion. Nonetheless, such high microglia viability compared to my data is likely due to quicker processing times as whole brains were used in these experiments and not due to differences in myelin removal as the Miltenyi Biotech brain dissociation kit utilises a Percol-like gradient. Equally it could be that the use of whole brains rather than dissected tissue could mean that there is less initial cell trauma and death leading to high cell viability or a combination of the two. Other studies isolating microglia, specifically for sequencing have not reported cell viability in their workflow and it is therefore difficult to make comparisons (Matcovitch-Natan et al. 2016; Hammond et al. 2019b). Cell yield was also another important factor here as I wanted to achieve the maximal number of sorted cells for RNA extraction. I reported that the cell count from the FACS machine was not an accurate reflection of the number of cells sorted with purity of the sorted samples ranging from 31-78%. This is a common problem in FACS experiments

and has been attributed to different factors such as droplet formation and electronic setup/parameters (Petersen and van den Engh 2003). Other factors that could influence these results could be that the extreme forces that are placed on the cells as they travel through the FACS machine impact cell viability and therefore yield. Interestingly (Osborne 2010) demonstrated that HEK cells loaded with fluorescent beads showed bigger yields upon sorting when performed with nozzles of a greater diameter. Therefore, it may be advantageous to think about using a wider nozzle for future microglial FACS experiments.

A major limitation of using the *Cx3cr1*$^{+/GFP}$ mouse is that one allele of the endogenous *Cx3cr1* gene is functionally knocked out and it is not completely understood what functional effect this may have. The chemokine Cx3cl1 is the sole ligand for the Cx3cr1 receptor which is constitutively expressed on the cell membrane of neurons. The binding of Cx3cl1 to Cx3cr1 suggests a discrete signalling pathway between neurons and microglia which may cause the release of neuromodulators. Despite this key link between neurons and microglia, the group that generated the *Cx3cr1*^{GFP} line did not observe any overt phenotype relating to the genetic manipulation at the time (Jung et al. 2000). However, since the publication of this study, there have been conflicting reports on the effect of manipulating the Cx3c axis. Neuron - microglial cross talk via Cx3cr1-Cx3cl1 is now thought to be important for regulating the neurotoxic effects of microglia (Sheridan and Murphy 2013). One study has demonstrated an absence of Cx3cl1 expression in immature neurons and suggests therefore, Cx3cl1 may play a protective role in mature neurons from over active microglia. Conversely, the restricted expression of Cx3cl1 in mature neurons may play a role in regulating the generation of new neurons through indirect microglial action (Bachstetter et al. 2011). Furthermore, there are opposing reports of the effects from completely knocking out the Cx3cr1 gene with some studies showing negative impacts and others reporting resilience in disease models (Cardona et al. 2006; Fuhrmann et

al. 2010; Grizenkova et al. 2014; Zhan et al. 2014; Liu et al. 2020). For example, (Zhan et al. 2014) have shown, using *Cx3cr1* KO mice, that the absence of this receptor in adult mice results in a deficiency in the number of synapses per axonal input, decreased functional connectivity between brain regions and decreased social interaction. However, there appears to be less evidence on the functional impact of knocking out one allele. One study has looked at the role of the Cx3c axis in cognition and synaptic plasticity comparing 3-month-old *Cx3cr1*$^{-/-}$, *Cx3cr1*$^{+/-}$ and wild type mice (Rogers et al. 2011). Both *Cx3cr1*$^{-/-}$ and *Cx3cr1*$^{+/-}$ showed deficits in contextual fear learning, Morris water maze memory function and motor learning which correlated with an impairment in long term potentiation compared to wild type. Interestingly there appeared to be significant differences recorded in the number of doublecortin (Dcx) positive and BrdU positive cells in the sub granular zone in a gene-dosage manner. With wild type mice displaying the greatest number of both Dcx positive and BrdU positive cells, *Cx3cr1*$^{-/-}$ with the least and *Cx3cr1*$^{+/-}$ lying in the middle. Reduced Dcx expression and BrdU labelling, in both *Cx3cr1*$^{-/-}$ and *Cx3cr1*$^{+/-}$ mice compared to wild type, indicate decreased rates of hippocampal neurogenesis. Another group has performed RNA-seq, comparing whole brain microglia from wild type, *Cx3cr1*$^{GFP/GFP}$ and *Cx3cr1*$^{+/GFP}$ mice (Gyoneva et al. 2019). In two month old mice, principal component analysis showed that *Cx3cr1*$^{GFP/GFP}$ and *Cx3cr1*$^{+/GFP}$ clustered together away from wild type samples. Further analysis revealed that *Cx3cr1*$^{GFP/GFP}$ and *Cx3cr1*$^{+/GFP}$ shared many differentially expressed genes including those encoding *Mhc class II* genes as well as chemokine receptors and ligands. Furthermore, Cx3cr1 deficient microglia from young mice appeared to show an aged transcriptional profile similar to that of wild type microglia from aged mice. Overall, these results demonstrate that the loss of one allele is enough to see disturbances in transcriptional phenotype as well as impairments in receptor function which likely reflect the important role that the Cx3c axis plays in neuron microglia signalling. It would have been highly interesting

to perform RNA-seq on microglia from the dentate gyrus comparing wild type mice with *Cx3cr1*$^{GFP/GFP}$ and *Cx3cr1*$^{+/GFP}$ mice to see if there were transcriptional differences in a gene dosage dependant manner. However, owing to Covid-19 restrictions this was not possible for logistical reasons.

A second limitation of using the *Cx3cr1*^{GFP} mouse line is that expression of *Cx3cr1* is not exclusively limited to microglia and has been shown to be expressed in monocytes, NK cells, dendritic cells and some T-cells (Jung et al. 2000). It has been reported elsewhere that *Cx3cr1* mRNA is expressed in cultured human neurons as well as microglia determined by reverse-transcription PCR, however, in this study they did not show whether the mRNA was translated into protein (Hatori et al. 2002). A different group has also suggested that *Cx3cr1* expression is not restricted to microglia. They report *Cx3cr1* expression in cultured hippocampal neurons from rat embryos (E17-18), but they did not demonstrate whether this was maintained into adulthood or whether it could be an artefact of culturing (Meucci et al. 2000). My results do not agree with these findings as over 99% of all GFP labelled cells were also shown to express Iba1. However, this result was performed *in vitro* and could be biased by the fact that microglia are by their nature more likely to stick to cell culture plates and awaits *in vivo* validation. Interestingly one group has published a recent report of a mouse line that has been generated with enhanced GFP expression under the recently discovered microglial specific gene: Tmem119 (Bennett et al. 2016; Kaiser and Feng 2019). (Kaiser and Feng 2019) aimed to create a mouse line in which microglia could be selectively visualised without compromising the endogenous expression of the targeted gene. They utilised CRISPR/Cas9 technology to insert eGFP into the stop codon of Tmem119 and this was validated via PCR. Furthermore, endogenous Tmem119 expression was validated by quantifying *Tmem119* transcript levels via qPCR and this was found to be comparable between wild type and Tmem119-eGFP$^{+/-}$. There

was also no reported difference at the protein level of Tmem119 between wild type and experimental animals as measured by immunofluorescence. This suggests that they have successfully generated a mouse line in which microglia are exclusively targeted and endogenous gene expression is maintained. This will be another useful tool in the investigation of microglia that will aid in distinguishing microglia from other myeloid derived cells.

As a result of these limitations I have decided to use wild type mice for RNA-seq experiments and I will isolate microglia instead using P2ry12-PE. P2ry12 is a microglial signature gene that has been identified in several transcriptomic studies (Hickman et al. 2013; Butovsky et al. 2014). There is some evidence that *P2ry12* – like other signature microglia genes- is downregulated in activated microglia and in diseased states, but as I will be using wild type mice this is not of too much concern (Butovsky et al. 2015). *P2ry12* has also been identified in a meta-analysis using five published mouse transcriptional studies as a top microglia gene that is differentially expressed between microglia and spleen monocytes/macrophages (Haage et al. 2019). To further validate this result (Haage et al. 2019) generated proteomic data from microglia and spleen monocytes/macrophages from 12-week-old wild type mice. Of the proteins that were evaluated between the two populations p2ry12 showed the greatest enrichment and the highest t-test difference for microglia. I have validated the use of this antibody in my work by back-gating P2ry12-PE staining onto GFP expression using existing data. As mentioned early, unfortunately a blocking procedure was omitted during antibody staining and so there will be some unspecific binding in this data. However, the mice used were perfused with PBS and as over 96% of P2ry12-PE stained cells were strongly expressing GFP. I am confident that I can extract the same population of cells in wild type mice using P2ry12-PE antibody.

6.4 Conclusion

In conclusion, I have established that the *Cx3cr1*$^{+/GFP}$ mouse model labels microglial cells via the expression of GFP as confirmed with Iba1 antibody co-labelling. Moreover, I have shown that I can successfully isolate a purified population of GFP expressing cells from discrete brain regions of *Cx3cr1*$^{+/GFP}$ mice by performing microdissection, including the cortex, hippocampus and DG and that these cells are viable post cell sorting. Since reviewing the very recent literature around *Cx3cr1*^{GFP} mice, I have opted to advance this work using wild type mice and selectively isolate microglia using P2ry12 antibody and FACS which I have validated through back gating. Although I have decided to move forward without using the *Cx3cr1*$^{+/GFP}$ mice it would be interesting in future work to further investigate levels of neurogenesis of *Cx3cr1*$^{+/GFP}$ mice at a young age compared to wild type animals and whether these differences could be observed at a transcriptomic level. Furthermore, I have validated my DG microdissections using previously reported genes that show enriched expression in the DG and CA1/CA3 regions and I am satisfied that my dissections reflect these regions accurately. I have also demonstrated that I can extract RNA from small populations of sorted cells in preparation for bulk RNA-seq.

7. Bulk RNA-sequencing of acutely isolated microglia from the dentate gyrus, surrounding hippocampus and cortex

7.1.0 Introduction

Distinct areas of the brain differ in their composition by cell type, myelination, architecture, chemical make up as well as varying levels of blood brain barrier properties. These differences between brain regions implies differential requirements that need to be met by supporting cells such as microglia and astrocytes. In the previous chapters I was unable to show a functional regional dependant neurogenic effect of cultured microglia on hippocampal neural progenitor cultures. This result could be due to a loss of specialised microglial phenotype when taken out of their endogenous microenvironment and into an artificial culture condition (Butovsky et al. 2014; Bohlen et al. 2017). Additionally, the method of microglial isolation has also been demonstrated to alter transcriptional phenotype as well as microglia surface and intracellular marker expression in flow cytometric analysis (Mattei et al. 2020). Therefore, a different approach was taken to investigate potential regional dependant neurogenic properties in microglia. The transcriptomic landscape of acutely isolated microglia extracted from discrete brain regions of wild type mice was investigated. In this way, any regional specific microglial transcriptomic phenotype should be captured. Here, I propose that microglia from different brain regions will have specialised transcriptomic phenotypes which is informed by and in

response to their local microenvironment. By comparing the transcriptome of microglia from the dentate gyrus with other brain regions I hope to show genes that are differentially expressed in the dentate gyrus and that these genes are relevant to its neurogenic capacity. Differentially expressed genes that are considered good candidates would then be used as targets in culture to confirm these findings. As discussed in the previous chapter, initially, *Cx3cr1-GFP* mice were to be used in these experiments, however, after reviewing the literature I decided to opt for wild type mice as *Cx3cr1-GFP* mice have been associated with deficits in neurogenesis, learning and memory as well as a premature aging of the transcriptome (Rogers et al. 2011; Gyoneva et al. 2019). Previous research in the field of microglia transcriptomics have made important advancements in highlighting key microglial signature genes as well as showing that microglia are highly dynamic and are capable of altering their phenotype across time and space as well as other factors (Erny et al. 2015; Grabert et al. 2016; Matcovitch-Natan et al. 2016). Further advancements in transcriptomics have included the emergence of single cell technologies, such as single cell RNA-seq, cytometry by time of flight mass spectrometry (CyTOF) and other 'omics' technologies, which are providing researchers with a greater holistic understanding of microglia cell biology (Artegiani et al. 2017; Hammond et al. 2019a; Sankowski et al. 2019).

7.1.1 Evidence of differential regional transcriptional phenotypes of microglia

It has been well documented that tissue resident macrophages have distinct transcriptional profiles dependent on their physical location in the body (Gautiar et al. 2012; Okabe and Medzhitov 2014). This reflects the ability of tissue resident macrophages to respond to their local microenvironment with differences in cell types, tissue architecture, degree of vasculature

and extracellular milieu evident in distinct tissues. Similarly, it is thought that the tissue resident macrophages of the brain -microglia- display distinct transcriptomic phenotypes across development, owing to the different needs of the tissue including, neurogenesis, neuronal migration, synaptic remodelling and homeostatic functions. Transcriptomic studies in recent years have demonstrated that the microglial transcriptional phenotype is altered across different parameters including time and space (Grabert et al. 2016; Matcovitch-Natan et al. 2016; Hammond et al. 2019a; Kreisel et al. 2019; Li et al. 2019; Masuda et al. 2019; Sankowski et al. 2019). Matcovitch-Natan et al. (2016) performed RNA-sequencing on isolated microglia across four developmental timepoints including yolk sac myeloid progenitors, embryonic, postnatal and adult microglia. A large number of genes were found to be differentially expressed across developmental timepoints where transitional states were determined as: early microglia, pre-microglia and adult microglia. Additionally, microglia from adult (8-week-old) mice were compared across different brain regions including: the cortex, hippocampus and spinal cord and here 76 genes were found to be differentially expressed between brain regions. Regional differences in microglial gene expression has been corroborated by Grabert et al. (2016). Here microglia were extracted from the cortex, cerebellum, hippocampus and striatum and transcriptional profiling was performed using gene expression micro arrays. Principal component analysis demonstrated that within each region, samples generally clustered together well, indicating heterogeneity between microglia from the brain regions that were examined. Samples from the cortex and striatum clustered more closely together while samples from the cerebellum and hippocampus clustered further away from each other. Additionally, differentially expressed gene expression has been shown between the dentate gyrus and CA1 regions in the *Cx3cr1-GFP* mouse model as discussed in the previous chapter (Kreisel et al. 2019). In further support that microglia are capable of specialised regional/temporal functionality Hammond et al. (2019b) demonstrated a distinct population of *Spp1* positive

microglia in the early post-natal brain which was not found at any other time point. Through validation with smFISH this highly concentrated population was identified as axon tract associated microglia which were localised to subcortical axon tracts of the corpus callosum as well as distinct axon tracts in the cerebellum. These reports provide good evidence that microglia are capable of distinct transcriptional phenotypes which may inform specialised functionality.

7.1.2 Aims

The aim of this chapter was to assess differential gene expression in microglia from three different brain regions from male C57 BL/6J mice: the dentate gyrus, hippocampus minus the dentate gyrus (rest of the hippocampus), and the cortex by performing bulk RNA-sequencing. In this way I aimed to confirm what has been performed in previously published work in transgenic mice and possibly identify new targets that are relevant to neurogenesis and therefore specific to the dentate gyrus to inform future experiments.

7.2.0 Results

7.2.1 Raw fastq files undergo adaptor trimming and quality control

In order to investigate possible regional-dependant neurogenic properties of microglia. The dentate gyrus (DG) was micro dissected along with the rest of the hippocampus (RH) and a section of the cortex from 6 male C57BL/6 mice (General Methods 2.2.4). The tissue for separate brain regions was pooled, dissociated, underwent myelin removal (General Methods 2.2.6) and then enriched for microglia by FAC sorting with the microglial specific P2ry12 fluorescent antibody (General Methods 2.2.7). After 3 independent experiments were performed and samples collected, total RNA was extracted and sent to Novogene (Cambridge, UK) for paired end (150bp reads) RNA sequencing with an approximate read depth of 30 million reads, on an Illumina Novaseq (General Methods 2.2.11 - 2.2.12). Once raw fastq files were received, files underwent adapter trimming and quality control assessment using fastqc report (General Methods 2.2.13). Upon initial adapter trimming it was found that there was a significant portion of over represented sequences identified as Clontech SMART CDS primers. These relate to the primers used to perform RNA amplification and once identified were also trimmed. Typical per base sequence quality reads are shown before adapter trimming (**Fig.33 B**) and after (**Fig.33 C**) adapter trimming.

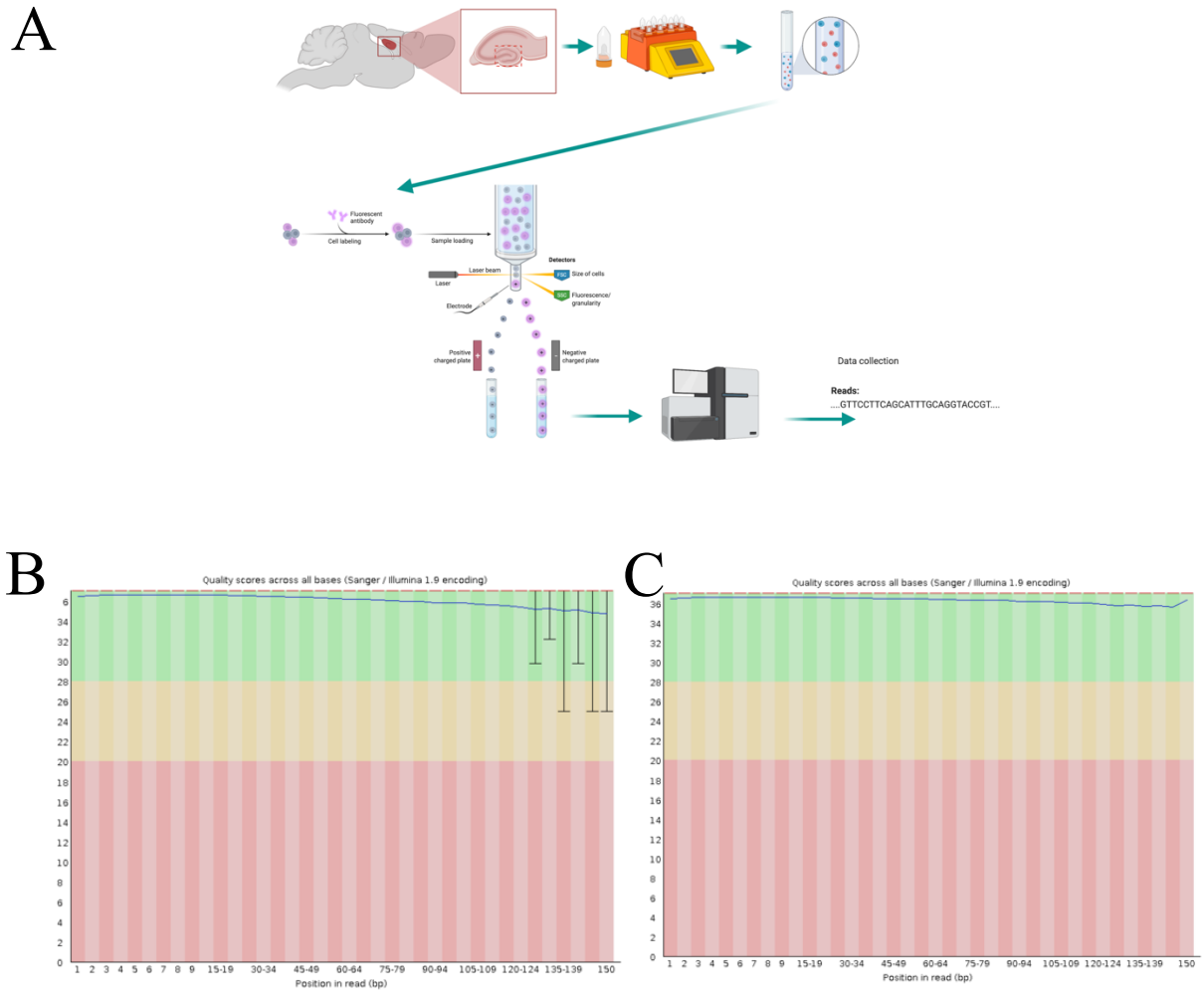

Figure 33. Fastqc quality scores improve upon adaptor trimming.

(A) shows the experimental design where microglia are isolated from mouse brain regions, mechanically dissociated and sorted by fluorescence activated cell sorting before undergoing RNA sequencing *(*Created with BioRender.com*)*. (B) a fastQC quality score pre illumina adaptor trim, (C) fastQC quality score post illumina and clonetech SMART primer trim.

7.2.2 Raw read counts are normalised with Deseq2

To perform differential expression analysis using the Desq2 package, un-normalised counts are required as the default input. The model that is used within the Deseq2 package corrects for library size internally and normalised counts are produced in the results. To examine the effect of normalisation, raw counts and normalised counts, they were plotted as box plots for each sample (**Fig.34 A**) (General Methods 2.2.14). For visualisation of the data it can be helpful to transformed versions of the data such as logarithm. There are several different methods that

can be used for transformation as suggested in the Desqeq2 vignette. MeanSDPlots were generated on raw (**Fig.34 B**), variance stabilising transformation (VSD, **Fig.34 C**), regularised log transformation (rlog, **Fig. 34 D**) and log2(n+1) (**Fig. 34 E**) transformed versions of the data set. Both rlog and VSD are equivalent to log2 transformed data where the data has been normalised with respect to library size. MeanSDPlots plot the standard deviation of the data, across all samples, against the mean. The raw data shows that the data is shifted to the left indicating that there are a large number of genes with a small number of counts and smaller number of genes with larger counts and larger variation. The transformation log2(n+1) results in a dramatic increase in the standard deviation of counts in the lower range, whereas VSD and rlog transformations stabilise the variance across all counts. For visualisation of the data from this point onwards rlog transformed data was used unless stated otherwise.

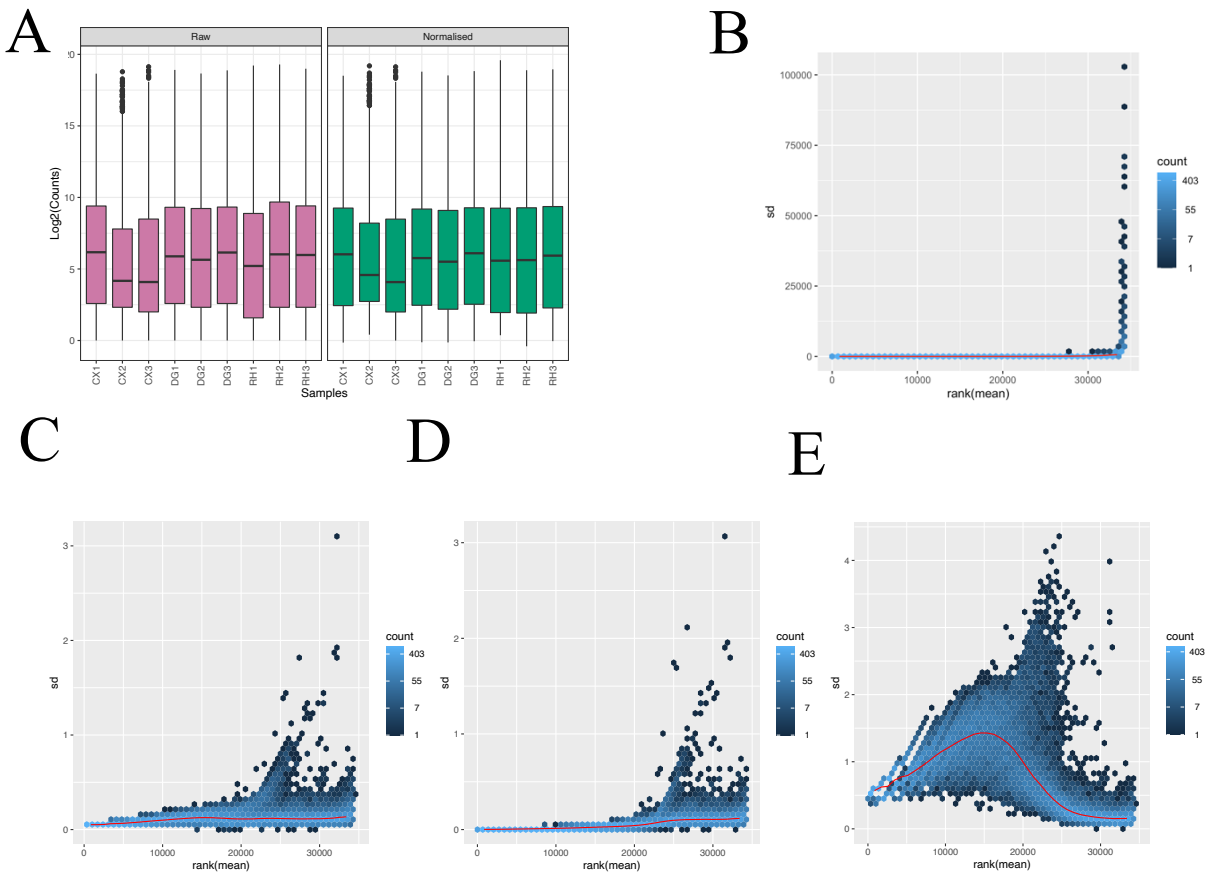

Figure 34. Effect of DeSeq2 normalization on count distribution.

The deseq2 package for differential analysis requires raw gene counts as its input and corrects for library size internally. To assess the effect of library size correction by deseq2, $\log_2$ raw and normalised gene counts were plotted for all samples (A). The suitability of data transformations were visualised using meanSDplot for (B) raw counts, (C) Variance stabilising transformation (VST), (D) regularised logarithm (rLog), (E) log2(n+1). MeanSDplot plots the standard deviation of the transformed data across all samples, against the mean. Both VST and rLog produce data on the log2 scale which is normalised with respect to library size. N= 3 independent samples per group, 6 mice per sample.

7.2.3 Microglia cell type specific signature genes are enriched

Freshly isolated microglia were purified by FACS sorting using the microglial specific marker, P2ry12. In order to validate the purity of the isolated microglia, the transcriptome data was probed for a curated list of well-known and previously published cell type specific genes for microglia (e.g. *Trem2, Tmem119, Selpig, Sall1, P2ry12, Cx3cr1, C1qa*), brain associated macrophages (these are phenotypically and ontogenically distinct from parenchymal microglia e.g. *Pf4, Mgl2, Ifitm3, F13a1, Clec12a*), monocytes (e.g. *Sell, MKi67, Hp, Gda, F5, F10,*

Emilin2, C3), astrocytes (e.g.*Slc6a11, Slc4a4, Grm3, Gfap, Fgfr3, Aqp4*), neurons (e.g. *Tubb3, Tmem130, Sst, Snap25, Reln, Npy, Neu1, Map2*) and oligodendrocytes (e.g. *Sox10, Ppp1r14a, Olig1, Mog, Mbp*) (Zhang et al. 2014; Matcovitch-Natan et al. 2016; Haage et al. 2019; Hammond et al. 2019b). FPKM values were plotted for each brain region against the cell type specific genes. The cell type specific markers used to identify microglia all exhibited high expression levels except for *Sall1* in all brain regions and undetectable or extremely low expression of other cell type specific genes were observed. This result indicates that a pure population of microglia were isolated and sequenced, providing further confidence to the results obtained in this chapter.

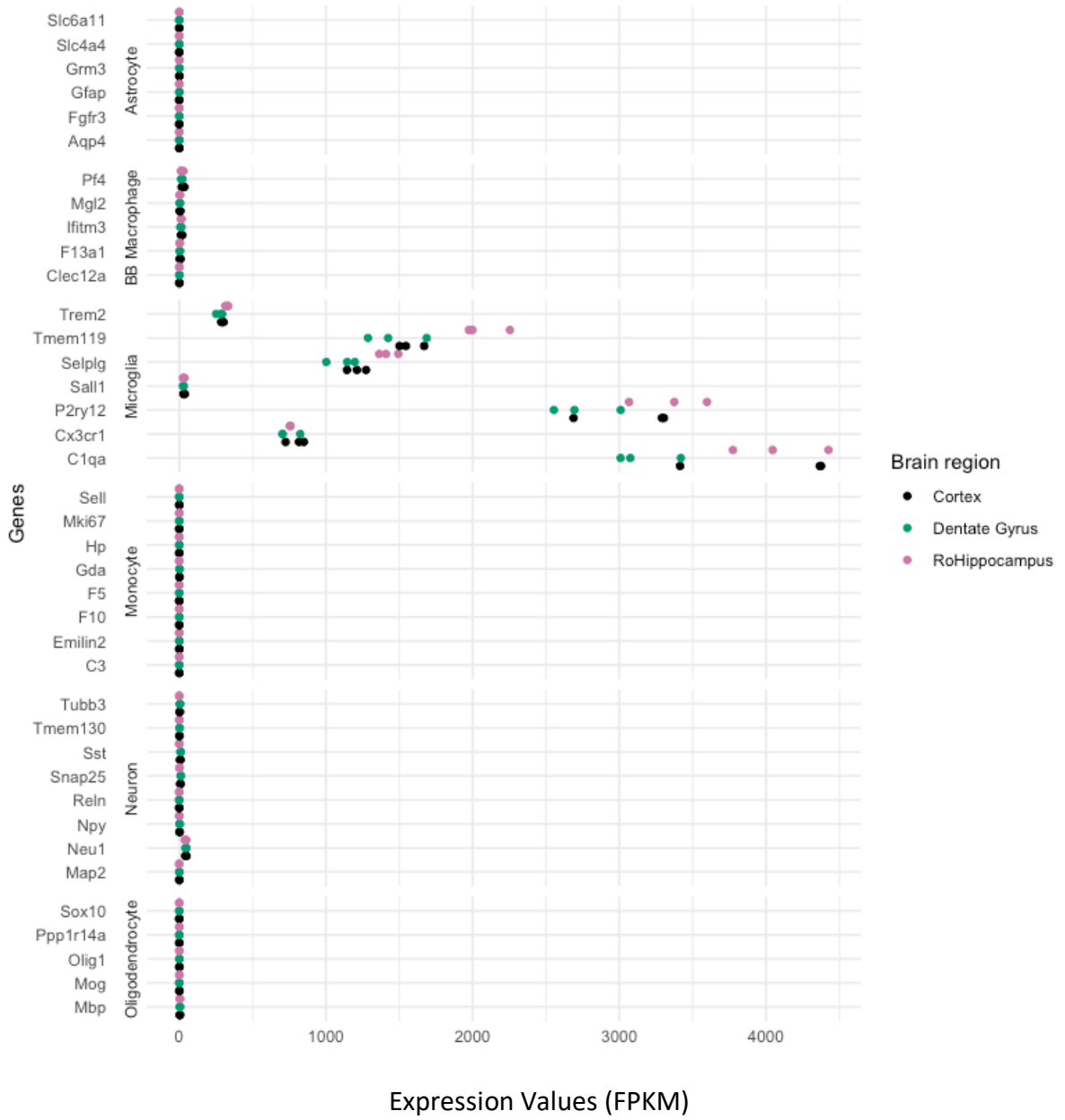

Figure 35. Microglia specific transcriptomic signatures show an enriched expression compared to non-microglia cell type specific genes.

FPKM values were calculated and plotted for the cell type specific genes selected and for each brain region that microglia were isolated from (n =3). High gene expression was observed in *Trem2, Tmem119, Selpig, P2ry12, Cx3cr1 and C1qa*. Undetectable or extremely low values were observed for non-microglia specific genes. N= 3 independent samples per group, 6 mice per sample.

7.2.4 Dentate gyrus microglia cluster away from microglia isolated from the rest of the hippocampus

In order to assess and visualise the variability within the dataset a principal component analysis (PCA) was performed (General Methods 2.2.14). PCA is a method that is used to reduce the number of dimensions – in this case number of genes- of a large set of variables into a smaller one while preserving as much information as possible. A PCA should reflect the total variation of the dataset and is commonly presented as a two-dimensional plot in which the data is visualised along axes that describe variation within the dataset known as principal components (PC). Typically, PC's are plotted against each other with PC1 describing the biggest amount of variation in the data set with further decreases attributed successively to each further PC. The PCA was plotted using rlog values (**Fig.36 A**) and displays PC1 and PC2, indicating that samples from the DG and RH cluster away from each other and that this directionally is responsible for the largest amount of variation. This was also corroborated in the scree plot (**Fig.36 B**). The second biggest attributer to variability is the separation of samples from DG and Cortex. One of the samples from the cortex appears to cluster together with DG samples. The separation in variability within the cortical samples may be due to RNA quality as the 2 samples that cluster away were described as moderately degraded by Novogene QC. Another way to interrogate inter and intra group variability is by calculating Pearson's correlation coefficient (**Fig.36 D, E**) which demonstrates the linear relationship between two variables accounting for differences in their mean and standard deviation. All pairwise Pearson's coefficients were greater than 0.999, with the highest coefficients observed within groups for DG and RoHippocampus. Similarly, sample clustering of the transformed data provides sample to sample distance which when plotted in a heatmap gives an overview of the similarities and

dissimilarities between samples (**Fig.36 C**). These results indicate that overall there was very little variation between all samples but of the variation that could be seen, this could be explained by the brain region that microglia were isolated from, particularly for DG and RH samples.

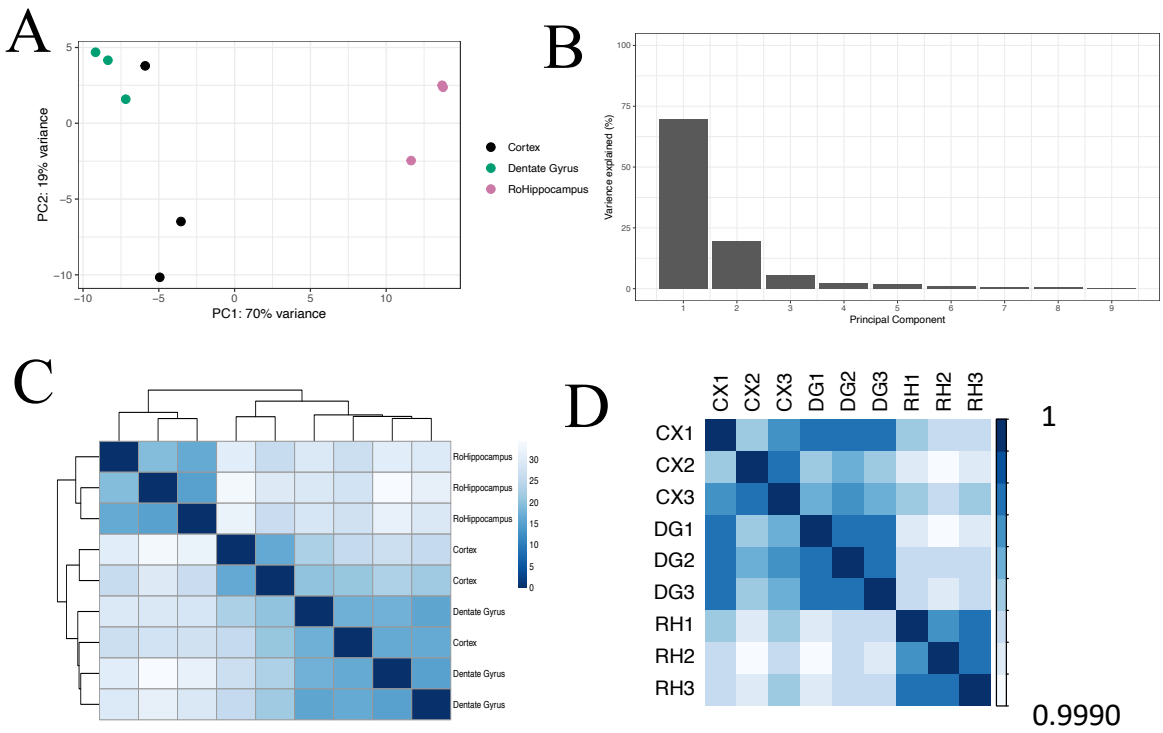

E

	CX1	CX2	CX3	DG1	DG2	DG3	RH1	RH2	RH3
CX1	1	0.9995	0.9997	0.9998	0.9998	0.9998	0.9994	0.9994	0.9994
CX2	0.9995	1	0.9998	0.9995	0.9996	0.9995	0.9993	0.9991	0.9992
CX3	0.9997	0.9998	1	0.9996	0.9997	0.9996	0.9995	0.9993	0.9995
DG1	0.9998	0.9995	0.9996	1	0.9998	0.9998	0.9993	0.9991	0.9992
DG2	0.9998	0.9996	0.9997	0.9998	1	0.9998	0.9993	0.9993	0.9994
DG3	0.9998	0.9995	0.9996	0.9998	0.9998	1	0.9993	0.9992	0.9993
RH1	0.9994	0.9993	0.9995	0.9993	0.9993	0.9993	1	0.9997	0.9998
RH2	0.9994	0.9991	0.9993	0.9991	0.9993	0.9992	0.9997	1	0.9998
RH3	0.9994	0.9992	0.9995	0.9992	0.9994	0.9993	0.9998	0.9998	1

Figure 36. Samples from the Dentate Gyrus and the RoHippocampus cluster away from each other.

To assess source of variation between samples a principal component analysis was plotted (A) using rlog values for cortex, dentate gyrus and Rest of hippocampus (RoHippocampus). PC1 (70%) and PC2 (19%) account for over 80% of the variation observed. The Scree plot (B) further demonstrates that variation between samples is accounted for mainly in the first 3 PC. Heatmap (C) provides an overview of the similarities and dissimilarities between samples. Pearson's correlation plot (D, E) to assess inter and intra group variability using FPKM normalised values. There are 3 independent samples per group, each sample is pooled from 6 mice.

7.2.5 Top expressed genes across all samples are enriched for microglial signature genes

In order to assess the similarities across all 9 samples, the top 50 expressed genes were plotted in a heatmap using rlog transformed values (**Fig.37**). Many of these genes were microglia signature genes such as *Hexb, P2ry12, Csf1r, Tmem119*, and *Cx3cr1* giving further confidence that data represents microglia populations from these brain regions. Other very highly expressed genes included immediate early genes including Fos and Jun, which could be due to cellular stress inflicted on microglia during isolation and handling procedures despite efforts to maintain 4ºC throughout (Mattei et al. 2020).

Figure 37. Top expressed genes across all microglial samples from the dentate gyrus, rest of hippocampus and cortex include microglial signature genes and immediate early genes.

The top 50 genes that were expressed in all microglia samples from the dentate gyrus (DG), rest of the hippocampus (RoHippocampus) and cortex (CX) were plotted in a heatmap using regularised log (rlog) transformed values. Red = Highest level of gene expression, blue = lower level of gene expression. N= 3 independent samples per group, 6 mice per sample.

7.2.6 Microglia isolated from the Dentate gyrus display over a 1000 differentially expressed genes compared to microglia from the rest of the hippocampus

To investigate divergence of gene expression between DG and RH microglia in C57BL/6J mice, DESeq2 was used to identify genes that were differentially expressed (General Methods 2.2.14) (Love et al. 2014). Raw reads were mapped to the mouse genome (GRCm39) with

53,700 possible genes for annotation including, coding, non-coding and pseudo genes. After filtering out genes that contained less than one read across all samples, 34,262 remained at a false discovery rate (FDR) of 0.01. 88 genes were also removed from the data as they are no longer represented in the Ensembl mouse database. Of the 34,174 annotated genes remaining, 1728 (5.06%) genes were identified as being differentially expressed with a p-adjusted value of less than 0.01, this was further reduced to 1221 (3.57%) when selecting for genes with a log fold change of less than -1 and greater than 1 (**Table.3** listing top 20 significant DEGs – see Appendix 9.0 for full list). Hierarchical clustering analysis was performed on this subset of differentially expressed genes (DEG) using calculated z-scores and samples were found to be clustered by brain region (**Fig.38 A**). To visualise the highest DEG, the top 50 DEGs were plotted in a heat map using their z-scores with top DEGs including *Olfm1, Stmn3, Bex2* and *Snca* (**Fig.38 B**). DEGs were also interrogated to see which genes were up or down regulated by plotting a volcano plot. Of the 1221 DEGs, 1210 had a log fold change greater than 1 and were deemed to be upregulated in DG microglia. A further 11 genes had a log fold change of less than -1 and were deemed to be down regulated in DG microglia (**Fig. 38 C**). This demonstrates that there were significant differences in gene expression between microglia isolated from the DG and RH.

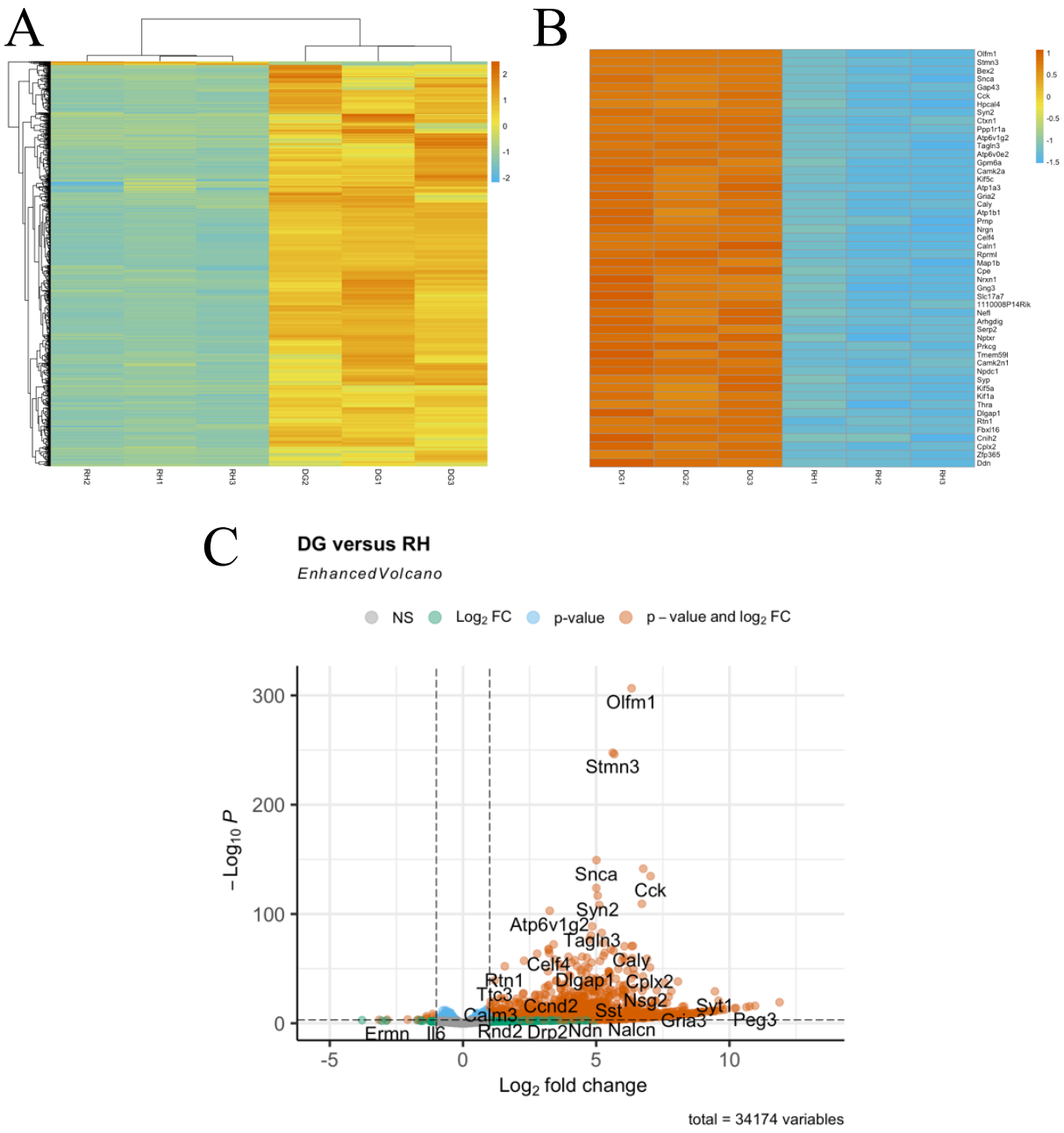

Figure 38. Over 1000 genes are differentially expressed between microglia isolated from the dentate gyrus (DG) and rest of the hippocampus (RH).

Deseq2 package was used to perform differential expression analysis on un normalised counts. A pairwise comparison was performed between DG and RH samples with a $p<0.01$ and log fold change < -1 or > 1. (A) Hierarchical clustering of significantly differentially expressed genes (DEG), (B) top 50 DEG plotted using calculated z-scores and (C) volcano plot showing up and down regulated genes. For (A) and (B) red = up regulated, blue = down regulated. N= 3 independent samples per group, 6 mice per sample.

Gene name	Description	log2FoldChange	Padj-value
Olfm1	olfactomedin 1	6.3302	5.86E-303
Stmn3	stathmin-like 3	5.6231	2.81E-244
Bex2	brain expressed X-linked 2	5.6789	3.87E-243
Snca	synuclein, alpha	5.0098	2.68E-146
Gap43	growth associated protein 43	6.7681	1.43E-138
Cck	cholecystokinin	7.04	7.38E-132
Hpcal4	hippocalcin-like 4	5.0072	4.87E-121
Syn2	synapsin II	5.0558	4.12E-114
Ctxn1	cortexin 1	6.717	1.10E-106
Ppp1r1a	protein phosphatase 1, regulatory inhibitor subunit 1A	5.118	1.42E-105
Atp6v1g2	ATPase, H+ transporting, lysosomal V1 subunit G2	3.254	2.01E-100
Tagln3	transgelin 3	4.8481	3.41E-86
Atp6v0e2	ATPase, H+ transporting, lysosomal V0 subunit E2	5.2072	3.06E-80
Gpm6a	glycoprotein m6a	4.8014	6.23E-78
Camk2a	calcium/calmodulin-dependent protein kinase II alpha	4.7413	3.14E-74
Kif5c	kinesin family member 5C	5.2663	4.50E-71
Atp1a3	ATPase, Na+/K+ transporting, alpha 3 polypeptide	3.4	8.21E-70
Gria2	glutamate receptor, ionotropic, AMPA2 (alpha 2)	6.378	2.04E-68
Caly	calcyon neuron-specific vesicular protein	6.3284	2.18E-68
Atp1b1	ATPase, Na+/K+ transporting, beta 1 polypeptide	6.0596	3.69E-68

Table 3. Top 20 differentially expressed genes in DG and RH microglia P<0.01 and log2fold change -1>X>1.

7.2.7 Dentate gyrus microglia display few differentially expressed genes compared to cortical microglia

To investigate the divergence of gene expression between DG and CX microglia in C57BL/6J mice, DESeq2 was used to identify genes that were differentially expressed (General Methods 2.2.14) (Love et al. 2014). Raw reads were mapped to the mouse genome (GRCm39) with 53,700 possible genes for annotation including, coding, non-coding and pseudo genes. After filtering out genes that contained less than one read across all samples, 34,262 remained at a false discovery rate (FDR) of 0.01. 88 genes were also removed from the data as they are no

longer represented in the Ensembl mouse database. Of the 34,174 annotated genes remaining, 38 (0.111%) genes were identified as being differentially expressed with a p-adjusted value less than 0.01. 12 (0.035%) of these identified genes had a log fold change of greater than 1 or a log fold change of less than -1 (**Table.2** listing significant DEGs). Hierarchical clustering analysis was performed on this subset of differentially expressed genes (DEG) using calculated z-scores and samples were found to be clustered by brain region (**Fig. 39 A**). To visualise the highest DEG, the top DEGs were plotted in a heat map using their z-scores with top DEGs including Ptger3, Lpl, Hes1 and Tcim (**Fig.39 B**). DEGs were also interrogated to see which genes were up or down regulated by plotting a volcano plot. Of the 38 DEGs, 6 displayed a log fold change greater than 1 and were deemed to be upregulated in DG microglia. A further 6 genes had a log fold change of less than -1 and were deemed to be down regulated in DG microglia (**Fig. 39 C**). This demonstrates that there were few significant differences in gene expression between microglia isolated from the DG and CX.

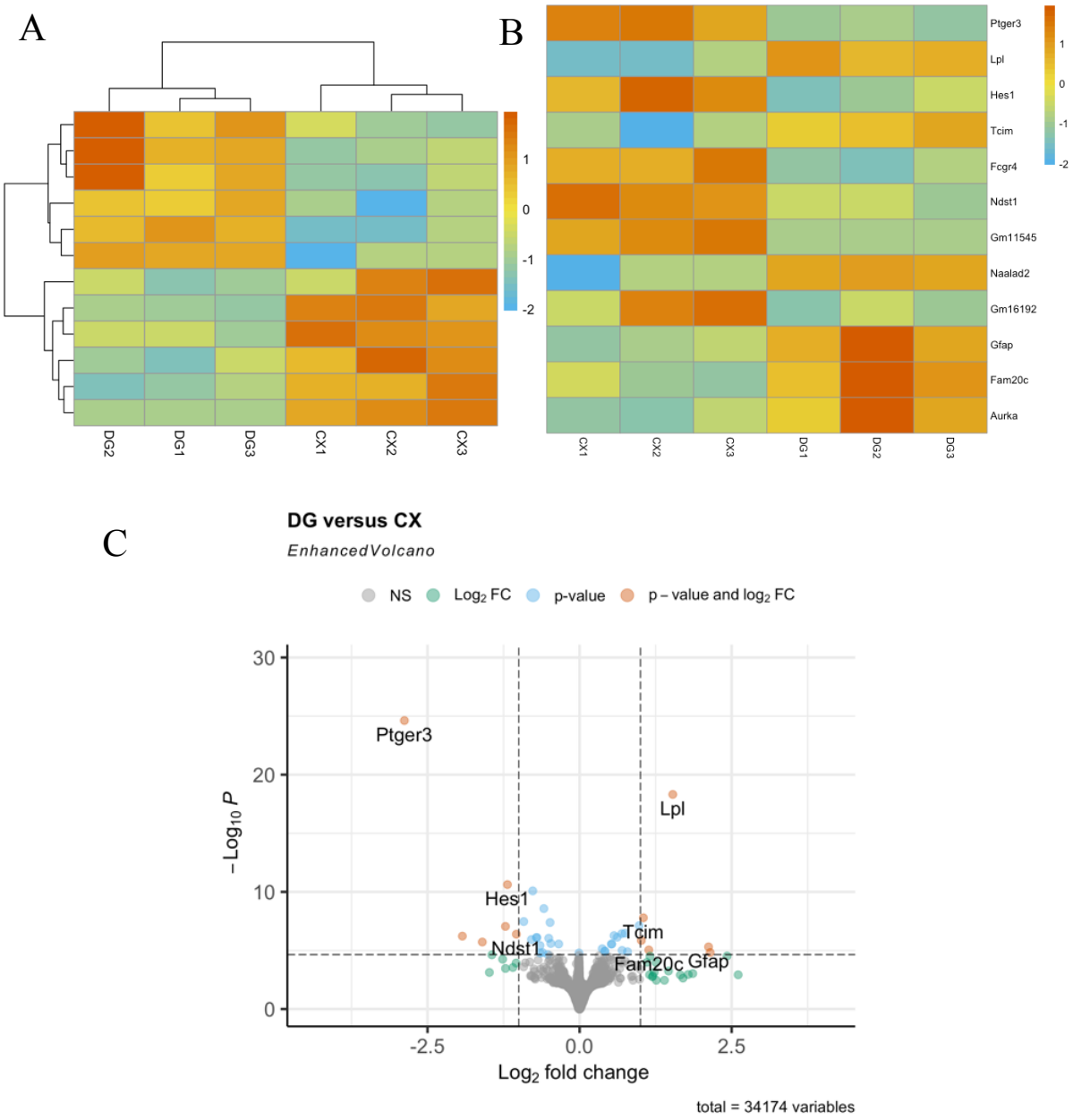

Figure 39. Few genes were differentially expressed between microglia isolated from the dentate gyrus (DG) and cortex (CX).

Deseq2 package was used to perform differential expression analysis on un normalised counts. A pairwise comparison was performed between DG and CX samples with a $p<0.01$ and log fold change < -1 or > 1. (A) Hierarchical clustering of significantly differentially expressed genes (DEG), (B) top DEG plotted using calculated z-scores and (C) volcano plot showing up and down regulated genes. N= 3 independent samples per group, 6 mice per sample.

Table 4. Differentially expressed genes of RNAseq analysis between DG and CX microglia from wild type mice

Gene name	Description	log2FoldChange	padj
Ptger3	prostaglandin E receptor 3 (subtype EP3)	-2.8802	4.70E-21
Lpl	lipoprotein lipase	1.532	4.75E-15
Hes1	hes family bHLH transcription factor 1	-1.1861	1.57E-07
Tcim	transcriptional and immune response regulator	1.0484	5.35E-05
Fcgr4	Fc receptor, IgG, low affinity IV	-1.2191	0.00017455
Ndst1	N-deacetylase/N-sulfotransferase (heparan glucosaminyl) 1	-1.0398	0.0006228
Gm11545	predicted gene 11545	-1.9273	0.00078392
Naalad2	N-acetylated alpha-linked acidic dipeptidase 2	1.0149	0.00131439
Gm16192	predicted gene 16192	-1.5995	0.00170487
Gfap	glial fibrillary acidic protein	2.1199	0.00346877
Fam20c	FAM20C, golgi associated secretory pathway kinase	1.138	0.0059577
Aurka	aurora kinase A	2.1467	0.00831704

7.2.8 Genes of interest show variable levels of read counts

It can be useful to examine the counts for reads for a single gene across groups as reliance on log fold changes can prove ineffective if genes are expressed at very low levels. Normalised read counts were plotted for individual genes of interest using the plotCounts function from the Deseq2 package which normalises counts by estimated size factors and adds a pseudo count of ½ to allow for log scale plotting (General Methods 2.2.14). For example, the gene which was shown to be the most highly differentially expressed between DG and RH was *Olfm1* (**Fig.40 A**), which has a log fold change of 6.33 and a P-adjusted value of 5.86E-303. When the normalised counts are plotted there is clear and large difference in gene expression between DG and RH regions with an average count of 5777 for DG and 73 for RH. In comparison, the DEG *Bdnf* (**Fig.40 B**) has a log fold change of 4.19 and P-adjusted value of 1.26E-09. When the normalised counts are plotted there is an observed difference between brain regions but the difference in the number of counts is relatively small with an average of 87 counts for DG and

3 counts for RH. Similar graphs were plotted for *Tyro3, Tgfb2, Il-6*, and *Il-34*. This demonstrates that genes which are DEG are not necessarily very highly expressed and this has implications for inferring biological meaning. Genes that were found to be differentially expressed in DG microglia in the work of Kreisel et al. (2019) were also plotted **(Fig.40 G/H/I)**. Normalised read counts for the genes *Clec7a, Axl* and *Spp1* were found to be differentially expressed in the DG of *CX3CR1-GFP* mice compared to microglia from the CA1 region in. Here they were not found to be differentially expressed between DG and RH with all three genes showing consistent, relatively high expression across all brain regions.

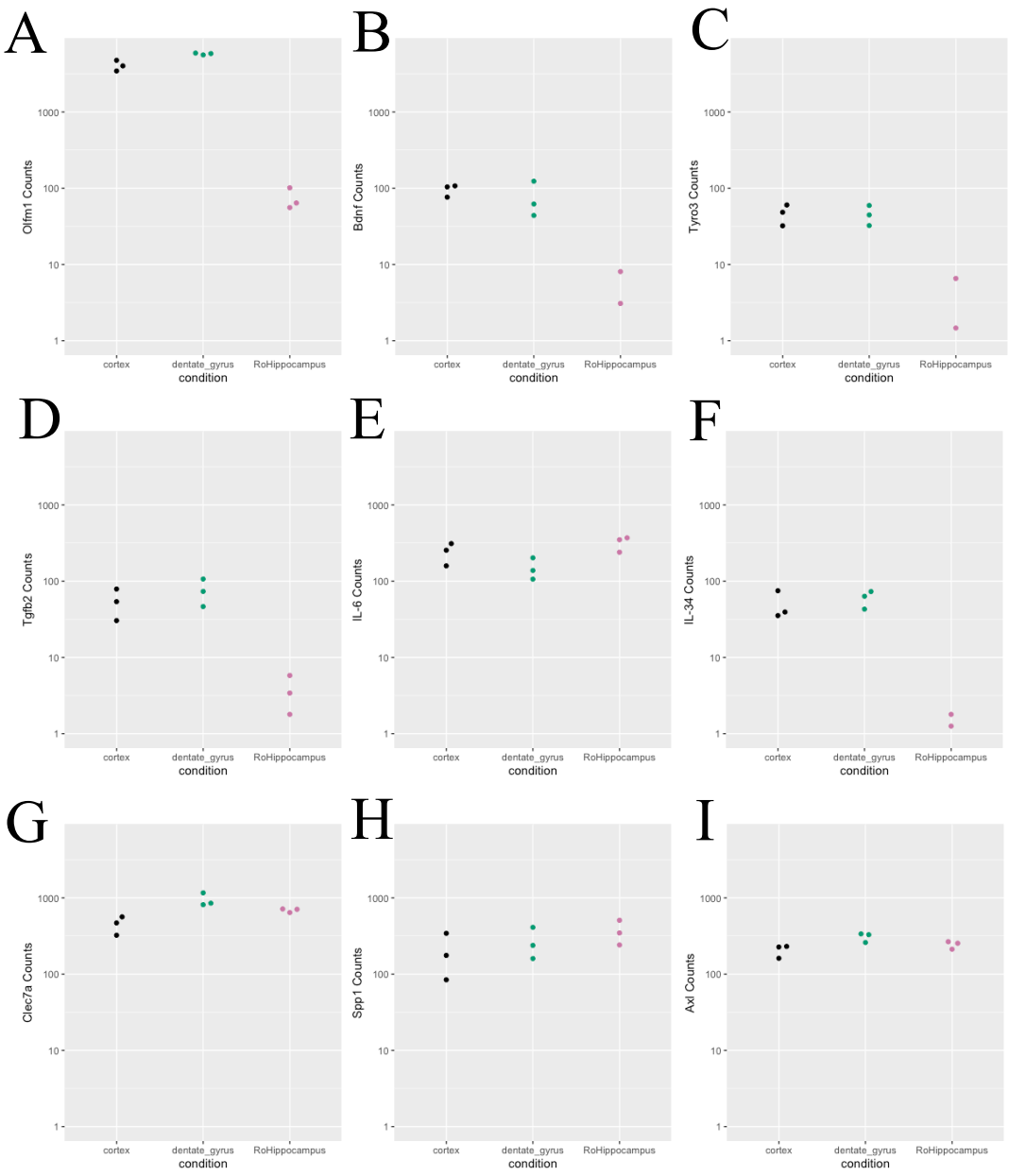

Figure 40. Significant log fold change in gene expression does not translate to relative high gene expression.

Plots were generated of normalised gene counts for individual genes for cortex, dentate gyrus and rest of hippocampus (RoHippocampus) using plotCounts from Deseq2 package. (A) *Olfm1,* (B)*Bdnf,* (C) *Tyro3*, (D)*Tgfb2*, (E) *Il-6*, (F) *Il-34*, (G) *Clec7a*, (H) *Spp1*, (I) *Axl*. N= 3 independent samples per group, 6 mice per sample.

7.2.9 GO term enrichment

Gene Ontology is a database that provides a logical structure to biological functions and pathways which are classed into terms. Gene ontology describes biological knowledge with respect to three broad categories: molecular function, cellular component and biological process. GO terms relating to molecular functions describe activities rather than molecules or complexes and cannot inform where, when or how an activity takes place e.g. toll-like receptor binding. GO terms relating to cellular component can inform the cellular and sub cellular compartment in which a gene product operates e.g. synapse. GO terms relating to biological process inform of the more conceptual biological programs which can be achieved through multiple molecular functions e.g. DNA repair. In order to investigate which biological processes were enriched in the DEG dataset GO term enrichment was performed (General Methods 2.2.15). The Ensembl gene IDs for the top DEG between pairwise comparisons where adjusted p-value < 0.01 and log fold change -1< >1 were uploaded to the AmiGO 2 online tool (http://amigo.geneontology.org/amigo) term enrichment service, selecting biological process and Mus musculus. Fisher's exact test was performed with a false discovery rate of < 0.05. There were no statistically significant enriched terms of biological processes found in the DEG list for DG v CX which is likely due to the low number of differentially expressed genes with a p-adjusted value < 0.01. For the DEG from the DG v RH pair wise comparison 750 biological processes were found to be statistically significant (FDR <0.05, P<0.01). **Fig. 41** displays the top 20 statistically significant biological process terms with a fold enrichment greater than 1. Many of the most significantly enriched GO terms that were over represented relate to synaptic signalling (eg. *Prrt, Grin3a, Cacng4*), neuronal development (e.g. *Vxn, Ntrk3, Cdkl5*) and neurogenesis (e.g. *Gpm6b, Dlg2, Camk2b*). This indicates that differential gene expression in DG microglia may relate to a specialised neurogenic function.

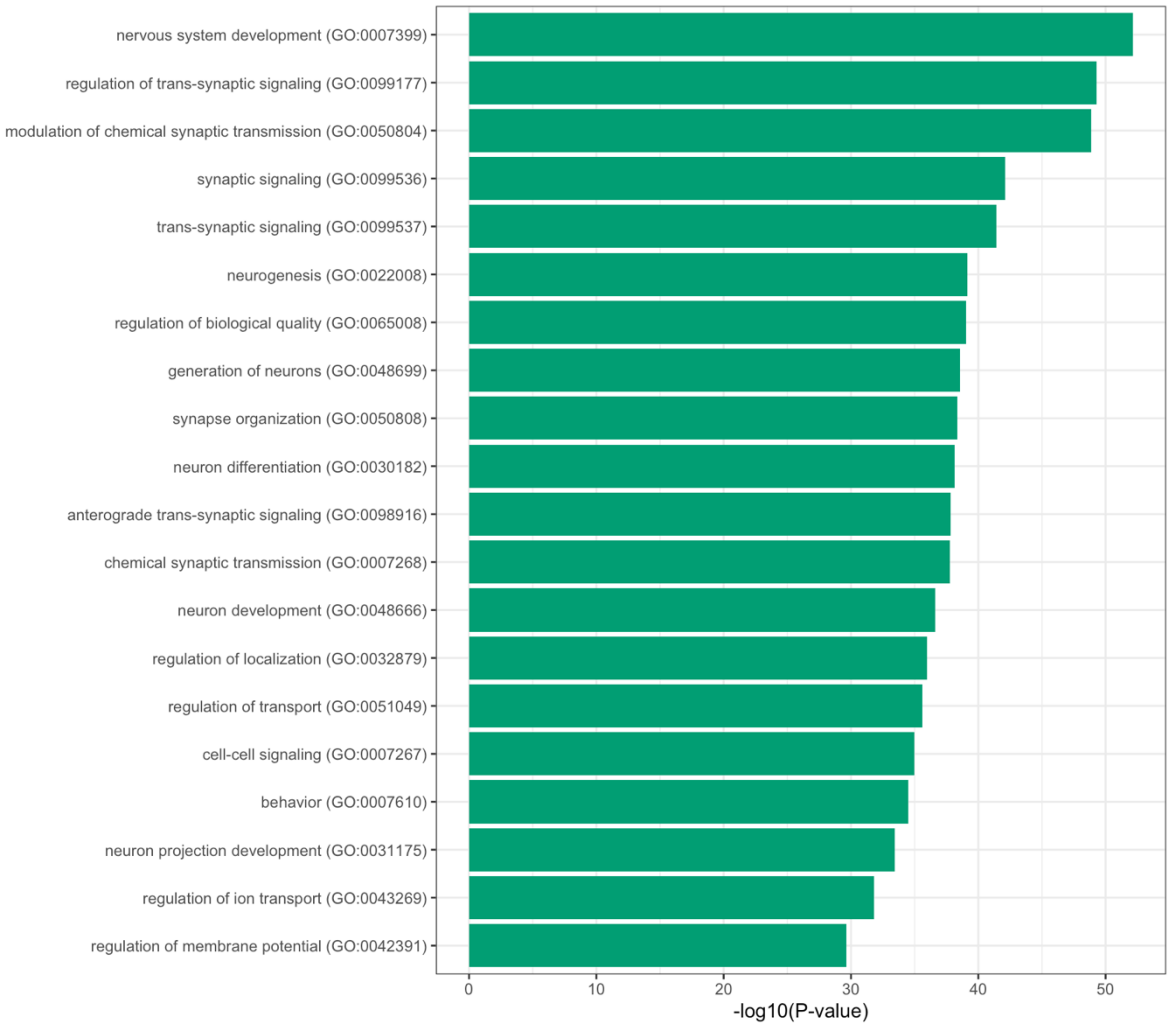

Figure 41. Dentate gyrus microglia show enrichment in neuronal differentiation, synapses and neurogenesis GO terms.

The Ensembl gene IDs for the top DEG between pairwise comparisons where adjusted p-value < 0.01 were uploaded to the AmiGO 2 online tool (http://amigo.geneontology.org/amigo) term enrichment service, selecting biological process and Mus musculus. Fisher's exact test was performed with a false discovery rate of < 0.05. N= 3 independent samples per group, 6 mice per sample.

7.2.10 Gene set enrichment analysis indicate an enrichment in metabolic processes for dentate gyrus microglia versus rest of hippocampus microglia

Data produced from RNA sequencing experiments result in a long list of differentially expressed genes which can be difficult to interpret and translate differences biologically. This

has been very useful in some fields such as cancer, where large perturbations in gene expression, observed in single genes are found to be responsible for particular phenotypes. However, in many biological questions it is becoming clear that it is not just one single gene that is perturbed or altered in a given state and it is more likely that there are moderate changes in gene expression across a number of genes related to a given pathway. A method to investigate significant differences of defined biological processes between experimental groups is gene set enrichment analysis (GSEA) (Mootha et al. 2003; Subramanian et al. 2005). GSEA is a computational method in which an *a priori* defined set of genes which are functionally related are used to assess if there are statistically significant, consistent differences between two experimental groups. GSEA analysis was performed (General Methods 2.2.16). Two of the top gene sets with the highest normalised enrichment score (NES) and an FDR < 0.25% are associated with metabolism (**Fig.42**). These gene sets require further investigation to decipher biological meaning. Gene sets that were overrepresented for RH all displayed an FDR - q value = 1.

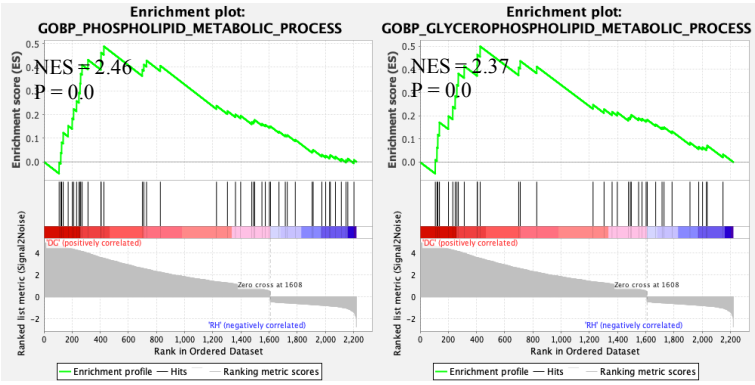

Figure 42. GSEA of data set DG v RoH, demonstrating gene sets that are overrepresented in each group.

Using molecular signatures database (MSigDB), the hallmark (H), curated (C2) and ontology (C5) gene sets were used to investigate differences between DG and rest of hippocampus (RoH). Gene set enrichment analysis (GSEA) plots show over represented gene sets of differentially expressed DG (A) genes compared to RoHippocampus microglial samples and include GOBP_phospholipid_metabolic_process and GOBP_Glycerophospholipid_metabolic process. N= 3 independent samples per group, 6 mice per sample.

7.2.11 Microglia gene list enrichment shows enrichment for ameboid microglia

Current gene enrichment tools such as GSEA allow comparison of differentially expressed genes in a data set to a predefined set of genes of biological cohesion. However, often these tools are not specific for particular cell types. Therefore, in order to perform direct gene list comparisons that are specific to microglia, Microglia Enrichment (MGEnrichment) analysis was performed (Jao and Ciernia 2021). MGEnrichment is a web-based tool that was developed for non-programming wet lab scientists to easily and efficiently perform enrichment analysis. MGEnrichment is a simple enrichment tool which performs a one-tailed Fisher's exact test to compare overlap between the supplied list of DEG and the gene lists in the database where statistical significance is established relative to a background gene list and an FDR correction. Ensembl IDs of differentially expressed genes between DG and RH with a P-value <0.01 and log fold change < -1 or >1 were uploaded to the platform with an FDR-value of 0.05 (General Methods 2.2.17). Gene list groups that were selected included: "microglia", "microglia development", "inflammation" and "neuropsychiatric & developmental disorders human brain". The background query was set to "all mm10 Genes or hg38 Genes". DEG were found to be enriched in 61 gene lists in the database. The most significant gene list that DEG were enriched in was "Amoeboid > Ramified" which is described as "DEGs with higher expression in amoeboid vs. ramified microglia" (Parakalan et al. 2012). 98 genes were found to overlap between the DEG list and "Amoeboid > Ramified" with a P-value of 3.13E-38 and FDR 2.14E-37. However, 50 genes were also enriched in "Ramified > Ameboid MG" gene list suggesting that DG microglia sit along a spectrum of these two phenotypes. Another gene list of potential interest called "decreased expression with age" showed enrichment for DEG where 54 genes were found to overlap, P-value = 4.65E-31 and FDR = 2.87E-30. This gene list is described as "DEGs negatively associated with human age" (Galatro et al. 2017). Significance in further

gene lists suggests enrichment for microglia over macrophage and monocytes and young mice over old mice.

7.3.0 Discussion

The aim of this chapter was to investigate regional differential gene expression in microglia from three different brain regions from male wild type C57 BL/6J mice including the DG, the RH, and cortex by performing bulk RNA-sequencing and downstream analysis. Firstly, the quality of the reads and effectiveness of the adapter trimming was assessed using fastqc reports. Next, alternative methods for transforming the data for visualisation purposes were evaluated by examining their effectiveness at stabilising the variation of the standard variation across all counts. The expression of cell type specific signature genes was investigated to further validate the effectiveness of acute microglia isolation. Intra and inter sample variation was then assessed using PCA and Pearson's correlation coefficient. Differential expression analysis was performed with the Deseq2 package where pairwise comparisons were performed: DG versus RH and DG versus cortex. Additional explorative analysis was conducted using DEGs by performing GO term enrichment, GSEA and MGEnrichment. Cell type specific gene interrogation gave further confirmation of microglial enrichment. DG microglial samples were found to possess over 1000 DEG compared to RH with only a few genes differentially expressed between DG and cortical microglial samples. These genes were found to be enriched for GO terms: nervous system development, neurogenesis and generation of neurons.

To examine whether microglia in DG represent a specialised subset of the microglia population that regulate hippocampal neurogenesis, DG microglia were compared to the non-neurogenic regions of the hippocampus termed RH as well as cortical microglia. Microglia were sorted on the basis of the microglial specific marker *P2ry12* and were compared with regards to their transcriptional phenotypes. Samples were shown to have a low degree of inter sample

variability with all samples displaying a high Pearson's correlation coefficient of 0.999 or over, suggesting that largely all samples have a similar expression profile with only a small number of genes accounting for these differences. Even with a very high Pearson's correlation coefficient, the analysis was still able to group microglia into DG and RH clusters with a less well-defined cluster for cortical microglial samples. This is concordant with other bulk RNA sequencing studies which have investigated regional differences in microglia. Matcovitch-Natan et al. (2016) compared gene expression in microglia from the cortex hippocampus and spinal cord and show similarity between brain region replicates are close to 1 with Pearson's correlation. In line with this result only 76 genes were found to be differentially expressed, however, they used a more stringent cut off for log fold change (log fold change >2). The high correlation of microglial samples from different brain regions likely reflects the high concordance of microglial signature genes and core functionality. Both Pearson's correlation and principal component analysis demonstrated that DG and RH samples clustered away from each other. The PCA and scree plot both showed that PC1 was responsible for the largest proportion of variance between samples. In comparison microglial samples from the DG and cortex showed a lower degree of separation. Looking back through the data notes received from Novogene who performed the RNA amplification, quality control checks, library preparation and RNA sequencing. After RNA amplification two of the cortical microglia samples (CX2 and CX3) were described as "moderately degraded" and this could have potentially introduced unwanted bias into these results. The fact that cortical sample CX1 clusters well with DG microglia samples may suggest that there is some contamination from SVZ (neurogenic region) microglia within this sample although further exploration would be required to confirm.

As expected, when investigating genes with the highest read counts across all samples, many of the genes identified were microglial signature genes including *Cx3cr1, Tmem119, Csfr1*,

Hexb and P2ry12 (Haage et al. 2019). Other genes which were highly expressed across all samples were immediate early genes including *Fos* and *Jun* Immediate early genes. From transcriptomic analysis of microglia isolated from the whole brain at varying developmental time points, Matcovitch-Natan et al. (2016) demonstrated that immediate early genes including Fos and Jun were upregulated in adult microglia compares to embryonic and postnatal populations. The authors postulate that *Jun* and *Fos* represent transcription factors that may be involved in establishing homeostatic microglial phenotypes or involved in the transition from pre-microglia to adult. Alternatively, a recent transcriptomic study demonstrated that the type of protocol used to isolate hippocampal mouse microglial cells had a significant effect on the expression levels of *Jun* and *Fos* in single cell RNA sequencing analysis (Mattei et al. 2020). Mouse hippocampal microglia isolated through enzymatic digestion at 37^{o}C showed high expression of *Jun* and *Fos* compared to microglia isolated by mechanical dissociation at 4^{o}C. The authors suggest that the increase of immediate early genes in microglia isolated by enzymatic dissociation at 37 ^{o}C is reflects an immediate microglia activation to the isolation paradigm. The enzymatic dissociation was performed using common dissociative agents including collagenase, DNAse I and 10% fetal calf serum. However, it is difficult to pinpoint exactly what is the causative agents of the change in expression of immediate early genes as this could be due to temperature, enzymatic dissociation, exposure to high levels of fetal calf serum or a combination of these factors. In the present study, microglia were isolated by enzymatic (enzyme p) and mechanical dissociation but were kept at 4^{o}C at all times where possible. As enzyme dissociation is a common denominator, this may indicate that enzymatic dissociation adversely affects microglia activation. Interestingly, Matcovitch-Natan et al. (2016) did not report using enzymatic dissociation however parts of the protocol were stated to be performed at room temperature and so fluctuations in temperature may have had some effect on global gene expression. However, the fact that differential expression of immediate

early genes was observed between developmental timepoints indicates that this may not be due to the isolation procedure.

Differential gene expression performed using Deseq2 produced many significant genes of interest particularly in the pair wise comparison of DG and RH. 1221 DEG were generated by filtering DESeq2 results for P-adjusted value < 0.01 and a log fold change of -1< > 1 with top hits including *Olfm1, Stmn3, Snca, Cck*. 1210 (99.1%) of the DEG were upregulated in DG microglial samples. In comparison, RNA sequencing and analysis of microglia from the DG and CA1 regions of Cx3cr1$^{+/GFP}$ mice found only 41 genes to be differentially expressed with a log fold change of -0.7 < > 0.7, adjusted p value < 0.05 (Kreisel et al. 2019). DEG in the DG were found to be associated to M1 (C*sf2ra* and *Cxcl10*) and M2 (*Axl, Spp1, Clec7a, Fabp5* ect.) phenotypes as well as fatty acid metabolism (*Fabp5, Lpl, Ldlr* ect.). 4 genes were found to be differentially expressed in both studies (Atp1a3, Fabp5, camk2a and Arhgef17). The large difference in the number of DEG found likely reflects a combination of factors including differences in the brain regions used (RH v CA1) as well as differences in mouse strain (C57BL/6J v *Cx3cr1$^{+/GFP}$*) which was discussed in the previous chapter. As the RH encompasses multiple hippocampal regions (CA1, CA2, CA3) this may have increased the variability of microglia gene expression from this region and resulted in a larger number of differentially expressed genes compared to microglia that are derived from the more discrete CA1 region. Supportive of a functional neurogenic role of DG microglia, GO term enrichment analysis, showed DEG in DG microglia samples were involved in neuronal development, regulation of synaptic signalling, neurogenesis as well as regulation of ion transport. However, these results require validation as some of the identified DEG are normally found in other cell types for example *Olfm1, Tubb3, Map2, Sst, Snca, Cx3cl1* and *Synaptophysin*, while differentially expressed are usually expressed in neuronal populations and may indicate low-

level neuronal contamination. Alternatively, the presence of neuronal associated genes may be remnants of synapses or dead neurons which have been engulfed by microglia. A study investigating the effects of aging on human microglia gene expression, found that some of the top genes affected by aging in microglia, included neuronal associated genes such as *Olfm1, Olfml3, Map2 and Nefh*. These neuronal associated genes showed reduced expression with age for which the authors suggest may reflect a loss of neurons or a dysfunction of microglia with age (Galatro et al. 2017).

7.3.1 Limitations

Several limitations in this work are recognised including a small sample size, amplification bias as well as potential contamination in cortical dissection. Firstly, significant effort was made to ensure that micro dissections of the dentate gyrus for microglia isolation was well validated. However, less attention was paid to cortical dissections and may well reflect some of the large variability seen in cortical microglial samples with potential contamination from the SVZ. Secondly, the small sample size is somewhat mitigated by the fact that microglia isolated from 6 mice were pooled to form one sample, which may reduce inter sample variability while maintaining power for testing DEG (Assefa et al. 2020). Thirdly, very low quantities of RNA were generated from microglial samples across all brain regions and for this reason it was decided that RNA amplification should be performed. RNA-sequencing in itself involves amplification of starting material to generate large enough cDNA libraries which can generate bias in the data (Parekh et al. 2016). As the samples have undergone 2 separate cycles of amplification it is acknowledged that bias may have been introduced which could have affected the precision and accuracy of the RNA quantification. This further magnifies the need

for validation of these results. In addition, GO and GSEA and MGEnrichment require further exploratory analysis to determine which genes are represented in which pathway and infer meaning relationships.

7.4.0 Conclusion

In conclusion, significant regional dependant transcriptional differences were observed between DG and RH microglial samples. Genes identified as DEG in the DG may represent good biological targets for inducing positive neurogenic effects particularly for diseases and brain disorders where hippocampal neurogenesis is dysregulated. Future work would involve pathway analysis to identify upstream regulators of the DEG as well as providing insight into molecular interactions. Replication and validation of these results with RT-QPCR is also required to make definitive conclusions. Replication of these findings in human microglia would also enhance translation of these results. Further experimental paradigms to explore this phenomenon would also probe targets of interest in cell culture models. Additionally, investigating transcriptional changes in the dentate gyrus of wild type mice undergoing a process which is known to have a positive neurogenic effect for example mice undergoing environmental enrichment compared to control animals. Single cell RNA sequencing as well as spatial transcriptomics of DG microglia may provide further information with regards to microglia heterogeneity within the DG as well as their physical location.

8.0 General Discussion

8.1 Overview

Adult hippocampal neurogenesis is a phenomenon that leads to the incorporation of new granule cells into the circuitry of the DG (Kempermann et al. 2004). Adult neurogenesis in and of itself is a rare phenomenon, with its occurrence in only two regions of the mammalian brain: the SGZ and SVZ. Adult hippocampal neurogenesis has been shown to be extremely important for memory processing by performing pattern integration, providing temporal valence as well as experience-based context (Aimone et al. 2009). There are many reports that hippocampal neurogenesis is dysregulated in neurodegenerative disorders such as Alzheimer's disease, Parkinson's disease, Huntington's disease as well as mood disorders including major depressive disorder, Schizophrenia and bipolar disorder (Anacker et al. 2018; Baptista and Andrade 2018; Moreno-Jiménez et al. 2019). A common symptom among these conditions is cognitive impairment which is often correlated with a dysregulation in hippocampal neurogenesis (Toda et al. 2019). This suggests that hippocampal neurogenesis dysregulation may underlie some of the negative symptoms in these patient populations. Therefore, hippocampal neurogenesis may represent a good biological target for treating symptoms of these disorders. However, the regulation of adult hippocampal neurogenesis is still poorly understood, which has impeded the development of new therapeutic strategies. An elegant study demonstrated the relevance of the local micro-environment in which NSPC reside, whereby spinal cord stem cells were shown to recover neurogenic potential upon transplantation into the DG but not when transplanted into the spinal cord or the non-

neurogenic CA1 region (Shihabuddin et al. 2000). This indicates, adult neuronal progenitors in the DG are not unique in their neurogenic capacity and that unique factors within the neurogenic niche facilitate this neurogenic phenomenon. There are many factors, external and internal that have been shown to affect rates of hippocampal neurogenesis such as environmental enrichment, wheel running in rodents as well as neurotrophic factors (Ahmed et al. 1995; van Praag et al. 1999; Kempermann 2011). Recent studies, have suggested a role for microglia in regulating hippocampal neurogenesis (Aarum et al. 2003; Morgan et al. 2004; Walton et al. 2006; Nunan et al. 2014). Microglia are the resident tissue macrophage of the of CNS and play many important roles in maintaining brain homeostasis by clearing dead cells and debris, responding to injury or to the invasion of pathogens and facilitating synaptic plasticity. Microglia are densely populated in the dentate gyrus compared to other brain regions and have been shown to display functions such as phagocytosing newly born cells and performing synaptic pruning that are important to maintain the neurogenic niche (Schafer et al. 2012; Tan et al. 2020).

Based on the published literature and previous work in our group, I hypothesised that microglia in the DG possessed specialised functional neurogenic properties that were regionally dependant that were due to differential gene expression (Nunan et al. 2014). This was explored via a two-pronged approach. Firstly, to examine differential functional neurogenic properties of microglia, hippocampal NSPCs were co-cultured microglia isolated from neurogenic and non-neurogenic brain regions or alternatively with their conditioned media. Limited evidence was found to support a neurogenic capacity of microglia in these culture paradigms and there were no differences found in the regional sourcing of microglia. The fact that I was unable to replicate previous work from within our group demonstrates the issue of replicability in science (Hirsch and Schildknecht 2019). Secondly, a transcriptomic approach was used to examine

differential gene expression between microglia isolated from the DG, RH and cortex. Here, a large number of differentially expressed genes were found to be identified when a pairwise comparison was performed between DG and RH with GO term enrichment showing biological pathways involving neurogenesis, neuronal development and synaptic signalling which was promising. How to resolve the differences seen *in vitro* versus *in vivo*? The fact that a significant amount of differentially expressed genes were found in DG microglia compared to RH microglia may infer that there are functional differences between these two populations or it could be that the results seen are due to low level contamination from other cell types as previously discussed or that these RNA transcripts are not translated into protein and therefore have no functional effects on phenotype. Alternatively, the DEG displayed between DG and RH microglia may not be directly linked to a pro-neurogenic action and could related instead to another microglial property, although this hypothesis would disagree with previously published data (Kreisel et al. 2019). However, without validation of these results it is hard to make any conclusions. As there were no significant regional differences in the co-culture paradigms this could indicate that there are no functional neurogenic differences between microglia from neurogenic and non-neurogenic regions. However, I suspect that the loss of signals from the local environment on microglia may have influenced these results. A wider discussion and investigation of the use of microglia in *in vitro* studies should be considered. New reports in the literature are also initiating conversations about the importance of microglia in the brain including Csfr1$^{fire/fire}$ mice which appear phenotypical normal despite lacking microglia in the brain (Rojo et al. 2019).

The regulation of hippocampal neurogenesis could of course be due contributions of non-microglial cells or other micro-environmental cues within the neurogenic niche and is likely to be a result from a combination of factors. The neurogenic niche consists of multiple cell types

including neurons, NSPCs, astrocytes, endothelial cells, and pericytes. One study has shown that neural stem cells are capable of secreting factors which actually facilitate neural stem cell differentiation as well as proliferation (Rhee et al. 2016). They were able to show that conditioned media from constitutional active (ca)-Raf induced neural stem cells caused neural stems to activate and proliferate into radial glial like astrocytes or adult neural stem cells. Likewise, there is also evidence that astrocytes contribute to the neurogenic capacity of the DG by, promoting proliferation and instructing stem cells to undergo neuronal differentiation (Song et al. 2002; Cao et al. 2013). Co-culture experiments of NSPC with endothelial cells have suggested a role for endothelial cells in precursor proliferation and neurosphere formation (Shen et al. 2004; Ehret et al. 2015). As many of the different cell types in the neurogenic niche appear to be capable of influencing the neurogenic capacity of NSPC it could be that a larger factor is at play that affects all cells in the neurogenic niche. For example, it is known that the DG is highly vascularised and that proliferating cells are found in clusters close to blood vessels (Palmer et al. 2000). The close proximity of NSPC to the blood brain barrier ensures that these cells have adequate supply of oxygen and sources of energy whilst also passing molecules from the periphery to the brain. This may expose NSPC to a wide range and potentially high concentration of pro-neurogenic factors. Other factors for consideration are cell to cell contact, the extracellular matrix as well as lymphatic vessels. These results demonstrate the need for multicellular approaches in investigating the regulation of hippocampal neurogenesis. Transcriptomic studies likely represent some of the best ways to approach this problem. Advances in transcriptomic technologies including, single cell RNA sequencing, spatial transcriptomics and RABID-seq coupled with improvements in mouse models will mean a greater resolution of these problems will be achieved (Artegiani et al. 2017; Masuda et al. 2020; Merritt et al. 2020; Vogt 2021).

Although the concept of hippocampal neurogenesis is now widely accepted in animal models, it still remains a controversial topic where adult humans are concerned, as demonstrated by recent opposing publications (Boldrini et al. 2018; Sorrells et al. 2018a). Post mortem tissue and postoperative neurosurgical tissue from epilepsy patients that spanned the human lifetime were used in one study to directly oppose this view. It was shown that hippocampal neurogenesis declines sharply during the first few years of life and is virtually absent thereafter (Sorrells et al. 2018b). Thus, supporting the long-held dogma that adult brain tissue is not capable of regenerating itself. In contrast a study by Boldrini (2018) used healthy subjects who were screened of neurological disorders and died of sudden death events, such as homicide. They provide data that hippocampal neurogenesis persists throughout the aging process. Immunocytochemistry demonstrated that quiescent neural progenitors that derive new neurons in the dentate gyrus decline with age but intermediate neural progenitors appear to remain stable over the lifetime and thus provide a source for new cells.

There are however many limitations in human studies. Many implore the use of post-mortem tissue, however, an issue with this method of sampling is the post mortem interval (PMI). This is the time between which the subject has been deceased and the tissue sample is taken and processed. Very often this is inconsistent between samples as demonstrated: the range cited in the study by Boldrini (2018) was 4-26hrs, in contrast tissue from epilepsy patients in Sorrells (2018b) study were fixed within 1hr of removal, 2 patients were perfused within 3-5hrs of death and infants within 2 days. Often this issue is out of the control of the processor's hands due to the matter of consent. However, to what extent the length of the PMI has on the quality of the data obtained is a valid question. Additional concerns to be aware of when using human hippocampal tissue post mortem is the prior health of the donor in which the tissue was acquired and whether this will impact the data observed. Boldrini's team appear to be sensitive

to this problem and as a result placed stringent discriminations on donors based not only on physical but also mental health. If this issue is not considered, it is difficult to disentangle differences in measures of hippocampal neurogenesis from cause of death or disease especially where control tissue is limited. A final challenge for the field, is to question whether it is possible to quantitatively assess whether the generation of new neurons in the adult hippocampus has any functional consequence for cognition directly in humans and thus comparisons between animal and human data should always be viewed with caution. However, advances in neuroimaging may help to overcome these limitations in the future

8.2 Concluding remarks

This body of work demonstrated that microglia show a limited neurogenic potential in the culture paradigm used irrelevant of the brain region they were isolated from. Additionally, it was shown that DG microglia display significant number of differential expressed genes compared to microglia from non-neurogenic regions of the hippocampus in wild type mice, which is novel. These differentially expressed genes may represent a good target to investigate hippocampal neurogenesis regulation by microglia.

References

Chapter 1 References

Aarum, J., Sandberg, K., Haeberlein, S.L.B. and Persson, M.A.A. 2003. Migration and differentiation of neural precursor cells can be directed by microglia. *Proceedings of the National Academy of Sciences* 100(26), pp. 15983–15988. Available at: https://www-pnas-org.abc.cardiff.ac.uk/content/100/26/15983 [Accessed: 12 December 2021].

Ahmed, S., Reynolds, B.A. and Weiss, S. 1995. *BDNF Enhances the Differentiation but Not the Survival of CNS Stem Cell-Derived Neuronal Precursors*. Available at: http://www.jneurosci.org/content/jneuro/15/8/5765.full.pdf [Accessed: 4 February 2019].

Aimone, J.B., Wiles, J. and Gage, F.H. 2009. Computational Influence of Adult Neurogenesis on Memory Encoding. *Neuron* 61(2), pp. 187–202. Available at: http://www.ncbi.nlm.nih.gov/pubmed/19186162 [Accessed: 4 May 2019].

Akers, K.G. et al. 2014. Hippocampal neurogenesis regulates forgetting during adulthood and infancy. *Science (New York, N.Y.)* 344(6184), pp. 598–602. Available at: http://www.ncbi.nlm.nih.gov/pubmed/24812394 [Accessed: 24 April 2021].

Alliot, F., Godin, I. and Pessac, B. 1999. Microglia derive from progenitors, originating from the yolk sac, and which proliferate in the brain. *Developmental Brain Research* 117(2), pp. 145–152. doi: 10.1016/S0165-3806(99)00113-3.

Alliot, F., Lecain, E., Grima, B. and Pessac, B. 1991. Microglial progenitors with a high proliferative potential in the embryonic and adult mouse brain (hemopoietic stem cels/macrophages/colony-stimulating factors). *Proc. Nadl. Acad. Sci. USA* 88, pp. 1541–1545.

Altman, J. and Das, G.D. 1965. Autoradiographic and histological evidence of postnatal hippocampal neurogenesis in rats. *The Journal of Comparative Neurology* 124(3), pp. 319–335. doi: 10.1002/cne.901240303.

Anacker, C. et al. 2018. Hippocampal neurogenesis confers stress resilience by inhibiting the ventral dentate gyrus. *Nature* 559(7712), pp. 98–102. Available at: http://www.nature.com/articles/s41586-018-0262-4 [Accessed: 27 January 2020].

Anacker, C. and Hen, R. 2017. Adult hippocampal neurogenesis and cognitive flexibility — linking memory and mood. *Nature Reviews Neuroscience* 18(6), pp. 335–346. Available at: http://www.nature.com/articles/nrn.2017.45 [Accessed: 24 April 2021].

Antony, J.M., Paquin, A., Nutt, S.L., Kaplan, D.R. and Miller, F.D. 2011. Endogenous microglia regulate development of embryonic cortical precursor cells. *Journal of Neuroscience Research* 89(3), pp. 286–298. Available at: https://onlinelibrary.wiley.com/doi/full/10.1002/jnr.22533 [Accessed: 7 December 2021].

Askew, K. et al. 2017. Coupled Proliferation and Apoptosis Maintain the Rapid Turnover of Microglia in the Adult Brain. *Cell Reports* 18(2), pp. 391–405. doi: 10.1016/j.celrep.2016.12.041.

Atoji, Y. and Wild, J.M. 2006. Anatomy of the avian hippocampal formation. *Reviews in the Neurosciences* 17(1–2), pp. 3–15. Available at: https://www-degruyter-com.abc.cardiff.ac.uk/document/doi/10.1515/revneuro.2006.17.1-2.3/html [Accessed: 19 November 2022].

Bannerman, D.M. et al. 2004. Regional dissociations within the hippocampus—memory and anxiety. *Neuroscience & Biobehavioral Reviews* 28(3), pp. 273–283. doi: 10.1016/J.NEUBIOREV.2004.03.004.

Bartrup, J.T., Moorman, J.M. and Newberry, N.R. 1997. BDNF enhances neuronal growth and synaptic activity in hippocampal cell cultures. *Neuroreport* 8(17), pp. 3791–4. Available at: http://www.ncbi.nlm.nih.gov/pubmed/9427372 [Accessed: 2 May 2019].

Battista, D., Ferrari, C.C., Gage, F.H. and Pitossi, F.J. 2006. Neurogenic niche modulation by activated microglia: transforming growth factor β increases neurogenesis in the adult dentate gyrus. *European Journal of Neuroscience* 23(1), pp. 83–93. Available at: https://onlinelibrary.wiley.com/doi/full/10.1111/j.1460-9568.2005.04539.x [Accessed: 11 November 2021].

Beltz, B.S., Tlusty, M.F., Benton, J.L. and Sandeman, D.C. 2007. Omega-3 fatty acids upregulate adult neurogenesis. *Neuroscience Letters* 415(2), pp. 154–158. doi: 10.1016/J.NEULET.2007.01.010.

Boekhoorn, K., Joels, M. and Lucassen, P.J. 2006. Increased proliferation reflects glial and vascular-associated changes, but not neurogenesis in the presenile Alzheimer hippocampus. *Neurobiology of Disease* 24(1), pp. 1–14. doi: 10.1016/J.NBD.2006.04.017.

van Bokhoven, P., Oomen, C.A., Hoogendijk, W.J.G., Smit, A.B., Lucassen, P.J. and Spijker, S. 2011. Reduction in hippocampal neurogenesis after social defeat is long-lasting and responsive to late antidepressant treatment. *European Journal of Neuroscience* 33(10), pp. 1833–1840. Available at: https://onlinelibrary.wiley.com/doi/full/10.1111/j.1460-9568.2011.07668.x [Accessed: 23 November 2022].

Boldrini, M., Hen, R., Underwood, M.D., Rosoklija, G.B., Dwork, A.J., Mann, J.J. and Arango, V. 2012. HIPPOCAMPAL ANGIOGENESIS AND PROGENITOR CELL PROLIFERATION ARE INCREASED WITH ANTIDEPRESSANT USE IN MAJOR DEPRESSION. *Biological psychiatry* 72(7), p. 562. Available at: /pmc/articles/PMC3438317/ [Accessed: 23 November 2022].

Bonaguidi, M.A., Wheeler, M.A., Shapiro, J.S., Stadel, R.P., Sun, G.J., Ming, G.L. and Song, H. 2011. In Vivo Clonal Analysis Reveals Self-Renewing and Multipotent Adult Neural Stem Cell Characteristics. *Cell* 145(7), pp. 1142–1155. doi: 10.1016/J.CELL.2011.05.024.

Bruttger, J. et al. 2015. Genetic Cell Ablation Reveals Clusters of Local Self-Renewing Microglia in the Mammalian Central Nervous System. *Immunity* 43(1), pp. 92–106. doi: 10.1016/J.IMMUNI.2015.06.012.

Burghardt, N.S., Park, E.H., Hen, R. and Fenton, A.A. 2012. Adult-born hippocampal neurons promote cognitive flexibility in mice. *Hippocampus* 22(9), pp. 1795–1808. Available at: https://onlinelibrary.wiley.com/doi/full/10.1002/hipo.22013 [Accessed: 22 November 2022].

Cameron, H.A. and Mckay, R.D.G. 2001. Adult neurogenesis produces a large pool of new granule cells in the dentate gyrus. *Journal of Comparative Neurology* 435(4), pp. 406–417. doi: 10.1002/cne.1040.

Campbell, S., Marriott, M., Nahmias, C. and MacQueen, G.M. 2004. Lower Hippocampal Volume in Patients Suffering from depression: A Meta-Analysis. *American Journal of Psychiatry* 161(4), pp. 598–607. Available at: https://ajp.psychiatryonline.org/doi/10.1176/appi.ajp.161.4.598 [Accessed: 23 November 2022].

Chaker, Z., Codega, P. and Doetsch, F. 2016. A mosaic world: puzzles revealed by adult neural stem cell heterogeneity. *Wiley Interdisciplinary Reviews: Developmental Biology* 5(6), pp. 640–658. Available at: https://onlinelibrary-wiley-com.abc.cardiff.ac.uk/doi/full/10.1002/wdev.248 [Accessed: 20 November 2022].

Chawla, M.K. et al. 2005. Sparse, environmentally selective expression of Arc RNA in the upper blade of the rodent fascia dentata by brief spatial experience. *Hippocampus* 15(5), pp. 579–586. Available at: https://onlinelibrary.wiley.com/doi/full/10.1002/hipo.20091 [Accessed: 19 November 2022].

Chu, Y., Jin, X., Parada, I., Pesic, A., Stevens, B., Barres, B. and Prince, D.A. 2010. Enhanced synaptic connectivity and epilepsy in C1q knockout mice. *Proceedings of the National Academy of Sciences* 107(17), pp. 7975–7980. Available at: https://www-pnas-org.abc.cardiff.ac.uk/content/107/17/7975 [Accessed: 11 December 2021].

Clark, R.E. and Squirea, L.R. 2013. Similarity in form and function of the hippocampus in rodents, monkeys, and humans. *Proceedings of the National Academy of Sciences of the United States of America* 110(SUPPL2), pp. 10365–10370. Available at: https://www.pnas.org/doi/abs/10.1073/pnas.1301225110 [Accessed: 21 November 2022].

Coleman, L.G., Zou, J. and Crews, F.T. 2020. Microglial depletion and repopulation in brain slice culture normalizes sensitized proinflammatory signaling. *Journal of Neuroinflammation* 17(1), pp. 1–20. Available at: https://jneuroinflammation-biomedcentral-com.abc.cardiff.ac.uk/articles/10.1186/s12974-019-1678-y [Accessed: 6 December 2021].

Crain, J.M., Nikodemova, M. and Watters, J.J. 2013. Microglia express distinct M1 and M2 phenotypic markers in the postnatal and adult central nervous system in male and female mice. *Journal of Neuroscience Research* 91(9), pp. 1143–1151. doi: 10.1002/jnr.23242.

Crews, L. et al. 2010. Increased BMP6 Levels in the Brains of Alzheimer's Disease Patients and APP Transgenic Mice Are Accompanied by Impaired Neurogenesis. *Journal of Neuroscience* 30(37), pp. 12252–12262. Available at: https://www.jneurosci.org/content/30/37/12252 [Accessed: 22 November 2022].

Cunningham, C.L., Martínez-Cerdeño, V. and Noctor, S.C. 2013. Microglia Regulate the Number of Neural Precursor Cells in the Developing Cerebral Cortex. *Journal of Neuroscience* 33(10), pp. 4216–4233. Available at: http://www.jneurosci.org/content/33/10/4216 [Accessed: 7 December 2021].

Davalos, D. et al. 2005. ATP mediates rapid microglial response to local brain injury in vivo. *Nature Neuroscience* 8(6), pp. 752–758. Available at: http://www.nature.com/articles/nn1472 [Accessed: 3 May 2020].

Diaz-Aparicio, I. et al. 2020. Microglia actively remodel adult hippocampal neurogenesis through the phagocytosis secretome. *Journal of Neuroscience* . Available at: https://www.jneurosci.org/content/early/2020/01/02/JNEUROSCI.0993-19.2019 [Accessed: 27 January 2020].

Doorn, K.J., Brevé, J.J.P., Drukarch, B., Boddeke, H.W., Huitinga, I., Lucassen, P.J. and van Dam, A.-M. 2015. Brain region-specific gene expression profiles in freshly isolated rat microglia. *Frontiers in cellular neuroscience* 9, p. 84. Available at: http://www.ncbi.nlm.nih.gov/pubmed/25814934 [Accessed: 2 May 2019].

Elmore, M.R.P. et al. 2014. Colony-Stimulating Factor 1 Receptor Signaling Is Necessary for Microglia Viability, Unmasking a Microglia Progenitor Cell in the Adult Brain. *Neuron* 82(2), pp. 380–397. doi: 10.1016/J.NEURON.2014.02.040.

Eriksson, P.S., Perfilieva, E., Björk-Eriksson, T., Alborn, A.-M., Nordborg, C., Peterson, D.A. and Gage, F.H. 1998. Neurogenesis in the adult human hippocampus. *Nature Medicine* 4(11), pp. 1313–1317. doi: 10.1038/3305.

Fabel, K., Wolf, S.A., Ehninger, D., Babu, H., Leal-Galicia, P. and Kempermann, G. 2009. Additive effects of physical exercise and environmental enrichment on adult hippocampal neurogenesis in mice. *Frontiers in Neuroscience* 3(NOV), p. 2. doi: 10.3389/NEURO.22.002.2009/BIBTEX.

Fares, R.P., Belmeguenai, A., Sanchez, P.E., Kouchi, H.Y. and Bodennec, J. 2013. Standardized Environmental Enrichment Supports Enhanced Brain Plasticity in Healthy Rats and Prevents Cognitive Impairment in Epileptic Rats. *PLoS ONE* 8(1), p. 53888. Available at: www.plosone.org.

Flajnik, M.F. and Kasahara, M. 2009. Origin and evolution of the adaptive immune system: genetic events and selective pressures. *Nature Reviews Genetics 2010 11:1* 11(1), pp. 47–59. Available at: https://www.nature.com/articles/nrg2703 [Accessed: 23 November 2022].

Fujita, S. and Kitamura, T. 1975. Origin of Brain Macrophages and the Nature of the So-Called Microglia. *Acta neuropathologica. Supplementum* Suppl 6, pp. 291–296. Available at: https://link-springer-com.abc.cardiff.ac.uk/chapter/10.1007/978-3-662-08456-4_51 [Accessed: 25 November 2021].

Gage, F.H. 2000. Mammalian neural stem cells. *Science* 287(5457), pp. 1433–1438. Available at: https://www-science-org.abc.cardiff.ac.uk/doi/abs/10.1126/science.287.5457.1433 [Accessed: 12 December 2021].

Garthe, A., Behr, J. and Kempermann, G. 2009. Adult-Generated Hippocampal Neurons Allow the Flexible Use of Spatially Precise Learning Strategies. *PLOS ONE* 4(5), p. e5464. Available at: https://journals.plos.org/plosone/article?id=10.1371/journal.pone.0005464 [Accessed: 22 November 2022].

Gebara, E., Sultan, S., Kocher-Braissant, J. and Toni, N. 2013. Adult hippocampal neurogenesis inversely correlates with microglia in conditions of voluntary running and aging. *Frontiers in Neuroscience* 7, p. 145. Available at: http://journal.frontiersin.org/article/10.3389/fnins.2013.00145/abstract [Accessed: 8 August 2019].

Ginhoux, F. et al. 2010. Fate Mapping Analysis Reveals That Adult Microglia Derive from Primitive Macrophages. *Science* 330(6005), pp. 841–845. Available at: https://science.sciencemag.org/content/330/6005/841.full [Accessed: 3 May 2020].

Gomez Perdiguero, E. et al. 2015. Tissue-resident macrophages originate from yolk-sac-derived erythro-myeloid progenitors. *Nature* 518(7540), pp. 547–551. Available at: http://www.nature.com/articles/nature13989 [Accessed: 6 June 2018].

Gonçalves, J.T., Schafer, S.T. and Gage, F.H. 2016. Adult Neurogenesis in the Hippocampus: From Stem Cells to Behavior. *Cell* 167(4), pp. 897–914. Available at: https://www.sciencedirect.com/science/article/pii/S0092867416314040?via%3Dihub [Accessed: 4 May 2019].

Gould, E., Tanapat, P., Mcewen, B.S., Flügge, G. and Fuchs, E. 1998. Proliferation of granule cell precursors in the dentate gyrus of adult monkeys is diminished by stress. *Proceedings of the National Academy of Sciences of the United States of America* 95(6), pp. 3168–3171. Available at: https://www.pnas.org/doi/abs/10.1073/pnas.95.6.3168 [Accessed: 23 November 2022].

Grabert, K. et al. 2016. Microglial brain region-dependent diversity and selective regional sensitivities to aging. *Nature Neuroscience* 19(3), pp. 504–516. doi: 10.1038/nn.4222.

Hagemeyer, N. et al. 2017. Microglia contribute to normal myelinogenesis and to oligodendrocyte progenitor maintenance during adulthood. *Acta Neuropathologica* 134(3), pp. 441–458. Available at: https://link-springer-com.abc.cardiff.ac.uk/article/10.1007/s00401-017-1747-1 [Accessed: 11 December 2021].

Hammond, T.R. et al. 2019. Single-Cell RNA Sequencing of Microglia throughout the Mouse Lifespan and in the Injured Brain Reveals Complex Cell-State Changes. *Immunity* 50(1), pp. 253-271.e6. Available at: https://www.sciencedirect.com/science/article/pii/S1074761318304850?via%3Dihub#sec4 [Accessed: 27 March 2019].

Harley, S.B.R. et al. 2021. Selective Ablation of BDNF from Microglia Reveals Novel Roles in Self-Renewal and Hippocampal Neurogenesis. Available at: https://doi.org/10.1523/JNEUROSCI.2539-20.2021 [Accessed: 1 June 2021].

Harrison, J.K. et al. 1998. Role for neuronally derived fractalkine in mediating interactions between neurons and CX3CR1-expressing microglia. *Proceedings of the National Academy of*

Sciences of the United States of America 95(18), pp. 10896–10901. doi: 10.1073/pnas.95.18.10896.

Hayes, N.L. and Nowakowski, R.S. 2002. Dynamics of cell proliferation in the adult dentate gyrus of two inbred strains of mice. *Brain research. Developmental brain research* 134(1–2), pp. 77–85. doi: 10.1016/S0165-3806(01)00324-8.

Haynes, S.E., Hollopeter, G., Yang, G., Kurpius, D., Dailey, M.E., Gan, W.B. and Julius, D. 2006. The P2Y12 receptor regulates microglial activation by extracellular nucleotides. *Nature Neuroscience* 9(12), pp. 1512–1519. Available at: https://www-nature-com.abc.cardiff.ac.uk/articles/nn1805 [Accessed: 12 December 2021].

Hill, A.S., Sahay, A. and Hen, R. 2015. Increasing Adult Hippocampal Neurogenesis is Sufficient to Reduce Anxiety and Depression-Like Behaviors. *Neuropsychopharmacology 2015 40:10* 40(10), pp. 2368–2378. Available at: https://www.nature.com/articles/npp201585 [Accessed: 23 November 2022].

Hoeffel, G. et al. 2015. C-Myb+ Erythro-Myeloid Progenitor-Derived Fetal Monocytes Give Rise to Adult Tissue-Resident Macrophages. *Immunity* 42(4), pp. 665–678. doi: 10.1016/J.IMMUNI.2015.03.011.

Huttenlocher., P.R. 1979. Synaptic density in human frontal cortex - Developmental changes and effects of aging. *Brain Research* 163(2), pp. 195–205. doi: 10.1016/0006-8993(79)90349-4.

Insausti, R. 1993. Comparative anatomy of the entorhinal cortex and hippocampus in mammals. *Hippocampus* 3(S1), pp. 19–26. Available at: https://onlinelibrary-wiley-com.abc.cardiff.ac.uk/doi/full/10.1002/hipo.1993.4500030705 [Accessed: 19 November 2022].

James Murphy, B.B. and Sturm, E. 1923. CONDITIONS D E T E R M I N I N G THE TRANSPLANTABILITY OF TISSUES IN THE BRAIN. *Journal of Experimental Medicine*

38(2), pp. 183–197. Available at: http://rupress.org/jem/article-pdf/38/2/183/1394659/183.pdf [Accessed: 29 November 2021].

Jin, K., Peel, A.L., Mao, X.O., Xie, L., Cottrell, B.A., Henshall, D.C. and Greenberg, D.A. 2004. Increased hippocampal neurogenesis in Alzheimer's disease. *Proceedings of the National Academy of Sciences of the United States of America* 101(1), pp. 343–347. Available at: https://pubmed.ncbi.nlm.nih.gov/14660786/ [Accessed: 23 November 2022].

Jordan, J.T. 2020a. The rodent hippocampus as a bilateral structure: A review of hemispheric lateralization. *Hippocampus* 30(3), pp. 278–292. Available at: https://onlinelibrary.wiley.com/doi/full/10.1002/hipo.23188 [Accessed: 21 November 2022].

Jordan, J.T. 2020b. The rodent hippocampus as a bilateral structure: A review of hemispheric lateralization. *Hippocampus* 30(3), pp. 278–292. Available at: https://onlinelibrary-wiley-com.abc.cardiff.ac.uk/doi/full/10.1002/hipo.23188 [Accessed: 11 December 2022].

Kempermann, G. 2012. New neurons for 'survival of the fittest'. *Nature Reviews Neuroscience 2012 13:10* 13(10), pp. 727–736. Available at: https://www-nature-com.abc.cardiff.ac.uk/articles/nrn3319 [Accessed: 10 December 2022].

Kempermann, G. 2019. Environmental enrichment, new neurons and the neurobiology of individuality. *Nature Reviews Neuroscience 2019 20:4* 20(4), pp. 235–245. Available at: https://www-nature-com.abc.cardiff.ac.uk/articles/s41583-019-0120-x [Accessed: 23 December 2021].

Kempermann, G., Brandon, E.P. and Gage, F.H. 1998. Environmental stimulation of 129/SvJ mice causes increased cell proliferation and neurogenesis in the adult dentate gyrus. *Current Biology* 8(16), pp. 939–944. Available at: http://www.cell.com/article/S0960982207003776/fulltext [Accessed: 23 December 2021].

Kempermann, G., Jessberger, S., Steiner, B. and Kronenberg, G. 2004a. Milestones of neuronal development in the adult hippocampus. *Trends in Neursciences* 27(8), pp. 447–452. Available at: www.sciencedirect.com [Accessed: 20 September 2018].

Kempermann, G., Kuhn, H.G. and Gage, F.H. 1997. More hippocampal neurons in adult mice living in an enriched environment. *Nature 1997 386:6624* 386(6624), pp. 493–495. Available at: https://www-nature-com.abc.cardiff.ac.uk/articles/386493a0 [Accessed: 23 December 2021].

Kempermann, G., Wiskott, L. and Gage, F.H. 2004b. Functional significance of adult neurogenesis. *Current Opinion in Neurobiology* 14(2), pp. 186–191. doi: 10.1016/J.CONB.2004.03.001.

Kheirbek, M.A. and Hen, R. 2014. Add neurons, subtract anxiety. *Scientific American* 311(1), pp. 62–7. doi: 10.1038/scientificamerican0714-62.

Kierdorf, K. et al. 2013. Microglia emerge from erythromyeloid precursors via Pu.1-and Irf8-dependent pathways. *Nature Neuroscience* 16(3), pp. 273–280. doi: 10.1038/NN.3318.

Kirby, E.D., Kuwahara, A.A., Messer, R.L. and Wyss-Coray, T. 2015. Adult hippocampal neural stem and progenitor cells regulate the neurogenic niche by secreting VEGF. *Proceedings of the National Academy of Sciences* . doi: 10.1073/pnas.1422448112.

Kowiański, P., Lietzau, G., Czuba, E., Waśkow, M., Steliga, A. and Moryś, J. 2018. BDNF: A Key Factor with Multipotent Impact on Brain Signaling and Synaptic Plasticity. *Cellular and Molecular Neurobiology* 38(3), pp. 579–593. Available at: http://link.springer.com/10.1007/s10571-017-0510-4 [Accessed: 2 May 2019].

Kreisel, T., Wolf, B., Keshet, E. and Licht, T. 2019. Unique role for dentate gyrus microglia in neuroblast survival and in VEGF-induced activation. *GLIA* 67(4), pp. 594–618. Available at: http://doi.wiley.com/10.1002/glia.23505 [Accessed: 27 March 2019].

Kyle, J., Wu, M., Gourzi, S. and Tsirka, S.E. 2019. Proliferation and differentiation in the adult subventricular zone are not affected by CSF1R inhibition. *Frontiers in Cellular Neuroscience* 13. Available at: www.frontiersin.org.

Lagace, D.C. et al. 2010. Adult hippocampal neurogenesis is functionally important for stress-induced social avoidance. *Proceedings of the National Academy of Sciences of the United States of America* 107(9), pp. 4436–4441. Available at: https://www.pnas.org/doi/abs/10.1073/pnas.0910072107 [Accessed: 23 November 2022].

Leutgeb, J.K., Leutgeb, S., Moser, M.B. and Moser, E.I. 2007. Pattern separation in the dentate gyrus and CA3 of the hippocampus. *Science (New York, N.Y.)* 315(5814), pp. 961–966. Available at: https://pubmed.ncbi.nlm.nih.gov/17303747/ [Accessed: 19 November 2022].

Li, B. et al. 2008a. Failure of Neuronal Maturation in Alzheimer Disease Dentate Gyrus. *Journal of Neuropathology & Experimental Neurology* 67(1), pp. 78–84. Available at: https://academic.oup.com/jnen/article/67/1/78/2916923 [Accessed: 22 November 2022].

Li, M. et al. 2017. Colony stimulating factor 1 receptor inhibition eliminates microglia and attenuates brain injury after intracerebral hemorrhage. *Journal of Cerebral Blood Flow and Metabolism* 37(7), pp. 2383–2395. Available at: https://journals-sagepub-com.abc.cardiff.ac.uk/doi/10.1177/0271678X16666551?url_ver=Z39.88-2003&rfr_id=ori%3Arid%3Acrossref.org&rfr_dat=cr_pub++0pubmed [Accessed: 6 December 2021].

Li, Y. et al. 2008b. TrkB Regulates Hippocampal Neurogenesis and Governs Sensitivity to Antidepressive Treatment. *Neuron* 59(3), pp. 399–412. Available at: http://www.cell.com/article/S0896627308005412/fulltext [Accessed: 23 November 2022].

Madar, A.D., Ewell, L.A. and Jones, M. v. 2019. Pattern separation of spiketrains in hippocampal neurons. *Scientific Reports 2019 9:1* 9(1), pp. 1–20. Available at: https://www.nature.com/articles/s41598-019-41503-8 [Accessed: 22 November 2022].

Malberg, J.E., Eisch, A.J., Nestler, E.J. and Duman, R.S. 2000. Chronic Antidepressant Treatment Increases Neurogenesis in Adult Rat Hippocampus. *Journal of Neuroscience* 20(24), pp. 9104–9110. Available at: https://www.jneurosci.org/content/20/24/9104 [Accessed: 22 November 2022].

Manns, J.R. and Eichenbaum, H. 2006. Evolution of declarative memory. *Hippocampus* 16(9), pp. 795–808. Available at: https://onlinelibrary-wiley-com.abc.cardiff.ac.uk/doi/full/10.1002/hipo.20205 [Accessed: 19 November 2022].

Marshall, J.S., Warrington, R., Watson, W. and Kim, H.L. 2018. An introduction to immunology and immunopathology. *Allergy, Asthma and Clinical Immunology* 14(2), pp. 1–10. Available at: https://aacijournal.biomedcentral.com/articles/10.1186/s13223-018-0278-1 [Accessed: 23 November 2022].

Matcovitch-Natan, O. et al. 2016. Microglia development follows a stepwise program to regulate brain homeostasis. *Science (New York, N.Y.)* 353(6301), p. aad8670. doi: 10.1126/science.aad8670.

Medawar, P.B. 1948. Immunity to homologous grafted skin; the fate of skin homografts. *British journal of experimental pathology* 29(1), pp. 58–69. Available at: http://www.ncbi.nlm.nih.gov/pubmed/18865105 [Accessed: 21 November 2018].

Meucci, O., Fatatis, A., Simen, A.A. and Miller, R.J. 2000. Expression of CX3CR1 chemokine receptors on neurons and their role in neuronal survival. *Proceedings of the National Academy of Sciences of the United States of America* 97(14), pp. 8075–80. Available at: http://www.ncbi.nlm.nih.gov/pubmed/10869418 [Accessed: 13 May 2020].

Mirescu, C., Peters, J.D., Noiman, L. and Gould, E. 2006. Sleep deprivation inhibits adult neurogenesis in the hippocampus by elevating glucocorticoids. *Proceedings of the National Academy of Sciences of the United States of America* 103(50), pp. 19170–19175. Available at: https://www.pnas.org/doi/abs/10.1073/pnas.0608644103 [Accessed: 23 November 2022].

Morgan, S.C., Taylor, D.L. and Pocock, J.M. 2004. Microglia release activators of neuronal proliferation mediated by activation of mitogen-activated protein kinase, phosphatidylinositol-3-kinase/Akt and delta-Notch signalling cascades. *Journal of Neurochemistry* 90(1), pp. 89–101. Available at: http://doi.wiley.com/10.1111/j.1471-4159.2004.02461.x [Accessed: 27 January 2020].

Muldoon, L.L. et al. 2013. Immunologic privilege in the central nervous system and the blood–brain barrier. *Journal of Cerebral Blood Flow & Metabolism* 33(1), p. 13. Available at: /pmc/articles/PMC3597357/ [Accessed: 23 November 2022].

Nandi, S. et al. 2012. The CSF-1 receptor ligands IL-34 and CSF-1 exhibit distinct developmental brain expression patterns and regulate neural progenitor cell maintenance and maturation. *Developmental Biology* 367(2), pp. 100–113. doi: 10.1016/J.YDBIO.2012.03.026.

Nikodemova, M., Kimyon, R.S., De, I., Small, A.L., Collier, L.S. and Watters, J.J. 2015. Microglial numbers attain adult levels after undergoing a rapid decrease in cell number in the third postnatal week. *Journal of Neuroimmunology* 278, pp. 280–288. doi: 10.1016/J.JNEUROIM.2014.11.018.

Nimmerjahn, A., Kirchhoff, F. and Helmchen, F. 2005. Neuroscience: Resting microglial cells are highly dynamic surveillants of brain parenchyma in vivo. *Science* 308(5726), pp. 1314–1318. Available at: https://science.sciencemag.org/content/308/5726/1314 [Accessed: 3 May 2020].

Nishiyori, A. et al. 1998. Localization of fractalkine and CX3CR1 mRNAs in rat brain: does fractalkine play a role in signaling from neuron to microglia? *FEBS Letters* 429(2), pp. 167–172. Available at: https://www.sciencedirect.com/science/article/pii/S0014579398005833 [Accessed: 2 May 2020].

Nunan, R., Sivasathiaseelan, H., Khan, D., Zaben, M. and Gray, W. 2014. Microglial VPAC1R mediates a novel mechanism of neuroimmune-modulation of hippocampal precursor cells via IL-4 release. *Glia* 62(8), pp. 1313–1327. doi: 10.1002/glia.22682.

Palmer, T.D., Willhoite, A.R. and Gage, F.H. 2000. Vascular niche for adult hippocampal neurogenesis. *The Journal of Comparative Neurology* 425(4), pp. 479–494. Available at: http://doi.wiley.com/10.1002/1096-9861%2820001002%29425%3A4%3C479%3A%3AAID-CNE2%3E3.0.CO%3B2-3 [Accessed: 4 May 2019].

Paolicelli, R.C. et al. 2011. Synaptic pruning by microglia is necessary for normal brain development. *Science* 333(6048), pp. 1456–1458. Available at: https://www-science-org.abc.cardiff.ac.uk/doi/abs/10.1126/science.1202529 [Accessed: 11 December 2021].

Parkhurst, C.N. et al. 2013. Microglia promote learning-dependent synapse formation through brain-derived neurotrophic factor. *Cell* 155(7), pp. 1596–609. Available at: http://www.ncbi.nlm.nih.gov/pubmed/24360280 [Accessed: 7 June 2018].

Pérez-Cerdá, F., Sánchez-Gómez, M.V. and Matute, C. 2015. Pío del Río Hortega and the discovery of the oligodendrocytes. *Frontiers in Neuroanatomy* 9(July). Available at: /pmc/articles/PMC4493393/ [Accessed: 25 November 2021].

Perry, V.H., Hume, D.A. and Gordon, S. 1985. Immunohistochemical localization of macrophages and microglia in the adult and developing mouse brain. *Neuroscience* 15(2), pp. 313–326. doi: 10.1016/0306-4522(85)90215-5.

Petersen, M.A. and Dailey, M.E. 2004. Diverse microglial motility behaviors during clearance of dead cells in hippocampal slices. *Glia* 46(2), pp. 195–206. Available at: https://onlinelibrary-wiley-com.abc.cardiff.ac.uk/doi/full/10.1002/glia.10362 [Accessed: 12 December 2021].

Pilz, G.A. et al. 2018. Live imaging of neurogenesis in the adult mouse hippocampus. *Science* 359(6376), pp. 658–662. Available at: https://www-science-org.abc.cardiff.ac.uk/doi/10.1126/science.aao5056 [Accessed: 29 August 2022].

Pont-Lezica, L., Beumer, W., Colasse, S., Drexhage, H., Versnel, M. and Bessis, A. 2014. Microglia shape corpus callosum axon tract fasciculation: functional impact of prenatal inflammation. *European Journal of Neuroscience* 39(10), pp. 1551–1557. Available at: https://onlinelibrary.wiley.com/doi/full/10.1111/ejn.12508 [Accessed: 11 December 2021].

van Praag, H. 2005. Exercise Enhances Learning and Hippocampal Neurogenesis in Aged Mice. *Journal of Neuroscience* 25(38), pp. 8680–8685. Available at: http://www.jneurosci.org/content/jneuro/25/38/8680.full.pdf [Accessed: 14 June 2018].

van Praag, H., Kempermann, G. and Gage, F.H. 1999. Running increases cell proliferation and neurogenesis in the adult mouse dentate gyrus. *Nature Neuroscience 1999 2:3* 2(3), pp. 266–270. Available at: https://www-nature-com.abc.cardiff.ac.uk/articles/nn0399_266 [Accessed: 23 December 2021].

Ransohoff, R.M. 2016. A polarizing question: Do M1 and M2 microglia exist. *Nature Neuroscience* 19(8), pp. 987–991. doi: 10.1038/nn.4338.

Ré, P. et al. 2017. The Lifespan and Turnover of Microglia in the Human Brain. *CellReports* 20, pp. 779–784. Available at: http://dx.doi.org/10.1016/j.celrep.2017.07.004http://dx.doi.org/10.1016/j.celrep.2017.07.004 [Accessed: 20 September 2018].

Reshef, R., Kudryavitskaya, E., Shani-Narkiss, H., Isaacson, B., Rimmerman, N., Mizrahi, A. and Yirmiya, R. 2017. The role of microglia and their CX3CR1 signaling in adult neurogenesis in the olfactory bulb. *eLife* 6. Available at: https://elifesciences.org/articles/30809.

Rice, R.A. et al. 2015. Elimination of Microglia Improves Functional Outcomes Following Extensive Neuronal Loss in the Hippocampus. *Journal of Neuroscience* 35(27), pp. 9977–

9989. Available at: https://www-jneurosci-org.abc.cardiff.ac.uk/content/35/27/9977 [Accessed: 6 December 2021].

del Río-Hortega Bereciartu, J. 2020. Pío del Río-Hortega: The Revolution of Glia. *Anatomical record (Hoboken, N.J. : 2007)* 303(5), pp. 1232–1241. Available at: https://pubmed-ncbi-nlm-nih-gov.abc.cardiff.ac.uk/31525279/ [Accessed: 25 November 2021].

Rodríguez, J.J. et al. 2008. Impaired Adult Neurogenesis in the Dentate Gyrus of a Triple Transgenic Mouse Model of Alzheimer's Disease. *PLOS ONE* 3(8), p. e2935. Available at: https://journals.plos.org/plosone/article?id=10.1371/journal.pone.0002935 [Accessed: 23 November 2022].

Rojo, R. et al. 2019. Deletion of a Csf1r enhancer selectively impacts CSF1R expression and development of tissue macrophage populations. *Nature Communications 2019 10:1* 10(1), pp. 1–17. Available at: https://www-nature-com.abc.cardiff.ac.uk/articles/s41467-019-11053-8 [Accessed: 14 December 2021].

Rolls, E.T. and Kesner, R.P. 2006. A computational theory of hippocampal function, and empirical tests of the theory. *Progress in Neurobiology* 79(1), pp. 1–48. doi: 10.1016/J.PNEUROBIO.2006.04.005.

Sahay, A. et al. 2011. Increasing adult hippocampal neurogenesis is sufficient to improve pattern separation. *Nature 2011 472:7344* 472(7344), pp. 466–470. Available at: https://www.nature.com/articles/nature09817 [Accessed: 22 November 2022].

Sankowski, R. et al. 2019. Mapping microglia states in the human brain through the integration of high-dimensional techniques. *Nature Neuroscience* 22(12), pp. 2098–2110. Available at: http://www.nature.com/articles/s41593-019-0532-y [Accessed: 10 February 2020].

Santarelli, L. et al. 2003. Requirement of hippocampal neurogenesis for the behavioral effects of antidepressants. *Science* 301(5634), pp. 805–809. Available at: https://www.science.org/doi/10.1126/science.1083328 [Accessed: 23 November 2022].

Sarma, J.V. and Ward, P.A. 2011. The complement system. *Cell and Tissue Research* 343(1), pp. 227–235. Available at: https://link.springer.com/article/10.1007/s00441-010-1034-0 [Accessed: 23 November 2022].

Sasaguri, H. et al. 2017. APP mouse models for Alzheimer's disease preclinical studies. *The EMBO Journal* 36(17), p. 2473. Available at: /pmc/articles/PMC5579350/ [Accessed: 23 November 2022].

Savchenko, V.L., McKanna, J.A., Nikonenko, I.R. and Skibo, G.G. 2000. Microglia and astrocytes in the adult rat brain: comparative immunocytochemical analysis demonstrates the efficacy of lipocortin 1 immunoreactivity. *Neuroscience* 96(1), pp. 195–203. doi: 10.1016/S0306-4522(99)00538-2.

Schafer, D.P. et al. 2012a. Article Microglia Sculpt Postnatal Neural Circuits in an Activity and Complement-Dependent Manner. *Neuron* 74, pp. 691–705. Available at: https://ac.els-cdn.com/S0896627312003340/1-s2.0-S0896627312003340-main.pdf?_tid=52d02daa-2f43-4cc1-8410-be818fe0caa4&acdnat=1543423946_c1736c06c743a197ea11e544c00a896f [Accessed: 28 November 2018].

Schafer, D.P. et al. 2012b. Microglia Sculpt Postnatal Neural Circuits in an Activity and Complement-Dependent Manner. *Neuron* 74(4), pp. 691–705. Available at: https://www.sciencedirect.com/science/article/pii/S0896627312003340?via%3Dihub [Accessed: 7 June 2018].

Schoenfeld, T.J. and Gould, E. 2012. Stress, Stress Hormones, and Adult Neurogenesis. *Experimental neurology* 233(1), p. 12. Available at: /pmc/articles/PMC3715962/ [Accessed: 23 November 2022].

Schulz, C. et al. 2012. A lineage of myeloid cells independent of myb and hematopoietic stem cells. *Science* 335(6077), pp. 86–90. Available at: https://www-science-org.abc.cardiff.ac.uk/doi/abs/10.1126/science.1219179 [Accessed: 30 November 2021].

Seress, L. 2007. Comparative anatomy of the hippocampal dentate gyrus in adult and developing rodents, non-human primates and humans. *Progress in Brain Research* 163, pp. 23–798. doi: 10.1016/S0079-6123(07)63002-7.

Shigemoto-Mogami, Y., Hoshikawa, K., Goldman, J.E., Sekino, Y. and Sato, K. 2014. Development/Plasticity/Repair Microglia Enhance Neurogenesis and Oligodendrogenesis in the Early Postnatal Subventricular Zone. doi: 10.1523/JNEUROSCI.1619-13.2014.

Shors, T.J., Miesegaes, G., Beylin, A., Zhao, M., Rydel, T. and Gould, E. 2001. Neurogenesis in the adult is involved in the formation of trace memories. *Nature* 410(6826), pp. 372–376. doi: 10.1038/35066584.

Sierra, A. et al. 2010. Microglia Shape Adult Hippocampal Neurogenesis through Apoptosis-Coupled Phagocytosis. *Cell Stem Cell* 7(4), pp. 483–495. Available at: https://www.sciencedirect.com/science/article/pii/S1934590910004376?via%3Dihub [Accessed: 26 October 2018].

Sipe, G.O., Lowery, R.L., Tremblay, M., Kelly, E.A., Lamantia, C.E. and Majewska, A.K. 2016. Microglial P2Y12 is necessary for synaptic plasticity in mouse visual cortex. *Nature Communications 2016 7:1* 7(1), pp. 1–15. Available at: https://www-nature-com.abc.cardiff.ac.uk/articles/ncomms10905 [Accessed: 11 December 2021].

Spalding, K.L. et al. 2013. Dynamics of Hippocampal Neurogenesis in Adult Humans. *Cell* 153(6), pp. 1219–1227. doi: 10.1016/j.cell.2013.05.002.

Stangl, D. and Thuret, S. 2009. Impact of diet on adult hippocampal neurogenesis. *Genes & Nutrition 2009 4:4* 4(4), pp. 271–282. Available at: https://link.springer.com/articles/10.1007/s12263-009-0134-5 [Accessed: 23 November 2022].

Stevens, B. et al. 2007. The Classical Complement Cascade Mediates CNS Synapse Elimination. *Cell* 131(6), pp. 1164–1178. Available at:

http://www.cell.com.abc.cardiff.ac.uk/article/S0092867407013554/fulltext [Accessed: 11 December 2021].

Tarozzo, G., Bortolazzi, S., Crochemore, C., Chen, S.-C., Lira, A.S., Abrams, J.S. and Beltramo, M. 2003. Fractalkine protein localization and gene expression in mouse brain. *Journal of Neuroscience Research* 73(1), pp. 81–88. Available at: http://doi.wiley.com/10.1002/jnr.10645 [Accessed: 2 May 2020].

Toda, T., Parylak, S.L., Linker, S.B. and Gage, F.H. 2019. The role of adult hippocampal neurogenesis in brain health and disease. *Molecular Psychiatry* 24(1), pp. 67–87. Available at: http://www.nature.com/articles/s41380-018-0036-2 [Accessed: 19 October 2019].

Tremblay, M.Ě., Lowery, R.L. and Majewska, A.K. 2010. Microglial Interactions with Synapses Are Modulated by Visual Experience. *PLOS Biology* 8(11), p. e1000527. Available at: https://journals.plos.org/plosbiology/article?id=10.1371/journal.pbio.1000527 [Accessed: 10 December 2021].

Ueno, M., Fujita, Y., Tanaka, T., Nakamura, Y., Kikuta, J., Ishii, M. and Yamashita, T. 2013. Layer V cortical neurons require microglial support for survival during postnatal development. *Nature Neuroscience 2013 16:5* 16(5), pp. 543–551. Available at: https://www-nature-com.abc.cardiff.ac.uk/articles/nn.3358 [Accessed: 11 December 2021].

Valente, T. et al. 2009. A Diet Enriched in Polyphenols and Polyunsaturated Fatty Acids, LMN Diet, Induces Neurogenesis in the Subventricular Zone and Hippocampus of Adult Mouse Brain. *Journal of Alzheimer's Disease* 18(4), pp. 849–865. doi: 10.3233/JAD-2009-1188.

Vukovic, J., Colditz, M.J., Blackmore, D.G., Ruitenberg, M.J. and Bartlett, P.F. 2012. Microglia modulate hippocampal neural precursor activity in response to exercise and aging. *Journal of Neuroscience* 32(19), pp. 6435–6443. Available at: http://www.jneurosci.org/content/jneuro/32/19/6435.full.pdf [Accessed: 28 November 2018].

Wake, H., Moorhouse, A.J., Jinno, S., Kohsaka, S. and Nabekura, J. 2009. Resting Microglia Directly Monitor the Functional State of Synapses In Vivo and Determine the Fate of Ischemic Terminals. *Journal of Neuroscience* 29(13), pp. 3974–3980. Available at: https://www-jneurosci-org.abc.cardiff.ac.uk/content/29/13/3974 [Accessed: 11 December 2021].

Walton, N.M. et al. 2006. Microglia instruct subventricular zone neurogenesis. *Glia* 54(8), pp. 815–825. Available at: https://onlinelibrary-wiley-com.abc.cardiff.ac.uk/doi/full/10.1002/glia.20419 [Accessed: 13 December 2021].

Wei, Z., Liao, J., Qi, F., Meng, Z. and Pan, S. 2015. Evidence for the contribution of BDNF-TrkB signal strength in neurogenesis: An organotypic study. *Neuroscience Letters* 606, pp. 48–52. Available at: https://www.sciencedirect.com/science/article/pii/S0304394015301026 [Accessed: 10 April 2019].

Weinhard, L. et al. 2018. Microglia remodel synapses by presynaptic trogocytosis and spine head filopodia induction. *Nature Communications* 9(1), p. 1228. doi: 10.1038/s41467-018-03566-5.

West, M.J. and Gundersen, H.J.G. 1990. Unbiased stereological estimation of the number of neurons in the human hippocampus. *Journal of Comparative Neurology* 296(1), pp. 1–22. Available at: https://onlinelibrary-wiley-com.abc.cardiff.ac.uk/doi/full/10.1002/cne.902960102 [Accessed: 10 December 2022].

Willis, A, R. 1935. Experiments on the intracerebral implantation of embryo tissues in rats. *Proceedings of the Royal Society of London. Series B - Biological Sciences* 117(805), pp. 400–412. Available at: https://royalsocietypublishing-org.abc.cardiff.ac.uk/doi/abs/10.1098/rspb.1935.0036 [Accessed: 29 November 2021].

Willis, E.F. et al. 2020. Repopulating Microglia Promote Brain Repair in an IL-6-Dependent Manner. *Cell* 180(5), pp. 833-846.e16. Available at:

http://www.cell.com.abc.cardiff.ac.uk/article/S0092867420301574/fulltext [Accessed: 26 December 2021].

Wirths, O. 2017. Altered neurogenesis in mouse models of Alzheimer disease. *Neurogenesis (Austin, Tex.)* 4(1), p. e1327002. Available at: http://www.ncbi.nlm.nih.gov/pubmed/29564360 [Accessed: 12 November 2019].

Xavier, A.L.R., Kress, B.T., Goldman, S.A., Menezes, J.R.L. de and Nedergaard, M. 2015. A Distinct Population of Microglia Supports Adult Neurogenesis in the Subventricular Zone. *Journal of Neuroscience* 35(34), pp. 11848–11861. Available at: https://www-jneurosci-org.abc.cardiff.ac.uk/content/35/34/11848 [Accessed: 16 October 2021].

Yu, Y. et al. 2009. Increased hippocampal neurogenesis in the progressive stage of Alzheimer's disease phenotype in an APP/PS1 double transgenic mouse model. *Hippocampus* 19(12), pp. 1247–1253. Available at: https://onlinelibrary.wiley.com/doi/full/10.1002/hipo.20587 [Accessed: 23 November 2022].

Zhan, Y. et al. 2014. Deficient neuron-microglia signaling results in impaired functional brain connectivity and social behavior. *Nature Neuroscience* 17(3), pp. 400–406. Available at: https://www.nature.com/articles/nn.3641 [Accessed: 9 June 2021].

Zhang, J. and Jiao, J. 2015. Molecular Biomarkers for Embryonic and Adult Neural Stem Cell and Neurogenesis. *BioMed research international* 2015, p. 727542. Available at: http://www.ncbi.nlm.nih.gov/pubmed/26421301 [Accessed: 2 May 2019].

Zhao, C., Deng, W. and Gage, F.H. 2008. Mechanisms and functional implications of adult neurogenesis. *Cell* 132(4), pp. 645–60. Available at: http://www.ncbi.nlm.nih.gov/pubmed/18295581 [Accessed: 12 April 2021].

Ziv, Y. et al. 2006. Immune cells contribute to the maintenance of neurogenesis and spatial learning abilities in adulthood. *Nature Neuroscience 2006 9:2* 9(2), pp. 268–275. Available at: https://www-nature-com.abc.cardiff.ac.uk/articles/nn1629 [Accessed: 23 December 2021].

Zusso, M., Methot, L., Lo, R., Greenhalgh, A.D., David, S. and Stifani, S. 2012. Regulation of Postnatal Forebrain Amoeboid Microglial Cell Proliferation and Development by the Transcription Factor Runx1. *The Journal of Neuroscience* 32(33), p. 11285. Available at: /pmc/articles/PMC6621177/ [Accessed: 3 December 2021].

Chapter 2 References

Brewer, G.J. and Cotman, C.W. (1989) 'Survival and growth of hippocampal neurons in defined medium at low density: advantages of a sandwich culture technique or low oxygen', *Brain Research*, 494(1), pp. 65–74. Available at: https://doi.org/10.1016/0006-8993(89)90144-3.

Hagihara, H. *et al.* (2009) 'Dissection of hippocampal dentate gyrus from adult mouse.', *Journal of visualized experiments : JoVE* [Preprint], (33). Available at: https://doi.org/10.3791/1543.

Jao, J. and Ciernia, A.V. (2021) 'MGEnrichment: A web application for microglia gene list enrichment analysis', *PLOS Computational Biology*, 17(11), p. e1009160. Available at: https://doi.org/10.1371/JOURNAL.PCBI.1009160.

Lein, E.S., Zhao, X. and Gage, F.H. (2004) 'Cellular/Molecular Defining a Molecular Atlas of the Hippocampus Using DNA Microarrays and High-Throughput In Situ Hybridization'. Available at: https://doi.org/10.1523/JNEUROSCI.4710-03.2004.

Liberzon, A. *et al.* (2011) 'Molecular signatures database (MSigDB) 3.0', *Bioinformatics*, 27(12), p. 1739. Available at: https://doi.org/10.1093/BIOINFORMATICS/BTR260.

Liberzon, A. *et al.* (2015) 'The Molecular Signatures Database (MSigDB) hallmark gene set collection', *Cell systems*, 1(6), p. 417. Available at: https://doi.org/10.1016/J.CELS.2015.12.004.

Love, M.I., Huber, W. and Anders, S. (2014) 'Moderated estimation of fold change and dispersion for RNA-seq data with DESeq2', *Genome Biology 2014 15:12*, 15(12), pp. 1–21. Available at: https://doi.org/10.1186/S13059-014-0550-8.

Mootha, V.K. *et al.* (2003) 'PGC-1α-responsive genes involved in oxidative phosphorylation are coordinately downregulated in human diabetes', *Nature Genetics 2003 34:3*, 34(3), pp. 267–273. Available at: https://doi.org/10.1038/NG1180.

Parker, G.E. *et al.* (2006) 'Gene expression profiling of mice with genetically modified muscle glycogen content.', *The Biochemical journal*, 395(1), pp. 137–45. Available at: https://doi.org/10.1042/BJ20051456.

Subramanian, A. *et al.* (2005) 'Gene set enrichment analysis: A knowledge-based approach for interpreting genome-wide expression profiles'. Available at: www.pnas.orgcgidoi10.1073pnas.0506580102 (Accessed: 27 July 2021).

Zhang, Y. and Wang, C. (2011) 'Nephroblastoma overexpressed (NOV/CCN3) gene: a paired-domain-specific PAX3-FKHR transcription target that promotes survival and motility in alveolar rhabdomyosarcoma cells', *Oncogene*, 30(32), pp. 3549–3562. Available at: https://doi.org/10.1038/onc.2011.69.

Chapter 3 References

Brewer, G.J. and Cotman, C.W. (1989) 'Survival and growth of hippocampal neurons in defined medium at low density: advantages of a sandwich culture technique or low oxygen', *Brain Research*, 494(1), pp. 65–74. Available at: https://doi.org/10.1016/0006-8993(89)90144-3.

Hagihara, H. *et al.* (2009) 'Dissection of hippocampal dentate gyrus from adult mouse.', *Journal of visualized experiments : JoVE* [Preprint], (33). Available at: https://doi.org/10.3791/1543.

Jao, J. and Ciernia, A.V. (2021) 'MGEnrichment: A web application for microglia gene list enrichment analysis', *PLOS Computational Biology*, 17(11), p. e1009160. Available at: https://doi.org/10.1371/JOURNAL.PCBI.1009160.

Lein, E.S., Zhao, X. and Gage, F.H. (2004) 'Cellular/Molecular Defining a Molecular Atlas of the Hippocampus Using DNA Microarrays and High-Throughput In Situ Hybridization'. Available at: https://doi.org/10.1523/JNEUROSCI.4710-03.2004.

Liberzon, A. *et al.* (2011) 'Molecular signatures database (MSigDB) 3.0', *Bioinformatics*, 27(12), p. 1739. Available at: https://doi.org/10.1093/BIOINFORMATICS/BTR260.

Liberzon, A. *et al.* (2015) 'The Molecular Signatures Database (MSigDB) hallmark gene set collection', *Cell systems*, 1(6), p. 417. Available at: https://doi.org/10.1016/J.CELS.2015.12.004.

Love, M.I., Huber, W. and Anders, S. (2014) 'Moderated estimation of fold change and dispersion for RNA-seq data with DESeq2', *Genome Biology 2014 15:12*, 15(12), pp. 1–21. Available at: https://doi.org/10.1186/S13059-014-0550-8.

Mootha, V.K. *et al.* (2003) 'PGC-1α-responsive genes involved in oxidative phosphorylation are coordinately downregulated in human diabetes', *Nature Genetics 2003 34:3*, 34(3), pp. 267–273. Available at: https://doi.org/10.1038/NG1180.

Parker, G.E. *et al.* (2006) 'Gene expression profiling of mice with genetically modified muscle glycogen content.', *The Biochemical journal*, 395(1), pp. 137–45. Available at: https://doi.org/10.1042/BJ20051456.

Subramanian, A. *et al.* (2005) 'Gene set enrichment analysis: A knowledge-based approach for interpreting genome-wide expression profiles'. Available at: www.pnas.orgcgidoi10.1073pnas.0506580102 (Accessed: 27 July 2021).

Zhang, Y. and Wang, C. (2011) 'Nephroblastoma overexpressed (NOV/CCN3) gene: a paired-domain-specific PAX3-FKHR transcription target that promotes survival and motility in alveolar rhabdomyosarcoma cells', *Oncogene*, 30(32), pp. 3549–3562. Available at: https://doi.org/10.1038/onc.2011.69.

Chapter 4 References

Aimone, J.B., Wiles, J. and Gage, F.H. 2009. Computational Influence of Adult Neurogenesis on Memory Encoding. *Neuron* 61(2), pp. 187–202. Available at: http://www.ncbi.nlm.nih.gov/pubmed/19186162 [Accessed: 4 May 2019].

Anacker, C. and Hen, R. 2017. Adult hippocampal neurogenesis and cognitive flexibility — linking memory and mood. *Nature Reviews Neuroscience* 18(6), pp. 335–346. Available at: http://www.nature.com/articles/nrn.2017.45 [Accessed: 24 April 2021].

Appel ', K., Honegger, P. and Gebicke-Haerter, P.J. 1995. Expression of interleukin-3 and tumor necrosis factor-p mRNAs in cultured microglia. *Journal of Neuroimmunology* 60, pp. 83–91.

Arnò, B. et al. 2014. Neural progenitor cells orchestrate microglia migration and positioning into the developing cortex. *Nature Communications 2014 5:1* 5(1), pp. 1–13. Available at: https://www-nature-com.abc.cardiff.ac.uk/articles/ncomms6611 [Accessed: 27 October 2021].

Battista, D., Ferrari, C.C., Gage, F.H. and Pitossi, F.J. 2006. Neurogenic niche modulation by activated microglia: transforming growth factor β increases neurogenesis in the adult dentate gyrus. *European Journal of Neuroscience* 23(1), pp. 83–93. Available at: https://onlinelibrary.wiley.com/doi/full/10.1111/j.1460-9568.2005.04539.x [Accessed: 11 November 2021].

Bennett, M.L. et al. 2016. New tools for studying microglia in the mouse and human CNS. *Proceedings of the National Academy of Sciences* 113(12), pp. E1738–E1746. doi: 10.1073/pnas.1525528113.

Bohlen, C.J., Bennett, F.C. and Bennett, M.L. 2019. Isolation and culture of microglia. *Current protocols in immunology* 125(1), p. e70. Available at: /pmc/articles/PMC6510657/ [Accessed: 14 November 2021].

Bohlen, C.J., Bennett, F.C., Tucker, A.F., Collins, H.Y., Mulinyawe, S.B. and Barres, B.A. 2017. Diverse Requirements for Microglial Survival, Specification, and Function Revealed by Defined-Medium Cultures. *Neuron* 94(4), pp. 759-773.e8. Available at: http://dx.doi.org/10.1016/j.neuron.2017.04.043.

Box, A. et al. 2020. Evaluating the Effects of Cell Sorting on Gene Expression. *Journal of Biomolecular Techniques : JBT* 31(3), p. 100. Available at: /pmc/articles/PMC7497499/ [Accessed: 16 November 2021].

Butovsky, O. et al. 2006. Microglia activated by IL-4 or IFN-γ differentially induce neurogenesis and oligodendrogenesis from adult stem/progenitor cells. *Molecular and Cellular Neuroscience* 31(1), pp. 149–160. doi: 10.1016/j.mcn.2005.10.006.

Cacao, E., Kapukotuwa, S. and Cucinotta, F.A. 2018. Modeling Reveals the Dependence of Hippocampal Neurogenesis Radiosensitivity on Age and Strain of Rats. *Frontiers in Neuroscience* 12. Available at: https://pubmed.ncbi.nlm.nih.gov/30618596/ [Accessed: 1 November 2021].

Chamak, B. and Mallat, M. 1991. Fibronectin and laminin regulate thein vitro differentiation of microglial cells. *Neuroscience* 45(3), pp. 513–527. doi: 10.1016/0306-4522(91)90267-R.

Diaz-Aparicio, I. et al. 2020. Microglia actively remodel adult hippocampal neurogenesis through the phagocytosis secretome. *Journal of Neuroscience* . Available at: https://www.jneurosci.org/content/early/2020/01/02/JNEUROSCI.0993-19.2019 [Accessed: 27 January 2020].

Doorn, K.J., Brevé, J.J.P., Drukarch, B., Boddeke, H.W., Huitinga, I., Lucassen, P.J. and van Dam, A.-M. 2015. Brain region-specific gene expression profiles in freshly isolated rat microglia. *Frontiers in cellular neuroscience* 9, p. 84. Available at: http://www.ncbi.nlm.nih.gov/pubmed/25814934 [Accessed: 2 May 2019].

Duke, D.C., Moran, L.B., Turkheimer, F.E., Banati, R. and Graeber, M.B. 2004. Microglia in culture: What genes do they express? *Developmental Neuroscience* 26(1), pp. 30–37. Available at: www.karger.comwww.karger.com/dne [Accessed: 9 January 2019].

Epp, J.R., Scott, N.A. and Galea, L.A.M. 2011. Strain differences in neurogenesis and activation of new neurons in the dentate gyrus in response to spatial learning. *Neuroscience* . doi: 10.1016/j.neuroscience.2010.10.025.

Ginhoux, F. et al. 2010a. Fate mapping analysis reveals that adult microglia derive from primitive macrophages. *Science* 330(6005), pp. 841–845. Available at: www.sciencemag.org/cgi/content/full/330/6005/838/DC1 [Accessed: 13 October 2021].

Ginhoux, F. et al. 2010b. Fate Mapping Analysis Reveals That Adult Microglia Derive from Primitive Macrophages. *Science* 330(6005), pp. 841–845. Available at: https://science.sciencemag.org/content/330/6005/841.full [Accessed: 3 May 2020].

Grabert, K. et al. 2016. Microglial brain region-dependent diversity and selective regional sensitivities to aging. *Nature Neuroscience* 19(3), pp. 504–516. doi: 10.1038/nn.4222.

Hammond, T.R. et al. 2019. Single-Cell RNA Sequencing of Microglia throughout the Mouse Lifespan and in the Injured Brain Reveals Complex Cell-State Changes. *Immunity* 50(1), pp. 253-271.e6. Available at: https://www.sciencedirect.com/science/article/pii/S1074761318304850?via%3Dihub#sec4 [Accessed: 27 March 2019].

He, Y., Yao, X., Taylor, N., Bai, Y., Lovenberg, T. and Bhattacharya, A. 2018. RNA sequencing analysis reveals quiescent microglia isolation methods from postnatal mouse brains and limitations of BV2 cells. *Journal of Neuroinflammation* 15(1), p. 153. Available at: https://jneuroinflammation.biomedcentral.com/articles/10.1186/s12974-018-1195-4 [Accessed: 9 January 2019].

Ito, D., Imai, Y., Ohsawa, K., Nakajima, K., Fukuuchi, Y. and Kohsaka, S. 1998. Microglia-specific localisation of a novel calcium binding protein, Iba1. *Molecular Brain Research* . doi: 10.1016/S0169-328X(98)00040-0.

Ito, D., Tanaka, K., Suzuki, S., Dembo, T. and Fukuuchi, Y. 2001. Enhanced expression of Iba1, ionized calcium-binding adapter molecule 1, after transient focal cerebral ischemia in rat brain. *Stroke* . doi: 10.1161/01.STR.32.5.1208.

Ju, L., Zeng, H., Chen, Y., Wu, Y., Wang, B. and Xu, Q. 2015. Dual polarization of microglia isolated from mixed glial cell cultures. *Journal of Neuroscience Research* 93(9), pp. 1345–1352. Available at: http://doi.wiley.com/10.1002/jnr.23563 [Accessed: 2 February 2021].

Kierdorf, K. et al. 2013. Microglia emerge from erythromyeloid precursors via Pu.1- and Irf8-dependent pathways. *Nature Neuroscience* 16(3), pp. 273–280. Available at: http://www.nature.com/articles/nn.3318 [Accessed: 3 May 2020].

Kitamura, Y., Taniguchi, T., Kimura, H., Nomura, Y. and Gebicke-Haerter, P.J. 2000. Interleukin-4-inhibited mRNA expression in mixed rat glial and in isolated microglial cultures. *Journal of Neuroimmunology* 106(1–2), pp. 95–104. Available at: https://www.sciencedirect.com/science/article/pii/S0165572800002393?via%3Dihub [Accessed: 4 December 2019].

Kreisel, T., Wolf, B., Keshet, E. and Licht, T. 2019. Unique role for dentate gyrus microglia in neuroblast survival and in VEGF-induced activation. *GLIA* 67(4), pp. 594–618. Available at: http://doi.wiley.com/10.1002/glia.23505 [Accessed: 27 March 2019].

Lam, D., Lively, S. and Schlichter, L.C. 2017. Responses of rat and mouse primary microglia to pro- and anti-inflammatory stimuli: Molecular profiles, K+ channels and migration. *Journal of Neuroinflammation* 14(1), pp. 1–30. doi: 10.1186/s12974-017-0941-3.

Lin, L., Desai, R., Wang, X., Lo, E.H. and Xing, C. 2017. Characteristics of primary rat microglia isolated from mixed cultures using two different methods. *Journal of*

Neuroinflammation 14(1). Available at: https://www.ncbi.nlm.nih.gov/pmc/articles/PMC5422983/pdf/12974_2017_Article_877.pdf [Accessed: 2 May 2019].

Lünemann, A. et al. 2006. Macrophage/microglia activation factor expression is restricted to lesion-associated microglial cells after brain trauma. *Glia* 53(4), pp. 412–419. Available at: https://onlinelibrary-wiley-com.abc.cardiff.ac.uk/doi/full/10.1002/glia.20301 [Accessed: 1 November 2021].

Malik, S. et al. 2013. Neurogenesis Continues in the Third Trimester of Pregnancy and Is Suppressed by Premature Birth. *Journal of Neuroscience* 33(2), pp. 411–423. Available at: https://www-jneurosci-org.abc.cardiff.ac.uk/content/33/2/411 [Accessed: 26 October 2021].

Marek, R., Caruso, M., Rostami, A., Grinspan, J.B. and Sarma, J. das 2008. Magnetic cell sorting: A fast and effective method of concurrent isolation of high purity viable astrocytes and microglia from neonatal mouse brain tissue. *Journal of Neuroscience Methods* . doi: 10.1016/j.jneumeth.2008.08.016.

Matcovitch-Natan, O. et al. 2016. Microglia development follows a stepwise program to regulate brain homeostasis. *Science (New York, N.Y.)* 353(6301), p. aad8670. doi: 10.1126/science.aad8670.

Moussaud, S. and Draheim, H.J. 2010. A new method to isolate microglia from adult mice and culture them for an extended period of time. *Journal of Neuroscience Methods* 187, pp. 243–253. Available at: https://ac.els-cdn.com/S0165027010000397/1-s2.0-S0165027010000397-main.pdf?_tid=7325cba6-6bc7-419e-b1fb-2d53c7bee4af&acdnat=1537437154_5e17e26c5ff4638c88b24222dc4e3043 [Accessed: 20 September 2018].

Nagata, S., Hanayama, R. and Kawane, K. 2010. Autoimmunity and the Clearance of Dead Cells. *Cell* 140(5), pp. 619–630. doi: 10.1016/J.CELL.2010.02.014.

Nandi, S. et al. 2012. The CSF-1 receptor ligands IL-34 and CSF-1 exhibit distinct developmental brain expression patterns and regulate neural progenitor cell maintenance and maturation. *Developmental Biology* 367(2), pp. 100–113. doi: 10.1016/J.YDBIO.2012.03.026.

Nunan, R., Sivasathiaseelan, H., Khan, D., Zaben, M. and Gray, W. 2014. Microglial VPAC1R mediates a novel mechanism of neuroimmune-modulation of hippocampal precursor cells via IL-4 release. *Glia* 62(8), pp. 1313–1327. doi: 10.1002/glia.22682.

Parkhurst, C.N. et al. 2013. Microglia promote learning-dependent synapse formation through brain-derived neurotrophic factor. *Cell* 155(7), pp. 1596–609. Available at: http://www.ncbi.nlm.nih.gov/pubmed/24360280 [Accessed: 7 June 2018].

Ransohoff, R.M. 2016. A polarizing question: Do M1 and M2 microglia exist. *Nature Neuroscience* 19(8), pp. 987–991. doi: 10.1038/nn.4338.

Satoh, J. ichi, Kino, Y., Asahina, N., Takitani, M., Miyoshi, J., Ishida, T. and Saito, Y. 2016. TMEM119 marks a subset of microglia in the human brain. *Neuropathology* . doi: 10.1111/neup.12235.

Sedgwick, J.D., Schwender, S., Imrich, H., Dorries, R., Butcher, G.W. and ter Meulen, V. 2006. Isolation and direct characterization of resident microglial cells from the normal and inflamed central nervous system. *Proceedings of the National Academy of Sciences* . doi: 10.1073/pnas.88.16.7438.

Sierra, A. et al. 2010. Microglia Shape Adult Hippocampal Neurogenesis through Apoptosis-Coupled Phagocytosis. *Cell Stem Cell* 7(4), pp. 483–495. Available at: https://www.sciencedirect.com/science/article/pii/S1934590910004376?via%3Dihub [Accessed: 26 October 2018].

Tamashiro, T.T., Dalgard, C.L. and Byrnes, K.R. 2012. Primary Microglia Isolation from Mixed Glial Cell Cultures of Neonatal Rat Brain Tissue. *Journal of Visualized Experiments*

(66), pp. 1–5. Available at: http://www.jove.com/video/3814/primary-microglia-isolation-from-mixed-glial-cell-cultures-neonatal.

Tanaka, J., Toku, K., Matsuda, S., Sudo, S., Fujita, H., Sakanaka, M. and Maeda, N. 1998. Induction of resting microglia in culture medium devoid of glycine and serine. *Glia* 24(2), pp. 198–215. Available at: http://doi.wiley.com/10.1002/%28SICI%291098-1136%28199810%2924%3A2%3C198%3A%3AAID-GLIA5%3E3.0.CO%3B2-0 [Accessed: 2 May 2019].

Toda, T., Parylak, S.L., Linker, S.B. and Gage, F.H. 2019. The role of adult hippocampal neurogenesis in brain health and disease. *Molecular Psychiatry* 24(1), pp. 67–87. Available at: http://www.nature.com/articles/s41380-018-0036-2 [Accessed: 19 October 2019].

Tong, C.K. and Vidyadaran, S. 2016. Role of microglia in embryonic neurogenesis: *https://doi-org.abc.cardiff.ac.uk/10.1177/1535370216664430* 241(15), pp. 1669–1675. Available at: https://journals-sagepub-com.abc.cardiff.ac.uk/doi/10.1177/1535370216664430 [Accessed: 11 October 2021].

Ziebell, J.M., Adelson, P.D. and Lifshitz, J. 2015. Microglia: Dismantling and rebuilding circuits after acute neurological injury. *Metabolic brain disease* 30(2), p. 393. Available at: /pmc/articles/PMC4198517/ [Accessed: 1 November 2021].

Chapter 5 References

Artegiani, B., Lyubimova, A., Muraro, M., Es, J. H. van, Oudenaarden, A. van, & Clevers, H. (2017). A Single-Cell RNA Sequencing Study Reveals Cellular and Molecular Dynamics of the Hippocampal Neurogenic Niche. *Cell Reports*, *21*(11), 3271–3284. https://doi.org/10.1016/J.CELREP.2017.11.050

Battista, D., Ferrari, C. C., Gage, F. H., & Pitossi, F. J. (2006). Neurogenic niche modulation by activated microglia: transforming growth factor β increases neurogenesis in the adult dentate gyrus. *European Journal of Neuroscience*, *23*(1), 83–93. https://doi.org/10.1111/J.1460-9568.2005.04539.X

He, Y., Yao, X., Taylor, N., Bai, Y., Lovenberg, T., & Bhattacharya, A. (2018). RNA sequencing analysis reveals quiescent microglia isolation methods from postnatal mouse brains and limitations of BV2 cells. *Journal of Neuroinflammation*, *15*(1), 153. https://doi.org/10.1186/s12974-018-1195-4

Iwano, T., Masuda, A., Kiyonari, H., Enomoto, H., & Matsuzaki, F. (2012). Prox1 postmitotically defines dentate gyrus cells by specifying granule cell identity over CA3 pyramidal cell fate in the hippocampus. *Development (Cambridge, England)*, *139*(16), 3051–3062. https://doi.org/10.1242/dev.080002

Kreisel, T., Wolf, B., Keshet, E., & Licht, T. (2019). Unique role for dentate gyrus microglia in neuroblast survival and in VEGF-induced activation. *GLIA*, *67*(4), 594–618. https://doi.org/10.1002/glia.23505

Lawson, L. J., Perry, V. H., Dri, P., & Gordon, S. (1990). Heterogeneity in the distribution and morphology of microglia in the normal adult mouse brain. *Neuroscience*, *39*(1), 151–170. https://doi.org/10.1016/0306-4522(90)90229-W

Marshall, G. P. I., Deleyrolle, L. P., Reynolds, B. A., Steindler, D. A., & Laywell, E. D. (2014). Microglia from neurogenic and non-neurogenic regions display differential proliferative potential and neuroblast support. *Frontiers in Cellular Neuroscience*, *0*(JULY), 180. https://doi.org/10.3389/FNCEL.2014.00180

Nikolakopoulou, A. M., Dutta, R., Chen, Z., Miller, R. H., & Trapp, B. D. (n.d.). *Activated microglia enhance neurogenesis via trypsinogen secretion*. https://doi.org/10.1073/pnas.1218856110

Nunan, R., Sivasathiaseelan, H., Khan, D., Zaben, M., & Gray, W. (2014). Microglial VPAC1R mediates a novel mechanism of neuroimmune-modulation of hippocampal precursor cells via IL-4 release. *Glia*, *62*(8), 1313–1327. https://doi.org/10.1002/glia.22682

Pannell, M., Szulzewsky, F., Matyash, V., Wolf, S. A., & Kettenmann, H. (2014). The subpopulation of microglia sensitive to neurotransmitters/neurohormones is modulated by stimulation with LPS, interferon-γ, and IL-4. *GLIA*, *62*(5), 667–679. https://doi.org/10.1002/GLIA.22633

Xavier, A. L. R., Kress, B. T., Goldman, S. A., Menezes, J. R. L. de, & Nedergaard, M. (2015). A Distinct Population of Microglia Supports Adult Neurogenesis in the Subventricular Zone. *Journal of Neuroscience*, *35*(34), 11848–11861. https://doi.org/10.1523/JNEUROSCI.1217-15.2015

Chapter 6 References

Ajami, B., Bennett, J.L., Krieger, C., McNagny, K.M. and Rossi, F.M. V 2011. Infiltrating monocytes trigger EAE progression, but do not contribute to the resident microglia pool. *Nature Neuroscience* 14(9), pp. 1142–1149. doi: 10.1038/nn.2887.

Andersen, M.N., Al-Karradi, S.N.H., Kragstrup, T.W. and Hokland, M. 2016. Elimination of erroneous results in flow cytometry caused by antibody binding to Fc receptors on human monocytes and macrophages. *Cytometry Part A* 89(11), pp. 1001–1009. doi: 10.1002/cyto.a.22995.

Bachstetter, A.D. et al. 2011. Fractalkine and CX3CR1 regulate hippocampal neurogenesis in adult and aged rats. *Neurobiology of Aging* 32(11), pp. 2030–2044. doi: 10.1016/J.NEUROBIOLAGING.2009.11.022.

Bennett, M.L. et al. 2016. New tools for studying microglia in the mouse and human CNS. *Proceedings of the National Academy of Sciences* 113(12), pp. E1738–E1746. doi: 10.1073/pnas.1525528113.

Bohlen, C.J., Bennett, F.C., Tucker, A.F., Collins, H.Y., Mulinyawe, S.B. and Barres, B.A. 2017. Diverse Requirements for Microglial Survival, Specification, and Function Revealed by Defined-Medium Cultures. *Neuron* 94(4), pp. 759-773.e8. Available at: http://dx.doi.org/10.1016/j.neuron.2017.04.043.

van den Brink, S.C. et al. 2017. Single-cell sequencing reveals dissociation-induced gene expression in tissue subpopulations. *Nature Methods* 14(10), pp. 935–936. doi: 10.1038/nmeth.4437.

Butovsky, O. et al. 2014. Identification of a unique TGF-β-dependent molecular and functional signature in microglia. *Nature Neuroscience* 17(1), pp. 131–143. doi: 10.1038/nn.3599.

Butovsky, O. et al. 2015. Targeting miR-155 restores abnormal microglia and attenuates disease in SOD1 mice. *Annals of Neurology* 77(1), pp. 75–99. doi: 10.1002/ana.24304.

Cardona, A.E. et al. 2006. Control of microglial neurotoxicity by the fractalkine receptor. *Nature Neuroscience* 9(7), pp. 917–924. doi: 10.1038/nn1715.

Chen, Z. and Trapp, B.D. 2016. Microglia and neuroprotection. *Journal of Neurochemistry* 136, pp. 10–17. doi: 10.1111/jnc.13062.

Davalos, D. et al. 2005. ATP mediates rapid microglial response to local brain injury in vivo. *Nature Neuroscience* 8(6), pp. 752–758. Available at: http://www.nature.com/articles/nn1472 [Accessed: 3 May 2020].

Delbridge, A.R.D. et al. 2020. Organotypic Brain Slice Culture Microglia Exhibit Molecular Similarity to Acutely-Isolated Adult Microglia and Provide a Platform to Study Neuroinflammation. *Frontiers in Cellular Neuroscience* 14, p. 444. doi: 10.3389/fncel.2020.592005.

E. Hirbec, H., Noristani, H.N. and Perrin, F.E. 2017. Microglia Responses in Acute and Chronic Neurological Diseases: What Microglia-Specific Transcriptomic Studies Taught (and did Not Teach) Us. *Frontiers in Aging Neuroscience* 9, p. 227. doi: 10.3389/fnagi.2017.00227.

Fuhrmann, M. et al. 2010. Microglial Cx3cr1 knockout prevents neuron loss in a mouse model of Alzheimer's disease. *Nature Neuroscience* 13(4), pp. 411–413. doi: 10.1038/nn.2511.

Geissmann, F., Jung, S. and Littman, D.R. 2003. Blood Monocytes Consist of Two Principal Subsets with Distinct Migratory Properties. *Immunity* 19(1), pp. 71–82. doi: 10.1016/S1074-7613(03)00174-2.

Gonzalez-Pena, D. et al. 2016. Microglia transcriptome changes in a model of depressive behavior after immune challenge. *PLoS ONE* 11(3), pp. 1–28. doi: 10.1371/journal.pone.0150858.

Grabert, K. et al. 2016. Microglial brain region-dependent diversity and selective regional sensitivities to aging. *Nature Neuroscience* 19(3), pp. 504–516. doi: 10.1038/nn.4222.

Grizenkova, J., Akhtar, S., Brandner, S., Collinge, J. and Lloyd, S.E. 2014. Microglial Cx3cr1 knockout reduces prion disease incubation time in mice. *BMC Neuroscience* 15(1), p. 44. doi: 10.1186/1471-2202-15-44.

Gyoneva, S. et al. 2019. Cx3cr1-deficient microglia exhibit a premature aging transcriptome. *Life Science Alliance* 2(6). doi: 10.26508/lsa.201900453.

Haage, V. et al. 2019. Comprehensive gene expression meta-analysis identifies signature genes that distinguish microglia from peripheral monocytes/macrophages in health and glioma. *Acta Neuropathologica Communications* 7(1), p. 20. doi: 10.1186/s40478-019-0665-y.

Hagihara, H., Toyama, K., Yamasaki, N. and Miyakawa, T. 2009. Dissection of hippocampal dentate gyrus from adult mouse. *Journal of visualized experiments : JoVE* (33). Available at: http://www.ncbi.nlm.nih.gov/pubmed/19920804 [Accessed: 4 December 2019].

Hammond, T.R. et al. 2019a. Single-Cell RNA Sequencing of Microglia throughout the Mouse Lifespan and in the Injured Brain Reveals Complex Cell-State Changes. *Immunity* 50(1), pp. 253-271.e6. doi: 10.1016/j.immuni.2018.11.004.

Hammond, T.R. et al. 2019b. Single-Cell RNA Sequencing of Microglia throughout the Mouse Lifespan and in the Injured Brain Reveals Complex Cell-State Changes. *Immunity* 50(1), pp. 253-271.e6. Available at: https://www.sciencedirect.com/science/article/pii/S1074761318304850?via%3Dihub#sec4 [Accessed: 27 March 2019].

Hanamsagar, R. and Bilbo, S.D. 2017. Environment matters: microglia function and dysfunction in a changing world. *Current Opinion in Neurobiology* 47, pp. 146–155. doi: 10.1016/J.CONB.2017.10.007.

Hatori, K., Nagai, A., Heisel, R., Ryu, J.K. and Kim, S.U. 2002. Fractalkine and fractalkine receptors in human neurons and glial cells. *Journal of Neuroscience Research* 69(3), pp. 418–426. doi: 10.1002/jnr.10304.

He, Y., Yao, X., Taylor, N., Bai, Y., Lovenberg, T. and Bhattacharya, A. 2018. RNA sequencing analysis reveals quiescent microglia isolation methods from postnatal mouse brains and limitations of BV2 cells. *Journal of Neuroinflammation* 15(1), p. 153. Available at: https://jneuroinflammation.biomedcentral.com/articles/10.1186/s12974-018-1195-4 [Accessed: 9 January 2019].

Hickman, S.E., Kingery, N.D., Ohsumi, T.K., Borowsky, M.L., Wang, L.C., Means, T.K. and el Khoury, J. 2013. The microglial sensome revealed by direct RNA sequencing. *Nature Neuroscience* 16(12), pp. 1896–1905. Available at: http://www.nature.com/authors/editorial_policies/license.html#terms [Accessed: 27 November 2018].

Imbeaud, S. et al. 2005. Towards standardization of RNA quality assessment using user-independent classifiers of microcapillary electrophoresis traces. *Nucleic Acids Research* 33(6), p. e56. Available at: /pmc/articles/PMC1072807/ [Accessed: 11 December 2022].

Ju, L., Zeng, H., Chen, Y., Wu, Y., Wang, B. and Xu, Q. 2015. Dual polarization of microglia isolated from mixed glial cell cultures. *Journal of Neuroscience Research* 93(9), pp. 1345–1352. doi: 10.1002/jnr.23563.

Jung, S., Aliberti, J., Graemmel, P., Sunshine, M.J., Kreutzberg, G.W., Sher, A. and Littman, D.R. 2000. Analysis of Fractalkine Receptor CX3CR1 Function by Targeted Deletion and Green Fluorescent Protein Reporter Gene Insertion. *Molecular and Cellular Biology* 20(11), p. 4106. doi: 10.1128/MCB.20.11.4106-4114.2000.

Kaiser, T. and Feng, G. 2019. Tmem119-EGFP and Tmem119-CreERT2 Transgenic Mice for Labeling and Manipulating Microglia. *eNeuro* 6(4). doi: 10.1523/ENEURO.0448-18.2019.

Kreisel, T., Wolf, B., Keshet, E. and Licht, T. 2019. Unique role for dentate gyrus microglia in neuroblast survival and in VEGF-induced activation. *GLIA* 67(4), pp. 594–618. Available at: http://doi.wiley.com/10.1002/glia.23505 [Accessed: 27 March 2019].

Kuonen, F., Touvrey, C., Laurent, J. and Ruegg, C. 2010. Fc block treatment, dead cells exclusion, and cell aggregates discrimination concur to prevent phenotypical artifacts in the analysis of subpopulations of tumor-infiltrating CD11b+ myelomonocytic cells. *Cytometry Part A* 77A(11), pp. 1082–1090. doi: 10.1002/cyto.a.20969.

Lam, D., Lively, S. and Schlichter, L.C. 2017. Responses of rat and mouse primary microglia to pro- and anti-inflammatory stimuli: Molecular profiles, K+ channels and migration. *Journal of Neuroinflammation* 14(1), pp. 1–30. doi: 10.1186/s12974-017-0941-3.

Lawson, L.J., Perry, V.H., Dri, P. and Gordon, S. 1990. Heterogeneity in the distribution and morphology of microglia in the normal adult mouse brain. *Neuroscience* 39(1), pp. 151–170. Available at: https://www.sciencedirect.com/science/article/pii/030645229090229W?via%3Dihub [Accessed: 11 February 2021].

Lein, E.S. et al. 2007. Genome-wide atlas of gene expression in the adult mouse brain. *Nature* 445(7124), pp. 168–176. doi: 10.1038/nature05453.

Lein, E.S., Zhao, X. and Gage, F.H. 2004. Cellular/Molecular Defining a Molecular Atlas of the Hippocampus Using DNA Microarrays and High-Throughput In Situ Hybridization. Available at: www.jneurosci.org [Accessed: 4 December 2019].

Liu, C. et al. 1999. Nephroblastoma overexpressed gene (NOV) codes for a growth factor that induces protein tyrosine phosphorylation. *Gene* 238(2), pp. 471–478. doi: 10.1016/S0378-1119(99)00364-9.

Liu, Y., Zhang, T., Meng, D., Sun, L., Yang, G., He, Y. and Zhang, C. 2020. Involvement of CX3CL1/CX3CR1 in depression and cognitive impairment induced by chronic unpredictable

stress and relevant underlying mechanism. *Behavioural Brain Research* 381, p. 112371. doi: 10.1016/J.BBR.2019.112371.

Lund, S. et al. 2006. The dynamics of the LPS triggered inflammatory response of murine microglia under different culture and in vivo conditions. *Journal of Neuroimmunology* 180(1–2), pp. 71–87. doi: 10.1016/J.JNEUROIM.2006.07.007.

Luo, W., Xu, C., Ayello, J., Dela Cruz, F., Rosenblum, J.M., Lessnick, S.L. and Cairo, M.S. 2018. Protein phosphatase 1 regulatory subunit 1A in ewing sarcoma tumorigenesis and metastasis. *Oncogene* 37(6), pp. 798–809. doi: 10.1038/onc.2017.378.

Martin, E., El-Behi, M., Fontaine, B. and Delarasse, C. 2017. Analysis of Microglia and Monocyte-derived Macrophages from the Central Nervous System by Flow Cytometry. *Journal of visualized experiments : JoVE* (124). doi: 10.3791/55781.

Masuda, T. et al. 2020. Novel Hexb-based tools for studying microglia in the CNS. *Nature Immunology* 21(7), pp. 802–815. Available at: http://www.nature.com/articles/s41590-020-0707-4 [Accessed: 3 February 2021].

Matcovitch-Natan, O. et al. 2016. Microglia development follows a stepwise program to regulate brain homeostasis. *Science (New York, N.Y.)* 353(6301), p. aad8670. doi: 10.1126/science.aad8670.

McCarthy, G.M., Farris, S.P., Blednov, Y.A., Harris, R.A. and Mayfield, R.D. 2018. Microglial-specific transcriptome changes following chronic alcohol consumption. *Neuropharmacology* 128, pp. 416–424. doi: 10.1016/j.neuropharm.2017.10.035.

Meucci, O., Fatatis, A., Simen, A.A. and Miller, R.J. 2000. Expression of CX3CR1 chemokine receptors on neurons and their role in neuronal survival. *Proceedings of the National Academy of Sciences of the United States of America* 97(14), pp. 8075–80. Available at: http://www.ncbi.nlm.nih.gov/pubmed/10869418 [Accessed: 13 May 2020].

Mizutani, M., Pino, P.A., Saederup, N., Charo, I.F., Ransohoff, R.M. and Cardona, A.E. 2012. The fractalkine receptor but not CCR2 is present on microglia from embryonic development throughout adulthood. *Journal of immunology (Baltimore, Md. : 1950)* 188(1), pp. 29–36. doi: 10.4049/jimmunol.1100421.

Nikodemova, M. and Watters, J.J. 2012. Efficient isolation of live microglia with preserved phenotypes from adult mouse brain. *Journal of neuroinflammation* 9, p. 147. doi: 10.1186/1742-2094-9-147.

Nimmerjahn, A., Kirchhoff, F. and Helmchen, F. 2005. Neuroscience: Resting microglial cells are highly dynamic surveillants of brain parenchyma in vivo. *Science* 308(5726), pp. 1314–1318. Available at: https://science.sciencemag.org/content/308/5726/1314 [Accessed: 3 May 2020].

Nishiyori, A. et al. 1998. Localization of fractalkine and CX3CR1 mRNAs in rat brain: does fractalkine play a role in signaling from neuron to microglia? *FEBS Letters* 429(2), pp. 167–172. Available at: https://www.sciencedirect.com/science/article/pii/S0014579398005833 [Accessed: 2 May 2020].

Noristani, H.N. et al. 2017. RNA-Seq Analysis of Microglia Reveals Time-Dependent Activation of Specific Genetic Programs following Spinal Cord Injury. *Frontiers in Molecular Neuroscience* 10, p. 90. doi: 10.3389/fnmol.2017.00090.

Ohira, K. et al. 2010. Expression of tryptophan 2,3-dioxygenase in mature granule cells of the adult mouse dentate gyrus. *Molecular Brain* 3(1), p. 26. doi: 10.1186/1756-6606-3-26.

Osborne, G.W. 2010. A method of quantifying cell sorting yield in “real time.” *Cytometry Part A* 77A(10), pp. 983–989. doi: 10.1002/cyto.a.20950.

Petersen, T.W. and van den Engh, G. 2003. Stability of the breakoff point in a high-speed cell sorter. *Cytometry* 56A(2), pp. 63–70. doi: 10.1002/cyto.a.10090.

Prinz, M. and Priller, J. 2014. Microglia and brain macrophages in the molecular age: From origin to neuropsychiatric disease. *Nature Reviews Neuroscience* 15(5), pp. 300–312. doi: 10.1038/nrn3722.

Rogers, J.T. et al. 2011. CX3CR1 Deficiency Leads to Impairment of Hippocampal Cognitive Function and Synaptic Plasticity. *Journal of Neuroscience* 31(45), pp. 16241–16250. doi: 10.1523/JNEUROSCI.3667-11.2011.

Ruan, C. et al. 2020. A novel Tmem119-tdTomato reporter mouse model for studying microglia in the central nervous system. *Brain, Behavior, and Immunity* 83, pp. 180–191. doi: 10.1016/J.BBI.2019.10.009.

Sheridan, G.K. and Murphy, K.J. 2013. Neuron–glia crosstalk in health and disease: fractalkine and CX3CR1 take centre stage. *Open Biology* 3(12). doi: 10.1098/RSOB.130181.

Si, Y., Tsou, C.-L., Croft, K. and Charo, I.F. 2010. CCR2 mediates hematopoietic stem and progenitor cell trafficking to sites of inflammation in mice. *The Journal of Clinical Investigation* 120(4), p. 1192. doi: 10.1172/JCI40310.

Solga, A.C. et al. 2015. RNA-sequencing reveals oligodendrocyte and neuronal transcripts in microglia relevant to central nervous system disease. *Glia* 63(4), pp. 531–548. doi: 10.1002/glia.22754.

Sutermaster, B.A. and Darling, E.M. 2019. Considerations for high-yield, high-throughput cell enrichment: fluorescence versus magnetic sorting. *Scientific Reports* 9(1), p. 227. doi: 10.1038/s41598-018-36698-1.

Takasato, M. et al. 2004. Identification of kidney mesenchymal genes by a combination of microarray analysis and Sall1-GFP knockin mice. *Mechanisms of Development* 121(6), pp. 547–557. doi: 10.1016/J.MOD.2004.04.007.

Tomlinson, M.J., Tomlinson, S., Yang, X.B. and Kirkham, J. 2013. Cell separation: Terminology and practical considerations. *Journal of tissue engineering* 4, p. 2041731412472690. doi: 10.1177/2041731412472690.

Vankriekelsvenne, E. et al. 2022. Transmembrane protein 119 is neither a specific nor a reliable marker for microglia. *Glia* 70(6), pp. 1170–1190. Available at: https://onlinelibrary-wiley-com.abc.cardiff.ac.uk/doi/full/10.1002/glia.24164 [Accessed: 12 December 2022].

Wu, W. et al. 2013. Expression of Tryptophan 2,3-Dioxygenase and Production of Kynurenine Pathway Metabolites in Triple Transgenic Mice and Human Alzheimer's Disease Brain. Adlard, P. A. ed. *PLoS ONE* 8(4), p. e59749. doi: 10.1371/journal.pone.0059749.

Yamasaki, N. et al. 2008. Alpha-CaMKII deficiency causes immature dentate gyrus, a novel candidate endophenotype of psychiatric disorders. *Molecular Brain* 1(1), p. 6. doi: 10.1186/1756-6606-1-6.

Zhan, Y. et al. 2014. Deficient neuron-microglia signaling results in impaired functional brain connectivity and social behavior. *Nature Neuroscience* 17(3), pp. 400–406. doi: 10.1038/nn.3641.

Zhao, X., Lein, E.S., He, A., Smith, S.C., Aston, C. and Gage, F.H. 2001. Transcriptional profiling reveals strict boundaries between hippocampal subregions. *The Journal of Comparative Neurology* 441(3), pp. 187–196. doi: 10.1002/cne.1406.

Chapter 7 References

Artegiani, B., Lyubimova, A., Muraro, M., Es, J.H. van, Oudenaarden, A. van and Clevers, H. 2017. A Single-Cell RNA Sequencing Study Reveals Cellular and Molecular Dynamics of the Hippocampal Neurogenic Niche. *Cell Reports* 21(11), pp. 3271–3284. Available at: https://www.cell.com/cell-reports/fulltext/S2211-1247(17)31702-3?_returnURL=https%3A%2F%2Flinkinghub.elsevier.com%2Fretrieve%2Fpii%2FS2211124717317023%3Fshowall%3Dtrue [Accessed: 9 May 2020].

Assefa, A.T., Vandesompele, J. and Thas, O. 2020. On the utility of RNA sample pooling to optimize cost and statistical power in RNA sequencing experiments. *BMC Genomics* 21(1), pp. 1–14. Available at: https://bmcgenomics-biomedcentral-com.abc.cardiff.ac.uk/articles/10.1186/s12864-020-6721-y [Accessed: 17 January 2022].

Bohlen, C.J., Bennett, F.C., Tucker, A.F., Collins, H.Y., Mulinyawe, S.B. and Barres, B.A. 2017. Diverse Requirements for Microglial Survival, Specification, and Function Revealed by Defined-Medium Cultures. *Neuron* 94(4), pp. 759-773.e8. Available at: http://dx.doi.org/10.1016/j.neuron.2017.04.043.

Butovsky, O. et al. 2014. Identification of a unique TGF-β-dependent molecular and functional signature in microglia. *Nature Neuroscience* 17(1), pp. 131–143. doi: 10.1038/nn.3599.

Erny, D. et al. 2015. Host microbiota constantly control maturation and function of microglia in the CNS. *Nature Neuroscience* 18(7), pp. 965–977. doi: 10.1038/nn.4030.

Galatro, T.F. et al. 2017. Transcriptomic analysis of purified human cortical microglia reveals age-associated changes. *Nature Neuroscience 2017 20:8* 20(8), pp. 1162–1171. Available at: https://www.nature.com/articles/nn.4597 [Accessed: 16 January 2022].

Gautiar, E.L. et al. 2012. Gene-expression profiles and transcriptional regulatory pathways that underlie the identity and diversity of mouse tissue macrophages. *Nature Immunology 2012*

13:11 13(11), pp. 1118–1128. Available at: https://www-nature-com.abc.cardiff.ac.uk/articles/ni.2419 [Accessed: 10 January 2022].

Grabert, K. et al. 2016. Microglial brain region-dependent diversity and selective regional sensitivities to aging. *Nature Neuroscience* 19(3), pp. 504–516. doi: 10.1038/nn.4222.

Gyoneva, S. et al. 2019. Cx3cr1-deficient microglia exhibit a premature aging transcriptome. *Life Science Alliance* 2(6). doi: 10.26508/lsa.201900453.

Haage, V. et al. 2019. Comprehensive gene expression meta-analysis identifies signature genes that distinguish microglia from peripheral monocytes/macrophages in health and glioma. *Acta Neuropathologica Communications 2019 7:1* 7(1), pp. 1–18. Available at: https://actaneurocomms-biomedcentral-com.abc.cardiff.ac.uk/articles/10.1186/s40478-019-0665-y [Accessed: 3 August 2021].

Hammond, T.R. et al. 2019a. Single-Cell RNA Sequencing of Microglia throughout the Mouse Lifespan and in the Injured Brain Reveals Complex Cell-State Changes. *Immunity* 50(1), pp. 253-271.e6. doi: 10.1016/j.immuni.2018.11.004.

Hammond, T.R. et al. 2019b. Single-Cell RNA Sequencing of Microglia throughout the Mouse Lifespan and in the Injured Brain Reveals Complex Cell-State Changes. *Immunity* 50(1), pp. 253-271.e6. Available at: https://www.sciencedirect.com/science/article/pii/S1074761318304850?via%3Dihub#sec4 [Accessed: 27 March 2019].

Jao, J. and Ciernia, A.V. 2021. MGEnrichment: A web application for microglia gene list enrichment analysis. *PLOS Computational Biology* 17(11), p. e1009160. Available at: https://journals.plos.org/ploscompbiol/article?id=10.1371/journal.pcbi.1009160 [Accessed: 15 January 2022].

Kreisel, T., Wolf, B., Keshet, E. and Licht, T. 2019. Unique role for dentate gyrus microglia in neuroblast survival and in VEGF-induced activation. *GLIA* 67(4), pp. 594–618. Available at: http://doi.wiley.com/10.1002/glia.23505 [Accessed: 27 March 2019].

Li, Q. et al. 2019. Developmental Heterogeneity of Microglia and Brain Myeloid Cells Revealed by Deep Single-Cell RNA Sequencing. *Neuron* 101(2), pp. 207-223.e10. Available at: https://www.sciencedirect.com/science/article/pii/S0896627318310821?via%3Dihub [Accessed: 4 December 2019].

Love, M.I., Huber, W. and Anders, S. 2014. Moderated estimation of fold change and dispersion for RNA-seq data with DESeq2. *Genome Biology 2014 15:12* 15(12), pp. 1–21. Available at: https://genomebiology.biomedcentral.com/articles/10.1186/s13059-014-0550-8 [Accessed: 20 July 2021].

Masuda, T. et al. 2019. Spatial and temporal heterogeneity of mouse and human microglia at single-cell resolution. *Nature 2019 566:7744* 566(7744), pp. 388–392. Available at: https://www.nature.com/articles/s41586-019-0924-x [Accessed: 4 December 2019].

Matcovitch-Natan, O. et al. 2016. Microglia development follows a stepwise program to regulate brain homeostasis. *Science (New York, N.Y.)* 353(6301), p. aad8670. doi: 10.1126/science.aad8670.

Mattei, D. et al. 2020. Enzymatic dissociation induces transcriptional and proteotype bias in brain cell populations. *International Journal of Molecular Sciences* 21(21), pp. 1–20. Available at: www.mdpi.com/journal/ijms.

Mootha, V.K. et al. 2003. PGC-1α-responsive genes involved in oxidative phosphorylation are coordinately downregulated in human diabetes. *Nature Genetics 2003 34:3* 34(3), pp. 267–273. Available at: https://www-nature-com.abc.cardiff.ac.uk/articles/ng1180 [Accessed: 7 January 2022].

Okabe, Y. and Medzhitov, R. 2014. Tissue-Specific Signals Control Reversible Program of Localization and Functional Polarization of Macrophages. *Cell* 157(4), pp. 832–844. doi: 10.1016/J.CELL.2014.04.016.

Parakalan, R. et al. 2012. Transcriptome analysis of amoeboid and ramified microglia isolated from the corpus callosum of rat brain. *BMC Neuroscience* 13(1), pp. 1–20. Available at: https://bmcneurosci-biomedcentral-com.abc.cardiff.ac.uk/articles/10.1186/1471-2202-13-64 [Accessed: 16 January 2022].

Parekh, S., Ziegenhain, C., Vieth, B., Enard, W. and Hellmann, I. 2016. The impact of amplification on differential expression analyses by RNA-seq. *Scientific Reports 2016 6:1* 6(1), pp. 1–11. Available at: https://www-nature-com.abc.cardiff.ac.uk/articles/srep25533 [Accessed: 17 January 2022].

Rogers, J.T. et al. 2011. CX3CR1 Deficiency Leads to Impairment of Hippocampal Cognitive Function and Synaptic Plasticity. *Journal of Neuroscience* 31(45), pp. 16241–16250. doi: 10.1523/JNEUROSCI.3667-11.2011.

Sankowski, R. et al. 2019. Mapping microglia states in the human brain through the integration of high-dimensional techniques. *Nature Neuroscience* 22(12), pp. 2098–2110. Available at: http://www.nature.com/articles/s41593-019-0532-y [Accessed: 10 February 2020].

Subramanian, A. et al. 2005. Gene set enrichment analysis: A knowledge-based approach for interpreting genome-wide expression profiles. Available at: www.pnas.orgcgidoi10.1073pnas.0506580102 [Accessed: 27 July 2021].

Zhang, Y. et al. 2014. An RNA-Sequencing Transcriptome and Splicing Database of Glia, Neurons, and Vascular Cells of the Cerebral Cortex. *Journal of Neuroscience* 34(36), pp. 11929–11947. Available at: http://www.jneurosci.org/cgi/doi/10.1523/JNEUROSCI.1860-14.2014.

Chapter 8 References

Aarum, J., Sandberg, K., Haeberlein, S.L.B. and Persson, M.A.A. 2003. Migration and differentiation of neural precursor cells can be directed by microglia. *Proceedings of the National Academy of Sciences* 100(26), pp. 15983–15988. Available at: https://www-pnas-org.abc.cardiff.ac.uk/content/100/26/15983 [Accessed: 12 December 2021].

Ahmed, S., Reynolds, B.A. and Weiss, S. 1995. *BDNF Enhances the Differentiation but Not the Survival of CNS Stem Cell-Derived Neuronal Precursors*. Available at: http://www.jneurosci.org/content/jneuro/15/8/5765.full.pdf [Accessed: 4 February 2019].

Aimone, J.B., Wiles, J. and Gage, F.H. 2009. Computational Influence of Adult Neurogenesis on Memory Encoding. *Neuron* 61(2), pp. 187–202. Available at: http://www.ncbi.nlm.nih.gov/pubmed/19186162 [Accessed: 4 May 2019].

Anacker, C. et al. 2018. Hippocampal neurogenesis confers stress resilience by inhibiting the ventral dentate gyrus. *Nature* 559(7712), pp. 98–102. Available at: http://www.nature.com/articles/s41586-018-0262-4 [Accessed: 27 January 2020].

Artegiani, B., Lyubimova, A., Muraro, M., Es, J.H. van, Oudenaarden, A. van and Clevers, H. 2017. A Single-Cell RNA Sequencing Study Reveals Cellular and Molecular Dynamics of the Hippocampal Neurogenic Niche. *Cell Reports* 21(11), pp. 3271–3284. Available at: https://www.cell.com/cell-reports/fulltext/S2211-1247(17)31702-3?_returnURL=https%3A%2F%2Flinkinghub.elsevier.com%2Fretrieve%2Fpii%2FS2211124717317023%3Fshowall%3Dtrue [Accessed: 9 May 2020].

Baptista, P. and Andrade, J.P. 2018. Adult Hippocampal Neurogenesis: Regulation and Possible Functional and Clinical Correlates. *Frontiers in Neuroanatomy* 12, p. 44. Available at: https://www.frontiersin.org/article/10.3389/fnana.2018.00044/full [Accessed: 10 February 2020].

Boldrini, M., Fulmore, C.A., Tartt, A.N. and ..., Andrew J. Dwork, Rene Hen, J.J.M. 2018. full-text. *Cell Stem Cell* 22(4), pp. 589-599.e5. Available at: http://www.ncbi.nlm.nih.gov/pubmed/29625071 [Accessed: 8 June 2018].

Cao, X. et al. 2013. Astrocytic Adenosine 5′-Triphosphate Release Regulates the Proliferation of Neural Stem Cells in the Adult Hippocampus. *Stem Cells* 31(8), pp. 1633–1643. Available at: https://academic-oup-com.abc.cardiff.ac.uk/stmcls/article/31/8/1633/6408209 [Accessed: 18 January 2022].

Ehret, F., Vogler, S. and Kempermann, G. 2015. A co-culture model of the hippocampal neurogenic niche reveals differential effects of astrocytes, endothelial cells and pericytes on proliferation and differentiation of adult murine precursor cells. *Stem Cell Research* 15(3), pp. 514–521. Available at: https://www.sciencedirect.com/science/article/pii/S1873506115001294?via%3Dihub [Accessed: 4 May 2019].

Hirsch, C. and Schildknecht, S. 2019. In Vitro Research Reproducibility: Keeping Up High Standards. *Frontiers in Pharmacology* 0, p. 1484. doi: 10.3389/FPHAR.2019.01484.

Kempermann, G. 2011. Seven principles in the regulation of adult neurogenesis. *European Journal of Neuroscience* 33(6), pp. 1018–1024. Available at: https://onlinelibrary-wiley-com.abc.cardiff.ac.uk/doi/full/10.1111/j.1460-9568.2011.07599.x [Accessed: 18 January 2022].

Kempermann, G., Jessberger, S., Steiner, B. and Kronenberg, G. 2004. Milestones of neuronal development in the adult hippocampus. *Trends in Neursciences* 27(8), pp. 447–452. Available at: www.sciencedirect.com [Accessed: 20 September 2018].

Kreisel, T., Wolf, B., Keshet, E. and Licht, T. 2019. Unique role for dentate gyrus microglia in neuroblast survival and in VEGF-induced activation. *GLIA* 67(4), pp. 594–618. Available at: http://doi.wiley.com/10.1002/glia.23505 [Accessed: 27 March 2019].

Masuda, T. et al. 2020. Novel Hexb-based tools for studying microglia in the CNS. *Nature Immunology* 21(7), pp. 802–815. Available at: http://www.nature.com/articles/s41590-020-0707-4 [Accessed: 3 February 2021].

Merritt, C.R. et al. 2020. Multiplex digital spatial profiling of proteins and RNA in fixed tissue. *Nature Biotechnology* 38(5), pp. 586–599. Available at: https://doi.org/10.1038/s41587-020-0472-9 [Accessed: 6 January 2022].

Moreno-Jiménez, E.P. et al. 2019. Adult hippocampal neurogenesis is abundant in neurologically healthy subjects and drops sharply in patients with Alzheimer's disease. *Nature Medicine* 25(4), pp. 554–560. Available at: http://www.nature.com/articles/s41591-019-0375-9 [Accessed: 2 May 2019].

Morgan, S.C., Taylor, D.L. and Pocock, J.M. 2004. Microglia release activators of neuronal proliferation mediated by activation of mitogen-activated protein kinase, phosphatidylinositol-3-kinase/Akt and delta-Notch signalling cascades. *Journal of Neurochemistry* 90(1), pp. 89–101. Available at: http://doi.wiley.com/10.1111/j.1471-4159.2004.02461.x [Accessed: 27 January 2020].

Nunan, R., Sivasathiaseelan, H., Khan, D., Zaben, M. and Gray, W. 2014. Microglial VPAC1R mediates a novel mechanism of neuroimmune-modulation of hippocampal precursor cells via IL-4 release. *Glia* 62(8), pp. 1313–1327. doi: 10.1002/glia.22682.

Palmer, T.D., Willhoite, A.R. and Gage, F.H. 2000. Vascular niche for adult hippocampal neurogenesis. *The Journal of Comparative Neurology* 425(4), pp. 479–494. Available at: http://doi.wiley.com/10.1002/1096-9861%2820001002%29425%3A4%3C479%3A%3AAID-CNE2%3E3.0.CO%3B2-3 [Accessed: 4 May 2019].

van Praag, H., Kempermann, G. and Gage, F.H. 1999. Running increases cell proliferation and neurogenesis in the adult mouse dentate gyrus. *Nature Neuroscience 1999 2:3* 2(3), pp. 266–293

270. Available at: https://www-nature-com.abc.cardiff.ac.uk/articles/nn0399_266 [Accessed: 23 December 2021].

Rhee, Y.-H. et al. 2016. Neural stem cells secrete factors facilitating brain regeneration upon constitutive Raf-Erk activation OPEN. *Nature Publishing Group* . Available at: www.nature.com/scientificreports.

Rojo, R. et al. 2019. Deletion of a Csf1r enhancer selectively impacts CSF1R expression and development of tissue macrophage populations. *Nature Communications 2019 10:1* 10(1), pp. 1–17. Available at: https://www-nature-com.abc.cardiff.ac.uk/articles/s41467-019-11053-8 [Accessed: 14 December 2021].

Schafer, D.P. et al. 2012. Microglia Sculpt Postnatal Neural Circuits in an Activity and Complement-Dependent Manner. *Neuron* 74(4), pp. 691–705. Available at: https://www.sciencedirect.com/science/article/pii/S0896627312003340?via%3Dihub [Accessed: 7 June 2018].

Shen, Q. et al. 2004. Endothelial cells stimulate self-renewal and expand neurogenesis of neural stem cells. *Science (New York, N.Y.)* 304(5675), pp. 1338–1340. Available at: https://pubmed.ncbi.nlm.nih.gov/15060285/ [Accessed: 18 January 2022].

Shihabuddin, L.S., Horner, P.J., Ray, J. and Gage, F.H. 2000. *Adult Spinal Cord Stem Cells Generate Neurons after Transplantation in the Adult Dentate Gyrus*. Available at: https://www.jneurosci.org/content/jneuro/20/23/8727.full.pdf [Accessed: 18 July 2019].

Song, H., Stevens, C.F. and Gage, F.H. 2002. *Astroglia induce neurogenesis from adult neural stem cells*. Available at: www.nature.com.

Sorrells, S.F. et al. 2018a. Human hippocampal neurogenesis drops sharply in children to undetectable levels in adults. *Nature* 555(7696), pp. 377–381. Available at: http://www.nature.com/doifinder/10.1038/nature25975 [Accessed: 8 June 2018].

Sorrells, S.F. et al. 2018b. Human hippocampal neurogenesis drops sharply in children to undetectable levels in adults. *Nature* . doi: 10.1038/nature25975.

Tan, Y.-L., Yuan, Y. and Tian, L. 2020. Microglial regional heterogeneity and its role in the brain. *Molecular Psychiatry* 25(2), pp. 351–367. Available at: http://www.nature.com/articles/s41380-019-0609-8 [Accessed: 10 February 2020].

Toda, T., Parylak, S.L., Linker, S.B. and Gage, F.H. 2019. The role of adult hippocampal neurogenesis in brain health and disease. *Molecular Psychiatry* 24(1), pp. 67–87. Available at: http://www.nature.com/articles/s41380-018-0036-2 [Accessed: 19 October 2019].

Vogt, N. 2021. Cell–cell interactions revealed with RABID-seq. *Nature Methods 2021 18:6* 18(6), pp. 593–593. Available at: https://www-nature-com.abc.cardiff.ac.uk/articles/s41592-021-01192-6 [Accessed: 18 January 2022].

Walton, N.M. et al. 2006. Microglia instruct subventricular zone neurogenesis. *Glia* 54(8), pp. 815–825. Available at: https://onlinelibrary-wiley-com.abc.cardiff.ac.uk/doi/full/10.1002/glia.20419 [Accessed: 13 December 2021].

9.0 Appendix

Gene name	Description	log2FoldChange	Padj-value
Olfm1	olfactomedin 1	6.3302	5.86E-303
Stmn3	stathmin-like 3	5.6234	2.34E-244
Bex2	brain expressed X-linked 2	5.6789	3.87E-243
Snca	synuclein, alpha	5.0098	2.68E-146
Gap43	growth associated protein 43	6.7681	1.43E-138
Cck	cholecystokinin	7.04	7.38E-132
Hpcal4	hippocalcin-like 4	5.0072	4.87E-121
Syn2	synapsin II	5.0558	4.12E-114
Ctxn1	cortexin 1	6.717	1.10E-106
Ppp1r1a	protein phosphatase 1, regulatory inhibitor subunit 1A	5.118	1.42E-105
Atp6v1g2	ATPase, H+ transporting, lysosomal V1 subunit G2	3.254	2.01E-100
Tagln3	transgelin 3	4.8481	3.41E-86
Atp6v0e2	ATPase, H+ transporting, lysosomal V0 subunit E2	5.2072	3.06E-80
Gpm6a	glycoprotein m6a	4.8014	6.23E-78
Camk2a	calcium/calmodulin-dependent protein kinase II alpha	4.7413	3.14E-74
Kif5c	kinesin family member 5C	5.2663	4.50E-71
Atp1a3	ATPase, Na+/K+ transporting, alpha 3 polypeptide	3.4	8.21E-70
Gria2	glutamate receptor, ionotropic, AMPA2 (alpha 2)	6.378	2.04E-68
Caly	calcyon neuron-specific vesicular protein	6.3284	2.18E-68
Atp1b1	ATPase, Na+/K+ transporting, beta 1 polypeptide	6.0596	3.69E-68
Prnp	prion protein	3.2118	6.82E-66
Nrgn	neurogranin	5.5422	1.75E-65
Celf4	CUGBP, Elav-like family member 4	3.2221	1.01E-64
Caln1	calneuron 1	5.6533	5.39E-64
Rprml	reprimo-like	5.3176	2.55E-62
Map1b	microtubule-associated protein 1B	3.2347	4.05E-62
Cpe	carboxypeptidase E	2.7835	1.72E-61
Nrxn1	neurexin I	5.2717	1.65E-59
Gng3	guanine nucleotide binding protein (G protein), gamma 3	4.4748	7.71E-59
Slc17a7	solute carrier family 17 (sodium-dependent inorganic phosphate cotransporter), member 7	6.0246	8.89E-59
1110008P14Rik	RIKEN cDNA 1110008P14 gene	3.9604	9.11E-59
Nefl	neurofilament, light polypeptide	4.6519	5.51E-58
Arhgdig	Rho GDP dissociation inhibitor (GDI) gamma	6.3493	1.59E-57
Serp2	stress-associated endoplasmic reticulum protein family member 2	6.91	5.20E-57
Nptxr	neuronal pentraxin receptor	3.4244	1.71E-56
Prkcg	protein kinase C, gamma	4.196	9.93E-56
Tmem59l	transmembrane protein 59-like	5.9628	1.24E-55

Camk2n1	calcium/calmodulin-dependent protein kinase II inhibitor 1	2.2926	3.15E-55
Npdc1	neural proliferation, differentiation and control 1	6.0757	3.54E-55
Syp	synaptophysin	5.1463	4.90E-55
Kif5a	kinesin family member 5A	4.0705	1.29E-53
Kif1a	kinesin family member 1A	4.8259	1.49E-53
Thra	thyroid hormone receptor alpha	3.5998	1.40E-52
Dlgap1	DLG associated protein 1	4.5961	1.73E-50
Rtn1	reticulon 1	1.5686	2.90E-50
Fbxl16	F-box and leucine-rich repeat protein 16	4.2852	3.91E-50
Cnih2	cornichon family AMPA receptor auxiliary protein 2	3.7357	2.65E-49
Cplx2	complexin 2	7.0135	3.28E-49
Zfp365	zinc finger protein 365	4.7061	6.33E-49
Ddn	dendrin	6.3963	5.28E-48
Ttc9b	tetratricopeptide repeat domain 9B	5.831	8.34E-48
Stmn2	stathmin-like 2	4.4158	7.29E-47
Meg3	maternally expressed 3	6.1735	3.06E-46
Ndrg4	N-myc downstream regulated gene 4	3.193	8.83E-46
Gria1	glutamate receptor, ionotropic, AMPA1 (alpha 1)	5.4729	1.06E-45
Nsg1	neuron specific gene family member 1	5.4679	1.54E-45
Cyfip2	cytoplasmic FMR1 interacting protein 2	5.4757	2.35E-44
Gnao1	guanine nucleotide binding protein, alpha O	4.4506	3.96E-44
Ncald	neurocalcin delta	5.5179	9.88E-44
Rasgef1a	RasGEF domain family, member 1A	4.6282	1.27E-43
Myt1l	myelin transcription factor 1-like	6.4326	6.94E-43
Camkv	CaM kinase-like vesicle-associated	3.9558	2.46E-42
Tmod2	tropomodulin 2	4.0209	8.92E-42
Tesc	tescalcin	6.7549	4.29E-41
Tceal3	transcription elongation factor A (SII)-like 3	4.8189	1.43E-39
Uchl1	ubiquitin carboxy-terminal hydrolase L1	5.0112	2.02E-39
Rab3c	RAB3C, member RAS oncogene family	5.2875	2.08E-39
Nnat	neuronatin	6.3233	2.26E-39
Chgb	chromogranin B	5.7334	5.07E-39
Cx3cl1	chemokine (C-X3-C motif) ligand 1	4.9544	1.40E-37
Ttc3	tetratricopeptide repeat domain 3	1.1882	1.75E-37

Fabp3	fatty acid binding protein 3, muscle and heart	3.505	2.02E-37
Itpka	inositol 1,4,5-trisphosphate 3-kinase A	5.0549	2.09E-37
Cntn1	contactin 1	5.4742	2.26E-37
Chn1	chimerin 1	3.5007	4.40E-37
Lmo3	LIM domain only 3	4.5981	8.14E-37
Gfra4	glial cell line derived neurotrophic factor family receptor alpha 4	4.9122	1.56E-36
Ly6h	lymphocyte antigen 6 complex, locus H	8.0674	1.74E-36
Gpr22	G protein-coupled receptor 22	5.213	4.10E-36
Kif21a	kinesin family member 21A	5.2562	8.36E-36
Dclk1	doublecortin-like kinase 1	4.6499	1.65E-35
Anks1b	ankyrin repeat and sterile alpha motif domain containing 1B	3.9386	1.94E-35
Snhg11	small nucleolar RNA host gene 11	7.5799	2.97E-35
Mapt	microtubule-associated protein tau	3.7538	6.97E-34
Lingo1	leucine rich repeat and Ig domain containing 1	6.1069	1.28E-33
Aplp1	amyloid beta (A4) precursor-like protein 1	3.2302	1.67E-33
Rasgrf1	RAS protein-specific guanine nucleotide-releasing factor 1	4.5651	2.62E-33
Bex1	brain expressed X-linked 1	5.887	2.62E-33
Rasgrp1	RAS guanyl releasing protein 1	5.1022	6.87E-33
Sv2b	synaptic vesicle glycoprotein 2 b	6.0191	9.48E-33
Chchd10	coiled-coil-helix-coiled-coil-helix domain containing 10	3.8048	1.45E-32
Crym	crystallin, mu	4.5095	1.98E-32
Rbfox3	RNA binding protein, fox-1 homolog (C. elegans) 3	3.1734	1.98E-32
Fam171b	family with sequence similarity 171, member B	4.5225	2.11E-32
Nsg2	neuron specific gene family member 2	6.858	2.15E-32
Ptprn	protein tyrosine phosphatase, receptor type, N	4.9942	5.04E-32
Eno2	enolase 2, gamma neuronal	3.0759	4.00E-31
Grin2b	glutamate receptor, ionotropic, NMDA2B (epsilon 2)	5.3498	8.17E-31
Map7d2	MAP7 domain containing 2	6.4253	9.44E-31
Cnksr2	connector enhancer of kinase suppressor of Ras 2	4.8092	1.79E-30
Shisa4	shisa family member 4	3.6654	2.70E-30
Syn1	synapsin I	3.6695	9.11E-30
Mal2	mal, T cell differentiation protein 2	5.5167	1.61E-29
Pcsk1n	proprotein convertase subtilisin/kexin type 1 inhibitor	5.9904	1.72E-29
Map2	microtubule-associated protein 2	5.997	5.66E-29

Ppp2r2c	protein phosphatase 2, regulatory subunit B, gamma	6.3283	1.01E-28
Scg5	secretogranin V	7.2648	1.25E-28
Alcam	activated leukocyte cell adhesion molecule	5.6525	1.51E-28
Nefm	neurofilament, medium polypeptide	4.8608	1.52E-28
Tubb3	tubulin, beta 3 class III	5.1131	2.38E-28
Gabrb1	gamma-aminobutyric acid (GABA) A receptor, subunit beta 1	6.0543	2.72E-28
Bmerb1	bMERB domain containing 1	4.4757	3.05E-28
Spint2	serine protease inhibitor, Kunitz type 2	4.7862	3.34E-28
Scn2a	sodium channel, voltage-gated, type II, alpha	6.7291	3.91E-28
Shank1	SH3 and multiple ankyrin repeat domains 1	7.8081	7.16E-28
Jph4	junctophilin 4	5.4092	7.54E-28
Cend1	cell cycle exit and neuronal differentiation 1	4.041	1.01E-27
Syt1	synaptotagmin I	9.4568	1.17E-27
Dgkb	diacylglycerol kinase, beta	4.9026	2.10E-27
Syt5	synaptotagmin V	6.0897	3.10E-27
Ccnd2	cyclin D2	3.3022	3.95E-27
Tceal6	transcription elongation factor A (SII)-like 6	5.8256	4.46E-27
Auts2	autism susceptibility candidate 2	5.0146	5.82E-27
Ppp2r2b	protein phosphatase 2, regulatory subunit B, beta	4.1298	7.19E-27
Snrpn	small nuclear ribonucleoprotein N	4.5332	1.11E-26
Fxyd6	FXYD domain-containing ion transport regulator 6	5.1505	1.81E-26
Map9	microtubule-associated protein 9	3.8116	2.73E-26
Pcdh10	protocadherin 10	4.6848	4.07E-26
Selenom	selenoprotein M	2.2697	4.50E-26
Erc2	ELKS/RAB6-interacting/CAST family member 2	5.6593	8.57E-26
Nr2f2	nuclear receptor subfamily 2, group F, member 2	6.0288	1.69E-25
Pgm2l1	phosphoglucomutase 2-like 1	2.2482	2.17E-25
Cpne6	copine VI	3.0328	2.69E-25
C1qtnf4	C1q and tumor necrosis factor related protein 4	5.9798	3.12E-25
Wasf1	WASP family, member 1	3.7383	5.80E-25
Map1a	microtubule-associated protein 1 A	4.3613	5.81E-25
Fabp5	fatty acid binding protein 5, epidermal	2.721	6.96E-25
Ociad2	OCIA domain containing 2	3.1026	1.34E-24
Nckap1	NCK-associated protein 1	2.8665	1.35E-24

Bcl11b	B cell leukemia/lymphoma 11B	5.3872	1.93E-24
Ina	internexin neuronal intermediate filament protein, alpha	3.9813	2.24E-24
Slc12a5	solute carrier family 12, member 5	4.9447	4.86E-24
Septin3	septin 3	4.237	5.68E-24
Faim2	Fas apoptotic inhibitory molecule 2	5.5329	6.26E-24
Pfn2	profilin 2	2.7057	8.93E-24
Pde1a	phosphodiesterase 1A, calmodulin-dependent	4.3105	1.19E-23
Gabbr2	gamma-aminobutyric acid (GABA) B receptor, 2	4.5561	1.37E-23
Igfbp6	insulin-like growth factor binding protein 6	4.4994	3.17E-23
Nedd4	neural precursor cell expressed, developmentally down-regulated 4	3.8185	3.86E-23
Sst	somatostatin	5.4724	4.20E-23
Grm5	glutamate receptor, metabotropic 5	6.0107	4.21E-23
Syt4	synaptotagmin IV	7.7259	7.36E-23
Ncam1	neural cell adhesion molecule 1	3.6875	9.48E-23
Snap91	synaptosomal-associated protein 91	3.9774	1.22E-22
Necab2	N-terminal EF-hand calcium binding protein 2	5.4794	2.20E-22
Mt3	metallothionein 3	4.5137	2.32E-22
Soga3	SOGA family member 3	4.5698	2.56E-22
Arpp21	cyclic AMP-regulated phosphoprotein, 21	5.7915	3.17E-22
Pak3	p21 (RAC1) activated kinase 3	5.2992	4.63E-22
Rab3a	RAB3A, member RAS oncogene family	1.4458	1.53E-21
Ube2ql1	ubiquitin-conjugating enzyme E2Q family-like 1	4.1794	1.96E-21
Fxyd7	FXYD domain-containing ion transport regulator 7	4.3205	2.93E-21
Acot7	acyl-CoA thioesterase 7	1.553	3.04E-21
Mapk8ip2	mitogen-activated protein kinase 8 interacting protein 2	6.3548	3.52E-21
Ahi1	Abelson helper integration site 1	2.0084	3.81E-21
Stmn1	stathmin 1	1.3617	4.29E-21
Pdlim7	PDZ and LIM domain 7	4.3649	5.21E-21
Ccn3	cellular communication network factor 3	6.1692	6.37E-21
Plcb1	phospholipase C, beta 1	4.4571	1.01E-20
Nap1l5	nucleosome assembly protein 1-like 5	3.0745	1.55E-20
Kctd4	potassium channel tetramerisation domain containing 4	3.4611	1.60E-20
Cbarp	calcium channel, voltage-dependent, beta subunit associated regulatory protein	4.1668	1.75E-20
Celsr2	cadherin, EGF LAG seven-pass G-type receptor 2	5.1039	2.50E-20

Sez6l2	seizure related 6 homolog like 2	3.632	3.22E-20
Ak5	adenylate kinase 5	3.4151	3.87E-20
Dnm1	dynamin 1	3.9592	7.14E-20
Vsnl1	visinin-like 1	6.2319	7.89E-20
Cplx1	complexin 1	2.8372	9.35E-20
Rprm	reprimo, TP53 dependent G2 arrest mediator candidate	6.732	9.73E-20
Cadm2	cell adhesion molecule 2	4.1574	1.04E-19
Frrs1l	ferric-chelate reductase 1 like	7.2035	1.48E-19
Crip2	cysteine rich protein 2	2.3009	1.69E-19
Lypd1	Ly6/Plaur domain containing 1	9.5935	2.04E-19
Clip3	CAP-GLY domain containing linker protein 3	3.7507	2.06E-19
Rims1	regulating synaptic membrane exocytosis 1	5.2297	3.86E-19
Adcy1	adenylate cyclase 1	7.0419	4.03E-19
Dbn1	drebrin 1	3.7476	4.36E-19
Epha5	Eph receptor A5	7.2468	4.49E-19
Nrn1	neuritin 1	3.6507	4.63E-19
Ntm	neurotrimin	4.4062	5.56E-19
St6galnac5	ST6 (alpha-N-acetyl-neuraminyl-2,3-beta-galactosyl-1,3)-N-acetylgalactosaminide alpha-2,6-sialyltransferase 5	4.7509	5.98E-19
Calm3	calmodulin 3	1.0442	7.63E-19
Nr2f1	nuclear receptor subfamily 2, group F, member 1	5.0558	8.49E-19
Lonrf2	LON peptidase N-terminal domain and ring finger 2	5.1452	9.61E-19
Lsamp	limbic system-associated membrane protein	4.2389	1.31E-18
Nat14	N-acetyltransferase 14	2.4981	1.45E-18
Dgkg	diacylglycerol kinase, gamma	4.216	1.78E-18
Zcchc18	zinc finger, CCHC domain containing 18	2.7057	2.49E-18
Sult4a1	sulfotransferase family 4A, member 1	2.1197	2.59E-18
Ldb2	LIM domain binding 2	4.9774	3.50E-18
Nrsn2	neurensin 2	6.3763	3.62E-18
Slc30a3	solute carrier family 30 (zinc transporter), member 3	6.1151	3.65E-18
Selenow	selenoprotein W	1.9624	4.34E-18
Ncdn	neurochondrin	1.1409	4.35E-18
Tmem179	transmembrane protein 179	5.283	5.13E-18
Resp18	regulated endocrine-specific protein 18	11.8808	6.05E-18
Svop	SV2 related protein	5.3668	6.70E-18

Tubg2	tubulin, gamma 2	3.8606	1.20E-17
Elavl3	ELAV like RNA binding protein 3	3.9629	1.25E-17
Stx1b	syntaxin 1B	4.8107	1.77E-17
Trim9	tripartite motif-containing 9	4.7821	2.31E-17
Pnmal2	PNMA-like 2	4.4544	2.33E-17
Fam81a	family with sequence similarity 81, member A	7.6503	2.56E-17
Slc1a2	solute carrier family 1 (glial high affinity glutamate transporter), member 2	2.7834	3.30E-17
Lysmd2	LysM, putative peptidoglycan-binding, domain containing 2	3.7308	4.18E-17
Cacnb3	calcium channel, voltage-dependent, beta 3 subunit	5.3445	6.01E-17
Nrcam	neuronal cell adhesion molecule	3.9359	7.35E-17
Sez6	seizure related gene 6	7.5335	7.55E-17
Klf9	Kruppel-like factor 9	2.1301	8.58E-17
Bex3	brain expressed X-linked 3	1.6006	9.41E-17
Ephx4	epoxide hydrolase 4	4.6906	9.41E-17
Plppr2	phospholipid phosphatase related 2	4.9194	1.01E-16
Pnmal1	PNMA-like 1	4.9514	1.13E-16
Ptpn5	protein tyrosine phosphatase, non-receptor type 5	5.0656	1.30E-16
Hpca	hippocalcin	2.0532	1.32E-16
Rgs17	regulator of G-protein signaling 17	4.8457	1.39E-16
Prickle2	prickle planar cell polarity protein 2	4.9675	2.06E-16
Tenm2	teneurin transmembrane protein 2	5.4543	2.31E-16
Dner	delta/notch-like EGF repeat containing	4.9284	2.41E-16
Negr1	neuronal growth regulator 1	4.0791	2.46E-16
Amph	amphiphysin	3.3447	2.55E-16
Mest	mesoderm specific transcript	4.2777	2.69E-16
Rnf208	ring finger protein 208	4.6461	3.44E-16
Scn8a	sodium channel, voltage-gated, type VIII, alpha	4.5109	3.53E-16
Tmem35a	transmembrane protein 35A	5.7736	3.64E-16
Spink8	serine peptidase inhibitor, Kazal type 8	6.1843	4.05E-16
Apba2	amyloid beta (A4) precursor protein-binding, family A, member 2	4.2406	4.09E-16
Napb	N-ethylmaleimide sensitive fusion protein attachment protein beta	1.7546	4.13E-16
Epha4	Eph receptor A4	5.1966	4.19E-16
Car11	carbonic anhydrase 11	2.3428	4.46E-16
Rab15	RAB15, member RAS oncogene family	3.6863	4.51E-16

Cap2	CAP, adenylate cyclase-associated protein, 2 (yeast)	5.556	4.94E-16
Tmem130	transmembrane protein 130	5.3118	5.15E-16
Camk2b	calcium/calmodulin-dependent protein kinase II, beta	1.7248	5.92E-16
1500011B03Rik	RIKEN cDNA 1500011B03 gene	1.2227	6.28E-16
Lin7b	lin-7 homolog B (C. elegans)	2.5331	6.46E-16
Adgrb2	adhesion G protein-coupled receptor B2	6.6062	7.45E-16
Gabrg2	gamma-aminobutyric acid (GABA) A receptor, subunit gamma 2	4.9623	1.26E-15
Astn1	astrotactin 1	4.7798	1.41E-15
Cit	citron	2.5889	1.62E-15
Ank3	ankyrin 3, epithelial	4.3531	1.81E-15
Sh3gl2	SH3-domain GRB2-like 2	2.878	2.53E-15
Rit2	Ras-like without CAAX 2	3.7343	2.94E-15
Car10	carbonic anhydrase 10	6.5595	3.63E-15
2010204K13Rik	RIKEN cDNA 2010204K13 gene	3.3841	5.24E-15
Cacna2d1	calcium channel, voltage-dependent, alpha2/delta subunit 1	5.4231	5.27E-15
Adgra1	adhesion G protein-coupled receptor A1	9.6965	5.39E-15
Opcml	opioid binding protein/cell adhesion molecule-like	5.174	5.45E-15
St8sia3	ST8 alpha-N-acetyl-neuraminide alpha-2,8-sialyltransferase 3	4.9595	6.81E-15
Gnaz	guanine nucleotide binding protein, alpha z subunit	3.1228	7.04E-15
Peg3	paternally expressed 3	10.9559	7.49E-15
Ccdc85b	coiled-coil domain containing 85B	1.0175	9.41E-15
Calb2	calbindin 2	4.6631	1.03E-14
Pgap4	post-GPI attachment to proteins GalNAc transferase 4	4.359	1.62E-14
Pcsk2	proprotein convertase subtilisin/kexin type 2	7.052	1.66E-14
Hap1	huntingtin-associated protein 1	2.9938	2.00E-14
Gria3	glutamate receptor, ionotropic, AMPA3 (alpha 3)	8.2992	2.24E-14
Mapk10	mitogen-activated protein kinase 10	3.7906	2.29E-14
Chl1	cell adhesion molecule L1-like	10.7615	2.41E-14
Gabra1	gamma-aminobutyric acid (GABA) A receptor, subunit alpha 1	4.786	3.09E-14
Neurod2	neurogenic differentiation 2	4.4169	3.10E-14
Cdkl5	cyclin-dependent kinase-like 5	4.3595	3.12E-14
Epdr1	ependymin related protein 1 (zebrafish)	3.8937	3.74E-14
Lrrn2	leucine rich repeat protein 2, neuronal	5.3097	3.97E-14
Rgs4	regulator of G-protein signaling 4	3.4684	4.17E-14

Syne1	spectrin repeat containing, nuclear envelope 1	4.1975	4.23E-14
Gda	guanine deaminase	8.2289	4.31E-14
Scg2	secretogranin II	3.8195	5.13E-14
Pianp	PILR alpha associated neural protein	5.8221	5.52E-14
Ildr2	immunoglobulin-like domain containing receptor 2	2.9316	5.98E-14
Gabra2	gamma-aminobutyric acid (GABA) A receptor, subunit alpha 2	7.0159	6.05E-14
Nell2	NEL-like 2	5.1648	6.98E-14
Sprn	shadow of prion protein	5.2588	7.80E-14
Limch1	LIM and calponin homology domains 1	4.374	8.44E-14
Rnf227	ring finger protein 227	1.289	1.24E-13
Cacng3	calcium channel, voltage-dependent, gamma subunit 3	10.628	1.26E-13
Unc80	unc-80, NALCN activator	6.2505	1.31E-13
Pcdh9	protocadherin 9	3.5647	1.40E-13
Enah	ENAH actin regulator	4.9391	1.42E-13
Cspg5	chondroitin sulfate proteoglycan 5	2.9534	1.51E-13
Mmp17	matrix metallopeptidase 17	4.4608	1.66E-13
Macrod2	mono-ADP ribosylhydrolase 2	3.099	1.80E-13
Cntnap2	contactin associated protein-like 2	5.2707	1.99E-13
Nrxn3	neurexin III	3.711	2.01E-13
Lynx1	Ly6/neurotoxin 1	6.8356	2.26E-13
Tafa1	TAFA chemokine like family member 1	6.2135	3.01E-13
Dcn	decorin	4.919	3.23E-13
Grik5	glutamate receptor, ionotropic, kainate 5 (gamma 2)	3.1245	3.46E-13
Slc24a2	solute carrier family 24 (sodium/potassium/calcium exchanger), member 2	5.15	3.46E-13
Pcdh17	protocadherin 17	3.5813	3.68E-13
Gabrb3	gamma-aminobutyric acid (GABA) A receptor, subunit beta 3	5.7106	3.84E-13
Akap6	A kinase (PRKA) anchor protein 6	5.1043	4.22E-13
Pfkp	phosphofructokinase, platelet	2.2838	4.74E-13
Rims2	regulating synaptic membrane exocytosis 2	3.9121	5.17E-13
Diras2	DIRAS family, GTP-binding RAS-like 2	3.7951	5.35E-13
Ptn	pleiotrophin	2.453	5.86E-13
Kctd16	potassium channel tetramerisation domain containing 16	6.062	5.91E-13
Pkia	protein kinase inhibitor, alpha	3.5541	7.35E-13
Thy1	thymus cell antigen 1, theta	10.2528	7.63E-13

Neto1	neuropilin (NRP) and tolloid (TLL)-like 1	5.4259	8.12E-13
Gdap1l1	ganglioside-induced differentiation-associated protein 1-like 1	2.5426	8.24E-13
Chrm1	cholinergic receptor, muscarinic 1, CNS	5.0926	9.27E-13
Fgf12	fibroblast growth factor 12	3.9604	9.92E-13
Actl6b	actin-like 6B	3.5286	9.92E-13
Rundc3a	RUN domain containing 3A	2.4559	1.10E-12
Mtfp1	mitochondrial fission process 1	1.4349	1.12E-12
Gabra4	gamma-aminobutyric acid (GABA) A receptor, subunit alpha 4	10.1901	1.15E-12
Dkk3	dickkopf WNT signaling pathway inhibitor 3	4.1287	1.19E-12
Tceal5	transcription elongation factor A (SII)-like 5	5.2273	1.23E-12
Apbb1	amyloid beta (A4) precursor protein-binding, family B, member 1	1.4344	1.39E-12
Prrt1	proline-rich transmembrane protein 1	4.4874	1.41E-12
Extl1	exostosin-like glycosyltransferase 1	3.5225	1.78E-12
Snap25	synaptosomal-associated protein 25	2.8394	2.32E-12
Vstm2b	V-set and transmembrane domain containing 2B	6.5568	2.33E-12
Spock1	sparc/osteonectin, cwcv and kazal-like domains proteoglycan 1	3.3427	2.64E-12
Ehd3	EH-domain containing 3	4.1697	2.64E-12
Ablim2	actin-binding LIM protein 2	2.5741	2.97E-12
Cystm1	cysteine-rich transmembrane module containing 1	2.2917	3.01E-12
Atp9a	ATPase, class II, type 9A	2.4422	3.39E-12
Ngef	neuronal guanine nucleotide exchange factor	3.7776	3.50E-12
Lzts1	leucine zipper, putative tumor suppressor 1	3.8807	3.60E-12
Stmn4	stathmin-like 4	2.8072	4.01E-12
Lhfpl4	lipoma HMGIC fusion partner-like protein 4	3.3824	4.11E-12
Srcin1	SRC kinase signaling inhibitor 1	4.6882	4.98E-12
Icam5	intercellular adhesion molecule 5, telencephalin	3.3565	5.66E-12
Slc4a3	solute carrier family 4 (anion exchanger), member 3	4.0062	6.09E-12
Cacnb4	calcium channel, voltage-dependent, beta 4 subunit	4.2468	6.21E-12
Ppfia2	protein tyrosine phosphatase, receptor type, f polypeptide (PTPRF), interacting protein (liprin), alpha 2	4.3093	6.87E-12
Vgf	VGF nerve growth factor inducible	5.0143	6.87E-12
Asphd2	aspartate beta-hydroxylase domain containing 2	3.2791	6.96E-12
Rab26	RAB26, member RAS oncogene family	3.7212	7.80E-12
Calb1	calbindin 1	3.1067	8.54E-12
Spock2	sparc/osteonectin, cwcv and kazal-like domains proteoglycan 2	4.1973	8.65E-12

Carmil2	capping protein regulator and myosin 1 linker 2	4.8306	8.69E-12
Pclo	piccolo (presynaptic cytomatrix protein)	5.2728	8.79E-12
Necab1	N-terminal EF-hand calcium binding protein 1	6.5183	9.55E-12
Ntrk3	neurotrophic tyrosine kinase, receptor, type 3	4.7574	9.93E-12
Ctxn2	cortexin 2	9.8468	1.05E-11
Sv2a	synaptic vesicle glycoprotein 2 a	1.5296	1.17E-11
Nrsn1	neurensin 1	2.2097	1.27E-11
Syt11	synaptotagmin XI	1.0364	1.48E-11
Clec2l	C-type lectin domain family 2, member L	4.1746	1.66E-11
Dcaf12l1	DDB1 and CUL4 associated factor 12-like 1	5.3379	2.00E-11
Pdxp	pyridoxal (pyridoxine, vitamin B6) phosphatase	2.4504	2.14E-11
Dusp26	dual specificity phosphatase 26 (putative)	3.1205	2.45E-11
Nptx1	neuronal pentraxin 1	4.8895	2.72E-11
A830018L16Rik	RIKEN cDNA A830018L16 gene	5.064	2.77E-11
Arxes2	adipocyte-related X-chromosome expressed sequence 2	2.9881	2.87E-11
Gdap1	ganglioside-induced differentiation-associated-protein 1	3.3632	3.02E-11
Kcna2	potassium voltage-gated channel, shaker-related subfamily, member 2	5.1477	3.14E-11
Slc4a10	solute carrier family 4, sodium bicarbonate cotransporter-like, member 10	5.1468	3.43E-11
Fam155a	family with sequence similarity 155, member A	6.4181	3.45E-11
Rab33a	RAB33A, member RAS oncogene family	4.535	3.46E-11
Arhgef28	Rho guanine nucleotide exchange factor (GEF) 28	3.0868	3.48E-11
Kcng1	potassium voltage-gated channel, subfamily G, member 1	9.7362	3.53E-11
Rasal1	RAS protein activator like 1 (GAP1 like)	5.352	3.61E-11
Shank2	SH3 and multiple ankyrin repeat domains 2	5.5414	4.10E-11
Phf24	PHD finger protein 24	3.6455	4.14E-11
Sptbn1	spectrin beta, non-erythrocytic 1	1.8925	4.20E-11
Cmbl	carboxymethylenebutenolidase-like (Pseudomonas)	4.3173	4.40E-11
Tspyl4	TSPY-like 4	2.6803	5.04E-11
Brinp1	bone morphogenic protein/retinoic acid inducible neural specific 1	5.5279	5.05E-11
Rgs7	regulator of G protein signaling 7	4.9641	5.05E-11
Tshz2	teashirt zinc finger family member 2	6.3816	5.47E-11
P4htm	prolyl 4-hydroxylase, transmembrane (endoplasmic reticulum)	2.8082	5.79E-11
Neto2	neuropilin (NRP) and tolloid (TLL)-like 2	4.397	5.96E-11
Gm10419	predicted gene 10419	4.8272	6.15E-11

Atp2b4	ATPase, Ca++ transporting, plasma membrane 4	8.3253	6.46E-11
Cd200	CD200 antigen	2.9724	6.76E-11
Dync1i1	dynein cytoplasmic 1 intermediate chain 1	3.8497	7.22E-11
Penk	preproenkephalin	9.608	7.22E-11
Ak4	adenylate kinase 4	4.0189	7.22E-11
Sowaha	sosondowah ankyrin repeat domain family member A	3.5264	7.47E-11
Gng4	guanine nucleotide binding protein (G protein), gamma 4	5.9574	7.83E-11
Kcnma1	potassium large conductance calcium-activated channel, subfamily M, alpha member 1	1.5342	8.05E-11
Arfgef3	ARFGEF family member 3	4.9456	8.35E-11
Susd4	sushi domain containing 4	5.1094	9.14E-11
Pgbd5	piggyBac transposable element derived 5	4.3951	9.14E-11
Nol4	nucleolar protein 4	4.6106	1.11E-10
Cadps	Ca2+-dependent secretion activator	4.8049	1.18E-10
Elmod1	ELMO/CED-12 domain containing 1	5.0339	1.18E-10
Rnf165	ring finger protein 165	4.4467	1.19E-10
Bhlhe22	basic helix-loop-helix family, member e22	9.4432	1.28E-10
Acyp2	acylphosphatase 2, muscle type	3.5417	1.30E-10
Hid1	HID1 domain containing	4.226	1.44E-10
Reep2	receptor accessory protein 2	2.7633	1.44E-10
Dnajc6	DnaJ heat shock protein family (Hsp40) member C6	4.7598	1.48E-10
Tmem14a	transmembrane protein 14A	1.7817	1.66E-10
Slc7a14	solute carrier family 7 (cationic amino acid transporter, y+ system), member 14	9.471	1.66E-10
Grin2a	glutamate receptor, ionotropic, NMDA2A (epsilon 1)	7.2084	1.66E-10
Crmp1	collapsin response mediator protein 1	3.3141	1.77E-10
Kcnq3	potassium voltage-gated channel, subfamily Q, member 3	6.2574	1.78E-10
Adcy5	adenylate cyclase 5	6.2467	1.78E-10
Nlgn1	neuroligin 1	6.1439	1.82E-10
H2bu2	H2B.U histone 2	2.8814	2.01E-10
Gnai1	guanine nucleotide binding protein (G protein), alpha inhibiting 1	2.6886	2.07E-10
Grin3a	glutamate receptor ionotropic, NMDA3A	3.4125	2.10E-10
Tro	trophinin	8.2287	2.33E-10
Tnik	TRAF2 and NCK interacting kinase	2.9275	2.61E-10
Lrrc4c	leucine rich repeat containing 4C	7.1173	2.62E-10
Cep170b	centrosomal protein 170B	3.5291	2.73E-10

Grp	gastrin releasing peptide	9.3487	2.88E-10
Fbxw7	F-box and WD-40 domain protein 7	1.0932	2.94E-10
Tenm4	teneurin transmembrane protein 4	4.2145	3.03E-10
Disp2	dispatched RND tramsporter family member 2	4.8563	3.07E-10
Prkcz	protein kinase C, zeta	1.8578	3.11E-10
1700086L19Rik	RIKEN cDNA 1700086L19 gene	8.0575	3.13E-10
Rbfox1	RNA binding protein, fox-1 homolog (C. elegans) 1	1.2799	3.13E-10
Tmeff2	transmembrane protein with EGF-like and two follistatin-like domains 2	2.692	3.15E-10
Kifap3	kinesin-associated protein 3	1.0194	3.25E-10
Rtl8c	retrotransposon Gag like 8C	1.137	3.28E-10
D430019H16Rik	RIKEN cDNA D430019H16 gene	9.2227	3.57E-10
Arnt2	aryl hydrocarbon receptor nuclear translocator 2	3.3639	3.86E-10
Gm9866	predicted gene 9866	6.2471	4.19E-10
Ryr2	ryanodine receptor 2, cardiac	4.711	4.19E-10
B230334C09Rik	RIKEN cDNA B230334C09 gene	9.2485	4.25E-10
Pcdh7	protocadherin 7	7.0825	4.28E-10
Clstn3	calsyntenin 3	8.0278	4.35E-10
Psd3	pleckstrin and Sec7 domain containing 3	1.7993	4.37E-10
Tafa5	TAFA chemokine like family member 5	3.8787	4.47E-10
Kcnd2	potassium voltage-gated channel, Shal-related family, member 2	9.4493	4.72E-10
Fezf2	Fez family zinc finger 2	5.0822	4.82E-10
Lrrc4b	leucine rich repeat containing 4B	9.2567	5.06E-10
Hcn1	hyperpolarization activated cyclic nucleotide gated potassium channel 1	5.0449	5.36E-10
Dlgap3	DLG associated protein 3	6.9737	5.39E-10
Cyb561	cytochrome b-561	6.1156	5.91E-10
Ngb	neuroglobin	5.452	6.76E-10
Kctd17	potassium channel tetramerisation domain containing 17	2.9621	6.87E-10
Ppp1r1b	protein phosphatase 1, regulatory inhibitor subunit 1B	2.6399	6.97E-10
Adgrl1	adhesion G protein-coupled receptor L1	1.7043	7.62E-10
Srrm3	serine/arginine repetitive matrix 3	3.8072	7.71E-10
Syt17	synaptotagmin XVII	3.854	7.80E-10
Ttll7	tubulin tyrosine ligase-like family, member 7	3.0933	8.01E-10
Clmn	calmin	4.4614	8.07E-10
Syt16	synaptotagmin XVI	5.1243	8.07E-10

Ccl27a	chemokine (C-C motif) ligand 27A	2.3701	9.62E-10
Cnnm1	cyclin M1	9.0054	9.77E-10
Gabra5	gamma-aminobutyric acid (GABA) A receptor, subunit alpha 5	4.0116	9.95E-10
Dbpht2	DNA binding protein with his-thr domain	7.8995	1.05E-09
Lrp11	low density lipoprotein receptor-related protein 11	2.1304	1.06E-09
Lrrtm1	leucine rich repeat transmembrane neuronal 1	5.5675	1.14E-09
Kcnq2	potassium voltage-gated channel, subfamily Q, member 2	7.7813	1.26E-09
Bdnf	brain derived neurotrophic factor	4.1883	1.26E-09
Tgfb2	transforming growth factor, beta 2	4.269	1.38E-09
Glrb	glycine receptor, beta subunit	3.5945	1.50E-09
Plppr4	phospholipid phosphatase related 4	1.5608	1.66E-09
Ajap1	adherens junction associated protein 1	7.7966	1.67E-09
Sema5a	sema domain, seven thrombospondin repeats (type 1 and type 1-like), transmembrane domain (TM) and short cytoplasmic domain, (semaphorin) 5A	4.8359	1.70E-09
Ptpru	protein tyrosine phosphatase, receptor type, U	5.1354	1.84E-09
Rapgef4	Rap guanine nucleotide exchange factor (GEF) 4	2.5698	2.02E-09
D430041D05Rik	RIKEN cDNA D430041D05 gene	8.9651	2.10E-09
Gabra3	gamma-aminobutyric acid (GABA) A receptor, subunit alpha 3	8.8806	2.42E-09
Sorbs2	sorbin and SH3 domain containing 2	3.7878	2.49E-09
1500009L16Rik	RIKEN cDNA 1500009L16 gene	6.7562	2.66E-09
Chd3	chromodomain helicase DNA binding protein 3	1.1628	2.72E-09
Sh3gl3	SH3-domain GRB2-like 3	3.2751	2.89E-09
Lrrtm3	leucine rich repeat transmembrane neuronal 3	9.0428	2.95E-09
Nmnat2	nicotinamide nucleotide adenylyltransferase 2	6.8259	3.04E-09
Pcdh19	protocadherin 19	7.629	3.26E-09
Mmd	monocyte to macrophage differentiation-associated	1.1473	3.50E-09
Nova2	NOVA alternative splicing regulator 2	3.3988	3.80E-09
Syt7	synaptotagmin VII	7.6672	3.84E-09
Gpr27	G protein-coupled receptor 27	3.5717	4.02E-09
Celf5	CUGBP, Elav-like family member 5	4.5581	4.02E-09
Fam241b	family with sequence similarity 241, member B	2.9677	4.25E-09
Syt13	synaptotagmin XIII	6.7991	4.35E-09
Add2	adducin 2 (beta)	3.8452	4.35E-09
Lgi1	leucine-rich repeat LGI family, member 1	3.9187	4.52E-09
Pitpnm3	PITPNM family member 3	8.9286	4.73E-09

Afdn	afadin, adherens junction formation factor	1.9343	4.96E-09
Bex4	brain expressed X-linked 4	7.5757	5.03E-09
Cntnap5a	contactin associated protein-like 5A	8.7877	5.60E-09
1700001L19Rik	RIKEN cDNA 1700001L19 gene	6.8348	5.75E-09
Kcnf1	potassium voltage-gated channel, subfamily F, member 1	7.6362	6.47E-09
Tpd52l1	tumor protein D52-like 1	4.0031	7.24E-09
B230217C12Rik	RIKEN cDNA B230217C12 gene	2.5345	7.80E-09
Gpr85	G protein-coupled receptor 85	4.5762	8.12E-09
Palm	paralemmin	1.8418	8.66E-09
Chga	chromogranin A	8.7689	9.23E-09
Atcay	ataxia, cerebellar, Cayman type	5.9746	9.71E-09
Nfib	nuclear factor I/B	2.6807	9.74E-09
Myo5a	myosin VA	1.1857	1.00E-08
Synpr	synaptoporin	4.7961	1.01E-08
Rragd	Ras-related GTP binding D	1.8412	1.01E-08
Enc1	ectodermal-neural cortex 1	1.135	1.02E-08
Flrt3	fibronectin leucine rich transmembrane protein 3	8.725	1.02E-08
Efnb3	ephrin B3	3.706	1.03E-08
Myo5b	myosin VB	4.1314	1.08E-08
Adgrb1	adhesion G protein-coupled receptor B1	7.5012	1.09E-08
Nkain3	Na+/K+ transporting ATPase interacting 3	8.897	1.11E-08
Cadps2	Ca2+-dependent activator protein for secretion 2	5.611	1.25E-08
Tmem178b	transmembrane protein 178B	6.5609	1.26E-08
Cnr1	cannabinoid receptor 1 (brain)	8.7637	1.26E-08
Sobp	sine oculis binding protein	6.4952	1.28E-08
Pbx4	pre B cell leukemia homeobox 4	2.6371	1.41E-08
Rnf112	ring finger protein 112	3.3689	1.46E-08
Ggt7	gamma-glutamyltransferase 7	5.2483	1.48E-08
Zfp428	zinc finger protein 428	1.8559	1.49E-08
Gsta4	glutathione S-transferase, alpha 4	2.1598	1.55E-08
Pnma2	paraneoplastic antigen MA2	1.7755	1.66E-08
Gm42517	predicted gene 42517	4.9951	1.69E-08
Acta1	actin, alpha 1, skeletal muscle	6.4921	1.71E-08
Cartpt	CART prepropeptide	8.5908	1.83E-08

Slit1	slit guidance ligand 1	4.0616	1.88E-08
Stox2	storkhead box 2	2.9282	2.00E-08
Cdh22	cadherin 22	8.5729	2.02E-08
Fzd3	frizzled class receptor 3	6.5806	2.03E-08
Arhgef9	CDC42 guanine nucleotide exchange factor (GEF) 9	1.8067	2.10E-08
Gas7	growth arrest specific 7	2.406	2.13E-08
Baiap2	brain-specific angiogenesis inhibitor 1-associated protein 2	1.1779	2.15E-08
Ccdc74a	coiled-coil domain containing 74A	7.3274	2.15E-08
Tmem198	transmembrane protein 198	5.6832	2.18E-08
Creg2	cellular repressor of E1A-stimulated genes 2	2.8394	2.37E-08
Wipf3	WAS/WASL interacting protein family, member 3	3.3753	2.41E-08
Gm42372	predicted gene, 42372	2.5349	2.42E-08
Scn2b	sodium channel, voltage-gated, type II, beta	6.4279	2.70E-08
Morn4	MORN repeat containing 4	2.7282	2.86E-08
Ptprf	protein tyrosine phosphatase, receptor type, F	4.7584	2.92E-08
Cdh13	cadherin 13	3.9051	3.05E-08
Sptbn2	spectrin beta, non-erythrocytic 2	3.0251	3.15E-08
Smim18	small integral membrane protein 18	4.7976	3.26E-08
Ap3b2	adaptor-related protein complex 3, beta 2 subunit	3.2952	3.27E-08
Kcnv1	potassium channel, subfamily V, member 1	8.4251	3.48E-08
Stum	mechanosensory transduction mediator	7.3333	3.67E-08
Elfn2	leucine rich repeat and fibronectin type III, extracellular 2	8.4358	3.77E-08
Tub	tubby bipartite transcription factor	5.6927	3.80E-08
Samd14	sterile alpha motif domain containing 14	4.3787	3.80E-08
Kcnc1	potassium voltage gated channel, Shaw-related subfamily, member 1	8.7023	3.80E-08
Mgst3	microsomal glutathione S-transferase 3	1.0997	5.04E-08
Ptprz1	protein tyrosine phosphatase, receptor type Z, polypeptide 1	4.5787	5.06E-08
Hapln4	hyaluronan and proteoglycan link protein 4	7.2159	5.13E-08
Rtn4rl2	reticulon 4 receptor-like 2	8.4582	5.41E-08
Slc1a1	solute carrier family 1 (neuronal/epithelial high affinity glutamate transporter, system Xag), member 1	3.478	5.41E-08
Slc6a17	solute carrier family 6 (neurotransmitter transporter), member 17	7.1173	5.74E-08
Adora1	adenosine A1 receptor	2.1254	6.08E-08
Brinp2	bone morphogenic protein/retinoic acid inducible neural-specific 2	8.209	6.12E-08
Bicd1	BICD cargo adaptor 1	5.6601	6.56E-08

Arhgap20	Rho GTPase activating protein 20	4.0005	6.64E-08
Kcnh3	potassium voltage-gated channel, subfamily H (eag-related), member 3	4.2814	6.86E-08
Epb41l1	erythrocyte membrane protein band 4.1 like 1	2.5615	7.20E-08
Galnt9	polypeptide N-acetylgalactosaminyltransferase 9	3.682	7.43E-08
Dpp6	dipeptidylpeptidase 6	7.0929	7.45E-08
Ntrk2	neurotrophic tyrosine kinase, receptor, type 2	2.6773	7.67E-08
Serpini1	serine (or cysteine) peptidase inhibitor, clade I, member 1	2.6072	8.07E-08
Myh7	myosin, heavy polypeptide 7, cardiac muscle, beta	8.2479	1.00E-07
Bcl2a1a	B cell leukemia/lymphoma 2 related protein A1a	-1.1362	1.01E-07
Jsrp1	junctional sarcoplasmic reticulum protein 1	5.4462	1.03E-07
Cdh8	cadherin 8	8.1754	1.11E-07
Mgat3	mannoside acetylglucosaminyltransferase 3	5.299	1.11E-07
Kcnd3	potassium voltage-gated channel, Shal-related family, member 3	4.7402	1.11E-07
Cobl	cordon-bleu WH2 repeat	4.9404	1.18E-07
Cox8a	cytochrome c oxidase subunit 8A	1.0231	1.25E-07
Map6	microtubule-associated protein 6	4.185	1.30E-07
Scg3	secretogranin III	2.4496	1.30E-07
Zfp575	zinc finger protein 575	8.3885	1.30E-07
Nap1l3	nucleosome assembly protein 1-like 3	8.3	1.38E-07
Scn3a	sodium channel, voltage-gated, type III, alpha	4.1418	1.52E-07
Kcnip4	Kv channel interacting protein 4	3.3743	1.64E-07
Dpp10	dipeptidylpeptidase 10	7.0126	1.66E-07
Gpr26	G protein-coupled receptor 26	8.1199	1.76E-07
Npy	neuropeptide Y	8.1655	1.76E-07
Fam110b	family with sequence similarity 110, member B	2.6114	1.78E-07
Unc119	unc-119 lipid binding chaperone	2.4478	1.81E-07
Timm8b	translocase of inner mitochondrial membrane 8B	1.2695	1.89E-07
Rragb	Ras-related GTP binding B	3.0366	2.05E-07
Thrb	thyroid hormone receptor beta	3.4419	2.06E-07
Fndc4	fibronectin type III domain containing 4	1.4607	2.08E-07
Sgip1	SH3-domain GRB2-like (endophilin) interacting protein 1	1.8841	2.10E-07
Vxn	vexin	2.7534	2.10E-07
Kcnj3	potassium inwardly-rectifying channel, subfamily J, member 3	5.6751	2.11E-07
Omg	oligodendrocyte myelin glycoprotein	3.2328	2.18E-07

Dnm3	dynamin 3	2.4685	2.18E-07
St8sia5	ST8 alpha-N-acetyl-neuraminide alpha-2,8-sialyltransferase 5	7.9196	2.28E-07
Cacna1e	calcium channel, voltage-dependent, R type, alpha 1E subunit	2.9832	2.33E-07
Tram1l1	translocation associated membrane protein 1-like 1	5.4134	2.43E-07
Sorcs3	sortilin-related VPS10 domain containing receptor 3	8.3419	2.44E-07
Psd	pleckstrin and Sec7 domain containing	1.2964	2.51E-07
Arhgef17	Rho guanine nucleotide exchange factor (GEF) 17	5.0086	2.53E-07
Nlgn3	neuroligin 3	4.475	2.55E-07
Uqcr11	ubiquinol-cytochrome c reductase, complex III subunit XI	1.3413	2.55E-07
Ccdc85a	coiled-coil domain containing 85A	5.3522	2.57E-07
Plxna2	plexin A2	6.8276	2.62E-07
Grin1	glutamate receptor, ionotropic, NMDA1 (zeta 1)	5.4028	2.63E-07
Nexmif	neurite extension and migration factor	8.1976	2.65E-07
Cgref1	cell growth regulator with EF hand domain 1	2.5795	2.69E-07
Il34	interleukin 34	6.1366	2.79E-07
Cox5b	cytochrome c oxidase subunit 5B	1.0205	2.79E-07
Gucy1a1	guanylate cyclase 1, soluble, alpha 1	4.4941	2.84E-07
Tmem132b	transmembrane protein 132B	6.8445	2.85E-07
6330403K07Rik	RIKEN cDNA 6330403K07 gene	3.7677	3.09E-07
Paqr9	progestin and adipoQ receptor family member IX	4.2644	3.14E-07
Rasl10a	RAS-like, family 10, member A	3.3919	3.26E-07
Ddx25	DEAD box helicase 25	3.5696	3.31E-07
Ckmt1	creatine kinase, mitochondrial 1, ubiquitous	2.5892	3.31E-07
Zcchc12	zinc finger, CCHC domain containing 12	4.8088	3.50E-07
Cnih3	cornichon family AMPA receptor auxiliary protein 3	5.7828	3.78E-07
Golga7b	golgi autoantigen, golgin subfamily a, 7B	6.8305	3.84E-07
Hecw1	HECT, C2 and WW domain containing E3 ubiquitin protein ligase 1	4.3952	3.86E-07
Grm2	glutamate receptor, metabotropic 2	8.1686	3.89E-07
Cacna1b	calcium channel, voltage-dependent, N type, alpha 1B subunit	8.121	3.94E-07
Ntng1	netrin G1	8.038	4.21E-07
Dpf1	D4, zinc and double PHD fingers family 1	2.8658	4.57E-07
Cttn	cortactin	2.6136	4.62E-07
Cox7a2	cytochrome c oxidase subunit 7A2	1.2496	4.63E-07
Jakmip2	janus kinase and microtubule interacting protein 2	3.3465	4.64E-07

Unc13c	unc-13 homolog C	3.3112	4.68E-07
Gprin1	G protein-regulated inducer of neurite outgrowth 1	3.0078	4.97E-07
Dlg2	discs large MAGUK scaffold protein 2	6.7228	4.99E-07
Fbxo41	F-box protein 41	6.9102	5.18E-07
Cdkl2	cyclin-dependent kinase-like 2 (CDC2-related kinase)	4.1774	5.47E-07
Actr3b	ARP3 actin-related protein 3B	3.6069	5.55E-07
Gm34466	predicted gene, 34466	3.9614	5.74E-07
Minar2	membrane integral NOTCH2 associated receptor 2	3.7377	5.89E-07
Emd	emerin	1.0805	5.98E-07
Cdh4	cadherin 4	3.6173	6.03E-07
Ar	androgen receptor	7.7881	6.20E-07
Slit3	slit guidance ligand 3	6.7731	6.21E-07
Bhlhe40	basic helix-loop-helix family, member e40	2.1317	6.50E-07
Lrrn3	leucine rich repeat protein 3, neuronal	5.2745	6.52E-07
B3galt2	UDP-Gal:betaGlcNAc beta 1,3-galactosyltransferase, polypeptide 2	4.4617	6.68E-07
Dusp14	dual specificity phosphatase 14	3.5696	6.81E-07
Mas1	MAS1 oncogene	4.9379	6.88E-07
Grm7	glutamate receptor, metabotropic 7	8.0496	7.20E-07
Vstm2a	V-set and transmembrane domain containing 2A	3.7797	7.84E-07
Camk1g	calcium/calmodulin-dependent protein kinase I gamma	5.1925	7.88E-07
Cdh7	cadherin 7, type 2	7.8928	7.88E-07
Scrn1	secernin 1	3.202	8.13E-07
Ralyl	RALY RNA binding protein-like	3.5533	8.49E-07
Fmn2	formin 2	7.998	8.62E-07
Pmm1	phosphomannomutase 1	1.0107	8.74E-07
Stk32c	serine/threonine kinase 32C	8.1337	9.31E-07
Dok6	docking protein 6	5.7997	9.41E-07
Lamp5	lysosomal-associated membrane protein family, member 5	8.0888	9.62E-07
Kcnb1	potassium voltage gated channel, Shab-related subfamily, member 1	2.5114	9.64E-07
Syndig1	synapse differentiation inducing 1	4.4048	1.00E-06
Slitrk5	SLIT and NTRK-like family, member 5	5.8467	1.00E-06
C1ql3	C1q-like 3	5.095	1.01E-06
Hs6st2	heparan sulfate 6-O-sulfotransferase 2	7.9129	1.04E-06
Srrm4	serine/arginine repetitive matrix 4	4.7863	1.05E-06

Kcna6	potassium voltage-gated channel, shaker-related, subfamily, member 6	5.8586	1.14E-06
Gm1673	predicted gene 1673	3.4549	1.16E-06
Hdgfl3	HDGF like 3	1.5026	1.20E-06
Gpr135	G protein-coupled receptor 135	7.7484	1.21E-06
Kcnj9	potassium inwardly-rectifying channel, subfamily J, member 9	1.7127	1.23E-06
Armcx1	armadillo repeat containing, X-linked 1	3.2347	1.29E-06
B4galnt4	beta-1,4-N-acetyl-galactosaminyl transferase 4	5.9424	1.29E-06
Hrk	harakiri, BCL2 interacting protein (contains only BH3 domain)	6.546	1.38E-06
Pcdh20	protocadherin 20	7.7333	1.39E-06
Grm1	glutamate receptor, metabotropic 1	7.8473	1.42E-06
4933416I08Rik	RIKEN cDNA 4933416I08 gene	1.4178	1.44E-06
Kcnip2	Kv channel-interacting protein 2	2.7876	1.61E-06
Nrxn2	neurexin II	4.1874	1.81E-06
Tmeff1	transmembrane protein with EGF-like and two follistatin-like domains 1	2.7644	1.85E-06
Tenm1	teneurin transmembrane protein 1	4.8345	1.87E-06
Tmem151a	transmembrane protein 151A	2.8905	2.07E-06
Tyro3	TYRO3 protein tyrosine kinase 3	3.7954	2.10E-06
Sphkap	SPHK1 interactor, AKAP domain containing	4.87	2.25E-06
Lrp3	low density lipoprotein receptor-related protein 3	7.5741	2.26E-06
Srgap3	SLIT-ROBO Rho GTPase activating protein 3	1.8443	2.40E-06
Id4	inhibitor of DNA binding 4	2.5981	2.45E-06
Chd5	chromodomain helicase DNA binding protein 5	3.2464	2.48E-06
Luzp2	leucine zipper protein 2	3.5155	2.53E-06
Vldlr	very low density lipoprotein receptor	3.7341	2.55E-06
Zdbf2	zinc finger, DBF-type containing 2	5.9042	2.55E-06
Tppp3	tubulin polymerization-promoting protein family member 3	1.3576	2.56E-06
Vstm2l	V-set and transmembrane domain containing 2-like	6.4405	2.69E-06
Galnt16	polypeptide N-acetylgalactosaminyltransferase 16	1.4199	2.81E-06
Dnajb13	DnaJ heat shock protein family (Hsp40) member B13	1.1359	2.97E-06
Nalcn	sodium leak channel, non-selective	6.3377	3.04E-06
Ccdc92	coiled-coil domain containing 92	3.333	3.04E-06
Slco3a1	solute carrier organic anion transporter family, member 3a1	3.2077	3.07E-06
Msantd3	Myb/SANT-like DNA-binding domain containing 3	7.5799	3.08E-06
Apc2	APC regulator of WNT signaling pathway 2	3.2056	3.20E-06

Gm47163	predicted gene, 47163	3.7521	3.27E-06
Rab11fip4	RAB11 family interacting protein 4 (class II)	1.9113	3.41E-06
Dok5	docking protein 5	4.081	3.48E-06
Trank1	tetratricopeptide repeat and ankyrin repeat containing 1	6.3232	3.62E-06
Htr2c	5-hydroxytryptamine (serotonin) receptor 2C	6.283	3.77E-06
Unc5d	unc-5 netrin receptor D	4.1582	3.78E-06
L1cam	L1 cell adhesion molecule	4.0192	3.85E-06
Reep1	receptor accessory protein 1	2.9237	3.95E-06
Cbln4	cerebellin 4 precursor protein	6.2624	3.97E-06
Sncb	synuclein, beta	3.2088	3.97E-06
Cttnbp2	cortactin binding protein 2	2.8473	3.97E-06
Rn18s	18S ribosomal RNA Source:NCBI gene (formerly Entrezgene);Acc:19791	1.5762	4.02E-06
Igsf21	immunoglobulin superfamily, member 21	4.227	4.04E-06
Eml2	echinoderm microtubule associated protein like 2	2.6626	4.07E-06
Capsl	calcyphosine-like	7.3841	4.08E-06
Fhl2	four and a half LIM domains 2	2.6499	4.11E-06
Sox5	SRY (sex determining region Y)-box 5	4.2285	4.20E-06
Me1	malic enzyme 1, NADP(+)-dependent, cytosolic	3.2193	4.26E-06
Galnt17	polypeptide N-acetylgalactosaminyltransferase 17	4.8806	4.31E-06
Lin7a	lin-7 homolog A (C. elegans)	3.2699	4.44E-06
2900079G21Rik	RIKEN cDNA 2900079G21 gene	4.9458	4.51E-06
C1ql2	complement component 1, q subcomponent-like 2	7.7743	5.02E-06
Nell1	NEL-like 1	7.4144	5.06E-06
Fam189a1	family with sequence similarity 189, member A1	6.1816	5.26E-06
Tac1	tachykinin 1	6.4785	5.46E-06
Tbr1	T-box brain transcription factor 1	7.3331	5.61E-06
Ndufa4	Ndufa4, mitochondrial complex associated	1.0725	5.63E-06
Fam135b	family with sequence similarity 135, member B	3.1306	5.87E-06
Cdh9	cadherin 9	7.4122	5.96E-06
Lrp1b	low density lipoprotein-related protein 1B	5.025	6.03E-06
Slc6a15	solute carrier family 6 (neurotransmitter transporter), member 15	3.8802	6.39E-06
Lpcat4	lysophosphatidylcholine acyltransferase 4	1.7988	6.42E-06
Pcdh8	protocadherin 8	4.9615	6.61E-06
Sema4f	sema domain, immunoglobulin domain (Ig), TM domain, and short cytoplasmic domain	7.2417	6.69E-06

Nkain4	Na+/K+ transporting ATPase interacting 4	4.4166	6.69E-06
D430036J16Rik	RIKEN cDNA D430036J16 gene	7.4019	6.84E-06
Il1rapl1	interleukin 1 receptor accessory protein-like 1	7.4167	6.90E-06
Fam163b	family with sequence similarity 163, member B	3.3348	6.90E-06
Fut9	fucosyltransferase 9	7.3893	6.99E-06
Sidt1	SID1 transmembrane family, member 1	3.449	7.02E-06
Osbpl6	oxysterol binding protein-like 6	3.1349	7.03E-06
Gpr158	G protein-coupled receptor 158	6.1072	7.07E-06
Ncan	neurocan	3.9647	7.47E-06
Cox6c	cytochrome c oxidase subunit 6C	1.1244	7.83E-06
Cdh15	cadherin 15	7.5167	7.94E-06
Adgrl3	adhesion G protein-coupled receptor L3	3.5115	8.14E-06
Cygb	cytoglobin	5.5164	8.17E-06
Ncam2	neural cell adhesion molecule 2	3.3036	8.29E-06
Foxg1	forkhead box G1	4.7941	8.39E-06
Fez1	fasciculation and elongation protein zeta 1 (zygin I)	1.9098	8.39E-06
Ccdc3	coiled-coil domain containing 3	4.4477	9.09E-06
Ackr1	atypical chemokine receptor 1 (Duffy blood group)	7.7009	9.21E-06
Larp6	La ribonucleoprotein domain family, member 6	5.7042	9.32E-06
Gm10699	predicted gene 10699	5.3442	9.32E-06
Ptger3	prostaglandin E receptor 3 (subtype EP3)	-1.3701	9.41E-06
AI593442	expressed sequence AI593442	5.5409	9.61E-06
Trpc7	transient receptor potential cation channel, subfamily C, member 7	7.2287	1.01E-05
Irak1bp1	interleukin-1 receptor-associated kinase 1 binding protein 1	1.4225	1.02E-05
Stxbp6	syntaxin binding protein 6 (amisyn)	2.9357	1.06E-05
Gm19531	predicted gene, 19531	4.8101	1.07E-05
Armcx4	armadillo repeat containing, X-linked 4	7.4075	1.08E-05
Cdh2	cadherin 2	4.3106	1.09E-05
Tspan6	tetraspanin 6	4.4467	1.09E-05
Rab40b	Rab40B, member RAS oncogene family	2.9653	1.11E-05
Rph3a	rabphilin 3A	3.3101	1.19E-05
Hook1	hook microtubule tethering protein 1	3.8203	1.19E-05
Wnt4	wingless-type MMTV integration site family, member 4	2.6359	1.19E-05
Adgrb3	adhesion G protein-coupled receptor B3	2.8973	1.23E-05

Csrnp3	cysteine-serine-rich nuclear protein 3	3.2487	1.26E-05
Ndn	necdin, MAGE family member	4.6021	1.27E-05
Mchr1	melanin-concentrating hormone receptor 1	7.3146	1.32E-05
Galnt18	polypeptide N-acetylgalactosaminyltransferase 18	7.1879	1.34E-05
Fam124a	family with sequence similarity 124, member A	7.458	1.35E-05
Gpm6b	glycoprotein m6b	1.3213	1.36E-05
Lyl1	lymphoblastomic leukemia 1	-1.1089	1.40E-05
Arhgap44	Rho GTPase activating protein 44	3.5366	1.40E-05
1700003E16Rik	RIKEN cDNA 1700003E16 gene	3.6867	1.45E-05
Iqsec3	IQ motif and Sec7 domain 3	3.8329	1.48E-05
Trim46	tripartite motif-containing 46	4.1431	1.61E-05
Spon1	spondin 1, (f-spondin) extracellular matrix protein	1.9647	1.69E-05
Dlgap2	DLG associated protein 2	3.8747	1.70E-05
Pak5	p21 (RAC1) activated kinase 5	2.8562	1.79E-05
Trpc5	transient receptor potential cation channel, subfamily C, member 5	7.0418	1.80E-05
Unc5c	unc-5 netrin receptor C	4.1185	1.86E-05
Pcbp4	poly(rC) binding protein 4	1.6982	1.87E-05
Atp1b2	ATPase, Na+/K+ transporting, beta 2 polypeptide	2.8931	1.90E-05
Gfod1	glucose-fructose oxidoreductase domain containing 1	5.2544	2.01E-05
Epha7	Eph receptor A7	4.1897	2.02E-05
Unc5a	unc-5 netrin receptor A	2.0111	2.06E-05
Shisal1	shisa like 1	4.286	2.11E-05
Scn3b	sodium channel, voltage-gated, type III, beta	3.6539	2.11E-05
Csdc2	cold shock domain containing C2, RNA binding	2.3069	2.14E-05
Cyp26b1	cytochrome P450, family 26, subfamily b, polypeptide 1	6.0161	2.17E-05
Adam22	a disintegrin and metallopeptidase domain 22	1.6107	2.26E-05
Gabrg3	gamma-aminobutyric acid (GABA) A receptor, subunit gamma 3	7.0523	2.27E-05
Lrfn5	leucine rich repeat and fibronectin type III domain containing 5	3.2947	2.27E-05
Abcg4	ATP binding cassette subfamily G member 4	5.3922	2.28E-05
Kazn	kazrin, periplakin interacting protein	3.1458	2.57E-05
Slc17a6	solute carrier family 17 (sodium-dependent inorganic phosphate cotransporter), member 6	7.1187	2.57E-05
Tmem158	transmembrane protein 158	1.7625	2.57E-05
Grik2	glutamate receptor, ionotropic, kainate 2 (beta 2)	5.8929	2.59E-05
Crtac1	cartilage acidic protein 1	3.5763	2.62E-05

St6gal2	beta galactoside alpha 2,6 sialyltransferase 2	7.0123	2.67E-05
S100a10	S100 calcium binding protein A10 (calpactin)	1.3709	2.78E-05
B4galt2	UDP-Gal:betaGlcNAc beta 1,4- galactosyltransferase, polypeptide 2	2.6266	2.80E-05
Mir124-2hg	Mir124-2 host gene (non-protein coding)	4.3614	2.82E-05
Rspo2	R-spondin 2	7.0927	2.90E-05
Smarca1	SWI/SNF related, matrix associated, actin dependent regulator of chromatin, subfamily a, member 1	6.9677	2.91E-05
Cracdl	capping protein inhibiting regulator of actin like	1.9035	2.93E-05
Slitrk4	SLIT and NTRK-like family, member 4	4.469	3.11E-05
Asphd1	aspartate beta-hydroxylase domain containing 1	5.8708	3.16E-05
Trnp1	TMF1-regulated nuclear protein 1	3.394	3.16E-05
Dzank1	double zinc ribbon and ankyrin repeat domains 1	1.9162	3.47E-05
Atp5md	ATP synthase membrane subunit DAPIT	1.2501	3.55E-05
Kcna1	potassium voltage-gated channel, shaker-related subfamily, member 1	3.3995	3.75E-05
Zfp612	zinc finger protein 612	2.2926	3.80E-05
Inka2	inka box actin regulator 2	2.0059	3.85E-05
Kcnh7	potassium voltage-gated channel, subfamily H (eag-related), member 7	3.8959	3.92E-05
Galnt14	polypeptide N-acetylgalactosaminyltransferase 14	4.0976	4.02E-05
Nlgn2	neuroligin 2	2.01	4.19E-05
Tmem255a	transmembrane protein 255A	3.8987	4.36E-05
Ube2e2	ubiquitin-conjugating enzyme E2E 2	1.5119	4.78E-05
Ptprt	protein tyrosine phosphatase, receptor type, T	5.8033	4.83E-05
Adra2c	adrenergic receptor, alpha 2c	7.0256	4.96E-05
Rnd2	Rho family GTPase 2	1.3979	5.09E-05
Aldh3b2	aldehyde dehydrogenase 3 family, member B2	7.3558	5.30E-05
Cacna1i	calcium channel, voltage-dependent, alpha 1I subunit	7.1428	5.66E-05
Pcp4	Purkinje cell protein 4	1.9985	5.71E-05
Gpr88	G-protein coupled receptor 88	6.884	5.82E-05
Shisa9	shisa family member 9	5.1644	5.94E-05
A230051N06Rik	RIKEN cDNA A230051N06 gene	6.9722	5.98E-05
Matn2	matrilin 2	2.3823	6.11E-05
Gm15631	predicted gene 15631	5.1494	6.16E-05
Sstr2	somatostatin receptor 2	4.4679	6.23E-05
Camk4	calcium/calmodulin-dependent protein kinase IV	5.2585	6.27E-05
Fign	fidgetin	6.7977	6.29E-05

Pbx1	pre B cell leukemia homeobox 1	1.2202	6.30E-05
Edil3	EGF-like repeats and discoidin I-like domains 3	2.4234	6.44E-05
Krt1	keratin 1	3.3936	6.63E-05
Wnt7b	wingless-type MMTV integration site family, member 7B	7.0456	6.75E-05
Tmem28	transmembrane protein 28	6.9387	6.81E-05
Hey1	hairy/enhancer-of-split related with YRPW motif 1	2.2603	6.94E-05
Dnah7a	dynein, axonemal, heavy chain 7A	3.563	7.02E-05
Meis2	Meis homeobox 2	2.5301	7.02E-05
Oprl1	opioid receptor-like 1	5.8137	7.03E-05
Ptprr	protein tyrosine phosphatase, receptor type, R	5.1811	7.26E-05
Samd12	sterile alpha motif domain containing 12	3.5035	7.29E-05
Shroom2	shroom family member 2	3.5654	7.59E-05
9330159F19Rik	RIKEN cDNA 9330159F19 gene	3.7235	7.59E-05
Adam11	a disintegrin and metallopeptidase domain 11	4.0514	7.92E-05
Wfs1	wolframin ER transmembrane glycoprotein	1.0378	8.10E-05
Pcsk1	proprotein convertase subtilisin/kexin type 1	7.0927	8.33E-05
Ankrd45	ankyrin repeat domain 45	4.1419	8.44E-05
Dtx1	deltex 1, E3 ubiquitin ligase	2.9226	8.72E-05
Krt12	keratin 12	6.7299	8.96E-05
AI115009	expressed sequence AI115009	6.7947	9.04E-05
Gstm6	glutathione S-transferase, mu 6	2.9879	9.07E-05
Adcy2	adenylate cyclase 2	2.7264	9.25E-05
Prcd	photoreceptor disc component	5.2971	9.50E-05
Prmt8	protein arginine N-methyltransferase 8	5.5559	9.67E-05
Mageh1	MAGE family member H1	1.8185	9.68E-05
Nos1	nitric oxide synthase 1, neuronal	2.9258	9.68E-05
Robo2	roundabout guidance receptor 2	4.9977	0.0001 0257
Sybu	syntabulin (syntaxin-interacting)	2.2986	0.0001 0269
C030017B01Rik	RIKEN cDNA C030017B01 gene	4.4884	0.0001 0376
Syngr3	synaptogyrin 3	3.6424	0.0001 0418
Cckbr	cholecystokinin B receptor	5.6458	0.0001 0438
Mark1	MAP/microtubule affinity regulating kinase 1	4.7542	0.0001 0569
Lingo2	leucine rich repeat and Ig domain containing 2	3.007	0.0001 0839
Synpo	synaptopodin	2.2175	0.0001 0951

Sertm1	serine rich and transmembrane domain containing 1	5.1987	0.0001 1279
Nrg3	neuregulin 3	5.7202	0.0001 1678
Cacng2	calcium channel, voltage-dependent, gamma subunit 2	4.3196	0.0001 1711
Rasgef1c	RasGEF domain family, member 1C	6.8896	0.0001 1778
Ramp2	receptor (calcitonin) activity modifying protein 2	1.3067	0.0001 235
Ccdc148	coiled-coil domain containing 148	3.1484	0.0001 2676
Prkar2b	protein kinase, cAMP dependent regulatory, type II beta	3.1271	0.0001 2676
Asic2	acid-sensing (proton-gated) ion channel 2	2.6847	0.0001 2761
Nt5dc3	5'-nucleotidase domain containing 3	1.5741	0.0001 2835
Ndufa5	NADH:ubiquinone oxidoreductase subunit A5	1.0927	0.0001 2965
Nudt11	nudix (nucleoside diphosphate linked moiety X)-type motif 11	5.6186	0.0001 387
Bok	BCL2-related ovarian killer	2.2916	0.0001 3997
Marchf4	membrane associated ring-CH-type finger 4	6.8246	0.0001 4019
Cdo1	cysteine dioxygenase 1, cytosolic	2.3365	0.0001 4314
Thsd7a	thrombospondin, type I, domain containing 7A	6.3207	0.0001 4829
Sdc2	syndecan 2	3.235	0.0001 4972
Ccdc136	coiled-coil domain containing 136	3.1843	0.0001 5344
Tnr	tenascin R	3.4418	0.0001 5568
Mpp2	membrane protein, palmitoylated 2 (MAGUK p55 subfamily member 2)	2.6877	0.0001 5922
Tnfaip8l3	tumor necrosis factor, alpha-induced protein 8-like 3	5.5529	0.0001 6759
Tafa2	TAFA chemokine like family member 2	4.7808	0.0001 7065
Prdm8	PR domain containing 8	3.7942	0.0001 7117
Efcab1	EF-hand calcium binding domain 1	3.8659	0.0001 7274
Gm10558	predicted gene 10558	3.6211	0.0001 7482
Pde10a	phosphodiesterase 10A	2.2164	0.0001 7755
Wasf3	WASP family, member 3	6.6609	0.0001 7961
Zfp941	zinc finger protein 941	3.6627	0.0001 8072
Nfasc	neurofascin	2.1645	0.0001 8437
Dab1	disabled 1	2.2874	0.0001 8506
Dcc	deleted in colorectal carcinoma	4.4962	0.0001 9296
Ano4	anoctamin 4	6.6308	0.0001 9594
Magi2	membrane associated guanylate kinase, WW and PDZ domain containing 2	2.4529	0.0001 9594
Tmem121	transmembrane protein 121	4.185	0.0002 0216
Gm45441	predicted gene 45441	6.56	0.0002 0359

3300002P13Rik	RIKEN cDNA 3300002P13 gene	5.4453	0.0002044
1500009C09Rik	RIKEN cDNA 1500009C09 gene	4.1303	0.0002056
Mturn	maturin, neural progenitor differentiation regulator homolog (Xenopus)	1.6549	0.0002072
A330076H08Rik	RIKEN cDNA A330076H08 gene	6.7236	0.0002113
Klf5	Kruppel-like factor 5	5.3874	0.0002117
Max	Max protein	1.1702	0.0002117
Tspyl5	testis-specific protein, Y-encoded-like 5	2.7123	0.0002127
Arhgap33	Rho GTPase activating protein 33	2.0297	0.0002132
Rab39b	RAB39B, member RAS oncogene family	3.1328	0.0002192
Snph	syntaphilin	1.3086	0.0002205
Arhgap6	Rho GTPase activating protein 6	3.5408	0.0002217
Plch2	phospholipase C, eta 2	4.3859	0.0002224
Nap1l2	nucleosome assembly protein 1-like 2	2.5016	0.0002287
Lor	loricrin	3.7019	0.0002287
Hipk4	homeodomain interacting protein kinase 4	3.389	0.0002288
Tnk2	tyrosine kinase, non-receptor, 2	2.4625	0.0002302
Drp2	dystrophin related protein 2	3.1805	0.0002325
C130026L21Rik	RIKEN cDNA C130026L21 gene	6.5164	0.0002325
Rtn2	reticulon 2 (Z-band associated protein)	1.8958	0.0002383
Bmp3	bone morphogenetic protein 3	3.6454	0.0002392
Kbtbd11	kelch repeat and BTB (POZ) domain containing 11	2.3356	0.0002398
B230303A05Rik	RIKEN cDNA B230303A05 gene	4.1326	0.0002412
Plppr5	phospholipid phosphatase related 5	4.7943	0.0002414
Nme5	NME/NM23 family member 5	2.9009	0.0002590
Efna2	ephrin A2	5.4697	0.0002591
Adcyap1	adenylate cyclase activating polypeptide 1	6.3554	0.0002735
Ano3	anoctamin 3	2.57	0.0002746
Cpeb1	cytoplasmic polyadenylation element binding protein 1	3.2078	0.0002753
Miat	myocardial infarction associated transcript (non-protein coding)	5.2498	0.0002780
9530077C05Rik	RIKEN cDNA 9530077C05 gene	4.3503	0.0002807
Aff3	AF4/FMR2 family, member 3	3.725	0.0002882
Rasl10b	RAS-like, family 10, member B	2.4735	0.0002888
Parm1	prostate androgen-regulated mucin-like protein 1	3.0784	0.0002985
Ptprd	protein tyrosine phosphatase, receptor type, D	2.1685	0.0003112

Nyap1	neuronal tyrosine-phosphorylated phosphoinositide 3-kinase adaptor 1	3.3137	0.0003 1464
Tnfaip8l1	tumor necrosis factor, alpha-induced protein 8-like 1	2.1591	0.0003 2198
Lhx2	LIM homeobox protein 2	2.728	0.0003 259
Pde9a	phosphodiesterase 9A	5.7189	0.0003 2622
Kcnc4	potassium voltage gated channel, Shaw-related subfamily, member 4	5.2806	0.0003 3263
Kcnh1	potassium voltage-gated channel, subfamily H (eag-related), member 1	6.7419	0.0003 3573
Pgr	progesterone receptor	4.3209	0.0003 47
Mpped1	metallophosphoesterase domain containing 1	3.3266	0.0003 5528
Mdga2	MAM domain containing glycosylphosphatidylinositol anchor 2	4.1911	0.0003 5529
Slc6a7	solute carrier family 6 (neurotransmitter transporter, L-proline), member 7	6.298	0.0003 5733
Tlcd3b	TLC domain containing 3B	5.2981	0.0003 6066
Adam23	a disintegrin and metallopeptidase domain 23	2.8667	0.0003 6312
Ripply2	ripply transcriptional repressor 2	6.2894	0.0003 6399
Acvr1c	activin A receptor, type IC	3.6087	0.0003 6739
Slc2a13	solute carrier family 2 (facilitated glucose transporter), member 13	5.1043	0.0003 6783
Dmwd	dystrophia myotonica-containing WD repeat motif	1.004	0.0003 7238
Scn1a	sodium channel, voltage-gated, type I, alpha	3.704	0.0003 7272
Filip1	filamin A interacting protein 1	3.231	0.0003 7729
Begain	brain-enriched guanylate kinase-associated	2.526	0.0003 8691
Cpne5	copine V	3.7781	0.0003 9317
Ndufc1	NADH:ubiquinone oxidoreductase subunit C1	1.0699	0.0003 9366
Celf6	CUGBP, Elav-like family member 6	2.5368	0.0003 98
Cadm3	cell adhesion molecule 3	4.5883	0.0004 0018
Atp1a2	ATPase, Na+/K+ transporting, alpha 2 polypeptide	1.4039	0.0004 0229
Tmem178	transmembrane protein 178	2.2163	0.0004 2549
Fkbp1b	FK506 binding protein 1b	1.1226	0.0004 3171
Rab3b	RAB3B, member RAS oncogene family	2.5171	0.0004 3355
Gria4	glutamate receptor, ionotropic, AMPA4 (alpha 4)	5.1279	0.0004 4351
Wnk2	WNK lysine deficient protein kinase 2	2.8433	0.0004 5122
Pigz	phosphatidylinositol glycan anchor biosynthesis, class Z	-1.3557	0.0004 6431
Tmem121b	transmembrane protein 121B	5.095	0.0004 7611
Cacna1h	calcium channel, voltage-dependent, T type, alpha 1H subunit	6.3787	0.0004 9055
Slc35f1	solute carrier family 35, member F1	4.0248	0.0004 9151
Nr4a3	nuclear receptor subfamily 4, group A, member 3	1.7366	0.0004 9338

Ptprk	protein tyrosine phosphatase, receptor type, K	2.3749	0.00049366
Sox11	SRY (sex determining region Y)-box 11	3.0621	0.00049366
Zdhhc2	zinc finger, DHHC domain containing 2	2.8998	0.00050459
Mgat4c	MGAT4 family, member C	5.1364	0.0005196
Gm20208	predicted gene, 20208	6.7989	0.00052402
Drd1	dopamine receptor D1	6.2152	0.00052455
Rmst	rhabdomyosarcoma 2 associated transcript (non-coding RNA)	5.9787	0.00053099
Mtss2	MTSS I-BAR domain containing 2	3.3081	0.00053394
Neurl1b	neuralized E3 ubiquitin protein ligase 1B	2.4379	0.00056482
Hspa12a	heat shock protein 12A	1.1039	0.00057785
Stk39	serine/threonine kinase 39	2.4356	0.00057897
Fcor	Foxo1 corepressor	6.131	0.00058353
Lrp8	low density lipoprotein receptor-related protein 8, apolipoprotein e receptor	2.1159	0.00062887
Brinp3	bone morphogenetic protein/retinoic acid inducible neural specific 3	3.2082	0.00063586
Nudt10	nudix (nucleoside diphosphate linked moiety X)-type motif 10	3.4167	0.00063674
Efna3	ephrin A3	3.7552	0.00064811
Lrrc73	leucine rich repeat containing 73	2.9551	0.00065569
Ppfia3	protein tyrosine phosphatase, receptor type, f polypeptide (PTPRF), interacting protein (liprin), alpha 3	1.8018	0.00066207
Rtn4r	reticulon 4 receptor	5.0865	0.00067595
Hs3st4	heparan sulfate (glucosamine) 3-O-sulfotransferase 4	4.052	0.00068154
Pitpnm2	phosphatidylinositol transfer protein, membrane-associated 2	3.27	0.00068626
Clip4	CAP-GLY domain containing linker protein family, member 4	2.7931	0.00068668
Arxes1	adipocyte-related X-chromosome expressed sequence 1	3.3532	0.00069728
Wdr54	WD repeat domain 54	2.3033	0.00069802
Kcns2	K+ voltage-gated channel, subfamily S, 2	6.0788	0.00070634
Dkkl1	dickkopf-like 1	3.8462	0.00070775
Atp5mpl	ATP synthase membrane subunit 6.8PL	1.0109	0.00077544
Ccdc106	coiled-coil domain containing 106	2.9483	0.00078063
Spink10	serine peptidase inhibitor, Kazal type 10	6.1701	0.00078113
Kcnn3	potassium intermediate/small conductance calcium-activated channel, subfamily N, member 3	6.1325	0.00078622
Ptpn3	protein tyrosine phosphatase, non-receptor type 3	4.8216	0.00078915
Ctnnd2	catenin (cadherin associated protein), delta 2	1.1216	0.00080766
Prkaa2	protein kinase, AMP-activated, alpha 2 catalytic subunit	3.1079	0.0008086
Rhov	ras homolog family member V	2.884	0.00087425

B230216N24Rik	RIKEN cDNA B230216N24 gene	3.0275	0.00090018
Fbxo16	F-box protein 16	6.1429	0.00090604
Slc35f4	solute carrier family 35, member F4	6.3749	0.00090604
Flywch2	FLYWCH family member 2	3.4597	0.00093818
Rsph1	radial spoke head 1 homolog (Chlamydomonas)	3.5756	0.00094257
Otof	otoferlin	4.4652	0.00095753
Necab3	N-terminal EF-hand calcium binding protein 3	2.676	0.00099746
Spock3	sparc/osteonectin, cwcv and kazal-like domains proteoglycan 3	2.7989	0.00099778
Gm26871	predicted gene, 26871	4.098	0.00101028
Lmo7	LIM domain only 7	2.4953	0.00101431
Dclk3	doublecortin-like kinase 3	4.8612	0.0010347
Gm9885	predicted gene 9885	6.4279	0.00104397
B3galt1	UDP-Gal:betaGlcNAc beta 1,3-galactosyltransferase, polypeptide 1	3.6067	0.00110677
Ppargc1a	peroxisome proliferative activated receptor, gamma, coactivator 1 alpha	2.1329	0.00113501
Slc35f3	solute carrier family 35, member F3	4.9058	0.00115215
Neurod6	neurogenic differentiation 6	1.5182	0.00116186
Kirrel3	kirre like nephrin family adhesion molecule 3	3.993	0.00119609
Pqlc3	PQ loop repeat containing	-1.3819	0.00119609
Tmem215	transmembrane protein 215	3.4236	0.00120896
Trpc1	transient receptor potential cation channel, subfamily C, member 1	3.5129	0.00121211
Lrrc3b	leucine rich repeat containing 3B	6.3662	0.00121473
Fhl1	four and a half LIM domains 1	2.1677	0.00123112
Dpysl3	dihydropyrimidinase-like 3	2.494	0.00124145
Cep126	centrosomal protein 126	5.8924	0.00126064
C130071C03Rik	RIKEN cDNA C130071C03 gene	4.6675	0.00128256
Sorcs2	sortilin-related VPS10 domain containing receptor 2	4.7842	0.00129995
Zfp971	zinc finger protein 971	1.1286	0.00130169
Cdk5r2	cyclin-dependent kinase 5, regulatory subunit 2 (p39)	3.2146	0.00131011
Xkr4	X-linked Kx blood group related 4	4.8556	0.00131011
Faah	fatty acid amide hydrolase	2.3316	0.00133558
Mmd2	monocyte to macrophage differentiation-associated 2	1.7273	0.00139217
Kcnj4	potassium inwardly-rectifying channel, subfamily J, member 4	5.9706	0.00139327
Hopx	HOP homeobox	1.7373	0.00139466
Lrrc7	leucine rich repeat containing 7	2.6095	0.00140358

Zfpm2	zinc finger protein, multitype 2	4.7347	0.0014 1113
Mcf2l	mcf.2 transforming sequence-like	3.0251	0.0014 3241
Abat	4-aminobutyrate aminotransferase	1.5382	0.0014 3241
Mlip	muscular LMNA-interacting protein	4.1942	0.0014 5997
Rbm24	RNA binding motif protein 24	4.9044	0.0014 7774
Epb41l4b	erythrocyte membrane protein band 4.1 like 4b	2.6319	0.0014 8171
Tox3	TOX high mobility group box family member 3	5.0181	0.0015 4782
Gucy1b1	guanylate cyclase 1, soluble, beta 1	3.4112	0.0015 5444
Cntn4	contactin 4	3.03	0.0015 7545
Coch	cochlin	3.7982	0.0015 7545
Pak6	p21 (RAC1) activated kinase 6	1.5328	0.0015 8889
Tmem205	transmembrane protein 205	1.1365	0.0016 0227
Atp2b3	ATPase, Ca++ transporting, plasma membrane 3	5.9701	0.0016 0227
Cacna1g	calcium channel, voltage-dependent, T type, alpha 1G subunit	4.2593	0.0016 1223
Dscaml1	DS cell adhesion molecule like 1	2.8328	0.0016 2115
Zfp423	zinc finger protein 423	5.6726	0.0016 3633
Asic1	acid-sensing (proton-gated) ion channel 1	2.3093	0.0016 37
Hrh3	histamine receptor H3	3.3866	0.0016 4332
Atp5k	ATP synthase, H+ transporting, mitochondrial F1F0 complex, subunit E	1.5727	0.0016 4332
Nkain2	Na+/K+ transporting ATPase interacting 2	2.6233	0.0016 5401
Ramp3	receptor (calcitonin) activity modifying protein 3	6.1025	0.0016 6412
Parva	parvin, alpha	2.8838	0.0016 7428
Wdr17	WD repeat domain 17	4.3212	0.0017 0548
B3gat1	beta-1,3-glucuronyltransferase 1 (glucuronosyltransferase P)	4.7296	0.0017 0548
Nefh	neurofilament, heavy polypeptide	2.8997	0.0017 162
Mboat2	membrane bound O-acyltransferase domain containing 2	2.9031	0.0017 3258
Elavl2	ELAV like RNA binding protein 1	2.235	0.0017 8834
Zfp831	zinc finger protein 831	6.0029	0.0017 8927
Flrt2	fibronectin leucine rich transmembrane protein 2	4.9235	0.0018 1087
Rasl2-9	RAS-like, family 2, locus 9	-1.0293	0.0018 5705
Gm5124	predicted pseudogene 5124	3.3401	0.0018 5915
Elovl6	ELOVL family member 6, elongation of long chain fatty acids (yeast)	1.8872	0.0018 7531
Ica1l	islet cell autoantigen 1-like	1.8841	0.0018 7531
Cracd	capping protein inhibiting regulator of actin	3.4653	0.0019 1259

Atrnl1	attractin like 1	2.4639	0.0019 3737
Gng13	guanine nucleotide binding protein (G protein), gamma 13	5.6062	0.0019 4286
Tmie	transmembrane inner ear	3.7367	0.0019 4517
Ppp1r16b	protein phosphatase 1, regulatory subunit 16B	1.6842	0.0020 7003
Rimbp2	RIMS binding protein 2	4.234	0.0020 8915
Gsg1l	GSG1-like	5.8951	0.0020 9125
Aldh1a1	aldehyde dehydrogenase family 1, subfamily A1	2.1468	0.0020 9319
Fsd1	fibronectin type 3 and SPRY domain-containing protein	2.594	0.0020 9826
Fndc5	fibronectin type III domain containing 5	2.6476	0.0021 0713
Pip5k1b	phosphatidylinositol-4-phosphate 5-kinase, type 1 beta	5.6279	0.0021 4104
Cabp1	calcium binding protein 1	3.5819	0.0021 4593
Lrch2	leucine-rich repeats and calponin homology (CH) domain containing 2	4.3921	0.0021 5923
Rsph9	radial spoke head 9 homolog (Chlamydomonas)	1.2125	0.0021 6592
mt-Rnr1	mitochondrially encoded 12S rRNA	1.4046	0.0021 682
Kcnb2	potassium voltage gated channel, Shab-related subfamily, member 2	5.7162	0.0021 788
Ctnna2	catenin (cadherin associated protein), alpha 2	2.2231	0.0022 154
Celf3	CUGBP, Elav-like family member 3	1.5295	0.0022 2048
Cntn3	contactin 3	5.9764	0.0023 3191
Dscam	DS cell adhesion molecule	4.2886	0.0023 3778
Sqle	squalene epoxidase	1.1846	0.0023 6563
Trpm3	transient receptor potential cation channel, subfamily M, member 3	2.2585	0.0023 8118
Zfp804a	zinc finger protein 804A	5.7435	0.0024 1077
Il17d	interleukin 17D	2.7048	0.0024 214
Ccdc159	coiled-coil domain containing 159	4.5677	0.0024 3375
Shisa6	shisa family member 6	3.3472	0.0024 5834
Pxdn	peroxidasin	3.5889	0.0025 4658
Dlk2	delta like non-canonical Notch ligand 2	4.57	0.0025 494
Cys1	cystin 1	4.0834	0.0025 494
Cdr1os	cerebellar degeneration related antigen 1, opposite strand	2.7748	0.0025 6199
Gm32224	predicted gene, 32224	5.8485	0.0025 754
Mir670hg	MIR670 host gene (non-protein coding)	3.6498	0.0025 8046
Rhof	ras homolog family member F (in filopodia)	1.0555	0.0025 9007
Efcab10	EF-hand calcium binding domain 10	5.4774	0.0025 9589
Pcsk2os1	proprotein convertase subtilisin/kexin type 2, opposite strand 1	6.1262	0.0026 3237

Vstm5	V-set and transmembrane domain containing 5	5.456	0.0026 5126
Fam13c	family with sequence similarity 13, member C	2.3839	0.0026 6117
Gm20063	predicted gene, 20063	5.8455	0.0026 9048
Neurod1	neurogenic differentiation 1	5.8568	0.0027 1415
Il6	interleukin 6	-1.0032	0.0027 1415
A230006K 03Rik	RIKEN cDNA A230006K03 gene	4.5727	0.0027 2868
Ptprn2	protein tyrosine phosphatase, receptor type, N polypeptide 2	3.1991	0.0027 4036
Cst6	cystatin E/M	5.6267	0.0027 9083
Ankrd63	ankyrin repeat domain 63	3.4776	0.0028 7429
Cacng4	calcium channel, voltage-dependent, gamma subunit 4	4.5017	0.0028 8865
Dtna	dystrobrevin alpha	1.6137	0.0029 3529
Ccdc177	coiled-coil domain containing 177	4.1987	0.0029 5044
Rasgrf2	RAS protein-specific guanine nucleotide-releasing factor 2	1.0909	0.0029 8147
Krt77	keratin 77	4.4882	0.0031 2398
Fam171a1	family with sequence similarity 171, member A1	1.2771	0.0031 3118
Kcnq5	potassium voltage-gated channel, subfamily Q, member 5	3.9982	0.0031 3362
Tmcc2	transmembrane and coiled-coil domains 2	1.3452	0.0031 3362
Slc16a2	solute carrier family 16 (monocarboxylic acid transporters), member 2	2.3434	0.0031 5422
Rap1gap	Rap1 GTPase-activating protein	1.5364	0.0032 4131
Cavin3	caveolae associated 3	2.6384	0.0032 4658
A830082 N09Rik	RIKEN cDNA A830082N09 gene	3.6409	0.0032 9937
Kcnt2	potassium channel, subfamily T, member 2	5.5015	0.0033 7021
Dll3	delta like canonical Notch ligand 3	3.5776	0.0034 7923
Pknox2	Pbx/knotted 1 homeobox 2	3.0658	0.0035 0105
1700030C 14Rik	RIKEN cDNA 1700030C14 gene	5.5207	0.0035 3913
Plagl1	pleiomorphic adenoma gene-like 1	3.9816	0.0035 8653
Tox	thymocyte selection-associated high mobility group box	3.0607	0.0035 978
Slc26a4	solute carrier family 26, member 4	3.9774	0.0036 0081
Htr1b	5-hydroxytryptamine (serotonin) receptor 1B	5.8799	0.0036 0846
Obsl1	obscurin-like 1	5.5395	0.0036 4922
Kndc1	kinase non-catalytic C-lobe domain (KIND) containing 1	3.2935	0.0037 2084
Glra3	glycine receptor, alpha 3 subunit	4.2189	0.0037 2629
Tmem200 a	transmembrane protein 200A	4.7089	0.0037 9691
Rims4	regulating synaptic membrane exocytosis 4	5.6037	0.0038 4296

Tlcd4	TLC domain containing 4	4.1442	0.0038 7446
Sdr39u1	short chain dehydrogenase/reductase family 39U, member 1	2.2316	0.0038 9495
Slc38a4	solute carrier family 38, member 4	5.57	0.0038 9758
Tmem74b	transmembrane protein 74B	4.594	0.0039 0155
Trh	thyrotropin releasing hormone	5.7945	0.0040 1467
Elapor2	endosome-lysosome associated apoptosis and autophagy regulator family member 2	3.5634	0.0040 798
Car4	carbonic anhydrase 4	1.8725	0.0040 8295
Dmrtc1a	DMRT-like family C1a	4.3951	0.0040 9345
Pygo1	pygopus 1	2.8443	0.0041 4737
Lancl2	LanC (bacterial lantibiotic synthetase component C)-like 2	1.1861	0.0042 5262
Gm20501	predicted gene 20501	3.6467	0.0043 655
Sv2c	synaptic vesicle glycoprotein 2c	3.753	0.0043 8208
Diras1	DIRAS family, GTP-binding RAS-like 1	4.2329	0.0044 5296
S100b	S100 protein, beta polypeptide, neural	1.7628	0.0045 2468
Cpne4	copine IV	2.7979	0.0045 382
Kcnt1	potassium channel, subfamily T, member 1	3.3408	0.0045 7583
Fabp7	fatty acid binding protein 7, brain	1.9689	0.0045 9053
Fgf14	fibroblast growth factor 14	3.5651	0.0047 4039
Ddit4l	DNA-damage-inducible transcript 4-like	4.4561	0.0047 8255
Sema3a	sema domain, immunoglobulin domain (Ig), short basic domain, secreted, (semaphorin) 3A	3.302	0.0047 8664
Mal	myelin and lymphocyte protein, T cell differentiation protein	-2.0764	0.0048 6621
Gm26984	predicted gene, 26984	2.9821	0.0049 0667
Cpne8	copine VIII	1.8622	0.0049 5903
Srsf12	serine and arginine-rich splicing factor 12	2.6445	0.0050 0106
Plcz1	phospholipase C, zeta 1	5.6971	0.0050 1876
Chac1	ChaC, cation transport regulator 1	4.1117	0.0050 8076
Dixdc1	DIX domain containing 1	2.0276	0.0052 5906
A330008L 17Rik	RIKEN cDNA A330008L17 gene	5.1801	0.0052 6599
Reps2	RALBP1 associated Eps domain containing protein 2	1.4389	0.0053 9285
Ttc39c	tetratricopeptide repeat domain 39C	3.6668	0.0055 5108
Mgat5b	mannoside acetylglucosaminyltransferase 5, isoenzyme B	5.1465	0.0058 2064
Kcnk4	potassium channel, subfamily K, member 4	4.0882	0.0058 8146
Akt3	thymoma viral proto-oncogene 3	1.2879	0.0058 8148
Nrip3	nuclear receptor interacting protein 3	1.6034	0.0058 9886

Usp29	ubiquitin specific peptidase 29	2.2586	0.0059 1743
Phactr3	phosphatase and actin regulator 3	2.0598	0.0059 4193
Slc8a2	solute carrier family 8 (sodium/calcium exchanger), member 2	4.1825	0.0060 6832
Ermn	ermin, ERM-like protein	-2.8384	0.0062 1362
Dact2	dishevelled-binding antagonist of beta-catenin 2	5.3625	0.0062 1814
Clstn2	calsyntenin 2	2.8267	0.0062 1814
Gm11223	predicted gene 11223	1.6398	0.0062 1814
Sult2b1	sulfotransferase family, cytosolic, 2B, member 1	1.9163	0.0063 0508
Csmd1	CUB and Sushi multiple domains 1	3.6749	0.0066 0767
Palm3	paralemmin 3	5.6252	0.0066 9995
Igf2r	insulin-like growth factor 2 receptor	2.9568	0.0066 9995
Rgs6	regulator of G-protein signaling 6	4.1215	0.0068 1774
Cpne7	copine VII	1.7294	0.0068 2626
Gm15441	predicted gene 15441	-1.6811	0.0069 0834
Ccdc92b	coiled-coil domain containing 92B	5.416	0.0069 099
Ikzf4	IKAROS family zinc finger 4	3.6212	0.0069 3047
Slitrk3	SLIT and NTRK-like family, member 3	3.116	0.0069 3124
Dlk1	delta like non-canonical Notch ligand 1	4.0754	0.0070 757
Cald1	caldesmon 1	1.9827	0.0071 326
Yap1	yes-associated protein 1	4.1624	0.0071 629
Erbb4	erb-b2 receptor tyrosine kinase 4	4.9461	0.0072 501
B230209E 15Rik	RIKEN cDNA B230209E15 gene	2.537	0.0072 7332
Mir124a-1hg	Mir124-1 host gene (non-protein coding)	5.129	0.0073 4033
Zfp618	zinc finger protein 618	3.5969	0.0073 738
Fam183b	family with sequence similarity 183, member B	5.2789	0.0074 1816
Gm19196	predicted gene, 19196	2.4752	0.0074 204
Prr36	proline rich 36	2.8094	0.0075 4606
Fgf9	fibroblast growth factor 9	2.7474	0.0075 9027
Nnmt	nicotinamide N-methyltransferase	4.2075	0.0076 2576
Pcbp3	poly(rC) binding protein 3	1.4285	0.0077 1811
Tgfb1i1	transforming growth factor beta 1 induced transcript 1	2.3216	0.0077 3257
Fxyd1	FXYD domain-containing ion transport regulator 1	2.7295	0.0077 4138
Rapgefl1	Rap guanine nucleotide exchange factor (GEF)-like 1	1.2644	0.0077 5319
Gm37899	predicted gene, 37899	3.8376	0.0078 2547

Klhl29	kelch-like 29	3.7015	0.0078 3692
Zfp462	zinc finger protein 462	4.8368	0.0079 0141
A830073 O21Rik	RIKEN cDNA A830073O21 gene	5.5888	0.0079 739
Fbll1	fibrillarin-like 1	3.6025	0.0079 739
B930095G 15Rik	RIKEN cDNA B930095G15 gene	1.5204	0.0079 8322
2900060N 12Rik	RIKEN cDNA 2900060N12 gene	4.7971	0.0079 8406
Kif26b	kinesin family member 26B	5.3375	0.0079 9013
Dipk1b	divergent protein kinase domain 1B	1.1927	0.0080 3235
Gm17024	predicted gene 17024	1.0976	0.0080 3283
Spin2c	spindlin family, member 2C	2.7531	0.0081 0685
Fam174b	family with sequence similarity 174, member B	4.2483	0.0081 3643
Cacna2d3	calcium channel, voltage-dependent, alpha2/delta subunit 3	2.26	0.0083 132
Garem1	GRB2 associated regulator of MAPK1 subtype 1	1.5615	0.0083 291
A830082K 12Rik	RIKEN cDNA A830082K12 gene	2.1283	0.0085 8556
Pcsk5	proprotein convertase subtilisin/kexin type 5	4.0228	0.0086 5566
Gm28374	predicted gene 28374	-3.1428	0.0087 0909
Prrg3	proline rich Gla (G-carboxyglutamic acid) 3 (transmembrane)	3.4905	0.0087 2632
Kcnab2	potassium voltage-gated channel, shaker-related subfamily, beta member 2	1.5702	0.0088 0991
Ankrd34a	ankyrin repeat domain 34A	2.0024	0.0088 2193
Zfp385b	zinc finger protein 385B	3.0465	0.0088 6895
Gpc6	glypican 6	4.631	0.0089 5584
Prr16	proline rich 16	4.6778	0.0091 0611
Nol3	nucleolar protein 3 (apoptosis repressor with CARD domain)	3.5132	0.0091 4528
Amot	angiomotin	5.1001	0.0092 8233
Ucma	upper zone of growth plate and cartilage matrix associated	5.0545	0.0093 2296
Aqp4	aquaporin 4	2.1269	0.0095 1887
Nck2	non-catalytic region of tyrosine kinase adaptor protein 2	2.9683	0.0097 1587
Me3	malic enzyme 3, NADP(+)-dependent, mitochondrial	1.9616	0.0097 3236